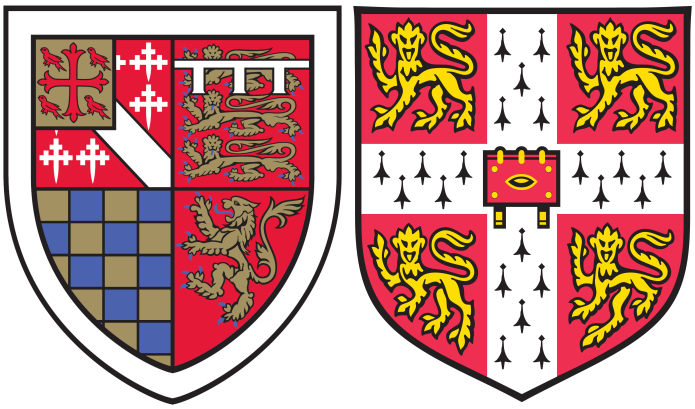
Novel regulators of antibiotic biosynthesis in *Serratia* sp. ATCC 39006



Daniel Orlando Plaza Sáez

Department of Biochemistry

St Edmund's College
University of Cambridge

This dissertation is submitted for the degree of
Doctor of Philosophy

August 2022

Novel regulators of antibiotic biosynthesis in *Serratia* sp. ATCC 39006

Daniel Orlando Plaza Sáez

Summary

Antibiotic resistance is an increasing global concern. Moreover, discovery of new antibiotics has dramatically declined over previous decades. Thus, there is a growing need for these compounds. Understanding of the regulatory processes that control antibiotic biosynthesis may prove exploitable in their controlled hyperproduction.

The enterobacterium *Serratia* sp. ATCC 39006 (S39006) is a useful Gram-negative model for studies on the biosynthesis and regulation of bioactive secondary metabolites, particularly two antibiotics – prodigiosin and a carbapenem. Both compounds are tightly regulated in response to various physiological and environmental signals, including quorum sensing.

This project aimed to identify and characterise new regulatory genes that modulate antibiotic biosynthesis in S39006. Novel regulators were sought through random transposon mutagenesis, using the wild type (WT) as parental strain and the prodigiosin production phenotype (red pigment) for screening of mutants. Colonies displaying altered pigmentation were thus selected. The transposon insertion effects on pigmentation were verified by transducing the mutations out into the WT genetic background using a generalised transducing phage. From the confirmed mutants, two strains were chosen for deeper characterisation: one carrying an insertion in *wzt* and another in an intergenic region. Disruption of *wzt*, encoding an ABC-transporter of the O-antigen, caused elevated production of both antibiotics. It was also pleiotropic, affecting features such as swimming motility and virulence. Pleiotropy was also found in the intergenic mutant: exhibiting enhanced antibiotic synthesis, and modified motility and virulence capacity. This intergenic insertion then led to the study of VfmE, an AraC-family transcription regulator, which activates antibiotic synthesis. This regulator was previously associated with virulence in phytopathogenic *Dickeya* strains, operating via a secondary quorum sensing system encoded in the *vfm* (virulence factor modulating) cluster, which uses an unknown signalling molecule. The members of this Vfm system were also found in S39006 and, by using transposon mutagenesis, their effect on antibiotic production was disclosed. To pinpoint the mechanisms by which *wzt*, the intergenic, and *vfmE* mutations act, double mutants with known S39006 regulators were generated to establish connections to the wider regulatory network. Finally, cutting-edge proteomics analysis was conducted for the intergenic mutant. In summary, functional characterisation of the regulatory mutations and their physiological impacts on the modulation of antibiotic production and associated wider pleiotropy were dissected here. This work thus provides insights into the mechanisms modulating antibiotic biosynthesis in S39006 via new regulators.

Declaration

This dissertation is the result of my own work and contains nothing which is the outcome of work carried out in collaboration, except where specifically expressed in the text.

It is not substantially the same as any that I have submitted for a degree, diploma, or other qualification at the University of Cambridge or any other institution. I further state that no substantial part of my dissertation has already been submitted or is being concurrently submitted for any such a degree, diploma, or other qualification at the University of Cambridge or any other institution.

This thesis does not exceed the length limit of 60,000 words, specified by the Biology Degree Committee.

Daniel Orlando Plaza Sáez

August 2022

Acknowledgements

Firstly, I want to express my infinite gratitude to my supervisor, Prof. George Salmond, who always encouraged and helped me to think more critically. The intellectual challenge was a constant motivation to do better. Moreover, the freedom to explore was an additional stimulus. The mentorship I received undoubtedly made me grow as a scientist. Many thanks for the patience, guidance, and unconditional support throughout this project; it was an honour.

I am also especially thankful to Dr. Rita Monson, not only for her crucial intelectual and technical support for moving this project forward, but also for making my life in Cambridge more enjoyable outside of the lab. Her wise advice and unforgettable events were very important at this stage.

Thanks to all the Salmond Lab members I met. Particularly, to Dr. Alex Quintero-Yanes, who supported me at the start of this project and in my new life in Cambridge. This is extended to my labmates with whom I shared most of this journey: Dr. Amy Hill, Maria Stroyakovski, Dr. Ziyue Zeng, Dr. Katherine Hucks, Dr. Carlo Sandoval, and Dr. Tomás Kappes. Thanks for being tremendously supportive and generous, especially during the tough pandemic time. My time accompanied by you will be always cherished. Moreover, thanks to Dr. Martin Welch and members of his lab for the fruitful discussions and willingness to help at any time.
The excellent technical support given by Diana Breitmaier and Josh Western in the lab was also tremendously important for this work, thank you. I also thank the support received from Dr. Mike Deery and Dr. Yagnesh Umrania for the proteomic analysis.

This new step would not have been possible without my supportive past mentors, Dr. Vilbett Briones, Dr. Ximena Moncada, and Dr. José Manuel Pérez Donoso. Thanks for trusting in me, even in my most mad ideas and dreams.

My heartfelt gratitude to ANID-Chile and The Cambridge Trust for their financial support of this PhD course, as well as the British Society for Plant Pathology, The Cambridge Trust, and the Department of Biochemistry for the COVID-19 extensions. Further gratitude to the International Society for Microbial Ecology, The Microbiology Society, and The Sanger Fund for travel grants awarded to present my work at conferences.

My endless gratitude also goes to Dr. Pamela Sotelo Hitschfeld (RIP), my beloved partner. Despite the distance, I never felt alone. Your constant support and love were always a pivotal incentive to never give up, particularly in difficult periods of uncertainty and hopelessness. Thank you for always being by my side and for loving me for over a decade. You are deeply missed.

Finally, I want to especially thank my beloved parents, Raquel Sáez and Orlando Plaza. For their ceaseless efforts in life to make me who I am. For always loving me and teaching me the value of striving to be better in life. Every single step in my life is thanks to you. You both are the reason that keeps me alive in the worst personal time of my life.

Este trabajo está dedicado a mis amados padres y a la memoria de mi amada Pamela. Gracias por tanto

Index

1. Introduction....12
1.1. Antibiotics....12
1.2. *Serratia* genus....12
1.2.1. *Serratia* sp. ATCC 39006....13
1.2.1.1. General features....14
1.2.1.2. Prodigiosin....15
1.2.1.3. Carbapenem....17
1.1.2.4. Genetic regulators of antibiotic biosynthesis....19
1.2.1.4.1. Central role of quorum sensing....19
1.2.1.4.2. PigP regulon....21
1.2.1.4.3. Connection to phosphate metabolism....22
1.2.1.4.4. RNA-binding proteins....22
1.2.1.4.5. Regulators from gas vesicle mutants....23
1.2.1.4.6. Other regulators....24
1.3. Aim of the project....25

2. Materials and methods....26
2.1. Media and solutions....27
2.2. Strains and growth conditions....27
2.3. DNA extraction....31
2.4. Polymerase chain reaction and gel separation....31
2.5. Random Transposon Mutagenesis....33
2.6. Determination of Transposon Insertion Sites....33
2.7. Phage Transduction....34
2.8. Antibiotic production....34
2.8.1. Prodigiosin....34
2.8.2. Carbapenem....35
2.9. Phenotypic assays....35
2.9.1. Gas vesicles....35
2.9.2. Acyl-homoserine lactones....35
2.9.3. Cell wall-degrading enzymes....35
2.9.4. Swimming and swarming motility....36
2.9.5. Cell and colony morphology....35
2.9.6. Potato infection assay....36
2.10. Plasmid construction and transformation....36
2.10.1. Preparation of competent cells....36
2.10.2. Cloning....37
2.11. β-galactosidase activity....38
2.11.1. Promoter activity....38
2.11.2. *In vivo* binding assays....38
2.12. RNA isolation....39

2.13. Determination of transcription ends 39
2.14. RNA sequencing data 39
2.15. Protein analysis 39
2.15.1. Extraction and separation 39
2.15.2. Western blot 40
2.15.3. Proteomics processing 40
2.16. Bioinformatics 41
2.16.1. Genome visualisation and homology matching 41
2.16.2. Specific growth rates 41
2.16.3. Sequence alignments and phylogeny 41
2.16.4. Gene elements prediction 41
2.16.5. RNA data analysis 42
2.16.6. Protein data analysis 42

3. Novel regulators of antibiotic production 43
3.1. Generation and selection of mutants 43
3.2. Transposon location in mutants 44
3.3. Novel regulators 46
3.3.1. Phosphopantetheinyl transferase 47
3.3.2. CysW: a sulfate-transport permease 47
3.3.3. An uncharacterized protein 51
3.4. Discussion 53

4. O-antigen transport Wzt modulates antibiotic production 57
4.1. Members of the O-antigen operon 57
4.2. The *wzt* mutation increases antibiotic production at transcriptional level 58
4.3. The *wzt* mutation has pleiotropic effects 60
4.3.1. Mutation in *wzt* alters transcription of the gas vesicle synthesis cluster 60
4.3.2. Secretion of cell-wall degrading enzymes and motility decreases in *wzt* strain 62
4.3.3. Mutation of *wzt* attenuates virulence in plants 62
4.3.4. Mutation in *wzt* diminishes the synthesis of acyl-homoserine lactones 63
4.3.2. Secretion of cell-wall degrading enzymes decreases in *wzt* strain 64
4.4. Overexpression of *wzt* and *1186* partially complements their correspondent mutants 64
4.5. The *wzt* mutation is epistatic to several known antibiotic synthesis regulators 66
4.6. Discussion 69

5. An intergenic mutation led to a novel antibiotic production regulator, VfmE 75
5.1. Genomic context of the intergenic transposon insertion 75
5.2. Intergenic and *vfmE* mutants have antagonistic effects on antibiotic synthesis 76
5.3. Intergenic and *vfmE* mutations are pleiotropic 79
5.3.1. Intergenic and *vfmE* mutations reduce transcription of gas vesicle operons 80
5.3.2. Intergenic mutation antagonises the VfmE effect on swimming but not on cellulase production 81
5.3.3. Intergenic and *vfmE* mutations weaken virulence in plants 82

5.3.4. Intergenic and *vfmE* mutations do not affect acyl-homoserine lactone synthesis 83
5.4. VfmE phenotype is epistatic to the intergenic 84
5.5. VfmE promotes expression of a putative gene in the intergenic region 87
5.6. Gene prediction and complementation attempts for the intergenic mutation 93
5.7. Several transcripts convergent to *vfmE* start in the intergenic region 98
5.8. VfmE *in trans* augments prodigiosin synthesis and perturbs cell growth 100
5.9. Intergenic and *vfmE* mutations are epistatic to several known regulators 102
5.10. Discussion 107

6. VfmE is essential in *vfm* secondary quorum sensing system 114
6.1. S39006 has the *vfm* quorum sensing system components 115
6.2. VfmE is predicted to interact with *vfm* proteins 117
6.3. A *vfm* gene *in trans* modulates transcription of the intergenic gene and contributes to producing the Vfm signal 118
6.4. Inactivation of all *vfm* transcription units reduces prodigiosin production 123
6.5. *vfmA* and *vfmE* inactivation attenuates virulence and overexpression of *vfmE* increases the Vfm signal 126
6.6. VfmE increases *vfmA* promoter activity and decreases that of *hlyD;* VfmH does not act on any *vfm* promoter 129
6.7. VfmE and VfmH do not influence expression of antibiotic operons, *carR,* or *rap* regulators 131
6.8. Discussion 132

7. Proteomes of the intergenic mutant and its *vfmE* double mutant exhibit opposite changes in antibiotic and Vfm synthesis proteins 136
7.1. The intergenic mutation induces more protein changes than the double with *vfmE* 137
7.2. The intergenic and the *vfmE* double mutant display opposite changes in antibiotic-synthesis protein levels 140
7.3. The intergenic and the *vfmE* double mutant display opposite changes in *vfm* protein levels 143
7.4. Discussion 145

8. Final discussion 147

9. References 154

List of figures

Chapter 1
1.1. Colonies of *Serratia* sp. ATCC 39006 13
1.2. Prodigiosin chemical structure 15
1.3. Biosynthetic gene cluster of prodigiosin 16
1.4. Biosynthetic route of prodigiosin 16
1.5. Carbapenem chemical structure 18
1.6. Biosynthetic gene cluster of prodigiosin 18
1.7. Biosynthetic route of carbapenem 19
1.8. Regulators associated with the carbapenem and prodigiosin production 20

Chapter 3
3.1. Experimental outline for generation of mutants 43
3.2. Examples of isolated strains displaying altered pigmentation 44
3.3. Phenotypic classification of mutants presenting changed pigmentation 45
3.4. Transposon insertions caused the changes in prodigiosin synthesis 46
3.5. Genomic neighbourhood of the transposon insertions in mutants OB5 and OB7 47
3.6. Production of antibiotics and AHL (BHL) over time by the *cysW* strain 48
3.7. Phenotypic characterisation of *cysW* strain 49
3.8. *cysW* mutant grows poorly in minimal medium 50
3.9. Genomic neighbourhood of the transposon insertion in mutant ND1 50
3.10. Representation of CysW domain 51
3.11. Production of antibiotics and acyl homoserine lactones over time of NB3 train 51
3.12. Phenotypic characterisation of NB3 train 52
3.13. NB3 mutant can grow in minimal medium 52
3.14. Genomic neighbourhood of the transposon insertion in mutant NB3 53

Chapter 4
4.1. Operonic organisation of *wzt* and *1186* and domain architecture of proteins 57
4.2. The mutation in *wzt* generates characteristic colonies and its phenotype is due to the transposon insertion 58
4.3. Mutations in *wzt* and *1186* increase the production of antibiotics 59
4.4. Mutation in *wzt* increases transcription of antibiotic biosynthesis operons 60
4.5. Mutation in *wzt* affects transcription of gas vesicle gene cluster 61
4.6. The *wzt* mutation reduced motility and secretion of cell-wall degrading enzymes 62
4.7. The wzt mutation decreases virulence in plants 63
4.8. The *wzt* mutation decreases synthesis of acyl-homoserine lactones 64
4.9. Overexpression of *wzt* and *1186* partially complements their corresponding mutant strains 65
4.10. The *wzt* mutation bypassed prodigiosin production control of several known regulators 66
4.11. The *wzt* mutation bypassed carbapenem production control of several known regulators 67

4.12. Mutation in *wzt* affects transcription of *pigS*, *pigX*, *pigZ*, and *caR* 68

Chapter 5
5.1. Genomic context of the transposon-disrupted intergenic region 75
5.2. Phylogenetic tree of S39006 VfmE and ArgG homologues 76
5.3. The intergenic mutation triggers overproduction of prodigiosin 77
5.4. The intergenic mutation increases *vfmE* expression but not *argG* expression 77
5.5. Intergenic and *vfmE* mutations generate opposite effects on production of antibiotics, and only prodigiosin is controlled at transcriptional level 79
5.6. Intergenic and *vfmE* mutations diminish expression of of gas vesicle gene cluster 81
5.7. The *vfmE* mutation reduced swimming and cellulase secretion, and intergenic mutation boosted motility 82
5.8. The intergenic and *vfmE* mutations diminish virulence in plants to different extents 83
5.9. Neither the intergenic or *vfmE* mutation alter synthesis of acyl-homoserine lactones 84
5.10. The IGR,*vfmE* double mutant has same pigmentation as the *vfmE* isogenic strain 85
5.11. The IGR,*vfmE* double mutant displays the same reduced antibiotic production as the *vfmE* strain 86
5.12. The *vfmE* and the double IGR,*vfmE* mutant show the same motility phenotype 86
5.13. The IGR,*vfmE* double mutant showed a decreased virulence in plants 87
5.14. Transcription direction in the transposon disrupted region is opposite to *vfmE* 88
5.15. VfmE activates expression of a putative gene interrupted by the transposon insertion .. 88
5.16. pNB9 region has maximal promoter activity 89
5.17. Predicted promoters for the region displaying maximal activity upstream of the insertion sites 90
5.18. A putative sigma 38 factor binding site drives transcription of the putative intergenic gene 91
5.19. The region upstream S38 might be a binding site for a ToxT homologue 92
5.20. VfmE and XylR regulators increase promoter activity of a putative intergenic gene 93
5.21. Schematic of the intergenic transposon insertions and similar regions in other bacteria 94
5.22. Location of the predicted genes in the intergenic region 95
5.23. Putative small RNA and the intergenic region in trans do not restore prodigiosin production 96
5.24. Putative small RNA and the intergenic region in trans boost swimming capacity of *vfmE* cells 97
5.25. Summary of inserts tested in genetic complementation of the intergenic mutant 98
5.26. Extensive transcriptional activity in the opposite direction of *vfmE* 98
5.27. Three transcripts are transcribed opposite to *vfmE* 100
5.28. Overexpression of *vfmE* leads to increased production of prodigiosin 101
5.29. Overexpression of *vfmE* negatively affects cell growth 102
5.30. The intergenic and *vfmE* mutations bypassed prodigiosin production of several known regulators 103
5.31. The intergenic and *vfmE* mutations bypassed carbapenem production of several known regulators 105
5.32. Mutation in the intergenic region augments transcription of *pigT* and decreases that of *pigP* and *caR* 106

5.33. Mutation in *vfmE* diminishes transcription of *pigR* and augments that of *pigW*..... 106

Chapter 6
6.1. Comparison of *vfm* clusters of *Dickeya dadantii* 3739 and *Serratia* sp. ATCC 39006 . 114
6.2. Domain architecture of *vfm* proteins in *Serratia* sp. ATCC 39006..... 116
6.3. Schematic of *vfm* quorum sensing system regulation in *Dickeya dadantii* 3937..... 117
6.4. Protein-protein interaction network predicted for S39006's VfmE..... 118
6.5. An example of transconjugants displaying different blue intensities that translate into diverse alteration levels of the intergenic transcription..... 119
6.6. The *hlyD* and IGR,*hlyD* transductants have the *vfmE* phenotype..... 121
6.7. Cross-feeding assay for antibiotic production..... 123
6.8. An example of a transconjugant colony displaying a light-pink (*vfm*) phenotype..... 124
6.9. Map and number of *vfm* genes hit by the transposons..... 125
6.10. Single and double *vfmA*, *vfmE*, and *vfmK* strains with the intergenic mutation display reduced prodigiosin synthesis..... 126
6.11. The *vfmA* and *vfmE* mutation decreases virulence in plants..... 127
6.12. Overexpression of *vfmE* increases production of an extracellular signal that augments carbapenem synthesis..... 128
6.13. VfmE from S39006 and *Dickeya dadantii* are highly similar at the sequence level 129
6.14. Motif prediction for the six regions bound by VfmE in *Dickeya dadantii*..... 130
6.15. VfmE activates *vfmA* and represses *hlyD* promoter activity in S39006..... 132
6.16. Overexpression of *vfmE* or *vfmH* has no effect on expression of biosynthesis clusters or *carR* or *rap* regulators..... 132

Chapter 7
7.1. Principal component analysis of the proteomes profiles..... 137
7.2. Volcano plots of the intergenic and double mutants proteomes..... 138
7.3. Relative abundance of differentially expressed proteins in the intergenic and double mutants' proteomes..... 139
7.4. Relative abundance of differentially expressed prodigiosin synthesis proteins in the intergenic and double mutants' proteomes..... 142
7.5. Relative abundance of differentially expressed carbapenem synthesis proteins in the intergenic and double mutants' proteomes..... 143
7.6. Relative abundance of differentially expressed *vfm* proteins in the intergenic and double mutants' proteomes..... 144

Chapter 8
8.1. Proposed model of antibiotic production regulation by the Wzt operon..... 148
8.2. Proposed model of antibiotic production regulation by the VfmE..... 150

List of tables

1.1. Regulators of antibiotic production in *Serratia* sp. ATCC 39006 20
2.1. Media and solutions used in this work 26
2.2. Antibiotic and supplements used in this work 27
2.3. Bacterial strains used in this work 28
2.4. PCR reaction concentrations 32
2.5. PCR program settings 32
2.6. Oligonucleotides used in this study 32
2.7. RP-PCR program settings 33
2.8. Plasmids used in this study 36
3.1. Transposon targets in genomes of prodigiosin mutants 45
6.1. Proteins of the *vfm* cluster present in *Serratia* sp. ATCC 39006 116
6.2. Regulators of antibiotic production in *Serratia* sp. ATCC 39006 121
7.1. Differentially expressed proteins in the intergenic and double mutants' proteomes .. 141

1. Introduction

1.1. Antibiotics

Antimicrobial discovery was one of the greatest advances in public health in the past century. Unfortunately, the pervasive use of these chemicals in medicine and many other human-related activities, has led to the evolution and selection of antibiotic-resistant microbes – to one or more compounds – leading to many deaths worldwide (Larsson and Flach, 2022). This resistance is spreading globally, posing a serious threat to humanity. New resistance mechanisms are emerging and spreading, putting our capacity to treat even common infectious diseases in jeopardy (Crofts *et al*, 2017). The current situation is concerning and necessitates immediate and intense action on new antibacterial agent developments (Brown and Wright, 2016; Surette and Wright, 2017; Church and McKillip, 2021). Furthermore, the rate of discovery and production of new antibiotics decreased dramatically over recent decades owing, at least in part, to a drop in profitability from the expensive commercial effort required to produce new antibiotics (Stanton *et al*, 2013; Wohlleben *et al*, 2016). The few new promising antibiotics discovered in recent years appear insufficient to address an increasing threat (Lewis, 2020). Thus, antibiotic resistance and the lack of novel antibacterial agents loom as an urgent issue for the health and welfare of both agriculture and humans.

The discovery of new antibiotics has been extensively sought from many sources (Spížek *et al*, 2016), where most traditional sources (bacteria and fungi) still prevail over synthetic compounds for clinical usage (Fischbach, 2009; Masschelein *et al*, 2017). Therefore, understanding antibiotic production pathways is crucial for developing new antibacterial drugs. *Streptomyces* strains are the most prolific and well-studied sources of bioactive chemicals, particularly antimicrobials, among bacteria (Hwang et al, 2014; van der Meij et al, 2017). Other bacteria evolutionarily distant from Gram-positive actinomycetes may provide novel products and synthetic mechanisms, however currently, far less is known about their respective antibiotic biosynthesis processes. Hence, examining diverse species and decoding their regulatory mechanisms may reveal novel and potentially useful antibiotic production processes. Such information may prove exploitable, for instance in industrial biotechnology – and this would be a worthwhile endeavour aimed at addressing current and future antibiotic problems.

1.2. *Serratia* genus

This genus consists of rod-shaped Gram-negative bacteria that belong to the *Enterobacteriaceae* family. Members are motile, facultative anaerobes, and their optimal growth temperature range between 30 and 37°C. They are found in diverse environmental sources including water, soil,

insects, and plants (Grimont and Grimont, 2006). Taxonomically, *Serratia* representatives are closely related to species from *Yersinia*, *Pectobacterium*, and *Dickeya* genera (Retchless and Lawrence, 2010). The most widely studied *Serratia* species is *S. marcescens*, an environmental pathogen capable of infecting a wide range of hosts, including plants, invertebrates, and vertebrates (Hejazi and Falkiner, 1997). This species has drawn most research attention, given it is a human opportunistic pathogen, able to colonise the digestive, respiratory, and urinary tracts, causing severe health problems in immunosuppressed patients (Mahlen, 2011). Several *Serratia* members are recognised producers of high-value compounds with biotechnological potential, such as pigments, biosurfactants, and cell-wall degrading enzymes (Soenens and Imperial, 2020).

1.2.1. *Serratia* sp. ATCC 39006

Serratia sp. ATCC 39006 (S39006) was originally found associated with halophytic plants from a salt marsh in Cheesequake (New Jersey, USA), when an expedition screened for new antibioticproducing microorganisms (Parker *et al*, 1982). Its genome sequence size is 4.94 Mb, with a GC content of 49.2%, and it comprises 4,413 protein-encoding genes (Fineran *et al*, 2013). This pigmented strain (Fig. 1.1) is motile through the use of flagella and spreads on surfaces by producing biosurfactants (Williamson *et al*, 2008). Furthermore, it is the only enterobacterium reported to date that synthesises gas vesicles naturally (Ramsay *et al*, 2011), which enable cells to maintain an optimal buoyancy at air/liquid interfaces to sustain adequate nutrition and oxygen supply (Pfeifer, 2012).

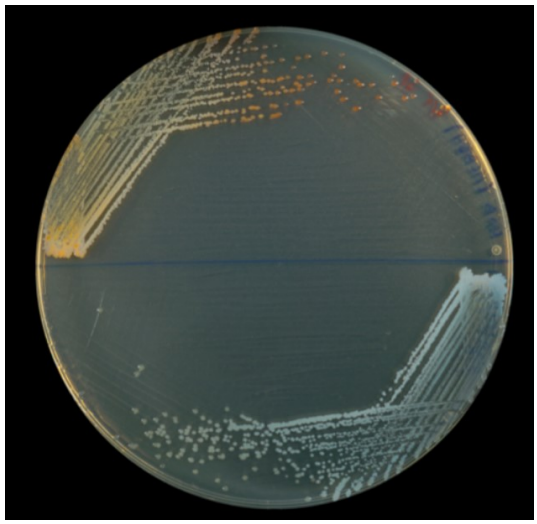


Fig. 1.1. Colonies of *Serratia* sp. ATCC 39006. Top: wild type strain; bottom: non pigmented strain (*pigA* mutant)

S39006 is virulent in plants, via secretion of cell wall-degrading enzymes, such as pectate lyase and cellulase (Slater *et al*, 2003), and in *Caenorhabditis elegans* through unidentified mechanisms (Coulthurst *et al*, 2004; Fineran *et al*, 2007). Lastly, this *Serratia* member produces at least two unrelated antibiotics - the distinctive red pigment named prodigiosin (Williamson *et*

al, 2006), and a carbapenem (Coulthurst *et al*, 2005). The strain is genetically amenable and this feature, along with the production of the two chemically defined antibiotics, makes it a useful Gram-negative model for the study of biosynthesis and regulation of bioactive secondary metabolites.

1.2.1.1. General features

Apart from antibiotic production, the most important attributes of S39006 are the synthesis of gas vesicles, motility, and exoenzymes production.

Gas vesicles are hollow intracellular nanostructures that allow microorganisms to move vertically through water by either producing dense conglomerations of vesicles (upward), or collapsing them (downward), seeking adequate oxygen and nutrient levels (Pfeifer, 2012). These unique structures are impermeable to water, but permeable to gases. Vesicles are composed completely of proteins and tend to form clusters, seen as bright "vacuoles" when cells are examined under phase contrast microscopy (Ramsey *et al*, 2011; Tashiro *et al*, 2016). Potential biotechnological applications of these gas chambers are in the biomedical field, such as components for engineered vaccines and contrast agents in magnetic resonance (reviewed in Hill and Salmond, 2020).

Gas-vesicle-containing microbes typically inhabit aquatic environments, and common examples are archaea, cyanobacteria, and some heterotrophic bacteria (Pfeifer, 2015). In S39006, the gas vesicles gene cluster (16.7 kb) is comprised of 19 genes, contained within two operons (*gvpA1gvpC* and *gvrA-gvrC*), with homologues found in other vesicle-producing organisms (Tashiro *et al*, 2016). The first operon carries the main structural genes (e.g. *gvpA1* and *gvpC*) whilst the second encodes some key regulatory genes, such as *gvrA* (Ramsay and Salmond, 2012).

*S*39006 is also a motile enterobacterium by mean of flagella, filamentous structures composed of more than 20 proteins, known as the motor system of the bacterial cell (Grognot and Taute, 2021). Among the existing types of motility, this species utilises swimming and swarming as active strategies for movement. Both kinds of bacterial locomotion are flagella-dependent, but there are marked differences between them Kearn, 2010). In short, swimming implies movement of individual cells through liquid environments, whereas swarming is a collective effort (multicellular) to move over semisolid surfaces in the presence of a wetting agent (Kearn, 2010; Xu *et al*, 2012). Flagellar machinery in S39006 comprises 35 genes that are scattered throughout its genome and are regulated by the FlhDC complex (Williamson *et al*, 2018).

As a plant pathogenic strain, S39006 secretes specialised enzymes in order to cause infection. To gain access to the plant, these bacteria release factors, termed cell wall-degrading enzymes (CWDE), that break down the host cell wall, allowing invaders to initate infection (Leonard *et al*, 2016). This strain uses pectate lyase and cellulase, targeting pectin and cellulose, respectively, to

enable the entry and subsequent colonisation of hosts. Simple soft rot assays in potato tubers have proved useful in testing virulence in S39006, through the maceration of soft tissue (Fineran *et al*, 2005, 2007).

1.2.1.2. Prodigiosin

Prodigiosin (2-methyl-3-pentyl-6-methoxyprodigiosin; Fig. 1.2) is a red compound that is part of a wider group of hydrophobic pigments called Prodiginines, which contain three pyrrole rings in their structure (Nisha and Kumar, 2015; Hu *et al*, 2016). They have sparked interest due to their versatile activities as antimicrobial, antimalarial, antitumor, immunosuppressive, and anti-inflammatory agents (Williamson *et al*, 2007; Pérez-Tomás and Viñas, 2010; Samrot *et al*, 2011; Pan *et al*, 2012; Darshan and Manonmani, 2015).

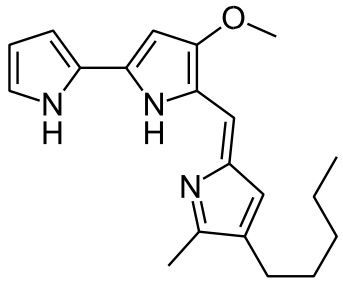


Fig. 1.2. Prodigiosin chemical structure.

The most promising members are undecylprodigiosin, cycloprodigiosin, metacycloprodigiosin, and prodigiosin made by *Serratia* and other bacteria such as streptomycetes (Hu *et al*, 2016). With a growing attention to prodigiosin in recent years due to its ample range of potential applications (Paul *et al*, 2020; Choi *et al*, 2021). For example, this tripyrrole can be used as a colorant since it is resistant to washing liquid ingredients, and so is relevant for the textile industry (Liu *et al*, 2013). It also has immunomodulating activity (Pandey *et al, 2007;* Rashidi and Jebali, 2019; Ji *et al*, 2019) and anticancer properties against some human carcinomas (Pérez-Tomás *et al*, 2003; Wang *et al*, 2016; Nguyen *et al*, 2020). As a biocide, it exerts antibacterial action against different species, including *Bacillus cereus* (Darshan *et al*, 2016), *Streptococcus pyogenes* (Lapenda *et al*, 2015), and *Staphylococcus aureus* (Lim *et al*, 2022). Nonetheless, its clinical usage is limited due to some cytotoxic effects (Williamson *et al*, 2006; Suryawanshi *et al*, 2017). Furthermore, it has potential as an antifungal (Jimtha *et al*, 2017), antiprotozoan (Arivizhivendhan *et al*, 2015), antimalarial (Papireddy *et al*, 2011), insecticidal (Tambong, 2013), algicidal (Chen *et al*, 2021), and nematocidal (Gomez-Valdez *et al*, 2022) compound.

Despite the rising interest spurred by its potential uses, the natural physiological role of prodigiosin in producing hosts is still poorly understood. Possible functions suggested include the

storage of light energy (Ryazantseva *et al*, 1995), protection from ultraviolet light (Boric *et al*, 2011) and as an interspecies competition advantage, since prodigiosin production aids in defeating other bacteria to gain niche advantages (Yip *et al*, 2021).

This pigment is a secondary metabolite that was discovered in *Serratia marcescens* (Harnet *et al*, 1954), the most studied prodigiosin-producing species. Different species from diverse genera synthesise this compound, such as *Streptomyces coelicolor*, *Hahella chejuensis*, *Vibrio spartinae*, and *Achromobacter denitrificans*, among others (Lin *et al*, 2020).

S39006 produces prodigiosin only at late growth stages and this production is highly regulated by an intricate network of regulators that are affected by both intra- and extra-cellular cues (Slater *et al*, 2003; Fineran *et al*, 2005; Williamson *et al*, 2006).

Its biosynthetic cluster includes 15 genes (*pigA-O*, often termed the *pig* cluster; Fig. 1.3), transcribed as polycistronic mRNA from a promoter usptream of *pigA* (Harris *et al*, 2004; Fineran *et al*, 2005).

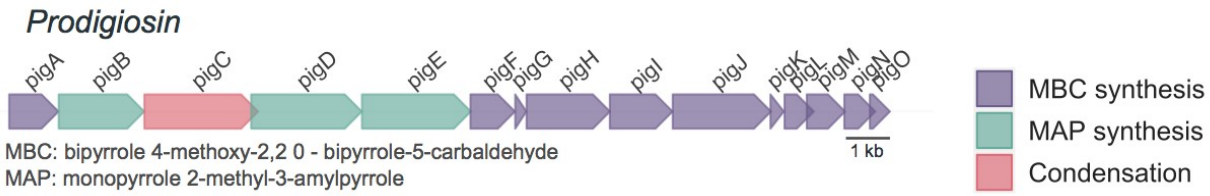


Fig. 1.3. Biosynthetic gene cluster of prodigiosin.

Prodigiosin biosynthesis involves a complex bifurcated pathway (Fig. 1.4). The first route produces a bipyrrole (4-methoxy-2,2′-bipyrrole-5-carbaldehyde; MBC), whereas the second produces a monopyrrole (2-methyl-3-n-amyl-pyrrole; MAP). These two compounds are then joined by an enzymatic condensation step to yield the final molecule (Harris *et al*, 2004).

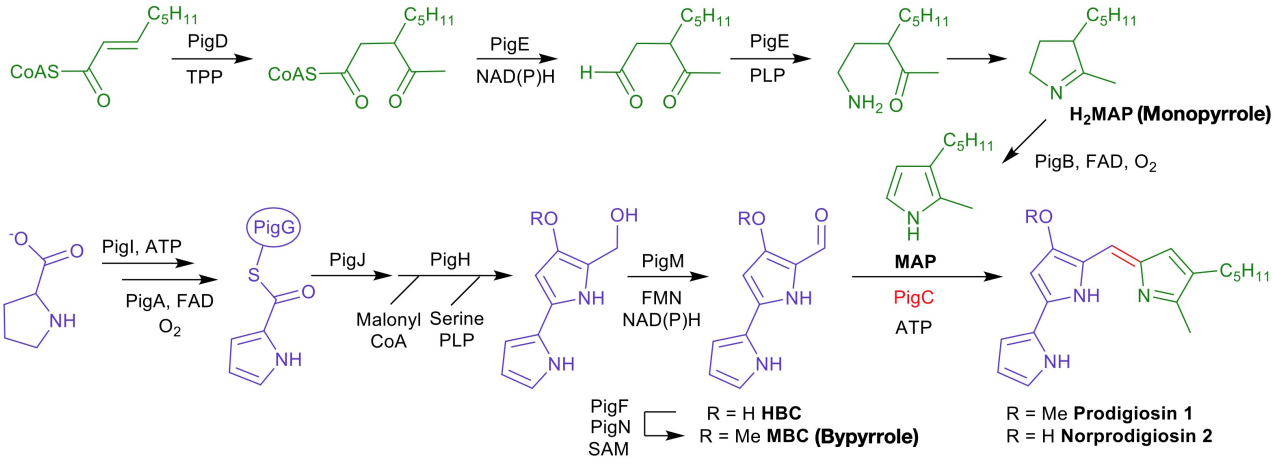


Fig. 1.4. Biosynthetic route of prodigiosin. Adapted from Couturier *et al* (2020).

The bypyrrole (MBC) is successively synthesised by PigI, PigL, PigG, PigA, PigJ, PigH, PigM, PigF and PigN, in multiple steps, while only three proteins, PigD, PigE and PigB, are required to form the monopyrrole (MAP; Williamson *et al*, 2005; Hu *et al*, 2016). The final step is carried out by the prodigiosin synthetase (PigC). Proteins PigK and PigO do not exert any obvious effect on prodigiosin production, and no function has been assigned to them (Williamson *et al*, 2005). The MBC pathway employs proline, acetate, serine, methione, and S-adenosylmethionine as precursors, whilst to form MAP, 2-octenal –mostly derived by oxidative degradation of unsaturated fatty acids– is the main precursor. Interestingly, the MBC pathway is highly conserved among prodigiosin producers, but the MAP pathway varies between species (Hu *et al*, 2016).

1.2.1.3. Carbapenem

The carbapenem produced by S39006 is a β-lactam, the most widely used class of antibiotics to treat infections. Their efficacy, safety, and versatility still make them the most successful antibacterials since they were discovered (Llarrull *et al*, 2010; Aminov, 2017).

They exert their bactericidal activity through inhibition of cell wall peptidoglycan biosynthesis, as they inactivate penicillin-binding proteins (Bush and Bradford, 2016). Penicillins, cephalosporins, monobactams, and carbapenem subclasses are members of this β-lactam class, which all share the characteristic β-lactam ring (Papp-Wallace *et al*, 2011; Townsend, 2016). Carbapenems have the broadest bactericidal activity against Gram-positive and Gram-negative bacteria and were originally not degraded by the majority of β-lactamases found in clinical settings (Potter *et al*, 2016; ElGamal *et al*, 2017) although carbapenemases have evolved in recent years, creating clinical problems. Nevertheless, they can still be employed as a useful "last resort" to fight against some multidrug-resistant pathogens (Gupta *et al*, 2017). Nevertheless, clinically proven compounds (meropenem, imipenem, and ertapenem) are synthetic due to the complexity of obtaining largescale concentrations from cell-based synthesis (El-Gamal *et al*, 2017). From over 60 naturally discovered, S39006 produces the simplest carbapenem structure known to date (1-carbapen-2-em3-carboxylic acid; Fig. 1.5; Coulthurst *et al*, 2005). The understanding of biosynthesis regulation of this simple antibiotic in S39006 in theory may be exploited potentially for large-scale production of carbapenems or their improvement by engineering regulatory pathways.

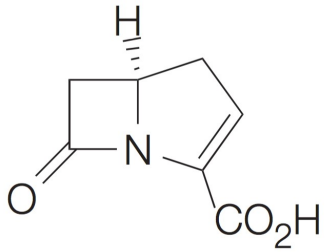


Fig. 1.5. Carbapenem chemical structure.

The carbapenem genetic cluster contains eight genes (*carA-H* operon; Fig. 1.6) and is regulated by a LuxR-type protein, CarR, which acts as a ligand-independent activator (McGowan *et al*, 1995; Thomson et al, 2000; Coulthurst *et al*, 2005).

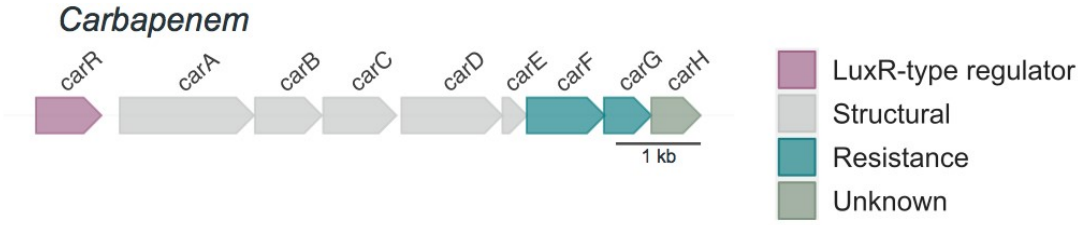


Fig. 1.6. Biosynthetic gene cluster for carbapenem.

Genes *carA-E* encode biosynthetic enzymes, and only CarA (carbapenem synthetase), CarB (carboxymethylproline synthase), and CarC (carbapenem synthase) are essential for carbapenem synthesis (Hamed *et al*, 2013). The intrinsic β-lactam resistance, to self-protect from the antibiotic, is driven by proteins encoded by *carF* and *carG* (McGowan *et al*, 1997). A structural report on CarG showed it has homology with a periplasmic *Aeromonas hydrophila* lysozyme inhibitor (PliI-Ah), and it was speculated that it might prevent toxicity by interacting with penicillin-binding proteins, the β-lactam targets (Tichy *et al*, 2014). Additionally, a structural study of CarF suggests the outer membrane porins as the target for interactions (Tichy *et al*, 2017). Lastly, the CarH specific function is not clear so far, but it is known that *carH* mutants are able to synthesise the antibiotic and are resistant to it (Slater et al, 2003; Coulthurst *et al*, 2005).

The pathways of carbapenem synthesis (Fig. 1.7) initiates when CarB converts the precursors (proline synthesis intermediates) into (2S,5S)-carboxymethylproline (CMP) which is next used by CarA to generate the β-lactam ring (3S,5S)-carbapenem. Subsequently, CarC catalyses an epimerization and a desaturation to yield the final compound. CarD (proline dehydrogenase) and CarE (2Fe-2S ferredoxin) roles are linked to proline oxidation catalysis and generation of cosubstrates for CarB, respectively (Stapon *et al*, 2003; Coulthurst *et al*, 2005; Hamed *et al*, 2013; Shomar *et al*, 2018).

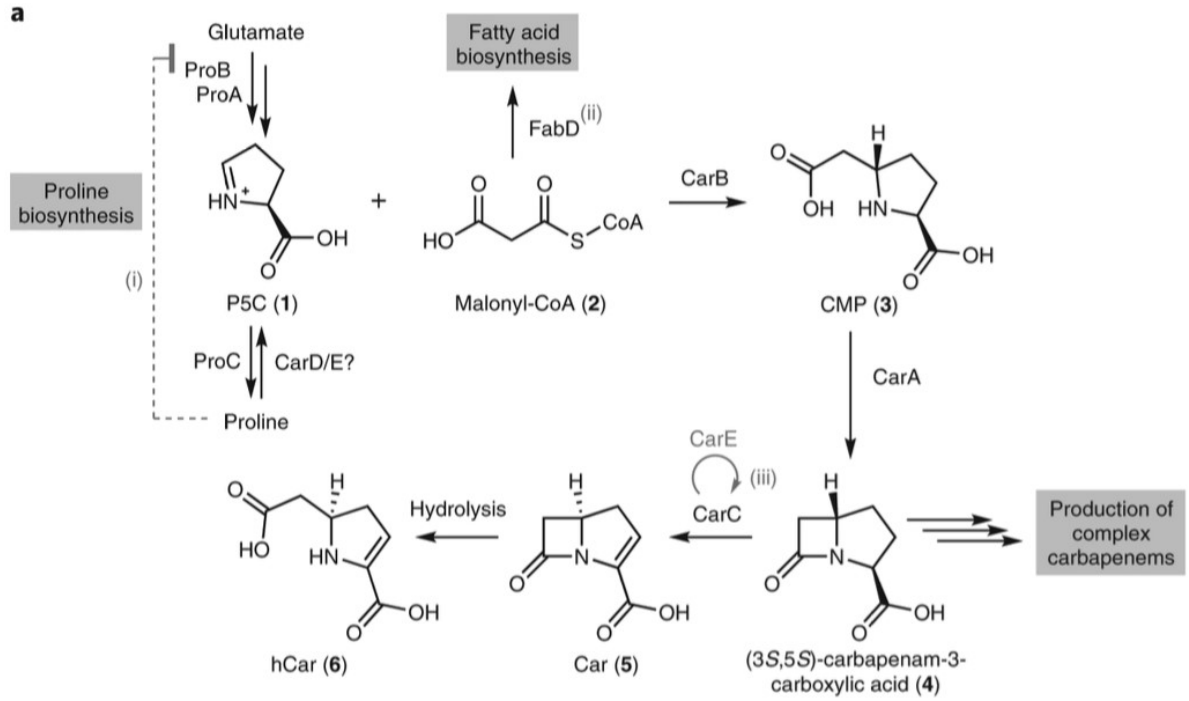


Fig. 1.7. Biosynthetic route of carbapenem. From Shomar *et al* (2018)

1.2.1.4. Genetic regulators of antibiotic biosynthesis

1.2.1.4.1. Central role of quorum sensing

Synthesis of antibiotics in S39006 is highly coordinated by different regulators that rely on various physiological and environmental signals (Table 1). Most of the regulators control the production of both antibacterials (Fig. 1.8) and depend on quorum sensing (QS) (Thomson *et al*, 2000; Slater *et al*, 2003; Fineran *et al*, 2005). This is a chemical cell-communication system based on the release and detection of small diffusible molecules known as "autoinducers," which cause a collective behaviour when a certain population cell density is reached (Papenfort and Bassler, 2016). S39006 produces two autoinducers: N-hexanoyl-L-homoserine lactone (HHL) and N-butanoyl-Lhomoserine lactone (BHL), which is the predominant product. Both signalling molecules, named collectively acyl homoserine lactones (AHLs), are synthetised by SmaI and recognised by SmaR, like their homologues LuxI and LuxR, respectively (Slater *et al*, 2003, Fineran *et al*, 2005; Williamson *et al*, 2005).

Name	Function	Reference
CarR	LuxR-type regulator	McGowan *et al* (1995)
SmaI	LuxI-type synthase	Thomson *et al* (2000)
SmaR	LuxR-type regulator	Thomson *et al* (2000)
Rap	SlyA/MarR regulator	Slater *et a*l (2003)
PstS	Phosphate transport	Slater *et al* (2003)
PigP	XRE family regulator	Fineran *et al* (2005)
PigQ	GacA response regulator homologue	Fineran *et al* (2005)
PigW	GacS sensor kinase homologue	Fineran *et al* (2005)
PigR	Class IV adenylate cyclase	Fineran *et al* (2005)
PigS	ArsR/SmtB family regulator	Fineran *et al* (2005)
PigT	GntR-type regulator	Fineran *et al* (2005)
PigU	LysR-type regulator	Fineran *et al* (2005)
PigV	YgfX membrane protein homologue	Fineran *et al* (2005)
PigX	CsrD homologue (GGDEF/EAL domain)	Fineran *et al* (2007)
PigZ	TetR/AcrR family regulator	Gristwood *et al* (2008)
RsmB	small RNA	Williamson *et al* (2008)
PhoB	Phosphate response regulator	Gristwood *et al* (2009)
PhoR	Phosphate sensor kinase	Gristwood *et al* (2009)
Hfq	RNA-binding protein	Wilf *et al* (2011)
RpoS	Sigma factor	Wilf and Salmond (2012)
RsmA	RNA-binding protein	Wilf *et al* (2013)
SdhE	Flavinylation factor	Hampton *et al* (2016)
RbsR	LacI family transcription factor	Lee *et al* (2017)
TrkH	Potassium transporter	Quintero-Yanes *et al* (2019)
FloR	DeoR family regulator	Quintero-Yanes *et al* (2020)
Fnr	Fumarate and nitrate reduction factor	Sun *et al* (2021)
OhrR	MarR family transcriptional	Sun *et al* (2021)

Table 1.1. Regulators of antibiotic production in *Serratia* sp. ATCC 39006.

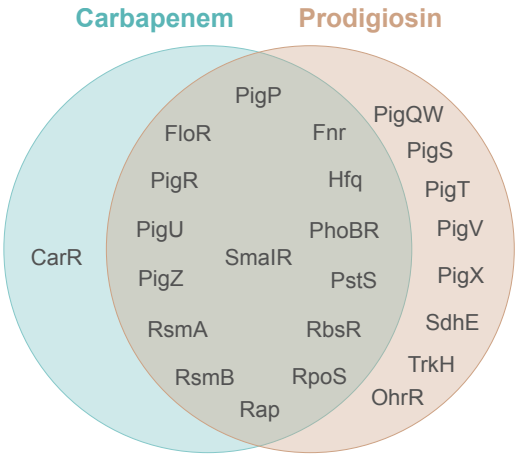


Fig. 1.8. Regulators associated with carbapenem and prodigiosin production. Overlap zone shows regulators affecting synthesis of both compounds.

1.2.1.4.2. PigP regulon

Some regulatory genes are critical for antibiotic production. Among these, PigP and Rap (regulator of antibiotic and pigment) are at the top of the hierarchy. PigP is a master regulator of secondary metabolites that in addition to control of the *pigA-O* gene cluster by promoter binding, in a QSindependent manner, it modulates at least another seven transcriptional regulators (*carR*, *pigQ*, *pigR*, *pigS*, *pigV*, *pigX* and *rap*; Fineran *et al*, 2005). Rap (SlyA/MarR family) is an activator of antibiotic production that operates by prompting direct transcription of the prodigiosin operon and *carR*, the carbapenem cluster activator. This regulator also connects overlapping inputs from QS, phosphate depletion, and other external cues sensed by the two-component system pigQW (Thomson *et al*, 1997; Slater *et al*, 2003; Fineran *et al*, 2005; Gristwood *et al*, 2011). This transduction system, a GacAS system homologue, is comprised of a sensor kinase (PigW) and a response regulator (PigQ) that modulate prodigiosin by binding its biosynthetic operon, which is additionally under QS signalling control (Fineran *et al*, 2005).

Along with PigQ and Rap, PigR (*cyaB* homologue) is another regulator under the control of both PigP and QS signals (Fineran *et al*, 2005). This enzyme converts ATP into cyclic adenosine monophosphate (cAMP), an ubiquituos molecule that fulfills diverse biological roles (Hentchel and Escalante-Semerena, 2015). In *E. coli*, cAMP interacts with the cAMP receptor protein (CRP; also termed catabolite activator protein, CAP) to influence global gene expression (Shimada *et al*, 2011). In S39006, the mechanisms used by PigR to modulate antibiotic production remain unknown. PigS is a metal-sensory regulator from the ArsR/SmtB family, which direct global gene expression to respond to harmful concentrations of various metal ions (Saha *et al*, 2017). This protein binds a sequence in the intergenic region between the divergently transcribed operons *blhAorfY* and *pigS-pmpABC*. Expression of the enzymes OrfY and BlhA gives rise to an undetermined S-containing compound that modulates prodigiosin production (Gristwood *et al*, 2011).

PigV is a regulator containing a DUF1434 domain, which only controls prodigiosin production (Fineran *et al*, 2005). More recently, it was renamed as YgfX, as its *E. coli* homologue, which forms a bicistronic operon with the succinate dehydrogenase protein E (SdhE), homologue of YgfY (McNeil et al, 2011). The latter is a DUF339 domain protein that flavinylates and activates the succinate dehydrogenase (McNeil *et al*, 2014). YgfX functions as a multimeric membrane protein that interacts with SdhE (McNeil *et al*, 2013). Independent studies on prodigiosin production showed that both mutants have the same effects on production, done either directly or indirectly, altering the pigment operon transcription levels (Fineran *et al*, 2005; Hampton *et al*, 2016). Hence, this operon may participate in the same function. The mechanism is not fully

understood, but YgfX interacts with cell division proteins, which might link the antibiotic production changes and cellular division (McNeil *et al*, 2013)

Another regulator is the GGDEF/EAL domain protein PigX (Fineran *et al*, 2007). Its homologue in *E. coli* is part of the carbon storage regulator system (CsrD), and it is involved in global transcriptional regulation (Esquerré *et al*, 2016). CsrD facilitates CsrA activity, a key regulator in bacteria, by inhibiting the synthesis of a small RNA, CsrB (Vakulskas *et al*, 2016). It might influence several transcriptional regulators through the c-di-GMP signaling pathway (Esquerré *et al*, 2016). In S39006, PigX was predicted to be bound to the inner membrane and proteomic analysis revealed that this mutation had impacted on many different proteins, and hence, its role in prodigiosin regulation still remains unclear (Finera *et al*, 2007).

For carbapenem synthesis, CarR is the only regulator known to exclusively activate its operon. This LuxR-like transcriptional factor is modulated by the SmaIR system. In the absence of AHLs, SmaR binds the *carR* promoter region repressing its activity, and hence, the transcription of the carbapenem operon. In the opposite scenario, at high cell density, AHLs bind SmaR, which allows the expression of *carR* by derepression, thereby augmenting the carbapenem operon transcription (Thomson *et al*, 2000; Slater *et al*, 2003).

1.2.1.4.3. Connection to phosphate metabolism

In S39006, vital regulators like *rap* and *smaI* are affected by phosphate availability (Gristwood *et al*, 2009). This strain employs the widely-distributed *pstSCAB-phoU* high-affinity phosphate transporter system, which was found to affect antibiotic synthesis (Slater *et al*, 2003). Changes in production are also dependent on a two-component system called PhoBR, where, in low concentrations of inorganic phosphate, the response regulator PhoB increases expression of *smaI*, and consequently both the AHLs and antibiotic levels. Accordingly, pstSCAB-phoU mutants imply phosphate depletion for cells, which means higher AHLs (Gristwood *et al*, 2009).

1.2.1.4.4. RNA-binding proteins

An example of post-transcriptional regulation is given by RNA-binding proteins, which play many different roles in prokaryotes (Holmqvist and Vogel, 2018). The RNA chaperone Hfq, involved in numerous processess such as bacterial adaptation during stress and pathogenesis, may bind to either sRNAs or mRNAs. Hfq is a hexameric protein that binds uracil-rich sequences that ultimately promote sRNA-mRNA interactions, avoiding RNase E cleavage (Kavita *et al*, 2018). In S39006, *hfq* mutants lack the normal capacity of producing gas vesicles and antibiotics. Hfq positively modulates secondary metabolism via CarR and SmaR, two QS-dependent regulators, thus impacting antibiotic synthesis (Wilf *et al*, 2011). It was suggested that different mechanisms

are utilised by this chaperone to regulate production of both compounds. To dissect those mechanisms, further work employed transcriptomics and proteomics to unveil the actors involved (Wilf *et al*, 2013). It was concluded that the *hfq* mutation leads to higher PigU levels, which in turn might repress pigment synthesis at a transcriptional level or may mediate this via an alternative sigma factor.

In addition to Hfq, the homologue of CsrA, RsmA is a key actor in posttranscriptional regulation of antibiotic production in S39006. CsrA (*carbon* storage regulator A) is a well-studied global regulator that sequesters mRNAs as its main mode of action (Romeo and Babitzke, 2018; Pourciau *et al*, 2020). Its counterpart in *Serratia*, RsmA (repressor of secondary metabolites A) was found to stimulate synthesis of gas vesicles (Ramsay *et al,* 2011) and impact production of antibiotics (Wilf *et al*, 2012). Transposon mutant *rsmA* had enhanced pigmentation but showed no carbapenem difference compared to WT. An ‘omics approach found that RsmA controls pigment synthesis through regulators such a PstS, PhoU, Rap, and RpoS. Interestingly, this study also showed an inverse correlation between genes regulated by this regulator and Hfq (Wilf *et al*, 2013). Furthermore, RsmA was later found to repress transcription of the membrane regulator YgfX (former PigV) by hindering the action of the flagellar master regulator FlhDC (Hampton *et al*, 2016). Moreover, there is an antagonist of RsmA activity called RsmB, which is a small RNA, and homologue of CsrB in *E. coli*, which had been earlier identified as a prodigiosin synthesis modulator (Williamson *et al*, 2008).

1.2.1.4.5. Regulators from gas vesicle mutants

Screening for gas vesicle mutants after random transposon mutagenesis has also enabled discovery of new regulators of antibiotic synthesis in S39006. This fact illustrates the complexity of regulation since regulators exert action in a concerted fashion to control diverse phenotypic features. Two of the novel regulators are pleiotropic transcription factors, modulating both antibiotics, and the other an ion transporter that only affects strain pigmentation. The first one uncovered was RbsR, which stands for "ribose repressor," a transcription factor from the LacI/GalR family that controls the operon involved in ribose catabolism and transport (Mauzy and Hermodson, 1992). This activity is carried out by an ATP-binding cassette transport system and a ribokinase in a single operonic arrangement (*rbsDACBKR*; Barroga et al, 1996). (Lee *et al*, 2017). This ribose-modulated transcription regulator not only affects gas vesicles and antibiotics but also other features such as motility and virulence, and its mechanism of action remain to be elucidated. Similar to RbsR, the flotation regulator FloR is a DeoR family transcription that, in addition to the control of production of gas vesicles also impacts both antibiotics (Quintero-Yanes *et al*, 2020). Proteomic analysis showed that this factor might exert its action via other known

regulators that include Rap, RpoS, RsmA, PigU, PstS and PigT, but this has not been experimentally proven so far. Finally, the potassium transporter TrkH alters prodigiosin production in addition to gas vesicles production. This ion transporter is a homodimer that facilitates mostly the passive transport of potassium (Cao *et al*, 2011). The *trkH* mutant strain showed a pleiotropic phenotype that produces elevated levels of pigment, which was diminished upon addition of increasing potassium concentrations (Quintero-Yanes *et al*, 2019).

1.2.1.4.6. Other regulators

Besides RbsR, another regulator involved in carbon usage is the GntR homologue, PigT. This transcription factor senses gluconate levels and responds by triggering expression of catabolic genes (Suvorova *et al*, 2015). In S39006, gluconate presence serves as an external signal that only directs prodigiosin production. Thus, when this sugar is present in high concentrations, transcription of the prodigiosin gene cluster is repressed by PigT, which might bind to a putative GntR-like operator located on the promoter (Fineran *et al,* 2005).

As shown previously, the *hfq* mutation halted antibiotic production in S39006, and as this chaperone, along with its related small RNAs, regulates the sigma factor RpoS, the latter was explored as possible explanation for the changes in antibiotic levels (Wilf and Salmond, 2012). Bacterial gene expression is mostly regulated by RNA polymerase sigma factors, from which the alternative factor RpoS (or Sigma 38) is pivotal during the stationary phase of growth. It orchestrates expression of multiple stress-response genes when starvation signals are perceived, such as high temperature, low pH, or nutrient deprivation (Hengge, 2009). It was shown that S39006 mutants lacking *rpoS* are hyper producers of antibiotics, opposite to what was observed for *hfq* strains. Nevertheless, Hfq regulates the synthesis of both compounds independently of RpoS, showing this sigma factor as an antibiotic regulator (Wilf and Salmond, 2012).

Another transcriptional factor affecting production of both antibacterials is a LysR-type protein named PigU. This regulator, homologue of HexA, was thought to repress pigment biosynthesis by direct binding to the biosynthesis operon promoter (Fineran et al, 2005). A high expression level of this gene was observed in the *hfq* genetic background, where it was speculated that this factor may lower *rpoS* expression (Wilf *et al*, 2013).

PigZ is a TetR/AcrR transcriptional regulator that modulates antibiotic biosynthesis via transcription repression of a resistance-nodulation-cell- division (RND) efflux pump named ZrpADBC. It regulates this pump through direct binding to a sequence located in the intergenic region between *pigZ* and the *zrpADBC* operon (Gristwood *et al*, 2008). Nonetheless, despite

finding the PigZ target, the exact mechanism of how antibiotic regulation proceeds is not fully determined.

More recently, two new antibiotic regulators in S39006 were discovered. The first one is Fnr, an oxygen sensor that is linked to several biological processes, and a MarR-type regulator named OhrR, linked to organic hydroperoxide stress. Fnr negatively controls antibiotic production via binding the spacer promoter of the prodigiosin biosynthetic operon. Carbapenem reduction was explored via quantitative PCR, and it was hypothesised that this effect operates via repression of CarR (Sun *et al*, 2021). The newest regulator is OhrR, an organic peroxide-sensing repressor that acts in response to high levels of hydroperoxides and peroxynitrite – harmful oxidants (Meireles *et al*, 2022). In S39006, organic hydroperoxide was noted as a prodigiosin inducer via the regulator, which binds to a previous region termed repressor of pigment 1 (ROP1), located in the prodigiosin operon (Slater *et al*, 2003). This promoter element, when mutated, generated enhanced pigmentation, but its binding factor was unknown at that time. Therefore, following the suggested model, hydroperoxide detaches OhrR from the ROP1 box, allowing transcription of the pigment operon (Sun *et al*, 2022).

1.3. Aim of the project

The present project sought to find and characterise novel regulatory genes controlling the biosynthesis of antibiotics in S39006, by exploiting random transposon mutagenesis. This approach yielded several candidate mutants that were examined. In addition to their antibiotic biosynthetic capacity, possible pleiotropic effects were also assessed. Furthermore, potential regulatory routes followed by the mutations investigated in more detail were addressed. Thus, this work aimed to elucidate new members of the intricate regulatory network involved in antibiotic production in S39006, which may result important for a controlled biosynthesis of these vital compounds.

2. Materials and methods

2.1. Media and solutions

All media and standard solutions used are listed in Table 2.1, while antibiotics and supplements are in Table 2.2. Media and solutions were sterilised by autoclaving at 121°C (20 min) and antibiotics by using 0.22 µm filters (Millipore), when needed.

Name	Composition	Reference
Lysogeny Broth (LB)	Tryptone [10 g/L] Yeast extract [5 g/L] NaCl [5 g/L]	Miler, 1972
Minimal medium	Na_2HPO_4 [5.4 g/L] NaH_2PO_4 [3.34 g/L] NH_4SO_4 [0.1 %] $MgSO_4$ [0.41 mM] Glucose [0.2%]	
Tryptone swimming agar (TSA)	Tryptone [10 g/L] Agar [3 g/L] NaCl [5 g/L]	
Eiken agar	Tryptone [8 g/L] Yeast extract [5 g/L] NaCl [5 g/L] Eiken agar [7.5 g/L]	
Minimal medium	Na_2HPO_4 [5.4 g/L] NaH_2PO_4 [3.34 g/L] NH_4SO_4 [0.1 %] $MgSO_4$ [0.41 mM] Glucose [0.2%]	
Pectate buffer (pH 8.0)	Na_2HPO_4 [15 g/L] $NaH_2PO_4.H_2O$ [0.7 g/L]	
Pectate agar	Yeast extract 20% w/v [5 mL] $(NH_4)_2SO_4$ 10% w/v [10 mL] Mg_2SO_4 1M [1 mL] Glycerol 50% v/v [10 mL] Polygalacturonic acid 2% w/v [250 mL] Pectate buffer [200 mL] Agar [16 g]	
Cellulase agar	Carboxymethyl cellulose [10 g/L] Yeast extract 20% w/v [25 mL] $(NH_4)_2SO_4$ 10% w/v [10 mL] $MgSO_4$ 1M [1 mL] Glycerol 50% v/v [4 mL] PBS 50X [20 mL] Agar [16 g/L]	
Solution A (heat shock)	$MnCl_2$ [8 g/L] $CaCl_2$ [5 g/L]	

	MES 50 mM [198 mL]
Lysis buffer	Tris Hcl [50 mM, pH 8] NaCl [0.2 M] Glycerol [10%] Imidazole [1 mM]
Phosphate-buffered saline (PBS)	NaCl [8 g/L] KCl [0.2 g/L] NaH_2PO_4 [1.15 g/L] KH_2PO_4 [0.2 g/L]
MUG reaction buffer	4'-Methylumbelliferyl-b-D-galactopyranose, MUG [250 μg/mL] Lysozyme (Sigma) [20 mg/mL] PBS
50X TAE buffer	Tris [242 g/L] Ethylenediaminetetraacetic acid [18.61 g/L] Glacial acetic acid [0.0571 % v/v]
10X Electrode buffer (pH 8.3)	Glycine [150 g in 600 mL H_2O] Tris [30 g] H_2O to 1L
Resolving gel (15% acrylamide)	Acrylamide 30% [20 mL] Stock running buffer [20 mL] Sodium dodecyl sulphate 20% [0.2 mL] Stock ammonium persulphate 80 mg/mL [0.4 mL] TEMED [25 μL]
SDS-PAGE solution A	Tris Hcl (pH 6.8) [240 mM] Glycerol [40 %] SDS [8 %] EDTA [50 mM]
Stacking gel (6 %)	Stock stacking gel buffer [10 % v/v] Acrylamide stock [6 % v/v]
Stock stacking gel buffer (pH 6.8)	Tris in 0.6 L H_2O [151.46 g] and adjust to 1 L
Transfer buffer	Glycine [14.4 g/L] Tris base [3.03 g/L] Methanol [150 mL] **H_2O to 1 L**

Table 2.1. Media and solutions used in this work.

2.2. Strains and growth conditions

Bacterial strains used are listed in Table 2.3. *Serratia* sp. ATCC 39006 (S39006) and *Escherichia coli* (*E. coli*) strains were grown in Lysogeny Broth (LB) at 30°C and 37°C, respectively. Overnight liquid cultures were set from single colonies into 5 mL LB in 30 mL universal tubes,

on a rotary wheel (300 rpm). LB agar (LBA) plates supplemented with 1.5% (w/v) agar were used for solid growth. Cell lawns on top of LBA plates (overlays) were prepare mixing 100 µL cells and 3 mL soft LBA (0.5%). When required, strains were grown in media including antibiotics and/or supplements at conventional concentrations (Table 2.2). Cell growth was monitored by optical density at 600 nm (OD_{600}) using a Unicam Heλios spectrophotometer. Strains were stored by mixing 500 µL overnight cultures with 500 µL glycerol (50 %) and saved at -80 °C.

Supplement	Abbreviation	Working concentration
Ampicillin	Ap	100 µg/mL
Chloramphenicol	Cm	50 µg/mL
Erythromycin	Em	200 µg/mL
Kanamycin	Km	50 µg/mL
Spectinomycin	Sp	50 µg/mL
Tetracycline	Tc	30 µg/mL
Diaminopimelic acid	DAPA	300 µM
Isopropyl β-d-1-thiogalactopyranoside	IPTG	300–500 µM

Table 2.2. Antibiotic and supplements used in this work.

For end-point measurements and growth curves, 25 mL LB in 250 mL Erlenmeyer flasks were inoculated with a seed overnight culture to a starting OD_{600} of 0.05 and incubated in water baths with shaking (215 rpm). For quantitative assays over time, sampling was performed every 2 h, removing 1mL for quantitation of antibiotic production and 100 µL for OD_{600} determination.

Strain	Features	Source
Escherichia coli		
*β*2163	F^- RP4-2-Tc::Mu Δ*dapA*::(*erm-pir*), [Km^R, Em^R]	Demarre *et al* (2005)
DH5α	F^- Ø80*lacZ*ΔM15, Δ(*lacZYA−argF*) U169, *deoR*, *recA1*, *endA1*, *hsdR17 (rK⁻, mK⁺),thi-1*, *supE44*, λ⁻, *gyrA96*, *relA1*	Hanahan (1983)
ESS	β-lactam super sensitive strain	Bainton *et al* (1992)
Serratia		
ATCC 39006	Wild type strain from ATCC	Bycroft *et al* (1987)
WT	Lac^- (LacA) strain referred to as WT	Thomson *et al* (2000)
MCA54 (*carA*)	*carA*::miniTn5LacZ1 [Km^R]	Thomson *et al* (2000)
MCP2L (*pigA*)	*pigA*::miniTn5LacZ1 [Km^R]	Slater *et al* (2003)
MCR14 (*carR*)	*carR*::miniTn5LacZ1 [Km^R]	Slater *et al* (2003)
HSPIG17 (*pigQ*)	*pigQ*::miniTn5LacZ1 [Km^R]	Fineran *et al* (2005)
HSPIG23 (*pigR*)	*pigR*::miniTn5LacZ1 [Km^R]	Fineran *et al* (2005)
HSPIG26 (*pigS*)	*pigS*::miniTn5LacZ1 [Km^R]	Fineran *et al* (2005)
HSPIG36 (*pigT*)	*pigT*::miniTn5LacZ1 [Km^R]	Fineran *et al* (2005)
HSPIG43 (*pigU*)	*pigUpro*::miniTn5LacZ1 [Km^R]	Fineran *et al* (2005)
HSPIG46 (*pigV*)	*pigV*::miniTn5LacZ1 [Km^R]	Fineran *et al* (2005)
HSPIG62 (*pigW*)	*pigW*::miniTn5LacZ1 [Km^R]	Fineran *et al* (2005)
HSPIG67 (*pigP*)	*pigP*::miniTn5LacZ1 [Km^R]	Fineran *et al* (2005)

HSPIG71 (*rsmB*)	*rsmB*::miniTn5LacZ1 [Km^R]	Fineran *et al* (2005)
RAPL (*rap*)	*rap*::miniTn5LacZ1 [Km^R]	Fineran *et al* (2005)
BR4 (*phoB*)	*phoB*::miniTn5LacZ1 [Km^R]	Fineran *et al* (2005)
ROP4 (*pigX*)	*pigX*::miniTn5LacZ1 [Km^R]	Fineran *et al* (2005)
TG39 (*pigZ*)	*pigZ*::miniTn5LacZ1 [Km^R]	Gristwood *et al* (2008)
LC13 (*smaI*)	*smaI*::miniTn5LacZ1 [Km^R]	Fineran *et al* (2005)
LIS (*smaI*)	*smaI*::miniTn5Sm/Sp [Sm^R,Sp^R]	Fineran *et al* (2005)
pigC	Δ*pigC*	Williamson *et al* (2005)
NWGV13 (*gvpA1*)	*gvpA1::*Tn-KRCPN1LacZ1, *pigC* [Km^R]	Williamson *et al* (2005)
JRTA6 (*gvrA*)	*gvrA::*Tn-KRCPN1LacZ1, *pigC* [Km^R]	Williamson *et al* (2005)
SP19 (biosensor)	*smaI::*miniTn5Sm/Sp, *pigX::*Tn-DS1028, *pigZ::*miniTn5lacZ1,[Sp^R, Cm^R, Km^R]	Poulter *et al* (2010)
NMW2 (*prf*)	*prf::*Tn-KRCPN1LacZ1 [Km^R]	Wilf *et al* (2011)
NMW7 (*rsmA*)	*rsmA::*Tn-KRCPN1LacZ1 [Km^R]	Wilf *et al* (2011)
NMW8 (*hfq*)	Δ*hfq*	Wilf *et al* (2011)
vfmE	*vfmE::*cat [Cm^R]	Williamson *et al* (2005)
IGR	IGR*::*Tn-DS1028 *cat* [Cm^R]	this study
wzt	*wzt::*Tn-DS1028 *cat* [Cm^R]	this study
cysW	*cysW::*Tn-DS1028 *cat* [Cm^R]	this study
ORF_5465	*5465::*Tn-DS1028 *cat* [Cm^R]	this study
ORF_2785	*2785::*Tn-DS1028 *cat* [Cm^R]	this study
cyaA	*cyaA::*Tn-DS1028 *cat* [Cm^R]	this study
sdhE	*sdhE,pro::*Tn-DS1028 *cat* [Cm^R]	this study
rsmA	*rsmA, pro::*Tn-DS1028 *cat* [Cm^R]	this study
flhC	*flhC::*Tn-DS1028 *cat* [Cm^R]	this study
tauD	*sdhE, pro::*Tn-DS1028 *cat* [Cm^R]	this study
fliD	*fliD::*Tn-DS1028 *cat* [Cm^R]	this study
hlyD	*hlyD::*Tn-DS1028 *cat* [Cm^R]	this study
vfmA	*vfmA::*Tn-KRCPN1LacZ1 [Km^R]	this study
vfmC	*vfmC::*Tn-KRCPN1LacZ1 [Km^R]	this study
vfmD	*vfmD::*Tn-KRCPN1LacZ1 [Km^R]	this study
vfmK	*vfmK::*Tn-KRCPN1LacZ1 [Km^R]	this study
vfmM	*vfmM::*Tn-KRCPN1LacZ1 [Km^R]	this study
vfmN	*vfmN::*Tn-KRCPN1LacZ1 [Km^R]	this study
vfmO	*vfmO::*Tn-KRCPN1LacZ1 [Km^R]	this study
vfmZ	*vfmZ::*Tn-KRCPN1LacZ1 [Km^R]	this study
gorA	*gorA::*Tn-KRCPN1LacZ1 [Km^R]	this study
mnmG	*mnmG::*Tn-KRCPN1LacZ1 [Km^R]	this study
rluD	*rluD::*Tn-KRCPN1LacZ1 [Km^R]	this study
prf, *pigC*	*prf::*Tn-KRCPN1LacZ1 [Km^R], Δ*pigC*	this study
prf,*vfmE*	*prf::*Tn-KRCPN1LacZ1 [Km^R],	this study
IGR,*hfq*	IGR*::*Tn-DS1028 *cat* [Cm^R], Δ*hfq*	this study
IGR, *phoB*	IGR*::*Tn-DS1028 *cat* [Cm^R], *phoB*::miniTn5LacZ1 [Km^R]	this study
IGR, *pigR*	IGR*::*Tn-DS1028 *cat* [Cm^R], *pigR*::miniTn5LacZ1 [Km^R]	this study
IGR, *pigS*	IGR*::*Tn-DS1028 *cat* [Cm^R], *pigS*::miniTn5LacZ1 [Km^R]	this study
IGR, *pigT*	IGR*::*Tn-DS1028 *cat* [Cm^R], *pigT*::miniTn5LacZ1 [Km^R]	this study
IGR, *pigU*	IGR*::*Tn-DS1028 *cat* [Cm^R], *pigUpro*::miniTn5LacZ1 [Km^R]	this study
IGR, *pigV*	IGR*::*Tn-DS1028 *cat* [Cm^R], *pigV*::miniTn5LacZ1 [Km^R]	this study
IGR, *pigW*	IGR*::*Tn-DS1028 *cat* [Cm^R], *pigW*::miniTn5LacZ1 [Km^R]	this study
IGR, *pigX*	IGR*::*Tn-DS1028 *cat* [Cm^R], *pigX*::miniTn5LacZ1 [Km^R]	this study
IGR, *pigZ*	IGR*::*Tn-DS1028 *cat* [Cm^R], *pigZ*::miniTn5LacZ1 [Km^R]	this study
IGR, *rap*	IGR*::*Tn-DS1028 *cat* [Cm^R], *rap*::miniTn5LacZ1 [Km^R]	this study
IGR, *rsmA*	IGR*::*Tn-DS1028 *cat* [Cm^R], *rsmA*::miniTn5LacZ1 [Km^R]	this study
IGR, *rsmB*	IGR*::*Tn-DS1028 *cat* [Cm^R], *rsmB*::miniTn5LacZ1 [Km^R]	this study
IGR, *carR*	IGR*::*Tn-DS1028 *cat* [Cm^R], *carR*::miniTn5LacZ1 [Km^R]	this study

IGR, *carA*	IGR*::*Tn-DS1028 *cat* [Cm^R], *carA*::miniTn5LacZ1 [Km^R]	this study
IGR, *pigA*	IGR*::*Tn-DS1028 *cat* [Cm^R], *pigA*::miniTn5LacZ1 [Km^R]	this study
IGR, *smaI*	IGR*::*Tn-DS1028 *cat* [Cm^R], *smaI*::miniTn5LacZ1 [Km^R]	this study
IGR, *gvpA1*	IGR*::*Tn-DS1028 *cat* [Cm^R], *gvpA1::*Tn-KRCPN1LacZ1, *pigC* [Km^R]	this study
IGR, *gvrA*	IGR*::*Tn-DS1028 *cat* [Cm^R], *gvrA::*Tn-KRCPN1LacZ1, *pigC* [Km^R]	this study
vfmE,*hfq*	*vfmE*::cat [Cm^R], Δ*hfq*	this study
vfmE, *phoB*	*vfmE*::cat [Cm^R], *phoB*::miniTn5LacZ1 [Km^R]	this study
vfmE, *pigR*	*vfmE*::cat [Cm^R], *pigR*::miniTn5LacZ1 [Km^R]	this study
vfmE, *pigS*	*vfmE*::cat [Cm^R], *pigS*::miniTn5LacZ1 [Km^R]	this study
vfmE, *pigT*	*vfmE*::cat [Cm^R], *pigT*::miniTn5LacZ1 [Km^R]	this study
vfmE, *pigU*	*vfmE*::cat [Cm^R], *pigUpro*::miniTn5LacZ1 [Km^R]	this study
vfmE, *pigV*	*vfmE*::cat [Cm^R], *pigV*::miniTn5LacZ1 [Km^R]	this study
vfmE, *pigW*	*vfmE*::cat [Cm^R], *pigW*::miniTn5LacZ1 [Km^R]	this study
vfmE, *pigX*	*vfmE*::cat [Cm^R], *pigX*::miniTn5LacZ1 [Km^R]	this study
vfmE, *pigZ*	*vfmE*::cat [Cm^R], *pigZ*::miniTn5LacZ1 [Km^R]	this study
vfmE, *rap*	*vfmE*::cat [Cm^R], *rap*::miniTn5LacZ1 [Km^R]	this study
vfmE, *rsmA*	*vfmE*::cat [Cm^R], *rsmA*::miniTn5LacZ1 [Km^R]	this study
vfmE, *rsmB*	*vfmE*::cat [Cm^R], *rsmB*::miniTn5LacZ1 [Km^R]	this study
vfmE, *carR*	*vfmE*::cat [Cm^R], *carR*::miniTn5LacZ1 [Km^R]	this study
vfmE, *carA*	*vfmE::*cat [Cm^R], *carA*::miniTn5LacZ1 [Km^R]	this study
vfmE, *pigA*	*vfmE::*Tn-DS1028 *cat* [Cm^R], *pigA*::miniTn5LacZ1 [Km^R]	this study
vfmE, *smaI*	*vfmE*::cat [Cm^R], *smaI*::miniTn5LacZ1 [Km^R]	this study
vfmE, *gvpA1*	*vfmE*::cat [Cm^R], *gvpA1::*Tn-KRCPN1LacZ1,*pigC* [Km^R]	this study
vfmE, *gvrA*	*vfmE*::cat [Cm^R], *gvrA::*Tn-KRCPN1LacZ1,*pigC* [Km^R]	this study
wzt,*hfq*	*wzt::*Tn-DS1028 *cat* [Cm^R], Δ*hfq*	this study
wzt, *phoB*	*wzt::*Tn-DS1028 *cat* [Cm^R], *phoB*::miniTn5LacZ1 [Km^R]	this study
wzt, *pigR*	*wzt::*Tn-DS1028 *cat* [Cm^R], *pigR*::miniTn5LacZ1 [Km^R]	this study
wzt, *pigS*	*wzt::*Tn-DS1028 *cat* [Cm^R], *pigS*::miniTn5LacZ1 [Km^R]	this study
wzt, *pigT*	*wzt::*Tn-DS1028 *cat* [Cm^R], *pigT*::miniTn5LacZ1 [Km^R]	this study
wzt, *pigU*	*wzt::*Tn-DS1028 *cat* [Cm^R], *pigUpro*::miniTn5LacZ1 [Km^R]	this study
wzt, *pigV*	*wzt::*Tn-DS1028 *cat* [Cm^R], *pigV*::miniTn5LacZ1 [Km^R]	this study
wzt, *pigW*	*wzt::*Tn-DS1028 *cat* [Cm^R], *pigW*::miniTn5LacZ1 [Km^R]	this study
wzt, *pigX*	*wzt::*Tn-DS1028 *cat* [Cm^R], *pigX*::miniTn5LacZ1 [Km^R]	this study
wzt, *pigZ*	*wzt::*Tn-DS1028 *cat* [Cm^R], *pigZ*::miniTn5LacZ1 [Km^R]	this study
wzt, *rap*	*wzt::*Tn-DS1028 *cat* [Cm^R], *rap*::miniTn5LacZ1 [Km^R]	this study
wzt,*rsmA*	*wzt::*Tn-DS1028 *cat* [Cm^R], *rsmA*::miniTn5LacZ1 [Km^R]	this study
wzt, *rsmB*	*wzt::*Tn-DS1028 *cat* [Cm^R], *rsmB*::miniTn5LacZ1 [Km^R]	this study
wzt,*carR*	*wzt::*Tn-DS1028 *cat* [Cm^R], *carR*::miniTn5LacZ1 [Km^R]	this study
wzt, *carA*	*wzt::*Tn-DS1028 *cat* [Cm^R], *carA*::miniTn5LacZ1 [Km^R]	this study
wzt, *pigA*	*wzt::*Tn-DS1028 *cat* [Cm^R], *pigA*::miniTn5LacZ1 [Km^R]	this study
wzt, *smaI*	*wzt::*Tn-DS1028 *cat* [Cm^R], *smaI*::miniTn5LacZ1 [Km^R]	this study
wzt, *gvpA1*	*wzt::*Tn-DS1028 *cat* [Cm^R], *gvpA1::*Tn-KRCPN1LacZ1, *pigC* [Km^R]	this study
wzt, *gvrA*	*wzt::*Tn-DS1028 *cat* [Cm^R], *gvrA::*Tn-KRCPN1LacZ1,*pigC* [Km^R]	this study

Table 2.3. Bacterial strains used in this work.

2.3. DNA extraction

Genomic DNA (gDNA) was isolated using the GeneJET Genomic DNA Purification Kit and plasmid DNA from the GeneJET Plasmid Miniprep Kit (both Thermo Fisher Scientific), following manufacturers' recommendations.

2.4 Polymerase chain reaction and gel separation

Polymerase chain reaction (PCR) experiments were conducted using Phusion® High-Fidelity DNA Polymerase (New England Biolabs; NEB) and gDNA as template, in a Veriti Thermal Cycler (Applied Biosystems). For colony PCR, a small cell sample was placed into 40 µL of sterile water and boiled at 98°C for 5 min. 1-2 µL cell extract was used for reactions. A general reaction and program are displayed in Tables 2.4 and 2.5, respectively. Volumes and PCR program settings were scaled and adjusted according to reaction requirements and specific oligonucleotides (Table 2.6; purchased from Sigma).

PCR Reagent	Volume (µL)
10 x reaction buffer	2.5
Polymerase	0.25
dNTPs (2 mM)	2.5
DMSO	1.25
Primer 1 (10 µM)	1.25
Primer 2 (10 µM)	1.25
DNA	0.5
dH_2O	15.5
Total	25

Table 2.4. PCR reaction concentrations.

Stage	Conditions	Cycles
Initial denaturation	98°C for 3 min	1
Denaturation	98°C for 15 s	25-30
Annealing	55°C for 30 s	
Elongation	72°C for 1.5 min	
Final elongation	72°C for 7 min	1
Hold	12°C	25

Table 2.5. PCR program settings.

Name	Sequence (5'– 3')	Function
oMAMV1	GGAATTGATCCGGTGGATG	RP-PCR specific primer
oMAMV2	GCATAAAGCTTGCTCAATCAATCAC	RP-PCR Sequencing primer
oPF106	GACCACACGTCGACTAGTGCNNNNNNNNNNAGAG	Random primer 1
oPF108	GACCACACGTCGACTAGTGCNNNNNNNNNNGATAC	Random primer 3
oPF107	GACCACACGTCGACTAGTGCNNNNNNNNNNACGCC	Random primer 2
oPF107	GACCACACGTCGACTAGTGC	Random adaptor primer

oDP1	ATTGCTGGATCCGTAACTTCATACTATGCTG	Fw sRNA
oDP2	TGCTTAAAGCTTTATCAACGGCCCTTTTCAAG	Rv sRNA
oDP3	GATAAAGGATCCAAATAACCGGCCGTTATAC	Fw IGR
oDP4	TCAAAAAGCTTGTAATTAATTCGTTATATGCTTAG	Rv IGR
oDP5	ATGGTGGATCCATTGTAATGGCAAATATATC	Fw *wzt*
oDP6	AAATTGAAGCTTTTTAACTCACTTAGCTACT	Rv w*zt*
oDP7	TTTTGGATCCAATGCCATGAATATACTACACG	Fw *vfmE*
oDP8	GCTAACTGCAGAACGAATTAATTACATAGG	Rv *vfmE*
oDP9	ACTAATCTGCAGCATTGCCAAAAAATCATCAC	Rv sRNA-II
oDP10	ATTGCGGATCCAGTAACTTCATACTATGCTG	Fw asRNA$_1$
oDP11	ATTGGGATCCTAGTAACTTCATACTATGCTG	Fw asRNA$_2$
oDP12	CCAGCTGCAGCATGAGAAATCCTCAGTGTATG	Fw asRNA$_3$
oDP13	GCTAAGTGGATCCAATATGATCAATTTTA	Fw *1186*
oDP14	GGCAAGAAGCTTATCTTATAAATTGTATC	Rv *1186*
oDP15	GATTGAATTCGTTTTTTTAATTTTGAGTG	Fw Sigma54
oDP16	GAAAACAAGCTTGTATGAAGTTACTATTGC	Rv Sigma54
oDP17	TTTTGAATTCGAGTGTTCATTGCTGCAATAG	Fw Sigma70
oDP18	GTCCAAGCTTGCTGAAAACAGCATAGTATG	Rv Sigma70
oDP19	GAAAACGGATCCTAATTAATGAATGTCTTA	Fw *1187*
oDP20	ACCCTCTGCAGATACTATTATTTATTC	Rv *1187*
oDP51	AAAGGCATGCTCAATGCACCTCGTTAAAAAC	Fw *hlyD$_{SS}$*
oDP52	GATTACTGCAGCTGTTATCTTTCTCGTAATGCC	Rv *hlyD$_{SS}$*
oDP58	CTGAGAGGATCCAGTATGGGCAAAAGATAC	vfmH
oDP59	CTCCAGGCTGCAGTCATCAGCTATTCT	vfmH
oDP62	CATTAACAGACATCTGTTATGCTTGTGGTTTTTCATCC	GSP2 5' RACE for IGR
oDP63	ATATCGTAAGTCTGTGTTTTCAGACAAAGAACG	GSP3 5' RACE for IGR
oDP64	CACCTCCAATGCTTTTCTTAAGTTAGGGTGG	GSP2 5' RACE for *vfmE*
oDP65	TGAATGAGGTTGTTATTGAAGCTTTCATTATCTAGTG	GSP3 5' RACE for *vfmE*
oDP66	TAGGTTTCAATAGGCGAGAAGGTGGCAAC	GSP2 3' RACE for IGR
oDP67	AGGGTAGGTCTCGCACCTGTAACG	GSP3 3' RACE for IGR
oDP68	CATCTGTTATGCTTGTGGTTTTTCATCCCTGC	GSP2 3' RACE for *vfmE*
oDP69	GTTTTCAGACAAAGAACGGCCTCGG	GSP3 3' RACE for *vfmE*
oDP70	GTGAAAGATGATAGGTATAAACGAAAAGTGGC	GSP3 3'RACE IGR
oDP71	ACATCCTTGACTTGCATCAGCC	GSP 5' for IGR
oDP72	GAGAATTCACCCGGTTGCCACCTTC	GSP2 5' RACE for IGR
oDP73	GAACGGCCTCGGACAATGAACAAC	GSP 5' for IGR
oDP74	CATGAGCTTTGATATTATTTTTGGCAAACAACGTC	GSP2 5' RACE for IGR
oDP75	ATGGGGATCCATCATCATGTTTGAGAAACG	Fw *xylR*
oDP76	GCATCTGCAGGAGTCAATCACTGTAATCG	Rv *xylR*
oDP77	ACTAATGAATTCCATTGCCAAAAAATCATCACA	Fw *vfmE* upstream
oDP78	AGTGAAGCTTTGTGAGCGTGTAGTATATTC	Rv *vfmE* upstream
oDP79	TTACGAATTCTTATTCACAACGAATATCATTC	Fw *vfmF1* upstream
oDP80	ACATAAGCTTGTTGAACCAGC	Rv *vfmF1* upstream
oDP81	GATTGAATTCTAGTAATAGGGTGTTTTTTCATAATG	Fw *vfmA* upstream
oDP82	TGATAAGCTTATCGGAAAGCTGATG	Rv *vfmA* upstream
oDP83	ATTGCTGAATTCTACTTTTTCTATTTTTTAATCC	Fw *vfmK* upstream
oDP84	CAAATTCAAGCTTGATAATTTTTTCAATACG	Rv *vfmK* upstream
oDP85	TATGAATTCATTGCCGGCATGATCATTTCTTG	Fw *hlyD* upstream
oDP86	AGTGAAGCTTCTGGTTTTACGCTGAACA	Rv *hlyD* upstream

Table 2.6. Oligonucleotides used in this study.

PCR products plus 1X Orange G loading buffer (NEB) were separated in agarose gels (1% w/v) stained with ethidium bromide (0.5 μg/mL) and run with appropriate reference ladders (Bioline). Gels run in 1X TAE buffer at 80V, and DNA bands under UV light were documented using the Gene Genius Bio-Imaging System (Bio-rad). Bands were excised and purified from gels using the GeneJET PCR Purification Kit (Thermo Fisher Scientific), based on manufacturer's

recommendations. Nucleic acid concentrations were measured using the NanoDropTM 1000 Spectrophotometer (NanoDrop Technologies). DNA was sequenced by GATC Biotech and the Sequencing Facility at Department of Biochemistry (University of Cambridge) and analysed with SnapGeneViewer software (V 5.2.1).

2.5. Random Transposon Mutagenesis

Random transposon mutagenesis was performed as described previously (Monson *et al*, 2015). Briefly, the plasmids pDS1028 or pKRCPN1 –incorporating the transposon Tn5 carrying Cm^R or Km^R, respectively– were conjugated from the donor *E. coli* β2163 (supplemented with Em and DAPA; Table 2.2) into S39006 recipient strains. The donor and recipient overnight cultures were mixed in a 1:1 ratio, to allow biparental conjugal mating. Subsequently, 25 µL of this mixture were spotted onto DAPA LBA plates and incubated overnight at 30°C. After conjugation, the mating patches were scraped off and resuspended in 1 mL LB, and 100 µL from serial dilutions (10^{-1} to 10^{-3}) were plated out on selection LBA and incubated for 48 h. Transconjugant colonies displaying phenotypes of interest were picked, isolated, and stored at -80°C.

2.6. Determination of Transposon Insertion Sites

Following transposon mutagenesis, the Random Primed PCR (RP-PCR) approach (Fineran *et al*, 2005) was used to identify the transposon insertion sites of mutants. This two-step method uses in the first round DNA from colony PCR (section 2.4), along with one transposon-specific (oMAMV1) and three degenerate primers (oPF106-108). For the second round, the preceding PCR product served as template and the second specific primer (oMAMV2) besides an oligo adapter (oPF109) enabled pinpointing of the insertion sites. PCR conditions are listed in Table 2.7.

Stage	Conditions	Cycles
Initial denaturation	94°C for 3 min	1
Denaturation	94°C for 15 s	6
Annealing	42°C for 30 s	
Elongation	72°C for 1.5 min	
Denaturation	94°C for 15 s	25-30
Annealing	55°C for 30 s	
Elongation	72°C for 1.5 min	
Final elongation	72°C for 7 min	1
Hold	12°C	25

Table 2.7. RP-PCR program settings.

2.7. Phage Transduction

The generalised transducing phage φOT8 was utilised to move markers between S39006 strains, as stated previously (Evans et al, 2010).

To generate a phage lysate containing the desired mutation, a lysate stock from S39006 WT strain, at sufficient titre to generate semi-confluent (merged) plaques, was used to infect a culture carrying such mutation (donor strain). Phage titres of lysates were confirmed by pouring 10 µL of serially diluted lysate mixed plus 100 µL of overnight cultures onto overlays of LBA plates. Plaques observed the following day were counted and titres expressed as plaque forming units per mL (pfu/mL).

To prepare phage lysates, overlays exhibiting semi-confluent lysis were rinsed with 3 mL phage buffer (Table 2.1) and scraped off into a 20 mL glass universal. 500 µL of $NaHCO_3$-treated chloroform were added to the mixture, which was vigorously vortexed (2 min) and centrifuged (2,219×g, 20 min, 4 °C) to remove cell debris. Supernantants containing the phages were decanted into 5 mL bijoux tubes, then 50 µL chloroform was added to ensure sterility, before storage at 4°C.

Overnight cultures of recipient hosts were pelleted (2,219×g, 10 min, 4°C), resuspended in 1 mL LB, and infected with 100 µL phage lysates generated from mutants. Following 20 min of adsorption at room temperature, the phage-host mixture was placed at 30°C for 20 min, then pelleted (2,219 g, 10 min). Cells were washed three times with 1 mL LB to significantly reduce phage levels, and resuspended in 250 µL LB. Finally, 100 µL were plated out on LBA selection plates, grown for 48 h, and transductant colonies were streaked out twice to diminish phage carry over.

2.8. Antibiotic production

2.8.1. Prodigiosin

Prodigiosin production was determined as described previously (Slater *et al*, 2003). 1 mL culture samples were centrifuged (13,200 *g,* 10 min, 4°C) to harvest cells and pellets were saved at -80°C until assayed. Samples were thawed and fully resuspended in 1 mL acidified ethanol (4% 1 M HCl) by vortexing (1 min). The resulting mixture was then centrifuged and 950 µL of clear supernatant was transferred to a 1 ml cuvette. Prodigiosin levels were obtained by reading absorbance at 534 nm (Unicam Heλios spectrophotometer) and expressed as (A_{534} mL^{-1}x$OD_{600\text{-}1}$) x 50.

2.8.2. Carbapenem

Carbapenem antibiotic production was assayed employing an *E. coli* sensitive strain (ESS) as bioindicator (Slater *et al*, 2003). For spot assays, normalised cells numbers (OD_{600}=1.0) were taken from overnight test cultures and 3 µL spotted over a dried overlay of 100 µL ESS and soft LBA (section 2.2). Plates were incubated for 16 h and the antibiosis cleared areas were examined. To quantitate carbapenem levels, 245x245x25 bioassay plates (Thermo Fisher Scientific) of LBA (400 mL) plus a soft LBA lawn (100 mL) containing ESS indicator (100 µL) were used. Once lawns were set, a sterile 0.5 cm core borer was used to make symmetrical holes. Next, 1 mL samples from flask-grown cells were centrifuged (13,200 rpm, 10 min, 4°C) and 800 µL supernatants were filter-sterilised and left on ice. Finally, 125 µL supernatants were used to fill the holes. After incubation, plates were imaged and growth inhibition zones were calculated using ImageJ (Abràmoff *et al,* 2004) and expressed as [cm^2*OD_{600}^{-1}].

2.9. Phenotypic assays

2.9.1. Gas vesicles

Gas vesicle production was inferred by the flotation assay, which assesses cell buoyancy capacity (Tashiro *et al*, 2016). Briefly, overnight cultures were used after 16 h to inoculate a second culture (OD_{600} adjusted to 0.05) for 24 h under the same conditions. New cultures were next set upright, left stationary at room temperature, then observed for 24-48 h. Flotation capacity of cells was evaluated by visual inspection.

2.9.2. Acyl-homoserine lactones

Analogous to carbapenem activity quantitation, acyl-homoserine lactone (AHL) production was also conducted via a S39006 bioindicator strain (SP19), which is a prodigiosin hyperproducer used for detection of AHLs (Poulter *et al*, 2010). As explained above, bioassay plates with SP19 bioindicator overlays were prepared and the sterile supernatants were used to fill the holes prepared. Following incubation, the pigmented area was calculated and expressed as in the carbapenem production assays.

2.9.3. Cell wall-degrading enzymes

The plate assay to determine cellulase activity was as described previously (Andro *et al*, 1984). Overnight cultures were adjusted to OD_{600} of 1, and 5 µL cells spotted onto cellulase agar plates (Table 2.1) and incubated for 48 h. Plates were then flooded with congo red solution (0.2% w/v) and left for 20 min, bleached (1 M NaCl) for another 20 min and finally stained (1 M HCL) for 5 min. Halo formation around the spots indicated enzyme activity.

Similarly, for pectate lyase synthesis, 5 µL from normalised cultures (OD_{600}=1) were spotted onto pectate agar plates (Table 2.1) and incubated for 48 h. Plates were then flooded with copper acetate solution (7.5% w/v) for 1-2 h. Pectate lyase activity was detected by halo formation.

2.9.4. Swimming and swarming motility

Motility of cells was assessed by plate assays, employing 5 µL normalised overnight cultures (OD_{600}=0.2 for swimming and OD_{600}=1 for swarming) which were spotted onto tryptone swarm agar (TSA) and Eiken agar (Table 2.1) plates, respectively. Halo size of swimming cells was examined after 16 h incubation, whereas swarming pattern motility was assessed after 36 h.

2.9.5. Cell and colony morphology

Phase contrast microscopy (PCM) images were captured from diluted liquid cultures placed on microscope glass slides, using an Olympus BX-51 (100x oil-immersion lens).

2.9.6. Potato infection assay

Virulence was tested via potato rotting assays as described earlier (Fineran *et al*, 2007). Maris Piper potatoes were sterilised by dipping in Virkon (10% w/v) for 10 min and then two sites per tuber (WT and test strain) were inoculated (10 µL of $1x10^7$ CFU). Infection sites were sealed with vacuum grease and tubers wrapped in wet tissue paper and cling film, which were incubated at 30°C over 4 days. After incubation, rotted tissue was removed and weighed.

2.10. Plasmid construction and transformation

2.10.1. Preparation of competent cells

To prepare chemically competent cells, overnight cultures of *E. coli* β2163 were used to inoculate 25 mL LB supplemented with 375 µL 1 M $MgCl_2$. Cells were grown to mid-exponential phase (OD_{600}~0.5) then were chilled on ice for 60 min. Cells were pelleted by centrifugation (2,219 g, 10 min, 4°C), washed twice with 10 mL of iced Solution A (Table 2.1), and pelleted. Finally, cells were resuspended in 1 mL solution A + glycerol, aliquoted, and either used immediately or stored at -80°C.

Similarly for preparation of cells for heat shock, electrocompetent cells were made from overnight cultures, but this time from *E. coli* DH5α, to an initial OD_{600} of 0.05. When at mid-exponential stage, cells were placed on ice for 30 min and harvested by centrifugation, as indicated previously. Three washing steps followed, using 10 mL chilled sterile H_2O, to finally collect the cells and resuspend them in 1 mL cold 10% glycerol (v/v), for use, or storage at -80 °C.

2.10.2. Cloning

Gene cloning and molecular biology techniques were conducted following standard methods (Green and Sambrook, 2012). To construct plasmids (Table 2.8), inserts were synthesized by PCR using gDNA (S39006 WT) as template, with designed primers (Table 2.6).

Name	Features	Source
pDS1028	*tetA*, *tnp*, *uidA*, *oriR6k*, *cat* [Cm^R, Tc^R]	Monson *et al* (2015)
pKRCPN1	*tetA*, *tnp*, *lacZ*, *oriR6k*, *aph* [Km^R, Tc^R]	Monson *et al* (2015)
pQE80-oriT	Derivative of pQE80 [Ap^R]	Ramsay *et al* (2011)
pRW50	Promotorless *lacZ* system [Tc^R]	Lodge *et al* (1992)
pQE-sRNA	pQE80-oriT with sRNA [Ap^R]	this study
pQE-asRNA	pQE80-oriT with sRNA [Ap^R]	this study
pQE-IGR	pQE80-oriT with sRNA [Ap^R]	this study
pQE-*vfmE*	pQE80-oriT with sRNA [Ap^R]	this study
pQE-*wzt*	pQE80-oriT with sRNA [Ap^R]	this study
pQE-*1186*	pQE80-oriT with sRNA [Ap^R]	this study
pQE-*vfmH*	pQE80-oriT with sRNA [Ap^R]	this study
pQE-*xylR*	pQE80-oriT with sRNA [Ap^R]	this study
p*S54*	pRW50 with Sigma54 promoter [Tc^R]	this study
p*S70*	pRW50 with Sigma70 promoter [Tc^R]	this study
p*vfmAprom*	pRW50 with *vfmA* promoter [Tc^R]	this study
p*vfmEprom*	pRW50 with *vfmE* promoter [Tc^R]	this study
p*vfmKprom*	pRW50 with *vfmK* promoter [Tc^R]	this study
p*hlyDprom*	pRW50 with *hlyD* promoter [Tc^R]	this study

Table 2.8. Plasmids used in this study.

PCR products and plasmids were digested with appropriate restriction enzymes (NEB) at 37 °C for 60 min, according to supplier's instructions. Later, vectors were dephosphorylated via Antarctic Phosphatase (NEB), electrophoresed (1% agarose) to estimate sizes, and finally purified by ethanol precipitation (Labrie *et al*, 2019).

Compatible digested products were ligated by using T4 DNA ligase (Thermo Fisher Scientific), following manufacturers' instructions. Mass of vector and insert ratios (varied from 1:3 to 1:5) for optimal ligation, was calculated using the online tool NEBioCalculator (v 1.15.0). Reactions were set overnight at 16°C and terminated by heating at 80°C for 10 min. Ligation products were introduced into host cells by either heat shock transformation or electroporation. For the former, 50-100 ng plasmid were mixed with 50 µL chemically competent cells in Eppendorf tubes and left on ice for 30 min. Subsequently, tubes were heated for 1 min at 42°C, iced for 3 min, and immediately added 900 µL SOC medium. Cells recovered for 60 min at 37°C, then were pelleted

(8,000 g, 2 min,), and resuspended in 200 µL LB. Finally, 50-100 µL cell suspensions were plated out onto selection LBA plates and incubated overnight.

For transformation via electroporation, 10-50 ng plasmid and 50 µL electrocompetent cells were mixed and placed into chilled 0.2-cm electroporation cuvettes (Bio-Rad). Cells were electroporated with pulse 2.5 kV, 200 Ω and 25 µFD (Bio-Rad Gene Pulser). Recovery and plating out of cells was the same as for the heat shock process.

To screen for positive clones, Colony PCR (section 2.3) was conducted using corresponding primers, and colonies harbouring the empty vector were used as control. Plasmids from positive clones were extracted and sequenced (section 2.4) for confirmation.

2.11. β-galactosidase activity

Transcription activity from fusion strains was monitored by measuring β-galactosidase activity (LacZ) –with 4'-methylumbelliferyl-β-D-galactoside (MUG) as substrate – in 96-well plates. 100 µL culture sample was placed in wells and immediately frozen at -80°C until analysed. Then samples were thawed at 37°C, 10 µL sampled and then freeze-thawed again to ensure cell lysis. Serial dilutions were performed and 100 µL MUG reaction buffer (Table 2.1) was added to wells and mixed by pipetting. Fluorimetric determinations were made on a Gemini XPS microplate reader (Molecular Devices) with the following parameters: excitation, 360 nm; emission, 450 nm; cut-off 435 nm; eight reads per well, measured every 30 s for 30 min at 37°C (Ramsay *et al*, 2011). Enzyme activity in cell extracts was normalised and expressed as RFU min-1 OD600-1.

2.11.1. Promoter activity

Putative promoter regions were cloned into the promoterless *lacZ* plasmid pRW50 (Lodge *et al*. 1992), and gene expression was measured as fluorescence from reporter activity. Constructs, including the empty vector as control, were used to transform electrocompetent *E. coli* DH5α cells (section 2.10). Overnight cultures were used to inoculate 25 mL LB cultures that grew until late exponential growth (10 h). Samples were then taken for OD_{600} determination and measuring expression changes as outlined above.

2.11.2. *In vivo* binding assays

To investigate whether transcriptional regulators can modulate promoter activity, *E. coli* DH5α harbouring putative regulatory regions cloned into pRW50 were employed, as described previously (Fineran *et al*, 2005b). Briefly, electrocompetent cells carrying those constructs were transformed with either pQE80-oriT intact or containing the candidiate regulator's coding sequences. At late exponential stage, sampling was conducted and promoter activity due to plasmid-expressed transcriptional regulators (leaky expression) was assessed via MUG assays.

2.12. RNA isolation

To extract total RNA from cells, the hot phenol method was utilised (Mattatall and Sanderson, 1996). In brief, S39006 cultures were grown in LB overnight (16 h) and used to start cultures at OD_{600} 0.05 in water baths. When cultures reached early stationary phase (10 h), 2 mL samples were taken, OD_{600} adjusted to 1.7, and mixed with 4mL RNA Later (Ambion).

Cells were next resuspended in 3 mL lysis buffer (Table 2.1) and added to 3 mL hot phenol (water saturated, 65°C, pH 4.3). Mixture was vortexed, incubated at 65°C for 5 min, placed on ice for 5 min, and pelleted (5,000 g, 30 min, 4°C). The aqueous phase was transferred to a new tube and the extraction process repeated, to finally extract RNA using 3 mL chloroform, which was ethanolprecipitated overnight (2.5 volumes at -20°C). The pellet was then washed twice (75% ethanol) and resuspended in 100 µL DEPC H2O. To eliminate DNA traces, TURBO DNase (Ambion) was used following the manufacturer's protocol. RNA was extracted with chloroform, precipitated, resuspended in 50 µL DEPC H_2O and stored at -80°C. PCR reactions with selected primers were carried out to confirm absence of gDNA from samples.

2.13. Determination of transcription ends

To locate both the 5' and 3' ends of transcription, a rapid amplification of cDNA ends (RACE) approach was followed by using the Roche 5'/3' RACE 2nd generation kit, following their instructions. Specific primers were designed for mapping in each case. As bacteria lack poly(A)tailed mRNA, RNA samples were treated with *E. coli* Poly(A) Polymerase (NEB) before generating the cDNAs for 3' end determination. In both types of RACE, the larger and predominant band from PCRs was excised and sequenced.

2.14. RNA sequencing data

Transcriptomic data was used to evaluate transcription on both strands, as it provides evidence about genes actively transcribed. Thus, recent paired-end RNA-sequencing of S39006 was searched at the Sequence Read Archive (SRA) database from NCBI. Raw data (accession number PRJNA635824; Chilczuk *et al*, 2020) from the control set (WT) was analysed. After a quality control check by using FastQC (Wingett and Andrews, 2018), reads were mapped and sorted by position to the reference genome (GCF_000463345) by Samtools (Li *et al*, 2009), generating a binary file (BAM extension). Reads were then filtered and separated by direction (sense and antisense). Resulting files were finally indexed and inspected in the Integrative Genome Viewer (IGV) software (Thorvaldsdottir *et al*, 2013).

2.15. Protein analysis

2.15.1. Extraction and separation

To obtain cell lysates, overnight cultures were grown and used to inoculate 25 mL LB cultures (section 2.2). After cultures grew for 14 h, 5 mL aliquot was taken and OD_{600} was adjusted to 1.7. Cells were then harvested (4,500 g, 10 min, 4 °C), resuspended in 500 µL lysis buffer (Dolan *et al*, 2020; Table 2.1), and lysed by 6 cycles of sonication (10 s on and 60 s off) on ice. Cell debris was sedimented (13,200 *g*, 15 min, 4 °C) twice and soluble protein extracts were transferred to icedchilled Eppendorf tubes. Standard Bradford Assay (Bio-Rad) was used to determine protein concentration.

For protein separation, sodium dodecyl sulfate polyacrylamide gel electrophoresis (SDS-PAGE) at 15% was conducted in A Bio-Rad Mini-PROTEAN Tetra Cell system (solutions in Table 2.1).

Lysates were mixed with 3X SDS loading buffer (NEB) incorporating 100 uM DTT per 100 µL sample, and heated (10 min, 80°C). 20 µL samples were next loaded into gel wells and run in 1X electrode buffer at 80 mV for 20 min (stacking gel passing) and later at 120 mV for 2 h. Following electrophoresis, protein samples were either stained (Coomassie Brilliant Blue G-250 0.05 %) or used for immunoblotting. For staining, gels were soaked in stain solution for 3 min, and destained with acetic acid (10%) until the background was cleared.

2.15.2. Western blot

After electrophoretic separation, protein bands were transferred by electro-blotting (Bio-Rad Mini Trans-Blot Cell) onto an Immobilon PVDF membrane (Millipore) and left overnight (100 mA at 4 °C) in transfer buffer (Table 2.1). Thereafter, membranes were washed three times (5 min each) with PBST buffer (0.1% Tween 20 in PBS) and blocked (5% skimmed milk) for 60 min at room temperature. A primary antibody was then included (anti-CarC; 1:20,000 dilution) and incubated again. Subsequently, membranes were washed four times as mentioned above, to remove unbound antibodies, and a LiCor dye 800 anti-rabbit antibody (Sigma; 1:10,000 dilution), was added and incubated for 40 min. Membranes were finally washed three times and developed with Bio-Rad Clarity TM Western ECL substrate, as indicated by the manufacturer, in sealed plastic bags. For blotting detection, X-ray films (Konika Minolta) were used in a dark room and blot images analysed.

2.15.3. Proteomics processing

To pinpoint differential protein abundance, cleared cell lysates derived from extraction were used for proteomic analysis. Extracts were diluted and 100 µg protein per sample was submitted to Cambridge Centre for Proteomics for processing. Individual samples were digested (trypsin),

labelled with tandem mass tags (TMT), and separated by liquid chromatography-mass spectrometry (LC-MS/MS).

2.16. Bioinformatics

2.16.1 Genome visualisation and homology matching

The Artemis genome browser v.16.0 (Carver *et al,* 2011) was used to identify transposon insertions by examining the Tn5-chromosomal junction regions in S39006 genome (accession ASM46334v3). To analyse the genomic context of genes, the EFI Genome Neighborhood Tool (GNT; Zallot *et al*, 2019) webserver was queried. Gene or protein homologues were obtained using the BLAST algorithm from NCBI (Boratyn *et al*, 2012). Pfam (Mistry *et al*, 2020) and the NCBI Conserved Domains Database (CCD; Marchler-Bauer *et al*, 2011) enabled identification of protein domains.

2.16.2 Specific growth rates

The Growthrates R package was used to obtain the specific growth rates (μ) following a logistic fit of OD data (Sprouffske and Wagner, 2016). Significant differences were tested by a one-way ANOVA followed by a Tukey Honest Significant Differences (HSD) for pairwise comparisons.

2.16.3 Sequence alignments and phylogeny

Amino acid and nucleotide sequence alignments were conducted using the MAFFT online tool (Katoh *et al*, 2018) with default parameters, with homologues obtained from BLAST (duplicates were removed). Neighbor-joining phylogenetic trees were built using the best scoring BLASTp hits (>70% identity), with a bootstrap of 1,000 using MEGA X (Kumar *et al*, 2018). Trees were visualised with the Interactive Tree Of Life (iTOL) v.4 server (Letunic and Bork, 2019).

2.16.4 Gene elements prediction

To predict open reading frames (ORFs), ORFfinder (NCBI), FgenesB (Solovyev and Salamov 2011), and getORF (Rice *et al*, 2020) tools were employed. Promoter elements were predicted by different tools, including BProm (Solovyev and and Salamov, 2011) for sigma 70 promoters, the neural network promoter prediction tool, BDGP (Reese, 2001), CNNProm (Umarov and Solovyev, 2017), and SEProm (Mishra *et al*, 2020). Rho-independent (intrinsic) terminators were predicted with ARNold (Naville *et al*, 2011) and FindTerm (Solovyev and Salamov, 2011).

MEME-Suite tools v.5.3.3 (Gupta *et al*, 2007) were used to uncover enriched sequence motifs in the CDS upstream regions of genes and search for known binding motifs via TomTom. The Prokaryotic combined database option was chosen and threshold of <0.05 was applied. Sequence logos were generated in the Weblogo online tool (Crooks *et al*, 2004).

Putative transcription factor binding sites were searched with Virtual Footprint (Dudek and Jahn, 2022) and Prediction of Prokaryote Promoter Elements and Regulons (PePPER; De Jong, 2012) by querying with putative promoter regions.

2.16.5 RNA data analysis

To search for RNA homologue sequences, the RFam database (Kalvari *et al*, 2018) was consulted. tRNAscanSE (Lowe and Chan, 2016) was used to scan presence of tRNAs.

2.16.6 Protein data analysis

To infer protein-protein interactions, network nodes were generated by the STRING database v.11.5 (Szklarczyk *et al*, 2021) by choosing a query protein. Raw data from proteomics were processed using Proteome Discoverer v.2.2 (Thermo Fisher Scientific) and the peptide search engine Mascot (www.matrixscience.com), to match peptides to S39006 proteome (Uniprot) and against the common repository of adventitious proteins (cRAP) v1.0. Multivariate data analysis was conducted with R package MSnbase (Gatto and Lilley, 2012) and Limma package (Smyth, 2005) was used to discern protein differential abundance. For detecting differentially expressed proteins, significant differences were ascertained by Student's *t*test ($p<0.05$) and log2 fold change (FC) threshold set to 1. Enrichment analysis was performed using the Gene Ontology (GO) tools from KEGG database (Kanehisa *et al*, 2007).

Chapter 3. Novel regulators of antibiotic production

3.1. Generation and selection of mutants

To find novel regulators of antibiotic production, a random transposon mutagenesis approach was followed (section 2.5; summarised in Fig. 3.1). Mutants were generated using the S39006 wild type (WT) as parental strain, and transconjugant colonies were visually screened to detect altered pigmentation compared with the WT strain. Thus, enhanced or reduced prodigiosin synthesis capacity served to directly identify strains carrying transposons in genes or regulatory regions involved, at least, in the control of this antibiotic. Transposons, mini-Tn*5* cassettes incorporating *cat* for selection, that are contained in the pDS1028 plasmid, were mobilised from donor (*E. coli* β2163) into S39006 WT via conjugation (Monson *et al*, 2015). The donor strain requires DAPA to grow, and hence it was used as counterselection of the *E coli* strain in the search for *Serratia* mutants. This transposon-transfer system was chosen because of the compatibility of its selection marker with most of the known regulator mutant markers that are part of the laboratory library. Moreover, the transposon cassette also includes *uidA*, which, if inserted in same orientation of transcription, generates fusions.

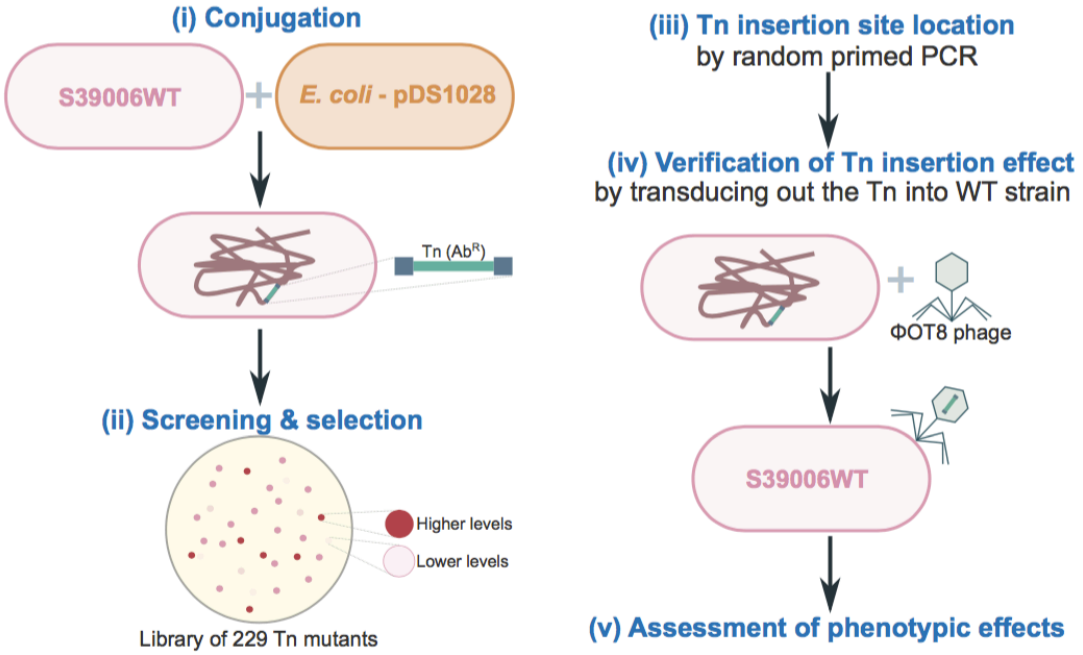


Fig. 3.1. Experimental outline for generation of mutants. (i) Conjugation: Recipient (S39006 WT) and donor (*E. coli* β2163) were mixed to allow conjugation of transposon (Tn) delivery system (pDS1028). (ii) Screening and selection: transconjugant colonies from overnight selection plates with altered pigmentation were isolated. (iii) Tn insertion site's location: novel regulators were confirmed by random primed PCR (iv). Verification of Tn insertion effect: Tn-disrupted regions of novel candidates were transduced back to S39006 via φOT8 phage, and phenotypic effects of Tn on resulted transductant strains were assessed (v).

To pinpoint the location of transposons in transconjugant genomes, a random primed PCR technique was employed (section 2.6; Fineran *et al*, 2005). In brief, this nested strategy uses primers annealing to the known end of the transposon cassette, along with a set of degenerate primers that align to an internal common sequence in the second round. Hence, the exact location of transposon disruption was ascertained from the transposon-genome junction by genomic search of the Tn5 end sequence. Those locations were confirmed with at least 20 bp of overlap.
Once mutants carrying transposons inserted into novel regulatory sites were confirmed, the generalised transducing phage φOT8 (Evans *et al*, 2010) was utilised to move the transposon-containing regions (Cm^R) back into S39006 WT. This gave additional genetic confirmation that transposon disruptions were indeed the cause of the phenotypes observed. Finally, the confirmed new regulators were subjected to further characterisation at phenotypic and molecular levels.

3.2. Transposon location in mutants

Overall, from independent conjugation events, approximately 13,000 colonies were screened, from which 229 mutants with modified pigmentation relative to the parental strain (Fig. 3.2) were obtained.



Fig. 3.2. Examples of isolated strains displaying altered pigmentation. Strains were streaked out on LBA plates along with the WT (top of each plate) for comparison.

These strains, around 1.7% from the total colonies screened, were grouped into three categories based on their pigmentation: “White” (no pigment), “Light pink” (faint colour), and “Hyper red” (hyperpigmented). The library of mutants comprised 85 isolates displaying White, 100 Light pink, and 44 Hyper red phenotypes. Almost half of the mutants isolated (43.5%) corresponded to the Light pink phenotype, followed by White (37.4%), and Hyper red, with around a fifth from the whole library (19.1%; Fig. 3.3).

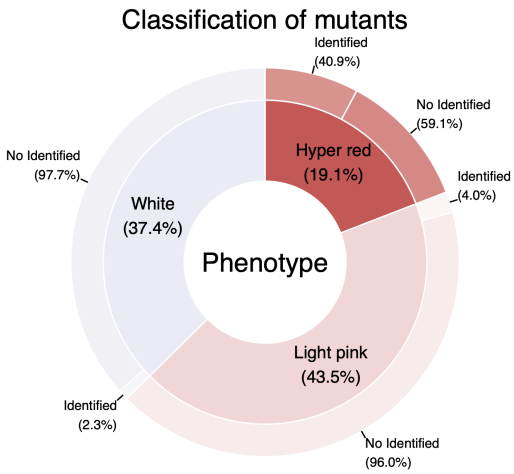


Fig. 3.3. Phenotypic classification of mutants presenting changed pigmentation. Percentage of each phenotypic group from the 229 isolates and the corresponding fraction of transposon insertion sites that were identified (outer ring).

Identifier	Target	Predicted function	Fusion	Match (bp)	Phenotype
ND6	*flhC*	Flagellar transcriptional regulator	Yes	71	Light Pink
NF8	*rap*	SlyA/MarR regulator	No	63	White
OI7	IGR	*rsmA* promoter	–	71	Hyper Red
OF5	IGR	*rsmA* promoter	–	51	Hyper Red
NF11	IGR	*sdhE* promoter	–	74	Light Red
NC6	*pigP*	XRE family regulator	No	21	White
OH15	*pigQ*	Response regulator (TCS)	Yes	69	Light pink
NA7	*pigW*	Sensor kinase (TCS)	No	74	Light pink
OA12	*pigX*	GGDEF/EAL domain	No	65	Hyper Red
NH4	*pigD*	Prodigiosin biosynthesis	Yes	74	White
OB6	IGR	PPT promoter	–	53	Hyper Red
OB7	IGR	PPT promoter	–	79	Hyper Red
OB5	*2785*	PPT	Yes	68	Hyper Red
OC1	*2785*	PPT	No	64	Hyper Red
OD3	*2785*	PPT	No	80	Hyper Red
OD5	*2785*	PPT	Yes	63	Hyper Red
OD8	*2785*	PPT	No	75	Hyper Red
OG3	*2785*	PPT	No	26	Hyper Red
NA4	*2785*	PPT	Yes	48	Hyper Red
NH5	*2785*	PPT	No	72	Hyper Red
ND1	*cysW*	Sulfate transporter permease	No	74	Light Red
NB3	*5465*	Hypothetical protein	No	65	Hyper Red
NF13	*wzt*	ABC-type transporter	Yes	48	Hyper Red
NJ1	*21635*	class I SAM dependent methyltransferase	Yes	68	Hyper Red
NJ6	IGR	Undefined	–	74	Hyper Red

Table 3.1. Transposon targets in genomes of prodigiosin mutants. Code: mutant name; Fusion: indicates if transposon-incorporated *uidA* forms a fusion strain; Match: genome overlap length in base pairs (bp). IGR= Intergenic region; TCS= Two-component system; PPT: phosphopantetheinyl transferase; ABC: ATPbinding cassette; SAM= S-adenosyl methionine. Known regulators and prodigiosin synthesis proteins are included.

Transposon location was defined for 25 mutants (Table 3.1), with eight inserted into previously known regulators (*flhC*, *rap*, *rsmA*, *sdhE*, *pigP*, *pigQ*, *pigW*, and *pigX*; section 1.2.1.4), and one mapped in *pigD* (from the prodigiosin operon; section 1.2.1.2). This finding validated the methodology employed as it identified several previously studied regulators (proof of principle). On the other hand, the remaining 17 strains had transposons inserted into previously unexplored regions. The transposon insertions disclosed a phosphopantetheinyl transferase (PPT) gene, *cysW* (a sulfate transporter, ND1 strain), *5465* (encoding a hypothetical protein, NB3 strain), an O-antigen transporter (NF13 strain), and an intergenic region (NJ6 strain), as new prodigiosin production regulators.

3.3. Novel regulators

After confirmation of transposon insertions in unexplored locations, transposants were subjected to transduction in order to confirm that the transposons caused the variation in prodigiosin levels. For the PPTase gene, two representative strains were evaluated: OB5, the transposon-disrupted CDS, and OB7, carrying the insertion in the putative PPT gene promoter. Hence, following transduction of mutations into a clean genetic background (WT), it was confirmed that both the original transconjugant and transductant strains displayed the same altered phenotype (Fig. 3.4).

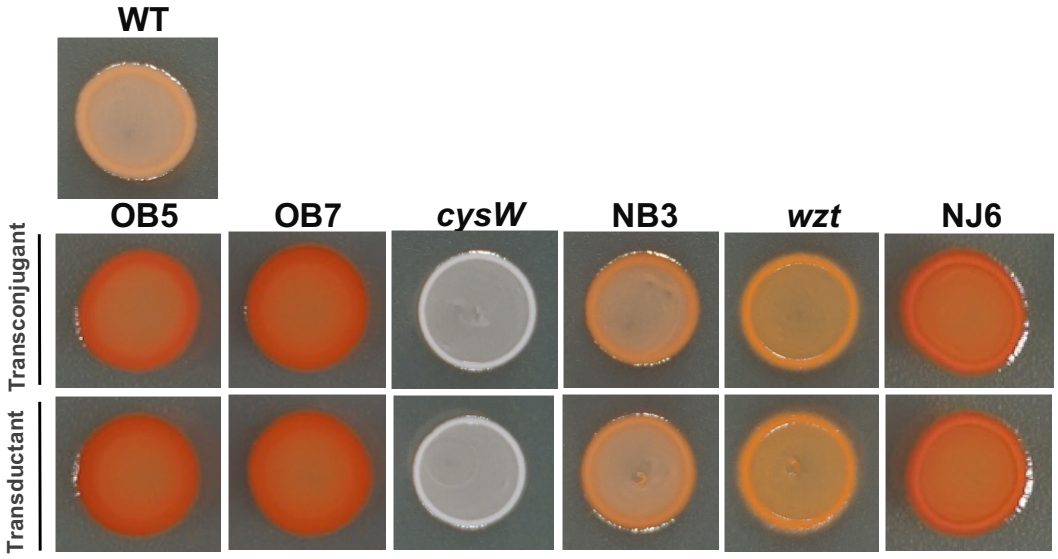


Fig. 3.4. Transposon insertions caused the changes in prodigiosin synthesis. Transposon mutations from transconjugants were moved back to S39006 WT strains via transduction, and their effects on pigment production were corroborated. OB5 and OB7: PPT, NB3: uncharacterized protein 5465, NJ6: intergenic region.

From the novel modulators of prodigiosin synthesis found, the initial characterisation of the phosphopantetheinyl transferase (*yieE*), *cysW*, and the uncharacterized protein-encoding *5465*,

are described in more detail in this chapter. The other two mutations, *wzt* and the intergenic region, were selected for subsequent detailed investigation (chapters 4 and 5, respectively).

3.3.1. Phosphopantetheinyl transferase

Several transposon insertions were mapped within the coding region of the *E. coli* homologue *yieE*, encoding a 4'-phosphopantetheinyl transferase, with two of them inserted upstream of the coding region. These transposons were located 61 and 85 bp upstream from the translation start site. This heavily transposed region constitutes almost a quarter of all prodigiosin hyperproducers found, with 10 representatives, out of 44 mutants in total. All strains from this set displayed the same elevated pigment production, and mutants OB5 and OB7 were chosen as representatives for transduction (Fig. 3.4) and genomic context exploration (Fig. 3.5). The *yieE* gene is not obviously part of an operon and it is surrounded by a gene coding for a nucleobase ascorbate transporter family protein (downstream) and an effector protein (upstream).

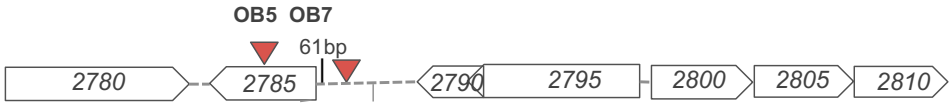


Fig. 3.5. Genomic neighbourhood of the transposon insertions in mutants OB5 and OB7. Locations disrupted by transposons (red triangles) are the *2785* (*yieE*) coding region (OB5) and an intergenic region (OB7) 61 bp upstream *2785* CDS. Putative functions: ***2780***: Nucleobase: Cation Symporter-2 (NCS2) family permease; ***2785***: Phosphopantetheinyl transferase (**PPT**); ***2790***: Effector protein; ***2795***: Oxidoreductase FeS-binding subunit; ***2800***: Hypothetical protein; ***2805***; DUF4810 domain protein; ***2810***: Hypothetical protein.

This gene encodes part of a family commonly abbreviated as PPTs or PPTases, which are involved in multiple biosynthetic pathways (Beld *et al*, 2014). Despite this being defined as a novel regulator in S39006, it has been previously used to manipulate antibiotic production in other species such as *Xanthomonas albilineans* (albicidin; Huang, *et al*, 2000) and *Streptomyces coelicolor* (actinorhodin and undecylprodigiosin; Lu *et al*, 2008), as a result it was not studied in this work.

3.3.2. CysW: a sulfate-transport permease

The only mutant that exhibited a drop in visual prodigiosin production (Fig. 3.4) from the set of novel regulators was *cysW*. Its product is an inner membrane protein that is part of a sulphate transport system called the CysAWPT complex. To confirm differential production of prodigiosin and explore any possible changes in production of carbapenem and acyl-homoserine lactones (AHLs), their quantification over time during batch culture was determined. AHLs were assayed because of their roles as quorum sensing (QS) inducers –mostly N-butanoyl-homoserine lactones

(BHL) in S39006– where BLH plays a crucial role in modulating the biosynthesis of both antibiotics, and therefore is important for regulation analysis. The CysW transport mutant produced decreased levels of prodigiosin but only before entering the stationary growth (p <0.037), after which no differences in production were detected. The opposite effect was observed for carbapenem production, as it rose significantly (p <0.027) after 8 hours of growth (Fig. 3.6). As in carbapenem production, BHL was produced following the same trend but only significant in the late stationary phase (p <0.029). This revealed that this mutation not only affects antibiotic biosynthesis but also the main communication signalling once the stationary phase is reached. Furthermore, the *cysW* strain did not grow as well as the WT strain, displaying a slower growth rate compared to the parental strain, confirming that this mutation had an impact on fitness and metabolism.

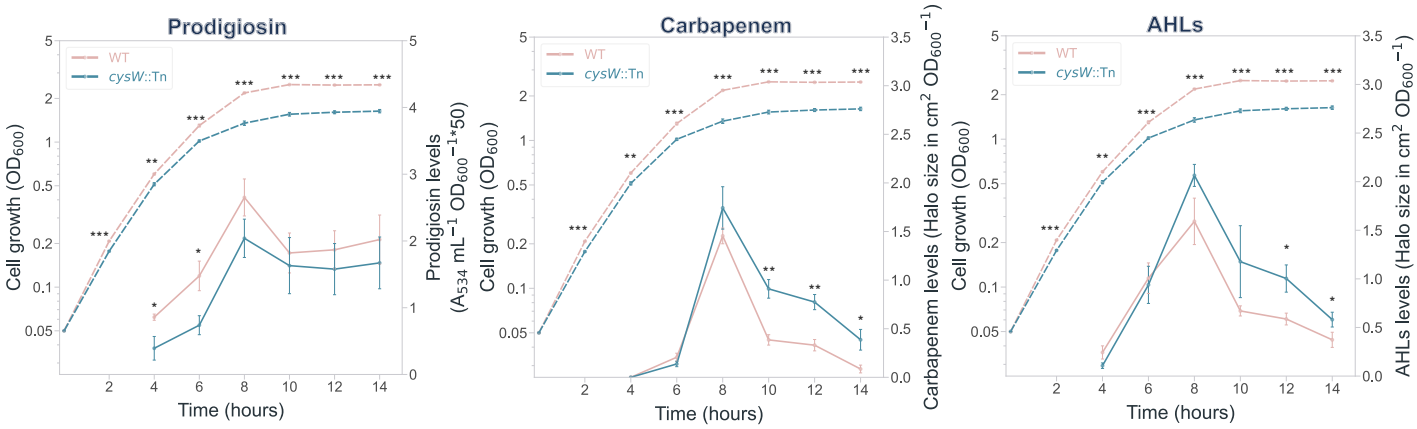


Fig. 3.6. Production of antibiotics and AHL (BHL) over time by the *cysW* strain. Dashed lines indicate cell growth (OD_{600}; left Y axes) whereas solid lines indicate cell product (right Y axes). Prodigiosin was quantified by spectrophotometry (A_{534}) while the carbapenem and AHL production were measured by halo formation using their corresponding indicator strain. Data are means ± SD of three biological replicates.

To explore to what extent this mutation affected other S39006 features, and thus determine whether it is acting at local or global level, a phenotypic characterisation was performed. Assays for production of two plant cell-wall degrading enzymes (pectate lyase and cellulase) were performed, along with swimming ability, and flotation assays. Flotation assays are useful indicators for the production of gas vesicles since these structures confer the ability to remain buoyant in liquid cultures. If production of gas vesicle organelles is reduced, cells tend to sink. To further assess the latter, cells were observed under phase-contrast microscopy to score for presence or absence of gas vesicles, as they can be seen as bright intracellular spots (gas "vacuoles") in bacterial cultures. Cells lacking CysW showed no swimming pattern difference when compared to the WT strain, but a dramatic effect on pectate lyase and cellulase production was seen (Fig. 3.7). Both activities were severely diminished in the mutant strain (p<0.0008 for

both enzymes), with pectate lyase nearly abolished. Moreover, these cells possess enhanced flotation capacity in relation to the parental strain as they remained buoyant, albeit no brighter spots from cell preparations were observed.

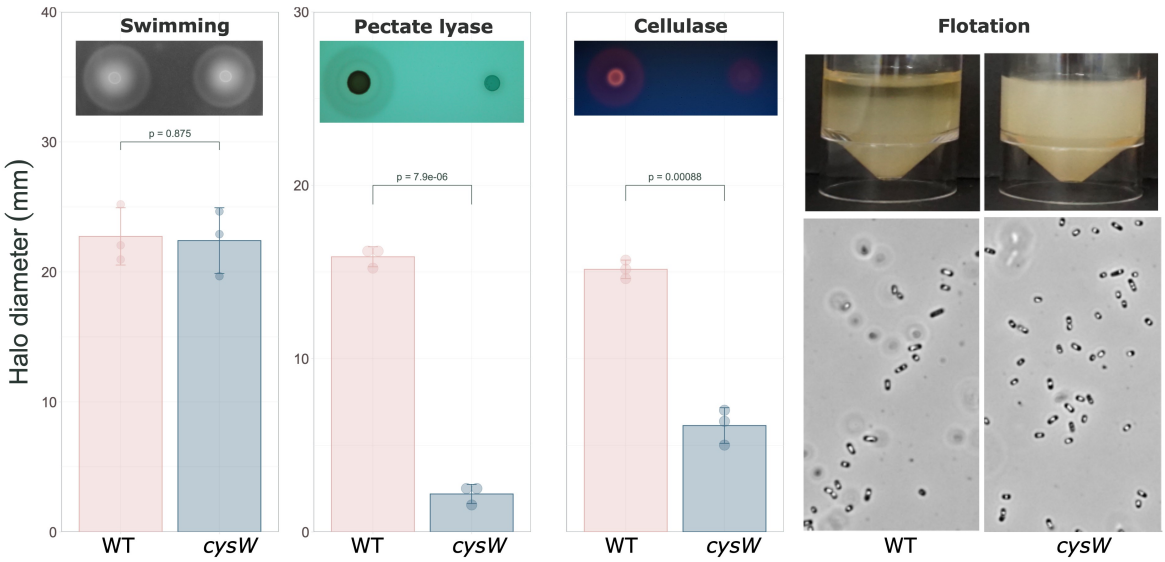


Fig. 3.7. Phenotypic characterisation of *cysW* strain. Swimming ability, pectate lyase, and cellulase production are expressed as halo diameter (means ± SD) and gas vesicle production as flotation capacity in liquid culture. All assays were performed with three biological replicates and significant differences set to $p<0.05$. Cells from flotation assays were observed under phase contrast microscopy (100X oil-immersion lens) after 48 h. Bright spots correspond to presence of gas vesicles.

As this mutant displayed a growth defect and the *cysW* function is involved in transport of sulfurcontaining molecules, it was speculated that auxotrophy may explain, at least partially, some of the effects observed. Thus, to test this hypothesis, the *cysW* mutant was grown in both LB and minimal medium, using only glucose as carbon source, and contrasted to WT growth. The mutant ND1, exhibited a noticeably defective growth in minimal medium plates, when compared to WT performance (Fig. 3.8). This fact suggests sulfur compound-dependance as the likely cause of the phenotypes observed.

Therefore, *cysW* disruption modified the production of antibiotic in opposite ways (lowered prodigiosin but elevated the carbapenem levels) and it boosted production of AHLs from exponential phase onwards. It also caused a detrimental effect on cell-wall degrading enzymes, and the buoyancy of cells was improved. Taken together, these results point to *cysW* as a pleiotropic regulator and some changes are most likely to relate to sulphate availability.

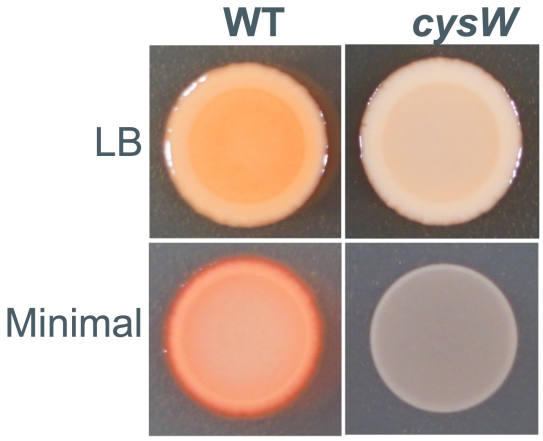


Fig. 3.8. *cysW* mutant grows poorly in minimal medium. Bacterial patches from normalized cell cultures were grown in both culture media (LB and M9 minimal medium supplemented with 0.2% glucose) for 24 h.

In *E. coli*, the CysAWPT complex is an ABC transport system that comprises the permease components CysW and CysT, the ATP-binding subunit CysA, and the sulfate/thiosulfate-binding protein CysP (Kertesz 2001; Barton, 2005; Pilsyk and Paszewski 2009). In S39006, three of these genes are arranged in a single operon *cysTWA*, with the putative *cysP* upstream thereof (Fig. 3.9).

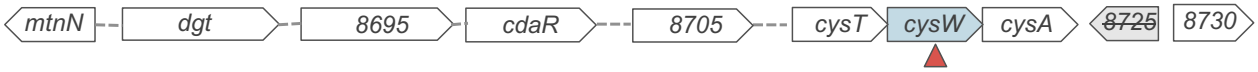


Fig. 3.9. Genomic neighbourhood of the transposon insertion in mutant ND1. Location disrupted by transposon (red triangles) is the *cysW* coding region. Putative functions: ***mtnN***: 5'-methylthioadenosine/Sadenosylhomocysteine nucleosidase; ***dgt***: Deoxyguanosinetriphosphate triphosphohydrolase; ***8695***: Periplasmic serine endoprotease DegP-like; ***cdaR***: CdaR family transcriptional regulator; ***8705***: Sulfate ABC transporter substrate-binding protein, putative *cysP*/*sbp*; ***cysT***: Sulfate ABC transporter permease subunit; ***cysW***: Sulfate ABC transporter; ***cysA***: Sulfate/thiosulfate import ATP-binding protein; ***8725***: hypothetical protein and ***8730***: Glycerol dehydrogenase.

CysW (293 aa) has only one protein domain, classified as an ABC type 1 transmembrane domain (Fig. 3.10), which is part of import systems that have only been found in bacteria and plants (Lewinson and Livnat-Levanon, 2017). Importer functions in prokaryotes rely on a substratebinding protein that captures substrates, generally sugars or amino acids, which are then transferred to the transmembrane domains to then enter the cells (Scheepers *et al*, 2016; Leisico *et al*, 2020).

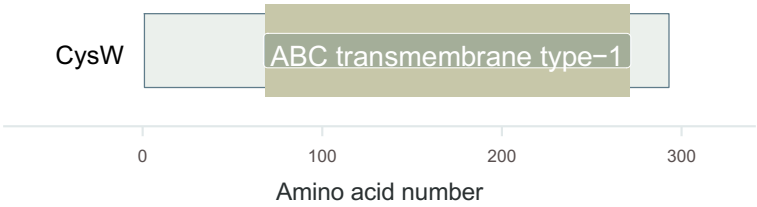


Fig. 3.10. Representation of CysW domain. Highlighted domain is located between positions 68 and 271 and correspond to Type 1 family of ATP-binding cassette (ABC) transporters (membrane proteins).

3.3.3. An uncharacterized protein

The mutant NB3, whose colonies was visually redder than WT (Fig. 3.4), contained a transposon inserted into a gene (*5465*) encoding an uncharacterized protein. As stated previously, quantitative evaluation of antibiotic production and AHLs synthesis was carried out. Despite the visual observation, prodigiosin synthesis was not affected throughout growth, and the same was confirmed for both carbapenem and AHL production (Fig. 3.11).

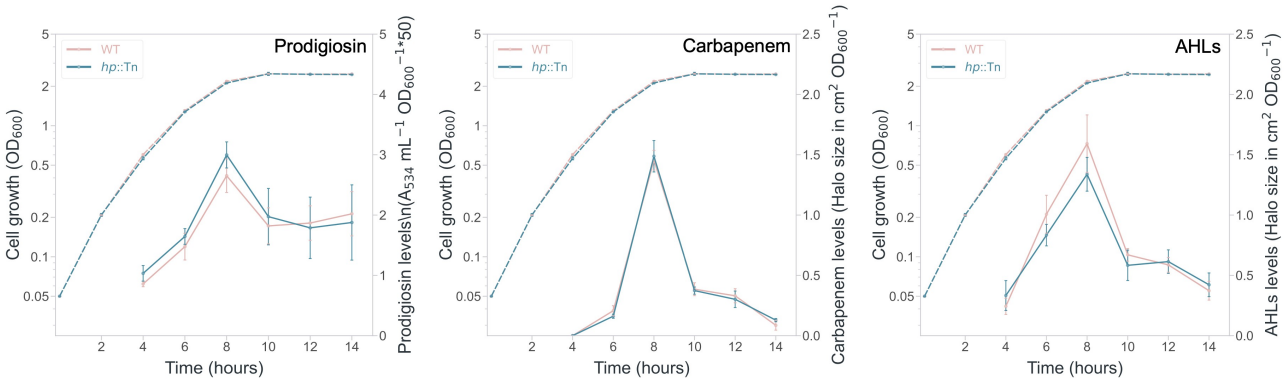


Fig. 3.11. Production of antibiotics and acyl homoserine lactones over time of NB3 train. Dashed lines indicate cell growth (OD_{600}; left Y axes) whereas solid lines indicate cell product (right Y axes). Prodigiosin was quantified by spectrophotometry (A_{534}) while the carbapenem and BHL production were measured by haloes formation using their corresponding indicator strain. Data are means ± SD of three biological replicates.

To investigate if this protein had a different role in S39006, a set of phenotypic assays was performed. The 5465 mutant exhibited enhanced swimming capacity (p=0.043) and a reduced cellulase activity (p=0.0059), whilst flotation capacity and pectate lyase remained unaffected (Fig.
3.12).

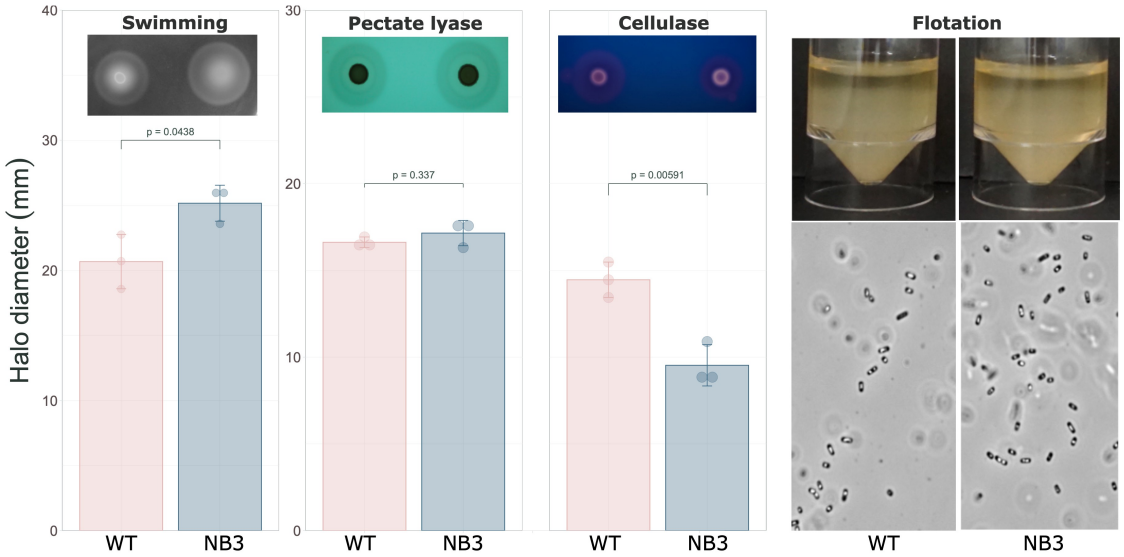


Fig. 3.12. Phenotypic characterisation of NB3 train. Swimming ability, pectate lyase, and cellulase production are expressed as haloes diameter (means ± SD) and gas vesicles production as flotability in liquid culture. All assays were performed with three biological replicates and significant differences set to $p<0.05$. Cells from flotation assays were observed under phase contrast microscopy (100X oil-immersion lens) after 48 h. Bright spots correspond to presence of gas vesicles (as gas vacuoles).

Subsequently, as these results showed that this mutation had effects other than in antibiotic production control, and because the protein had unknown function, cell growth was scrutinised in minimal conditions to rule out auxotrophic effects. The *5465*-transposon disruption mutant grew similarly to the parental strain in plates containing minimal medium (Fig. 3.13) and so is likely prototrophic.

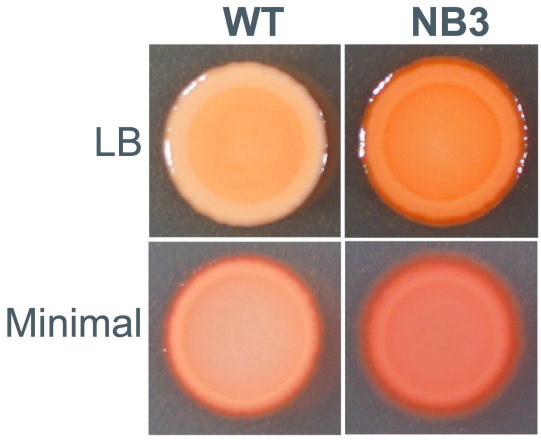


Fig. 3.13. NB3 mutant can grow in minimal medium. Bacterial patches from normalized cell cultures were grown in both culture media for 24 h.

Although the mutation found in NB3 does not affect antibiotic production, it impacts other phenotypic features, and attempts to assign it a putative function were made. Considering the genomic context, efforts to find similar syntenic regions in other species were not fruitful. The transposon-disrupted gene *5465* is not part of an operon (Fig. 3.14), which could have given clues

by association. It is followed downstream by a putative operon linked to peroxide stress response that transcribes in the opposite direction. The middle gene of this arrangement is *ohrR* and immediately upstream of *5465*, glycine tRNA synthetase is found, and further up, there is another putative operon encoding three hypothetical proteins.

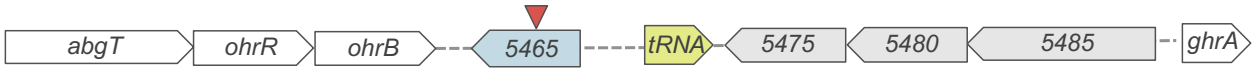


Fig. 3.14. Genomic neighbourhood of the transposon insertion in mutant NB3. Location disrupted by transposon (red triangles) is the *5465* coding region. Putative functions: ***abgT***: p-aminobenzoyl-glutamate transport protein; ***ohrR***: organic hydroperoxide resistance transcriptional regulator (MarR family); ***ohrB***: organic hydroperoxide resistance protein; ***5465***: hypothetical protein; **tRNA**: tRNA-Gly; ***5475-5485***: hypothetical proteins (in grey) and ***ghrA***: glyoxylate/hydroxidepyruvate reductase A

A homology search was performed using BLASTp, and only uncharacterised proteins were displayed. Since no information about function was drawn, possible similar domains were sought in the Conserved Domain Database (NCBI; Marchler-Bauer *et al*, 2015), Pfam (Mistry *et al*, 2020), InterProScan (Blum *et al*, 2021), CATH Protein Structure Classification database (Sillitoe *et al*, 2021) could not assign any domain. Likewise, no similar structures to 5465 deposited at the Protein Data Bank (PDB) were returned. Predictors for potential ligand-binding sites (3DLigandSite; Wass *et al*, 2010) and gene ontology terms by using DeepGO (Kulmanov *et al*, 2018) and DeepFri (Gligorijević *et al*, 2021) also failed to provide information. Finally, it was decided to keep abandon this mutant and concentrate on the remaining mutants.

3.4. Discussion

In this work, random transposon mutagenesis using the S39006 WT as parental strain, enabled identification of both known and "new" genes involved in prodigiosin production, based on altered pigmentation in colonies. This straightforward yet powerful approach proved to be effective in searching for regulators either up- or downregulating synthesis of antibiotics in S39006.

Transposon mutagenesis has been useful for studying gene regulation over decades. This robust technique makes it easy to connect a given phenotype with a transposon disruption (Kwon *et al*, 2016; Cain *et al*, 2020). The mutagenesis system used in this study, via plasmid conjugal transfer, was previously used successfully to uncover gas vesicle regulators, which in turn were found to also control prodigion synthesis and other phenotypes in this strain (Lee *et al*, 2017; QuinteroYanes *et al*, 2019; Quintero-Yanes *et al*, 2020). Here enhanced or decreased colony pigmentation was exploited to detect putative regulatory genes or loci influencing prodigiosin

synthesis. Previous reports aimed to identify novel antibiotic regulators using Tn5-based systems, have found 365 genes modulating changes in undecylprodisiosin (Xu *et al*, 2017) and 551 genes for actinorhodin synthesis (Xu *et al*, 2019) in the well-known Gram-positive model *Streptomyces coelicolor*. Key advantages of the system employed here are the generation of stable chromosomal insertions, and its capacity to construct gene fusion strains, when inserted in the appropriate transcriptional direction (Monson *et al*, 2015). Fusion strains are useful for the study of gene expression and regulation as they enable monitoring of changes by either spectrophotometric or fluorometric assays (Van Dik *et al*, 2001; Van der Meer and Belkin, 2010). Phenotypes from mutants of interest were verified by transducing the transposon, coupled with a resistance marker, back into the WT parental strain using phage OT8 (Evans *et al*, 2010) to confirm that phenotypes observed were due to the transposon insertions.

The new library of prodigiosin transposon mutants contains 229 strains in total, from which 25 disrupted regions were determined, most of them exhibiting a hyperpigmented phenotype. Thus, 204 strains with undefined transposon insertions could be used in the future to extend the regulatory network in the S39006 model.

From the identified pool of mutants, seven strains representing five genotypes were selected for transduction verification. From this confirmed set, two mutants carrying transposons in adjacent genomic positions, *wzt* and a SAM-dependent methyltransferase gene, plus an intergenic mutation, were subjected to more detailed investigation (chapters 4 and 5, respectively). Another two mutants were chosen as representatives for a PPTase gene (coding region and promoter), and the last two insertions were located at *cysW* and in a predicted gene.

All transposon targets identified were hit only once, except the gene *yieE* (PPTase) with eight disruptions of its coding sequence plus two insertions upstream of the translational start. This transposon target was overrepresented with almost a quarter of all hyperpigmented mutants isolated, perhaps suggesting this gene had preferential insertions over other insertion sites. Transposon Tn5 has been a reliable tool for mutagenesis (Barquist *et al*, 2013) even though it does not integrate into bacterial genomes at completely random locations, some target bias does occur (Herron *et al*, 2004; Green, 2012). DNA regions presenting a low number of insertions can be associated with essential genes or genes affecting fitness (Grazziotin *et al*, 2015; Rancati *et al*, 2018; Ma *et al*, 2022), hence, having a heavily transposon-hit zone such as the *yieE* locus might suggest an accessory function.

PPTases are found across all life domains and are essential for secondary metabolite activation, particularly in synthesis of compounds such as fatty acids, polyketides, and non-ribosomal peptides (Kim *et al*, 2018). In prokaryotes, they are usually biosynthetic-specific pathway modulators that act at a post-translational level, by modifying carrier proteins to render them

catalytically active (Cox *et al*, 2002; Cheng and Wang, 2020). Notably, at least two more PPTases are present in S39006's genome. One of them is PigL (Harris *et al*, 2004), part of the biosynthetic prodigiosin cluster that synthesizes the intermediate bypyrrole MBC (section 1.2.1.2) and the other is VfmJ, a homologue from *Dickeya*'s secondary quorum sensing system termed VFM (virulence factor modulating).

Another insertion generating diminished prodigiosin production was in *cysW*. This belongs to the complex CysAWPT, a widely used system for importing external sulfate and thiosulfate across the membrane from external sources (Han and Lee, 2006), although it was also found to import tellurate in *E. coli* (Goff and Yee, 2017). CysW is a membrane-bound protein that forms a heterodimer along with CysT, which allows the passage of sulfur-containing compounds into the cells. It is considered pivotal for cellular metabolism and its loss is associated with nutrient starvation (Hatzios and Bertozzi, 2011; Kim *et al*, 2018; Ma *et al*, 2021) and has been proposed as a drug target in *Mycobacterium tuberculosis* (Paritala and Carroll, 2013). Cells defective in *cysW* showed severely impacted growth in minimal medium, consistent with a sulfur auxotrophy Moreover, CysW mutants showed decreased production of prodigiosion until the cells entered stationary phase, when they started to produce WT levels. This effect might be due to the impaired uptake of sulfur-containing compounds as the importer system entry is constituted by both CysW and CysT. A study in *Serratia* sp. strain S2B, showed that increasing amounts of sulfur (as ammonium sulfate) enhanced prodigiosin biosynthesis, whereas the addition of other ammonium salts resulted in fewer effects on production (Rastegari and Karbalaei-Heidari, 2016). This suggests that sulfur uptake is crucial for that *Serratia* strain to produce the pigment, and this may have implications for strain S39006. For example, the synthesis of the pigment requires methionine as one of the main substrates for biosynthesis (Williamson *et al*, 2006; Sun *et al*, 2021) and therefore, this may have implications for delayed synthesis. This could be tested by supplementing minimal medium with increasing amounts of cysteine and methionine, and monitoring if a restored ability to produce the pigment is observed, as was shown for the potassium transporter *trkH* (QuinteroYanes *et al*, 2019).

On the other hand, carbapenem synthesis began to increase just before the stationary growth was initiated and it stayed high afterwards, in a similar fashion to increased levels of AHLs (BHL). The LuxR homologue in S39006, SmaR, is a negative regulator of *carR*, which in turn is a positive regulator of the *carA-H* carbapenem cluster (see section 1.2.1.4.2).

The CysW mutant showed an almost abolished synthesis of cell-wall degrading enzymes, which has also been reported for *cysB* mutants in *Pectobacterium carotovora* (formerly *Erwinina*

carotovora), another pythopatogen (Hinton *et al*, 1987). This is probably related to the decreased uptake of sulphated compounds, yet had an augmented capacity to remain buoyant in liquid culture. The latter observation is generally related to the presence of more gas vesicles, seen as bright spots (vacuoles) within cells (Ramsay *et al*, 2011; Monson *et al*, 2016; Tashiro *et al*, 2016). However, mutant cells appeared similar to those native strain in terms of "brightness" under phase-contrast microscopy. An alternative explanation would be enhanced swimming capacity, but that notion was discarded. Therefore, more detailed intracellular images by electron microscopy may help clarify the reason behind this behaviour.

The last mutant that was selected based on apparent hyperpigmentation by visual inspection was in a gene encoding an uncharacterised protein, Ser_005465 (in short 5465). Mutants carrying that insertion showed no obvious differences in growth, AHL production, carbapenem synthesis, or surprisingly, in prodigiosin production, in comparison to WT strain. Subsequent quantitation of the pigment then demonstrated that the "hyperproduction" of red colouration of mutant colonies was an artifact. S39006 WT strain naturally produces prodigiosin; this gives it a distinctive reddish colour. Colony appearance generally correlates tightly with pigment biosynthesis, but this can be affected also by levels of gas vesicle production. These intracellular nanostructures can refract light, and thus when sparse, colour of colonies may look more intense (Tashiro *et al*, 2016, Lee *et al*, 2017; Quintero-Yanes *et al*, 2020). Nonetheless, no noticeable changes were perceived from the cells observed under the microscope; bright spots from vacuoles appeared undistinguishable in the mutant and WT strains. However, some changes were noticed in this mutant for swimming capacity and cellulase production. Various attempts to gather information about the putative function of the 5465 protein were unsuccessful. None of the putative homologues found have been characterised. Thus, given the marginal phenotypic impacts seen in this mutant, no further analysis was undertaken.

Chapter 4. O-antigen transport Wzt modulates antibiotic production

From the screening of S39006 mutants displaying changes in pigmentation, two transposon insertions in two contiguous coding sequences were further studied. The altered genes were *S39006_1185* and *S39006_1186* (shortened as *1185* and *1186*) and both seem to be part of a larger operon. The former is a *wzt* homologue, part of an ABC transport system of O-antigen polysaccharide, and *1186* encodes an S-adenosyl methionine (SAM)-dependent methyltransferase. Both mutations were verified by phage transduction, and the resultant transductants showed the same hyperpigmented phenotype and distinctive colony morphology. The *wzt* gene mutation was chosen as representative in most of the experiments, which not only increased antibiotic production but also had pleiotropic effects.

4.1. Members of the O-antigen operon

The putative operon containing the transposon-disrupted genes appears to be comprised of six genes (*1182-1187;* Fig. 4.1, top) involved in O-antigen translocation through the Wzm/Wzt ABC transporter system. To gain more insights about their putative functions, the BLASTp tool was utilised to seek homologues and known domains were searched in the Uniprot database. Thus, the gene products from this operon contain the ABC transport elements (Wzm and Wzt), a nucleotidyl transferase and an isomerase (1182), a methyltransferase (1186), and phosphomannomutase/phosphoglucomutase domains (1183; Fig. 4.1, bottom). No domain was predicted for 1187, but based on homology, it is predicted to act as a glycosyltransferase. The gene *1184* encodes a Wzm homologue, which associates with Wzt to give rise to the active ABC transporter as reported for *E. coli* (Iguchi *et al*, 2015).

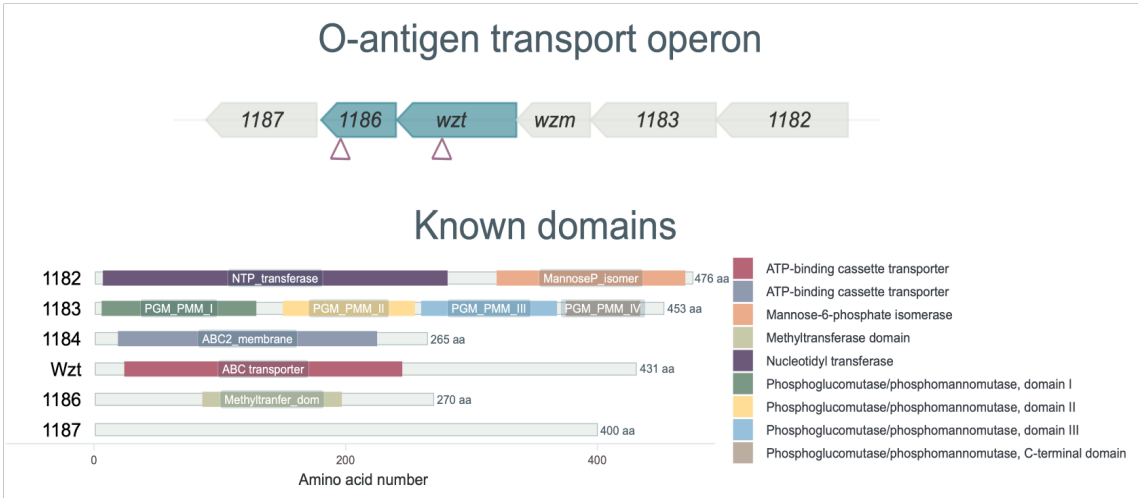


Figure 4.1. Operonic organisation of *wzt* and *1186* and domain architecture of proteins. Transposoninserted genes are highlighted in blue (top) and red triangles denote the approximate transposon insertion sites. Gene function (left to right): ***1187***: Putative glycosyltransferase; ***1186***: Class I S-adenosyl-Lmethionine (SAM)-dependent methyltransferase; ***wzt***: ATP-binding cassette (ABC) transporter; ***wzm***:

Putative O-antigen export permease; ***1183***: Phosphomannomutase/phosphoglucomutase; ***1182***: Mannose-1phosphate guanylyltransferase/mannose-6-phosphate isomerase. Known domains of proteins (bottom) extracted from Uniprot database and classified by Pfam have the following identifiers: NTP_transferase (PF00483), MannoseP_isomer (PF01050), PGM_PMM_I (PF02878), PGM_PMM_II (PF02879), PGM_PMM_III (PF02880), PGM_PMM_IV (PF00408), ABC2_membrane (PF01061), ABC_tran (PF00005), Methyltransf_dom (PF13847).

4.2. The *wzt* mutation increases antibiotic production at transcriptional level

The two mutants hit by the transposons in *wzt* and *1186* exhibited identical phenotypes on LBA plates (*wzt* strain is shown as an example in Fig. 4.2, top). Both are hyperpigmented and display a characteristic crusty/rough colony morphology with irregular edges, in marked contrast to WT colonies. To verify that transposons were the cause of such phenotypes, mutations were transduced back into the WT strain, which confirmed their impact (Fig. 4.2, bottom).

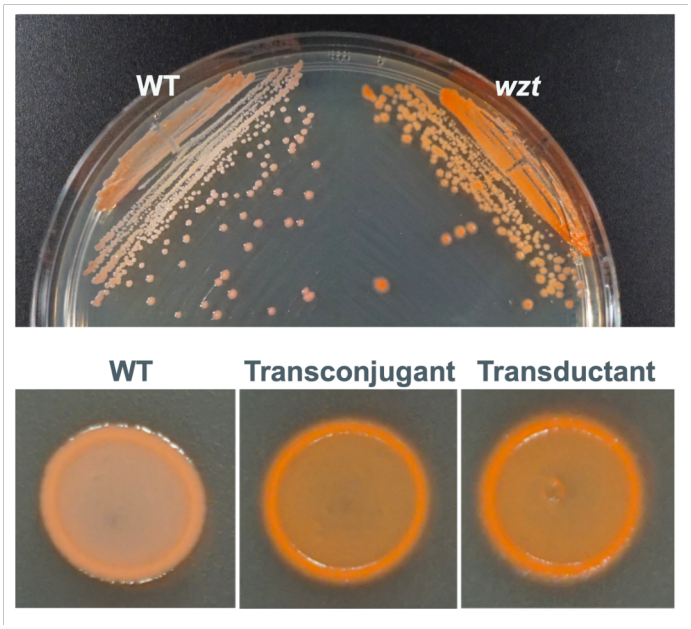


Fig. 4.2. The mutation in *wzt* generates characteristic colonies and its phenotype is due to the transposon insertion. Top: WT and *wzt* mutant strains streaked out in LBA plates grown for two days. Bottom: The transposon mutation transduced via φOT8 phage, from the original transconjugant *wzt* into the WT strain validated the insertion as the cause of the phenotype.

Subsequently, to corroborate whether both mutations have the same effect on synthesis of antibiotics, quantitation of prodigiosin and carbapenem levels over time was performed. Both mutants presented increased production of prodigiosin compared to WT synthesis (p <0.012) and between them (p <0.006) only when entering stationary growth phase, at 8 hours of growth (Fig. 4.3, left). In this phase, pigment synthesis of the *wzt* strain reached a peak of approximately fivefold upturn compared to WT strain, and doubled the values from the *1186* strain, confirming the two mutations to have disparate effects on prodigiosin production. In the case of carbapenem, again, both mutations caused significantly higher levels of this antibiotic compared to the WT

strain (p <0.012), but unlike prodigiosin synthesis, no difference between *wzt* and *1186* production was found, except at 10 hours (p =0.027; Fig. 4.3, right). The carbapenem production in the mutant strains was more than double that of WT cells.

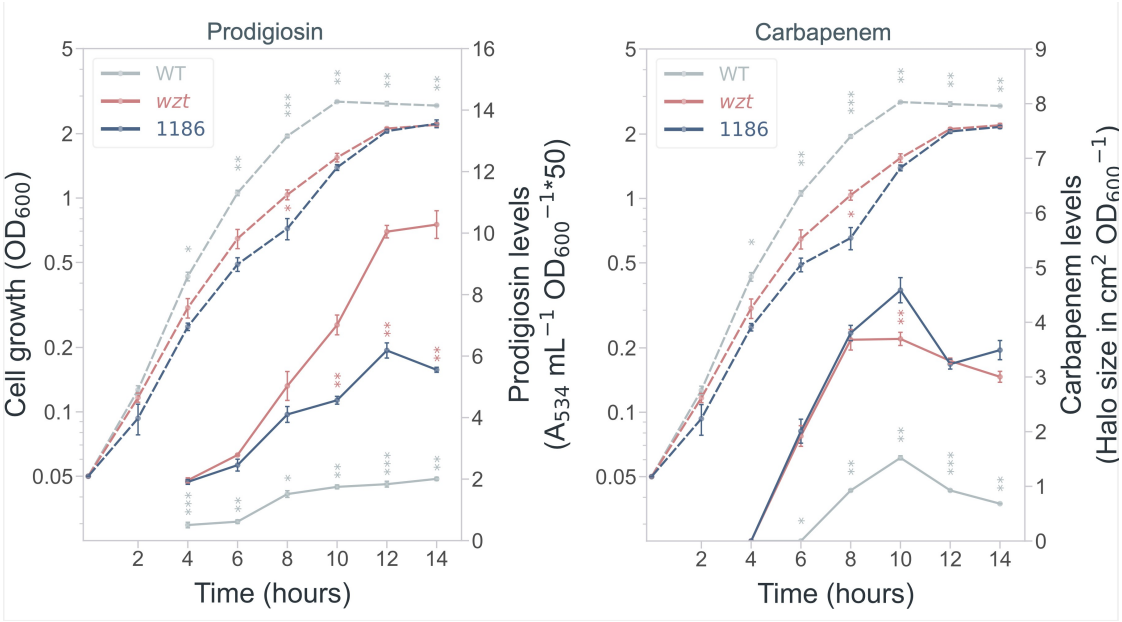


Fig. 4.3. Mutations in *wzt* and *1186* increase the production of antibiotics. Cell growth is depicted as dashed lines (OD_{600}; left Y axes) whereas normalised antibiotic synthesis is indicated as solid lines (right Y axes). Prodigiosin was quantified by spectrophotometry (A_{534}) and the carbapenem by halo formation using an indicator strain. Data from three biological replicates are shown as means ± standard deviation. Statistical analysis was conducted at each time point by multiple unpaired Student's t-test: *p < 0.05, **p < 0.01, ***p < 0.001. Grey stars: differences between WT and the closest mutant's corresponding values; red stars: differences between mutants.

Additionally, both mutants grew significantly slower than WT strain, as indicated by their specific growth rates (μ) comparison (p <0.001), indicating that both insertions affected growth to the same extent. These results confirm that the *wzt* mutation has a higher impact on prodigiosin synthesis than *1186*, carbapenem is produced at similar levels in both genetic backgrounds, and the two mutations have a detrimental effect on cell growth. Hence, as the *wzt* strain had a more marked effect on pigment synthesis, it was chosen as the representative mutation for further studies.

Next, to determine whether the modulation of antibiotic synthesis occurs at the transcriptional level, the *wzt* transposon insertion was transduced out into the fusion strains *pigA*::*lacZ* and *carA*::*lacZ* the first genes of the respective biosynthesis operons – to follow transcription over time through β-galatosidase (LacZ) activity. The prodigiosin cluster (*pigA-O*) transcription was significantly increased (p <0.043) from early growth in the *wzt* background relative to the parental fusion levels, and it was maintained throughout growth (Fig. 4.4, left). The

transcriptional levels of *pigA* in the *wzt* background were approximately 20% to 50% higher than the isogenic reporter.

For carbapenem operon (*carA-H*) transcription, an similar LacZ activity pattern was obtained for the *carA*,*wzt* strain, showing a significant difference (p <0.012) compared to the parental strain (Fig. 4.4, right). This upturn in transcription in the double mutant was between 1.18 and 2.5 times higher than the *carA* strain.

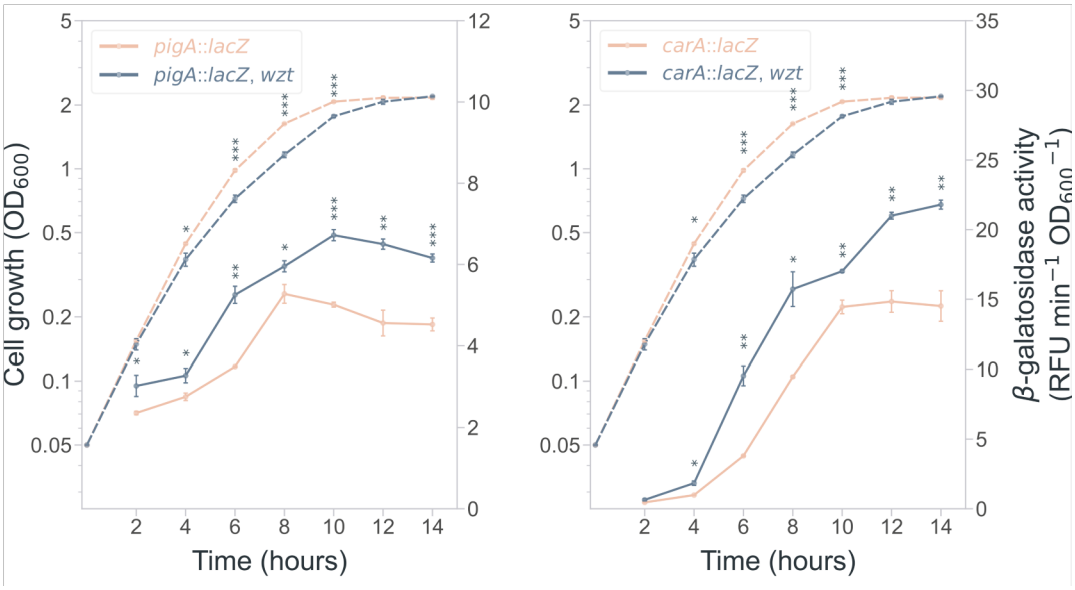


Fig. 4.4. Mutation in *wzt* increases transcription of antibiotic biosynthesis operons. Cell growth is depicted as dashed lines (OD_{600}; left Y axes) whereas normalised β-galatosidase activity is indicated as solid lines (right Y axes). Transcription activity is expressed as relative fluorescence units (RFU). Data from three biological replicates are shown as means ± standard deviation. Statistical analysis was conducted at each time point by multiple unpaired Student's t-test: *p < 0.05, **p < 0.01, ***p < 0.001.

Altogether, these findings confirm that both *wzt* and *1186* mutations, presenting a rough colony morphology, affect cell growth and increase antibiotic production. However, the effect of the *wzt* mutation on prodigiosin production was higher than in *1186*. Furthermore, the increased antibiotic levels in this strain were due to an augmented transcriptional activity of each operon.

4.3. The *wzt* mutation has pleiotropic effects

To further explore the effect of the *wzt* mutation on other phenotypic features of S39006, this mutant strain was characterised. This examination included analysis of gas vesicle production, swimming ability, synthesis of cell-wall degrading enzymes, virulence, and quorum sensing signalling.

4.3.1. Mutation in *wzt* alters transcription of the gas vesicle synthesis cluster

S39006 is capable of synthesising gas vesicles, which allow cells to float in liquid environments. The production of these intracellular structures is directed by two adjacent operons, whose first

genes are *gvpA1* and *gvrA* (Ramsay *et al*, 2011; Tashiro *et al*, 2016). Thus, to dissect the potential effects of *wzt* on gas vesicle production, flotation and transcription assays were conducted. For transcriptional monitoring, the *wzt* mutation was moved into *gvpA1*::*lacZ* and *gvrA*::*lacZ* reporter strains via phage transduction. Flotation assays displayed no visual differences between the mutant and WT strains; both stayed buoyant at comparable heights in liquid culture (Fig. 4.5, top left). Moreover, cells from the assay were inspected by phase contrast microscopy to directly assess differences in gas vesicle content, since they are visible as bright spots (gas vacuoles) (Fig. 4.5, bottom left). Both the mutant and WT gas vesicles content seemed similar, with no obvious differences between them.

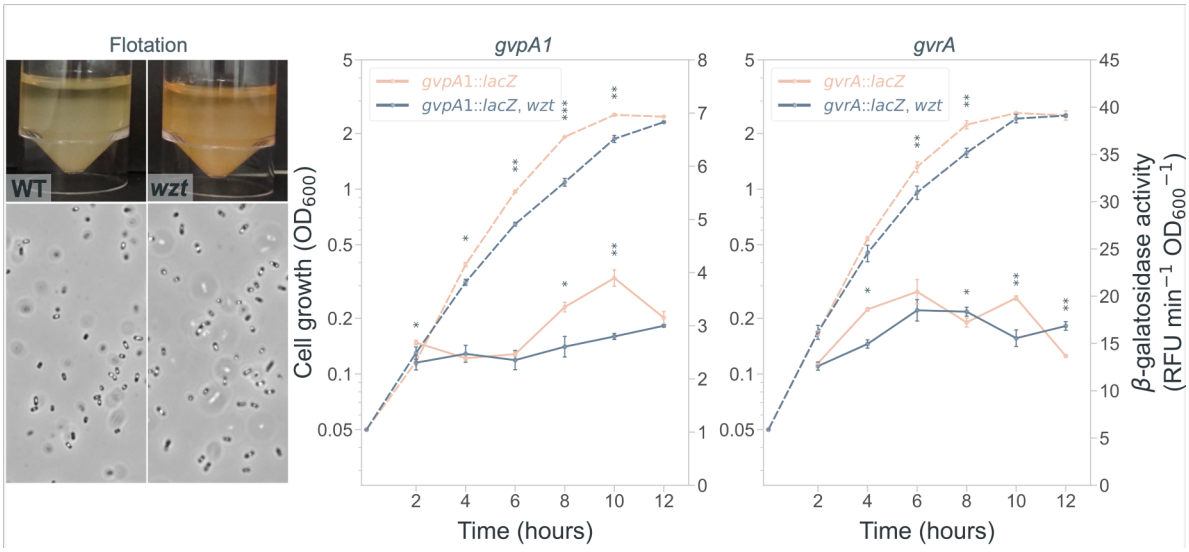


Fig. 4.5. Mutation in *wzt* affects transcription of gas vesicle gene cluster. Flotation cultures of WT and *wzt* strains were left static for 48 h, and cells were examined by phase contrast microscopy (100X oilimmersion lens) and recorded. Bright spots correspond to gas vesicles' presence. For transcription assays, dashed lines represent growth (OD_{600}; left Y axes) whereas solid lines indicate normalised β-galatosidase activity expressed as relative fluorescence units (RFU; right Y axes). Data from three biological replicates are shown as means ± standard deviation. Statistical analysis was conducted at each time point by multiple unpaired Student's t-test: *p < 0.05, **p < 0.01, ***p < 0.001.

To further evaluate whether *wzt* may affect synthesis of gas vesicles at the transcriptional level, LacZ activity from the *gvpA1* and *gvrA* reporter strains was monitored.

In the presence of the *wzt* mutation, *gvpA1* expression increased slightly over time and differed significantly from parental values at early log phase (p =0.032; 16% lower) and when cell growth began to plateau (p <0.01; 28% and 38% lower; Fig. 4.5, middle). Afterwards, the *lacZ* expression from the parental strain decreased. Transcriptional activity of *gvrA* with mutated *wzt* varied over time in the opposite manner to the parental strain (Fig. 4.5, right). Nonetheless, expression differences between the two strains are not clearly defined.

As a result, the *wzt* mutation seems to reduce transcription of *gvpA1-gvpY* and not that of *gvrA-gvrC*, only from log stage of growth. This effect appears negligible when examining gas vesicle

production using flotation assays or cell microscopy after two days, although it is possible that it might be more obvious at a later stage.

4.3.2. Secretion of cell-wall degrading enzymes and motility decreases in *wzt* strain

As a plant pathogen, S39006 produces two different types of cell-wall degrading enzymes, pectate lyase and cellulase, that allow cells to penetrate plant tissues, among others. This strain is also motile by flagella, allowing cells to migrate in liquid habitats. The effect of the *wzt* mutation on these attributes was investigated in plate assays. Swimming ability of mutant bacteria was decreased by the transposon mutation (p =0.004), as well as secretion of degrading enzymes (Fig. 4.6). Pectate lyase activity decreased by around 30% (p =0.0027), whilst cellulase was affected to a lesser extent, with a reduction of circa 17% (p =0.0013; Fig. 4.6, middle and right, respectively). Therefore, the *wzt* mutation reduces the production of plant cell-wall degrading enzymes in S39006.

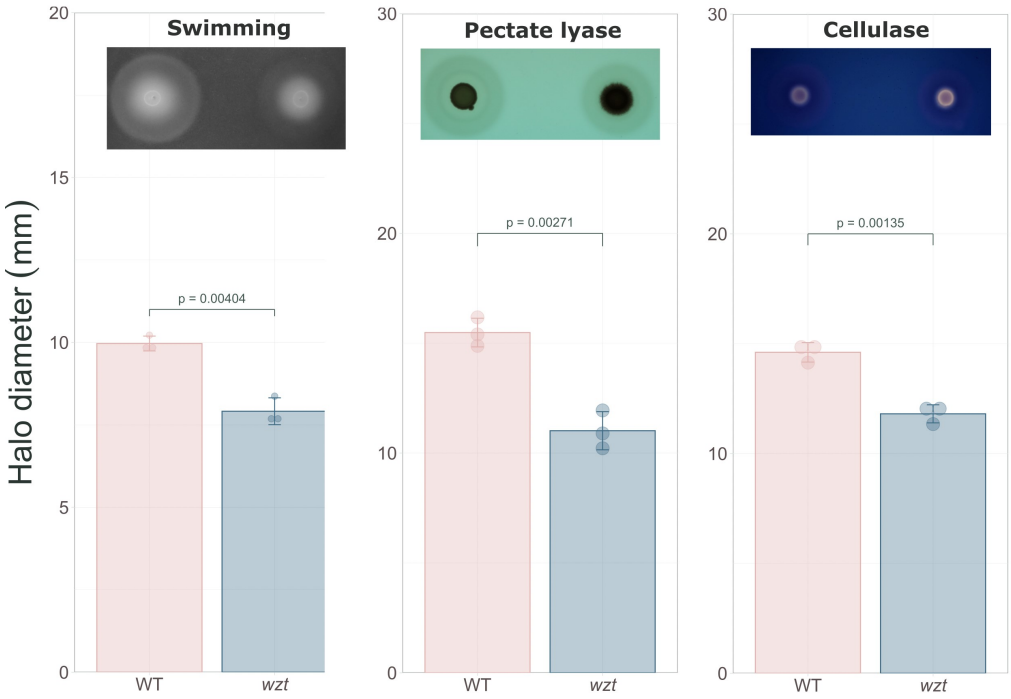


Fig. 4.6. The *wzt* mutation reduced motility and secretion of cell-wall degrading enzymes. Swimming ability, pectate lyase, and cellulase production were measured as halo diameters formed by bacteria from normalised cultures (OD_{600}=1) spots. Data from three biological replicates are shown as means ± standard deviation. Statistical analysis was conducted by Student's t-test (p <0.05). Insets show a representative plate assayed for each attribute.

4.3.3. Mutation of *wzt* attenuates virulence in plants

S39006 is a phytopathogen that causes rotting in potato tubers, and thereby its capacity to infect plants is a key characteristic that was assessed in the *wzt* mutant. The severity of potato infection by this strain versus the WT was evaluated by weighting the total necrotic tissue from rot lesions after 4 days of bacterial inoculation on opposite sides of tubers. The virulence was significantly

reduced in the *wzt* mutant (p =2.25e^{-5}) when compared to the WT rotting capacity (Fig. 4.7). The potato tuber slices exhibited a smaller rotted space at the *wzt* inoculation site compared to that of WT (Fig. 4.7, inset). The reduction of total macerated tissue was approximately 80%; a five-fold diminution in rotten tissue by the mutant.

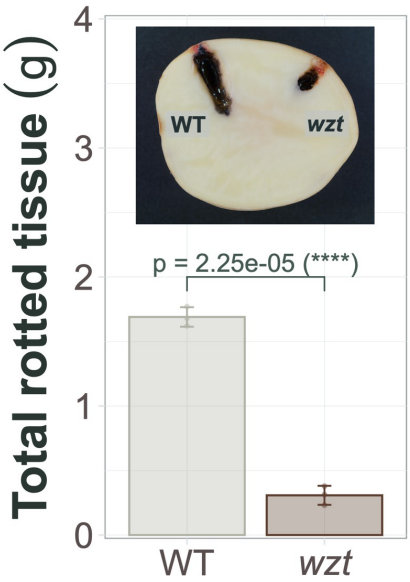


Fig. 4.7. The wzt mutation decreases virulence in plants. Tubers were infected with a normalised cell number (10^7 CFU) and scraped-off rotted tissue was weighted after 4 days. The average weights of three biological replicates (± standard deviation) and significance (Student's t-test) are displayed. Inset: cross section of a representative infected potato (iodine-stained rotten cavities for enhanced visualisation).

To investigate whether cell growth impairment is causing this dramatic effect on infection, bacterial cells recovered from necrotic tissue were serially diluted and grown in minimal medium to test their viability. The WT strain cell count was 10^6 colony forming units (CFU) per gram of tissue, whereas for *wzt* cells the values were 10^5 CFU, indicating a log growth reduction. Previously, an effect from the *wzt* mutation on growth had been ascertained, and hence, the CFU decrease might relate to the attenuated virulence observed given the extent of rotting reduction. Moreover, this outcome agrees with the reduced synthesis of cell-wall degrading enzymes exhibited by this mutant, which play a pivotal role in initiating the cell invasion. Therefore, it appears that this mutation reduces the synthesis of essential enzymes needed for plant invasion, which results in a weakened virulence capacity.

4.3.4. Mutation in *wzt* diminishes the synthesis of acyl-homoserine lactones

The cell-to-cell communication system called quorum sensing (QS) in S39006 is driven via two signalling molecules, but N-butanoyl-L-homoserine lactone (BHL) largely predominates. These molecules, commonly grouped and termed acyl-homoserine lactones, are synthesised in this strain by SmaI, a LuxI-type synthase. Consequently, to examine whether the *wzt* mutation impinges on QS signalling molecule production, the *smaI*::*lacZ* reporter strain was employed.

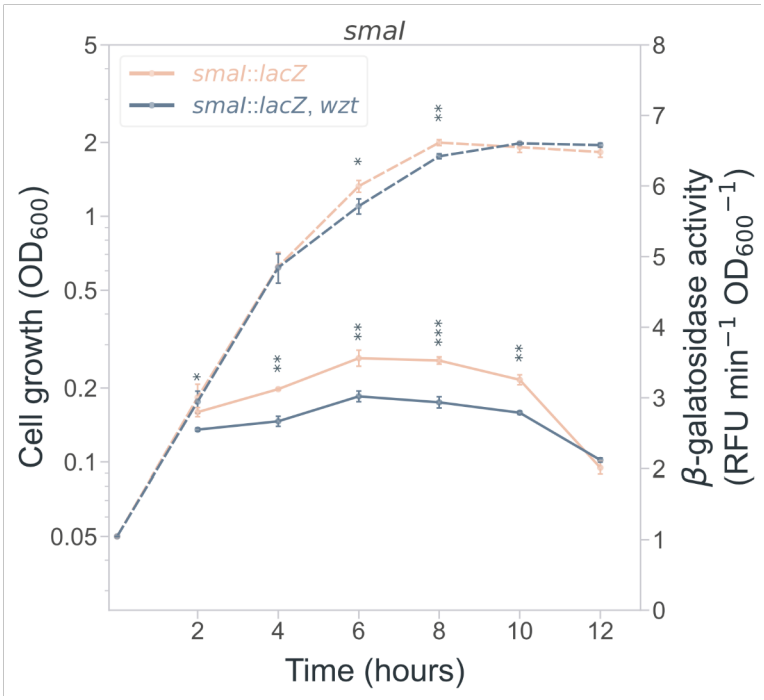


Fig. 4.8. The *wzt* mutation decreases synthesis of acyl-homoserine lactones. Cell growth is depicted as dashed lines (OD_{600}; left Y axis) whereas normalised β-galatosidase activity is indicated as solid lines (right Y axis). Transcription activity is expressed as relative fluorescence units (RFU). Data from three biological replicates are shown as means ± standard deviation. Statistical analysis was conducted at each time point by multiple unpaired Student's t-test: *p < 0.05, **p < 0.01, ***p < 0.001.

The additional mutation of *wzt* in the *smaI* reporter strain caused a reduction in LacZ activity through time, compared to its isogenic strain (p <0.013), and this activity reached the parental levels towards late stationary growth (Fig. 4.8). Such a reduction in expression ranged between 12-20% of the regular values observed in the *smaI* strain. Therefore, the *wzt* mutation appeared to slightly reduce the transcription of *smaI*, the acyl-homoserine lactone synthase, and in turn, the total synthesis of QS autoinducer molecules in this strain.

On the whole, the mutation of *wzt* has pleiotropic effects in S39006. Other than antibiotics, the inactivation of this gene also altered the colony morphology, reduced the synthesis of plant cell-wall degrading enzymes, motility, virulence, and the production of QS communication signals.

4.4. Overexpression of *wzt* and *1186* partially complements their correspondent mutants.

The two adjacent genes affected by the transposon insertions, *wzt* and *1186*, are within an operon (Fig. 4.9, top), and therefore, a single transposon insertion could lead to transcriptional termination of downstream genes and their loss of function (polar effects). To examine to what extent each of the two genes might restore the WT phenotype, plasmid-encoded leaky expression of *wzt* and *1186* was exploited. The coding sequences of these genes were cloned into the high-copy-number pQE80-oriT (*p*-) system, yielding the *p-1186* and *p-wzt* constructs, which were used to transform *E. coli* β2163. This strain was then used as a donor to conjugate the constructs into the recipient strains WT, *1186*, and *wzt*, to examine the corresponding expression effects.

The genetic complementation showed that the empty vector control caused no obvious effects on the tested strains, as expected (Fig. 4.9, *p-* row). However, the overexpression of *1186*, the penultimate gene of the operon, led to a surge in WT pigmentation, compared to the strain harbouring the empty vector. It reverted the colony roughness and irregular edges of the *1186* mutant, but not comparable to the WT colony aspect (Fig. 4.9, p-*1186* row). This might imply that 1187 activity is also required for complete phenotype restoration. The overexpression of *1186* had no discernible effects on the *wzt* mutant colonies.

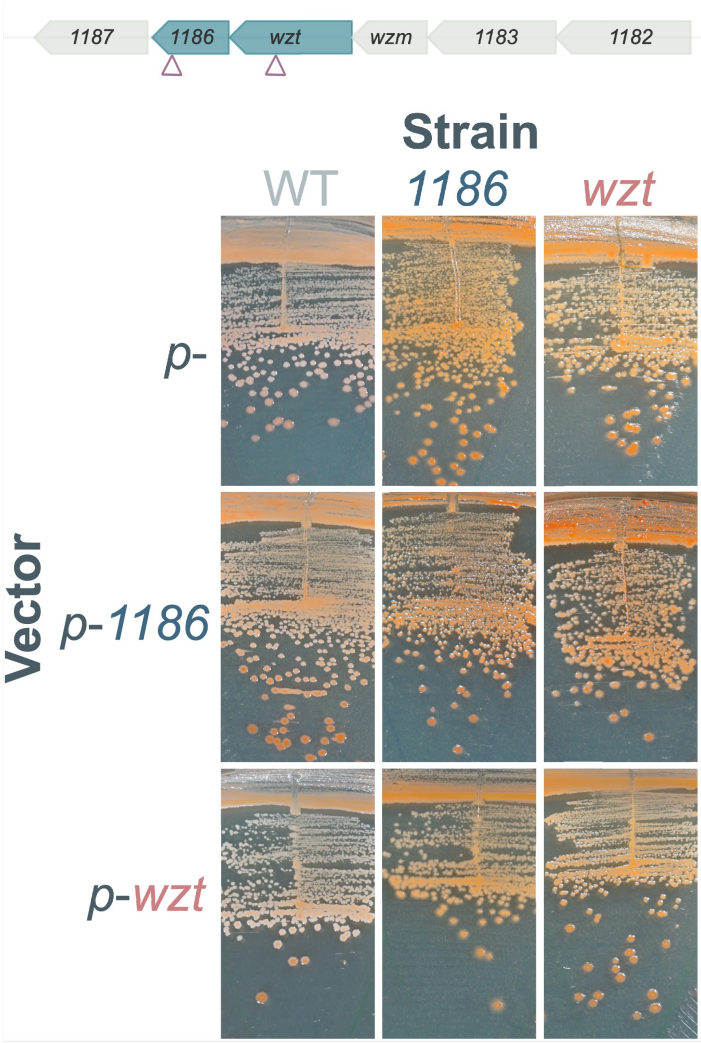


Fig. 4.9. Overexpression of *wzt* and *1186* partially complements their corresponding mutant strains. Transposon-inserted genes are highlighted in blue (top) and red triangles denote the transposon insertion sites. Panels display colonies of the three complemented strains (columns) grown on LBA selection plates for two days. The vectors (rows) used to complement the strains correspond to the pQE80-oriT (*p-*) system expressing either *1186* (*p-1186*) or *wzt* (*p-wzt*).

The expression of *wzt in trans* did not modify the visual morphology phenotype of WT or *1186* colonies (Fig. 4.9, p-*wzt* row), indicating that 1186 activity is necessary for normal colony morphology. However, its overexpression did largely restore the colony morphology of the *wzt* strain, bringing it closer to WT, albeit not full restoration, as the complemented colonies

remained slightly rough. This effect, equivalent to that observed from the complementation of *1186* on its mutant, suggests that the 1186 gene is at least partially active. Overall, these results show that both genes are independently important for maintaining at least the colony morphology in S39006. Unfortunately, the effect of 1187, encoded in the putative last gene of the operon, could not be tested on these strains due to time limitation, as the cloning of one of the DNA fragments spanning *wzt-1187* and *1186-1187* was not completed. Also, the quantitation of prodigiosin production to determine the level of restoration, if any, in complemented strains, could not be performed.

4.5. The *wzt* mutation is epistatic to several known antibiotic synthesis regulators

To infer possible mechanisms by which the *wzt* mutation enhances antibiotic synthesis in S39006, double mutants with 14 known regulators were generated via phage transduction. In this way the interaction of *wzt* with the current regulatory network was explored by quantifying antibiotic production at early stationary growth and comparing double mutant versus single isogenic mutant biosynthesis. Furthermore, given that some regulatory mutants are fusion strains, the effect of *wzt* on their transcription was also assayed. The double mutant *rsmA*,*wzt* displayed seriously defective growth, and therefore, it was not incorporated into the analysis. Hence, 13 double mutants, plus WT and *wzt* mutant as controls, were employed to examine functional interactions. The *wzt* mutation bypassed prodigiosin production of 10 regulatory strains, significantly rising their biosynthesis (Fig. 4.10).

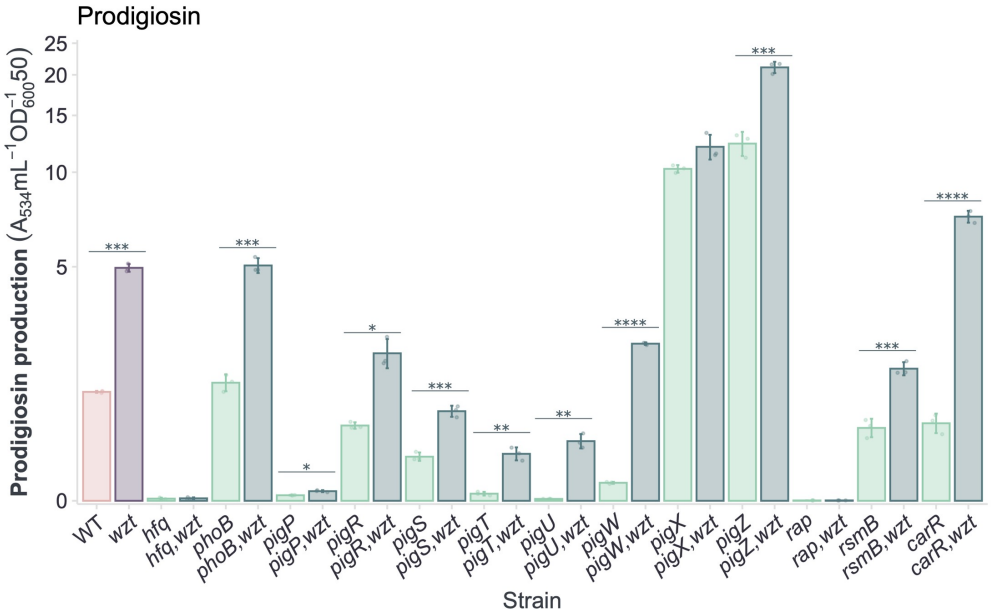


Fig. 4.10. The *wzt* mutation bypassed prodigiosin production control of several known regulators. Prodigiosin synthesis was quantified by spectrophotometry (A_{534}) and normalised by cell growth (OD_{600}). Darker-coloured bars indicate the presence of the *wzt* mutation. The means of data ± standard deviation from three biological replicates taken at an early stationary phase are shown. Statistical analysis was conducted by Student's t-test: *$p < 0.05$, ** $p < 0.01$, *** $p < 0.001$, **** $p < 0.0001$.

Major differences in pigment production were found for *carR* (p=9.18e^{-5}), *pigT* (p=0.0063), *pigW* (p=1.23e^{-6}), and *pigU* (p=0.0058), in which the increase in synthesis ranged from 6.3 (*carR*) up to 32 (*pigU*) times the isogenic levels. The production also increased for the rest of regulators, although to a lesser extent, displaying changes between 1.7 and 2.7 times relative to parental values. In increasing order, these regulators were *pigZ* (p=0.00041), *pigP* (p=0.0135), *rsmB* (p=0.00079), *pigS* (p=0.00082), *pigR* (p=0.0175), and *phoB* (p=0.00035). Mutations in *hfq* and *rap*, unable to synthesise antibiotics, were not bypassed by the *wzt* mutation, supporting their role as key drivers for antibiotic production. The only double mutant displaying no pigmentation changes when compared to its isogenic counterpart was *pigX*, encoding a cyclic dimeric guanosine monophosphate (GMP) phosphodiesterase, suggesting it might play a role in the boosted pigment production of *wzt* strain.

As observed in prodigiosin production, the additional mutation of *wzt* caused carbapenem synthesis to increase in the majority of known regulators' backgrounds (Fig. 4.11).

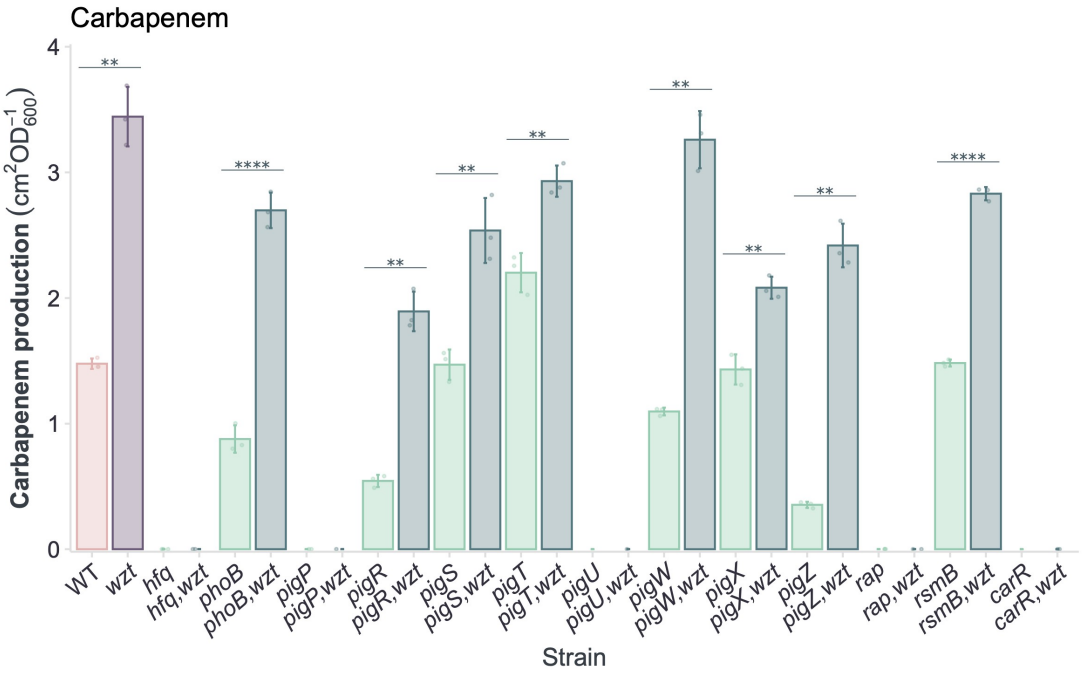


Fig. 4.11. The *wzt* mutation bypassed carbapenem production control of several known regulators. Carbapenem synthesis was quantified by halo formation using an indicator strain and normalised by cell growth (OD_{600}). Darker-coloured bars indicate the presence of the *wzt* mutation. The means of data ± standard deviation from three biological replicates taken at an early stationary phase are shown. Statistical analysis was conducted by Student's t-test: *$p < 0.05$, ** $p < 0.01$, *** $p < 0.001$, **** $p < 0.0001$.

Significant changes were detected for *pigX* (p =0.0023), *pigT* (p =0.0038), *pigS* (p =0.00886), *rsmB* (p =3.46e^{-5}), *pigW* (p =0.0032), *phoB* (p =9.40e^{-5}), *pigR* (p =0.00236), and *pigZ* (p =0.00198). Double mutants with *pigX*, *pigT*, *pigS*, and *rsmB* produced 1.3 to 1.9 times higher carbapanem levels than parental regulator strains, whilst *pigW*, *phoB*, *pigR*, and *pigZ*, produced

even more, with values that went from 2.9 to 6.8 times, respectively. Mutations that cease production of this antibiotic (*hfq*, *pigP*, *pigU*, *rap*, and *carR*) were not bypassed by the *wzt* disruption.

To investigate whether the *wzt* mutation influences the expression of the 8 reporter strains present in the library used for antibiotic quantitation, LacZ activity was measured. Disruption of *wzt* showed no effect on transcription of *pigR*, *pigT*, *pigU*, *pigW*, whose double mutants produced higher levels of both antibiotics, except *pigU*, on which carbapenem synthesis could not be restored by the *wzt* mutation (Fig. 4.12). In contrast, disrupted *wzt* had an effect on expression of *pigS* (p= 0.00876), *pigX* (p= 0.00126), *pigZ* (p= 0.00628), and *carR* (p= 0.0219). Transcriptional activity was thus increased by 19%, 28%, and 44% for *pigZ*, *pigX*, and *pigS*, respectively, whereas it diminished by 14% for *carR*. Antibiotic levels were higher for *pigZ* and *pigS* double mutants, whilst *pigX* exhibited unchanged pigmentation and increased synthesis of carbapenem.

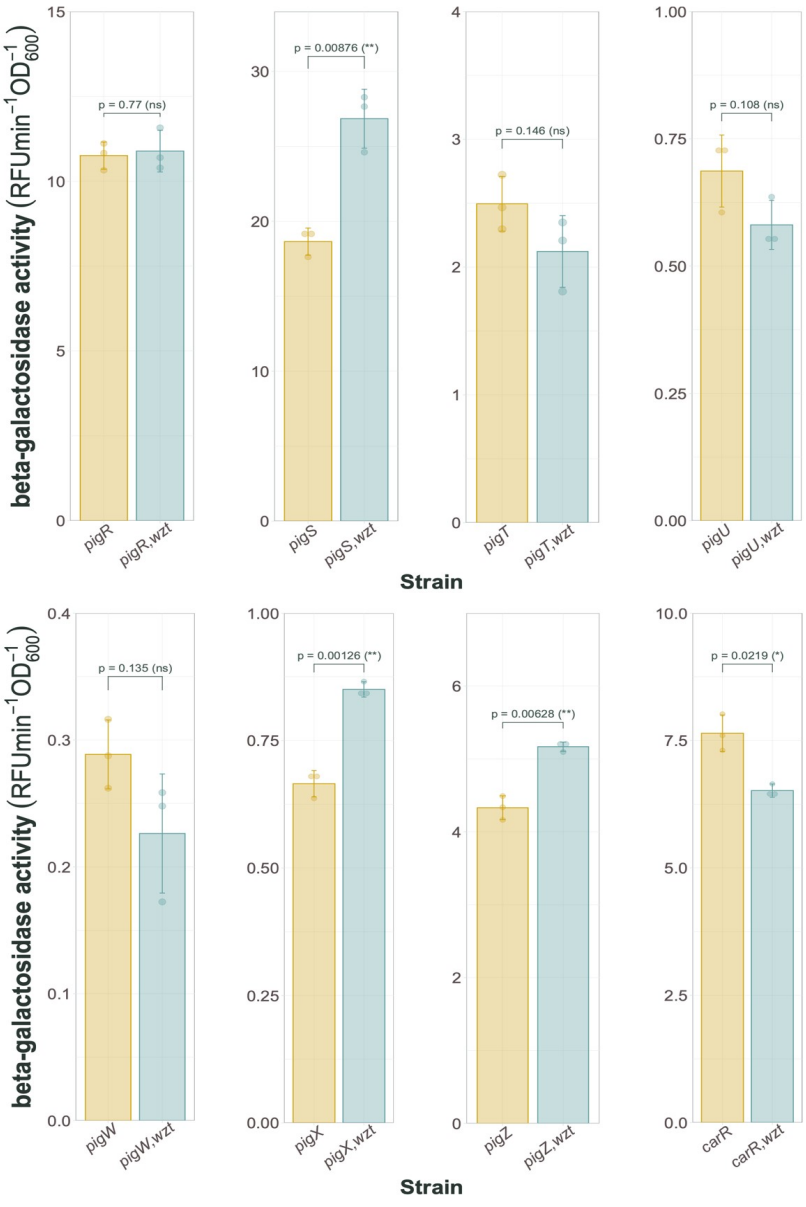


Fig. 4.12. Mutation in *wzt* affects transcription of *pigS*, *pigX*, *pigZ*, and *caR*. Normalised β-galactosidase (LacZ) activity is expressed as relative fluorescence units (RFU). The average of three biological replicates (± standard deviation) and significance (Student's *t*-test) are shown.

Taken together, these results show that the *wzt* mutation was epistatic over several known regulators of antibiotic production in S39006. This mutation in a *pigX* genetic background showed no changes in prodigiosin synthesis compared to the isogenic pigment regulator, suggesting that increased levels of prodigiosin in the insertion strain might be related to PigX activity. Moreover, the *wzt* mutation increased transcription of *pigX* at early stationary growth. In the case of the carbapenem, candidate regulators through which *wzt* acts are less clear. Possibly, PigP or Rap might drive the hyperproduction of this antibiotic, since there were no significant transcriptional changes in *pigU*, and expression of *carR* in *wzt* is reduced, in contrast to its effect on *carA*.

4.6. Discussion

This chapter describes the effect of an O-antigen transport gene on biosynthesis of antibiotics in S39006. Two transposon insertions in consecutive genes, that form an operon along with others, changed pleiotropically the colony morphology and enhanced the production of carbapenem, as well as the prodigiosin levels, but to different extents. Thus, the *wzt* mutation, having a greater effect on pigment synthesis, was selected for further characterisation.

The Gram-negative bacterial cell envelope comprises an inner and outer membrane, with a peptidoglycan-containing space in between; the periplasm. The vast majority of these bacteria contain phospholipids on the cytoplasmic inner side, whilst these molecules are only present in the inner leaflet of the outer membrane, whose external layer is predominantly made up of lipopolysaccharide (LPS; Henderson *et al*, 2016; Bertani and Ruiz, 2018; Di Lorenzo *et al*, 2021). LPS is constituted by three main zones: the hydrophobic lipid A, the core oligosaccharide, and the O-antigen polysaccharide. The lipid A is a widely conserved moiety that connects the LPS to the outer membrane, whereas its other end attaches the core oligosaccharide. Finally, the O-antigen polysaccharide–the most variable and distant component–lacking in several bacterial strains, is joined to the core, becoming the outermost part of the mature LPS (Raetz and Whitfield, 2002; Whitfield and Trent, 2014; Sperandeo *et al*, 2017; Simpson and Trent, 2019). The composition of this O-antigen chain are repeats of one or more sugar residues whose length varies widely, even within species, and usually are not essential for viability (Greenfield and Whitfield, 2012; Kalynych *et al*, 2014).

There are three mechanisms by which the synthesis and export of O-antigen is carried out: the synthase-dependent, the Wzy-dependent, and the ABC transport pathway. Regardless of the mechanism, undecaprenol phosphate (und-P) is the acceptor of O-antigen units to build the

nascent chain (Whitfield and Trent, 2014). The synthase-dependent mechanism is the least common and therefore poorly characterized pathway. It relies on a multifunctional synthase complex that synthesises and exports the repeat units through the inner membrane (Whitney, 2013; Low and Howell, 2018). In the Wzy-dependent pathway, the carbohydrate units are produced on the cytoplasmic side of the inner membrane and are individually exported to the periplasmic side by the Wzx flippase. Once there, the repeat units are joined together by the polymerase Wzy to yield the final chain (Hong *et al*, 2017). Finally, in the ABC transport-mediated mechanism, the entire O-antigen polymerisation takes place in the cytoplasm via glycosyltransferases, and when the polysaccharide is completed, it is translocated across the inner membrane via the Wzm/Wzt transport system, comprised of a transmembrane permease and an ATPase, respectively (Cuthbertson *et al*, 2010; Whitfield and Trent, 2014; Whitfield *et al*, 2020). Regardless of the mechanism, the full O-antigen chain, localised on the periplasmic side of the inner membrane, is finally ligated to the lipid-A core by WaaL to generate the mature LPS (Greenfield and Whitfield, 2012). In this system, the control of the O-antigen length is generally mediated by adding a methyl residue to the terminus by homologues of WbdD, and the extension of the polysaccharide chain by glycosyltransferases such as WbdA (Olsthoorn *et al*, 2000; Clarke *et al*, 2004; Greenfield and Whitfield, 2012; Mann *et al*, 2019). Recently, in the phytopathogen *Pseudomonas syringae*, an operon containing genes encoding homologues of the ABC transport system, WbdD, and WbdA was described (Jayaraman *et al*, 2022) and it resembles the predicted functions only from the *wzm* to the end of the S39006 operon. Hence, 1186 and 1187 might fulfill the WbdA and WbdD functions.

In the *Serratia* genus, the strain *S. marcescens* O16 was the first member examined for the presence of the *rfb* gene cluster (referring to the O-antigen gene cluster). The strain contained an ATPbinding cassete and a permease, almost identical to the corresponding genes present in *Klebsiella neumoniae* O1. This was the earliest evidence of the RfbAB, the Wzm/Wzt ABC-transport, operating in this genus (Szabo *et al*, 1995). Later, in *S. marcescens* O4, the O-antigen cluster was characterised, and it encompasses six genes: *rmlC*, *rmlD*, *wbbL*, *wzm*, *wzt*, and *wbbA* (Saigi et al, 1999). Their assigned functions, apart from *wzm*/*wzt*, were: *rmlC*: dTDP-4-dehydrorhamnose 3,5epimerase, *rmlD*: dTDP-rhamnose synthase, *wbbL*: rhamnosyltransferase, and *wbbA*: glycosyltransferase. Thus, most of them are involved in the rhamnose synthesis pathway. Furthermore, the authors demonstrated that the last enzyme, WbbA, is essential for O-antigen synthesis. Regarding other *Serratia* species, no specific information was found, hence, this is an open topic to explore further. According to the BLASTp analysis performed in this study, for all the six protein sequences comprising the O-antigen operon in S39006, the only *Serratia* member on the 100-best-hits list was *S. symbiotica* (42.1% identity), for the Wzt

sequence queried. No other member of this genus appeared in the search of the remaining proteins. Thus, this fact raised the question about how genetically close is S39006 to other *Serratia* members. To shed some light, a study on the phylogeny of *Dickeya* species revealed that S39006 –originally intended as an outgroup– clusters with other *Dickeya* strains. The authors also revealed that S39006, on average, shares more protein families with *Dickeya* (60.5%) than other defined *Serratia* species (51.2%). Nevertheless, S39006 was different enough from *Dickeya* species, and it was therefore suggested to define a new lineage under the name of *Prodigiosinella confusarubida* (Duprey *et al*, 2019). Following these relationships, it was discovered that some O-antigen operonic arrangements in *Dickeya*'s strains exhibit a pattern equivalent to that of S39006. The most similar operons are comprised of eight genes: *cpsB*, *cpsG*, *gmd*, *wzm*, *wzt*, *fcl*, *wbeA*, and *wbeB*, in some strains of *D. dadantii*, *D. dianthicola*, *D. fangzhongdai*, and *D. solani* species (Ranjan *et al*, 2021). Cps genes are involved in colanic acid production, and *cpsB* and *cpsG*, encoding a mannose-1-phosphate guanylyltransferase and a phosphomannomutase, respectively, seem homologues of *1182* and *1183*, given their function. On the other hand, *gmd* and *fcl*, related to GDP-L-fucose biosynthesis, have no homologues in the O-antigen locus in S39006.

This research group is responsible for the only study that reports the effects of O-antigen locus mutations in S39006. In the pursuit of gas vesicle regulators by random transposon mutagenesis, a *pigC* strain, lacking pigmentation to avoid interference in the screening, was used as parental strain. From the screening, three mutants displaying the so-called "bull's-eye transparent" phenotype were isolated (Quintero-Yanes, 2018). Two insertions were found on *wzt* and one in *1186*, which presented the colony morphology changes described here previously. This rough colony phenotype, displaying a dry and spread aspect, is often linked to mutations in O-chain biosynthetic genes, as this bestows the smooth aspect to colonies (Knirel *et al*, 2001; Mesarich *et al*, 2017). From the genetic complementation, it was observed that each gene could largely restore the colony morphology of their correspondent mutation, albeit not completely, and their overexpression on the opposite mutant caused no visible effect. This shows that each of the genes tested are important for at least the colony morphology.

Regarding gas vesicle production, the strains reported by Quintero-Yanes (2018) were shown to sink in flotation assays only after three days when the cultures were left static, a longer time period than it is usually tested, as conducted in this work. Hence, these O-antigen mutations might cause the cells to plunge at a slower pace compared to other gas vesicle regulators (e.g. Lee *et al*, 2017). Microscopy cell images demonstrated the presence of bright structures, comparable to WT, even after three days. That work suggested that cell aggregation in the O-antigen mutants

may impact flotation capability, despite retention of gas vesicles. No further characterisation of these strains was performed in that study.

In this work, both *wzt* and *1186* mutations, in addition to altering the colony shapes, seemed to enhance antibiotic production. Carbapenem synthesis was increased in a similar fashion by both insertions, whereas the *wzt* mutation showed a more profound effect on prodigiosin synthesis, and it was therefore chosen for analyses. In this genetic background, the expression of the biosynthesis operons, *pigA-O* and *carA-H*, increased, implying that the surge in antibiotic production occurs at a transcriptional level. The quantitation of prodigiosin and carbapenem levels in double mutants of *wzt* with 13 known regulators, provided some clues about possible regulatory connections through which this O-antigen transport gene might modulate antibiotic synthesis.

For pigment production, nearly all the known regulators were bypassed by the *wzt* mutation, except for *hfq*, *rap*, and *pigX*. Hfq is a well-known RNA-binding protein that regulates many physiological processes in prokaryotes at the post-transcriptional level (Updegrove *et al*, 2016), and its deletion in S39006 completely abrogates the synthesis of antibiotics (Wilf *et al*, 2011). Likewise, Rap is a key transcriptional regulator that activates production of both antibiotics, operating at the transcriptional level; mutants do not make the antibiotics (Thomson *et al*, 1997). The only known regulator whose pigment synthesis remained unchanged upon *wzt* insertion was *pigX*. The synthesis of both the double and the isogenic regulator were not significantly different from each other and reached higher levels than WT and *wzt* strains. Therefore, PigX activity might be important in Wzt's mode of action for prodigiosin control. This regulator is predicted to be a membrane protein and it only modulates pigment synthesis, by repressing the transcription of the biosynthesis operon. Its suggested mechanism is based on one of its domains, EAL, which was sufficient to successfully complement the *pigX* mutant, although a GGDEF domain is also present in the regulator (Fineran *et al*, 2007). Thus, the active EAL domain implies that this protein functions as a cyclic dimeric phosphodiesterase (PDE), involved in a conserved bacterial secondary messenger. This messenger is bis-(3′-5′)-cyclic dimeric guanosine monophosphate (c-di-GMP), an intracellular signalling molecule that modulates multiple processes. It is synthesised by diguanylate cyclases (DGCs), degraded by phosphodiesterases (PDEs), and it exerts action through c-di-GMP-controlled effectors (Valentini and Filloux, 2019). The *wzt* mutation was shown to increase the expression of *pigX* by 28%, which reveals a connection between these genes. However, an enhanced activity of PigX, a PDE, should be expected to reduce the c-di-GMP levels, which in turn would generate lower prodigiosin production. This is a contradictory observation given that *wzt* increased the pigment levels. Nonetheless, it is important to note that bacteria encode multiple producers and degraders of c-di-GMP, and the associated effector

proteins vary widely (Valentini and Filloux, 2019). Therefore, there must be more actors involved if the increase of this antibiotic in the *wzt* strain relates to c-di-GMP signalling.

In the literature, work connecting O-antigen and the c-di-GMP messenger, showed that a methyltransferase, WarA, which also has a GGDEF domain, interacts with the DGC SadC to modify the O-antigen modal distribution in *P. aeruginosa*. Furthermore, WarA binds to c-di-GMP and this interaction intensifies its enzymatic activity. As a result, the authors claimed that c-diGMP levels influence WarA methyltransferase activity, which leads to modified LPS profiles that help cells avoid immune host responses (McCarthy *et al*, 2017). WarA is a homologue of WbdD, which signals the O-antigen termination by sugar methylation and prepares its export in *E. coli* O9a (Hagelueken *et al*, 2012). Thus, 1186, the transposon-altered methyltransferase, that probably influences O-antigen synthesis by extending its length, might act through c-di-GMP levels or another molecule. In the case of the *wzt* mutation, the lack of the ATPase impedes the transport of O-antigen chains because pumping is not possible without ATP hydrolysis (Wilkens, 2015). In either case, it is not obvious how a mutation in the O-antigen locus could augment the c-di-GMP levels, which, following the PigX mechanism described, would increase the expression of the pigment biosynthesis cluster. This protein was the first regulator linked to c-di-GMP signalling reported in this laboratory to control antibiotic biosynthesis (Fineran *et al*, 2005; 2007). Later, this signalling molecule was also linked to antibiotic synthesis in *Streptomyces coelicolor* via BldD (den Hengst *et al*, 2010). More recently, this messenger has been associated with antibiotic biosynthesis in *Lysobacter enzymogenes* (Chen *et al*, 2017; Shu *et al*, 2018; Han *et al*, 2019; Xu *et al*, 2021; Shu *et al*, 2022) and *Streptomyces ghanaensis* (Nuzzo *et al*, 2020; Makitrynskyy *et al*, 2020), through multiple connections to different effectors and complexes.

An increase in the carbapenem levels of the majority of *wzt* double mutants versus their isogenic counterparts was detected, except in the backgrounds of five regulators. Excluding the above mentioned *hfq* and *rap*, the *wzt* mutation could not additionally revert the abolition of synthesis of carbapenem in *carR*, *pigU*, and *pigP* mutants. This outcome was expected for CarR as this is an exclusive LuxR-type activator of the carbapenem biosynthesis cluster (McGowan *et al*, 1995). PigU, is a HexA transcriptional regulator, and it was predicted to control the production of both antibiotics by repressing the expression of their biosynthetic cluster (Fineran *et al*, 2005), and the *wzt* mutation did not alter its transcription. Finally, PigP is a master transcriptional regulator that controls seven other regulators (*carR*, *pigQ*, *pigR*, *pigS*, *pigV*, *pigX*, and *rap*). As in the prodigiosin biosynthesis cluster, the *wzt* mutation increased the expression levels of the carbapenem operon, suggesting that the mechanism acting in this case should be at the transcriptional level. Unfortunately, it is not clear how some of the known mutations that abolish the production of this antibiotic help mediate the *wzt* effect.

The *wzt* insertion mutant exhibited an attenuated pathogenicity capacity when tested in potato rotting assays, relative to the WT strain. Supporting this finding, cells devoid of this gene synthesised lower levels of the exoenzymes required to initiate plant invasion, pectate lyase and cellulase, which is the most probable reason for the impaired virulence registered through this potato tuber assay. This diminished infection capacity in LPS mutants has been previously reported for other plant pathogens such as *Erwinia amylovora* (Berry *et al*, 2009) and *Pseudomonas syringae* (Kutschera *et al*, 2019). Another interesting effect of the inactivation of *wzt* was the decreased production of the QS signalling molecules collectively known as acyl-homoserine lactones. It has been reported that this chemical communication system plays a central role in antibiotic biosynthesis in S39006. This strain produces and senses the signalling molecules via homologues of the LuxI-R system: the synthase SmaI and the regulator SmaR (Thomson *et al*, 2000; Slater *et al*, 2003). This regulator controls the transcription of another four regulators (*pigQ*, *pigR*, *rap*, and *carR*) through which it modulates the production of antibiotics, in tight response to the acyl-homoserine lactones concentration (Slater *et al*, 2003; Fineran *et al*, 2005). By exploiting the *smaI*::*lacZ* reporter strain, the mutation in *wzt* was found to reduce the expression of this gene, and thus the total synthesis of the QS signals.

The evidence provided in this chapter shows that a mutation in an O-antigen transport gene *wzt* provokes enhanced antibiotic production in the S39006 model. Additionally, this surge in synthesis results from a transcriptional effect on the biosynthetic gene clusters. Possible mechanisms of action for the improved production of both compounds were also experimentally conducted by interrogating links to a large set of known regulators. Furthermore, other phenotypic effects in the wake of the wzt inactivation were ascertained, highlighting its highly pleiotropic consequences.

Chapter 5. An intergenic mutation led to a novel antibiotic production regulator, VfmE

The last transposon mutant investigated in this work had an insertion in an intergenic region that resulted in a hyperpigmented phenotype. This disruption occurred between two genes, *argG* and *vfmE*, which are convergently transcribed. Previous work provided some insights from the insertion region. The characterisation of the intergenic and *vfmE* mutations showed that they provoke contrary effects not only in antibiotic synthesis, suggesting an interplay between them.

5.1. Genomic context of the intergenic transposon insertion

The strain initially named NJ6, then termed IGR (which stands for **i**nter**g**enic **r**egion), was selected from the screening of mutants due to its hyperpigmented phenotype. This strain was found to harbour a transposon insertion in a region between two coding sequences that are convergently transcribed. These genes are single transcriptional units and the intergenic region between their coding areas is 477 bp long. The transposon interruption was mapped 330 and 147 bp away from the stop codons of genes *argG* and *vfmE*, respectively (Fig. 5.1, bottom). *argG* encodes an argininosuccinate synthetase, involved in arginine biosynthesis. The product of *vfmE* is an AraCfamily transcriptional regulator, associated with a virulence-linked quorum sensing system in *Dickeya*, as its name denotes (**v**irulence **f**actor **m**odulating, *vfm*). Upstream of the latter, two other homologue members of the *vfm* cluster, *vfmJ* and *vfmF1*, were also found, and further up, the gas vesicle operon locus (Fig. 5.1, top). On the other hand, upstream from *argG*, a gene encoding a ThiJ/PfPi protein, and *xylR*, a regulator known for controlling xylan and xylose utilisation, were also noted.

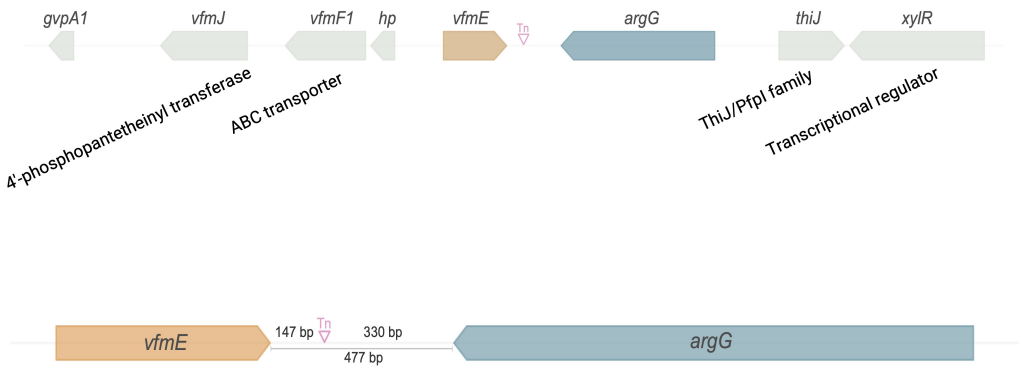


Fig. 5.1. Genomic context of the transposon-disrupted intergenic region. Transposon insertion (pink triangle) is located downstream of the *vfmE* (yellow) and *argG* (blue) coding sequences. Top: an overview of the genomic neighbourhood of the transposon insertion. Genes upstream of *vfmE*: *gvpA1*, a gas vesicle structural protein; *vfmJ* and *vfmF*, proteins from the virulence factor modulating system (*vfm*); *hp*, a hypothetical protein. Genes upstream of the argininosuccinate synthetase, *argG*: *thiJ*, a ThiJ/PfpI domaincontaining protein; *xylR*, a transcriptional regulator. Bottom: a zoomed-in insertion region shows the distances between the transposon location and the termination codons.

To explore the conserved degree of the genes and encoded products products surrounding the transposon insertion region, which might relate to the enhanced pigmentation, a phylogenetic tree for each protein was built. The resulting trees showed a contrast between ArgG and VfmE, with the former being highly conserved across many different genera, whereas VfmE homologues were only found in a few of them (Fig. 5.2). Over 90% identity in different bacterial genera was determined for ArgG from S39006, which groups with various *Dickeya* species in a separate clade from the rest of the hits. Its homologues cluster into five different groups, including species from *Dickeya*, *Brenneria*, *Pectobacterium*, *Yersinia*, and *Lonsdalea* (Fig. 5.2, colour coded groups). For VfmE, in contrast, only three main clusters present homologues of this regulatory protein (identities below 87.3%); a restricted niche of species. The clusters are mostly composed of *Dickeya*, the S39006's VfmE clade, *Pseudomonas*, and *Vibrio* species. Interestingly, no homologues from the *Serratia* genus were found for VfmE.

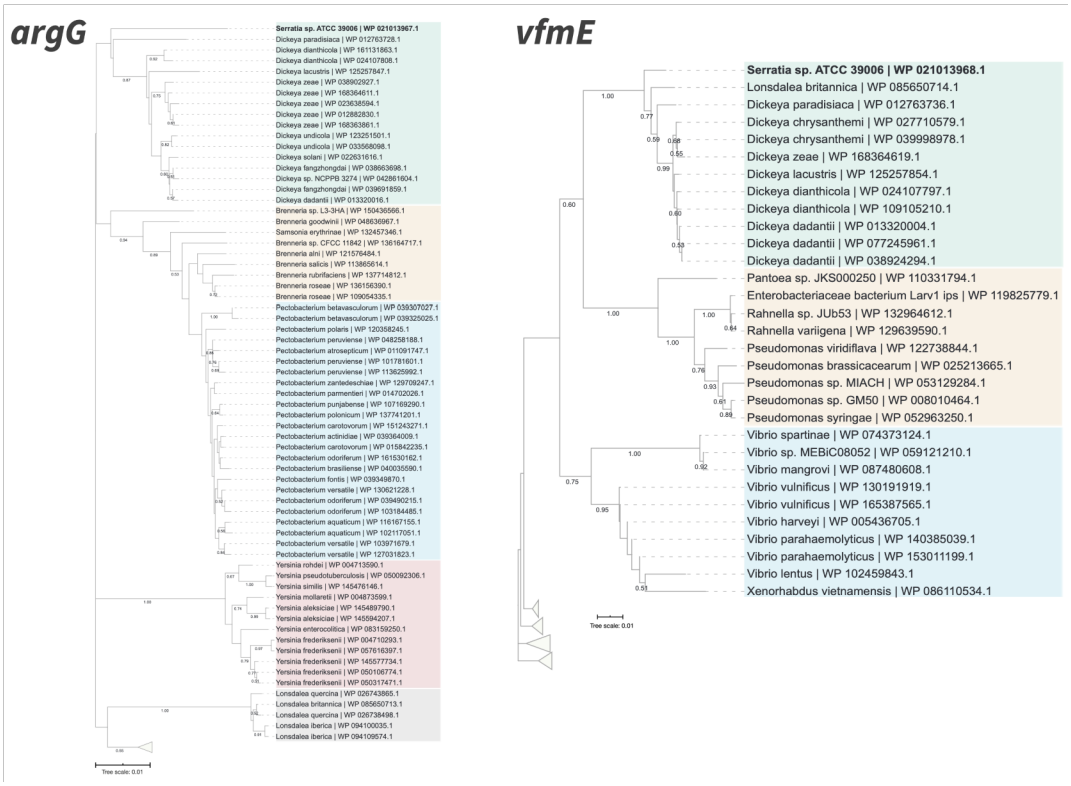


Figure 5.2. Phylogenetic tree of S39006 ArgG and VfmE homologues. Phylogenetic relationship among proteins is shown by a rooted Neighbour-Joining tree constructed with MEGAX. Different background colours in the rooted tree represent closely related protein groups. The node stability was assessed by bootstrap analysis (1,000 replications), and only significant values are displayed at the corresponding nodes.

5.2. Intergenic and vfmE mutants have antagonistic effects on antibiotic synthesis

To confirm that the intergenic region transposon led to the hyperpigmented phenotype, the mutated region was transduced out via the φOT8 phage from the original transconjugant into the

WT strain. The resulting transductant strain displayed the same phenotype as the transconjugant, corroborating the fact that the insertional disruption caused the phenotypic change (Fig. 5.3).

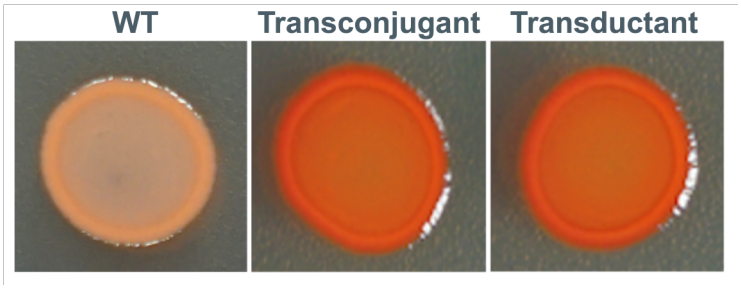


Fig. 5.3. The intergenic mutation triggers overproduction of prodigiosin. The transposon mutation transduced via φOT8 phage, from the intergenic transconjugant into the WT strain, showed the insertion causes the hyperpigmented phenotype. The WT and intergenic strains (transconjugant and transductant) were grown on LBA plates for two days.

The DNA locus affected by the transposon insertion investigated in this work had been hit before by a doctoral researcher in this research group (Wilf, 2011). That limited study provided insights that were considered relevant for the experimental design of the present work. First, a putative gene was predicted and termed *pigment regulatory factor* (*prf*), on which a set of independent insertions were observed to provoke prodigiosin overproduction. By using quantitative RT-PCR, it was shown that *vfmE* mRNA levels are increased in the mutated intergenic background in comparison to that of WT, whilst *argG* expression remained unaltered (Fig. 5.4). Therefore, to contrast the phenotypes of the intergenic mutation, the NJ6 (termed IGR) and *vfmE* strains, and thus infer a possible link, both mutants were characterised. A VfmE-lacking strain was previously constructed by marker exchange by N. Williamson (Salmond Lab collection).

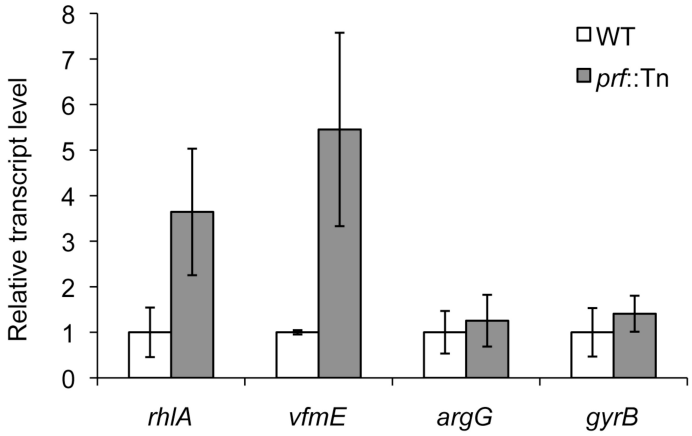


Figure 5.4. The intergenic mutation increases *vfmE* expression but not *argG* expression. Gene expression for *prf*::Tn (intergenic strain) was measured as transcript levels relative to WT at early stationary phase. Values represent the average gene expression ± standard deviation from three replicates (Wilf, 2011).

The first step was to quantify and compare the antibiotic production levels of the two mutants over time. The IGR (NJ6) and *vfmE* strains showed opposite results for the biosynthesis of prodigiosin and the carbapenem compounds. Prodigiosin synthesis was notably increased from the early growth phase (p <0.015) until reaching levels nearly 20-times higher than WT strain, when cells entered stationary growth (Fig. 5.5 A). In contrast, cells devoid of *vfmE* produced lower pigment levels compared with those obtained in WT (p <0.045). However, this change occurred to a much lesser extent compared to the intergenic mutation-induced upturn, from the IGR strain. In this case, the average reduction was approximately half of WT prodigiosin biosynthesis, which was maintained throughout growth. Likewise, the carbapenem synthesis was higher in the intergenic background (IGR strain) compared to the WT (p <0.024) strain, but only in the stationary growth, almost doubling WT synthesis (Fig. 5.5 B). Also in this growth phase, the reduction in carbapenem production observed in the *vfmE* cells was more modest but significant (p <0.039), in relation to WT synthesis. Furthermore, the intergenic mutation had a significant effect on cell growth (p <0.033), unlike the *vfmE* strain, whose growth did not differ significantly from that of WT cells. This was also confirmed by the specific growth rates of the strains (p <0.022). These results confirm that the intergenic and *vfmE* mutations have contrary effects on antibiotic synthesis, and only the intergenic insertion in the IGR strain prompted a negative effect on cell growth.

Following determination of antibiotic levels, it was investigated whether these changes occur at the transcriptional level. For this, both the intergenic (NJ6 strain) and the *vfmE* mutations were transferred to the *pigA*::*lacZ* and *carA*::*lacZ* transcriptional fusion reporter strains via phage transduction. These are the first genes of the prodigiosin and carbapenem biosynthesis operons, respectively. The β-galactosidase (LacZ) activity obtained from the *pigA*::*lacZ*,IGR strain was higher than that of the *pigA*::*lacZ* fusion (p <0.039). Despite this activity mirrors the IGR mutant prodigiosin production, the expression change was less than one-third in magnitude compared to the pigment synthesis difference (Fig. 5.5 C). The opposite effect was found for the *pigA*::*lacZ*,*vfmE* double strain, displaying a significantly reduced expression in comparison to the isogenic fusion (p <0.042), from 6 h onwards (Fig. 5.5 D). For the case of the carbapenem biosynthetic operon, the two mutations only provoked significant changes on *carA*::*lacZ* transcription at early exponential growth (p <0.03 and p <0.024, respectively). After this point, only a significant difference at 8 h between the *carA*::*lacZ* strain and its *vfmE* double mutant (p <0.012), and at 10 h, between the two double mutants (p <0.009) were observed. Hence, the converse effects of both the intergenic and *vfmE* in carbapenem production seems to be acting at posttranscriptional level.

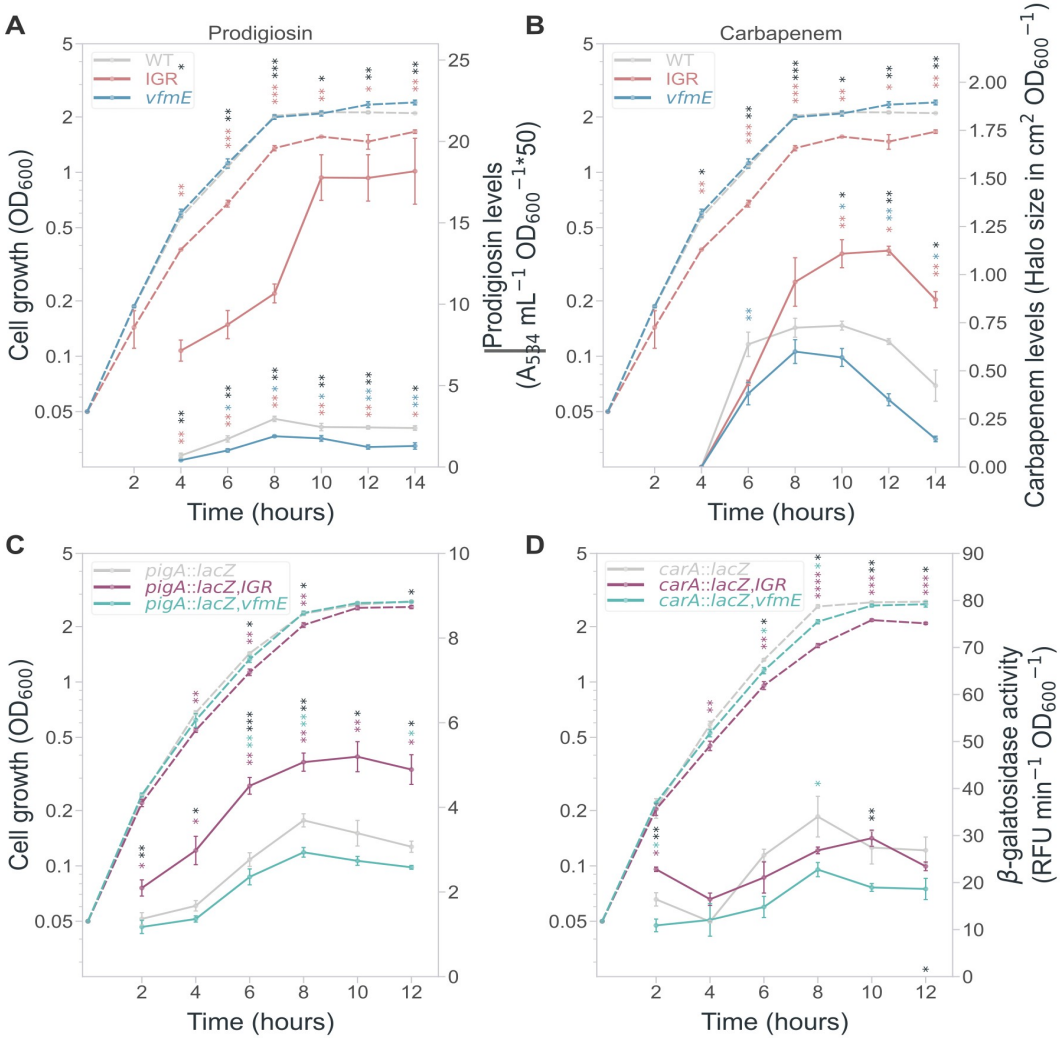


Fig. 5.5. Intergenic and *vfmE* mutations generate opposite effects on production of antibiotics, and only prodigiosin is controlled at the transcriptional level. Cell growth is depicted as dashed lines (OD_{600} ; left Y axes) whereas normalised antibiotic synthesis (A and B) and β-galatosidase activity (C and D) are indicated as solid lines (right Y axes). Prodigiosin was quantified by spectrophotometry (A_{534}) and the carbapenem by halo formation using an indicator strain. Transcription activity is expressed as relative fluorescence units (RFU). Data from three biological replicates are shown as means ± standard deviation. Statistical analysis was conducted at each time point by multiple unpaired Student's t-test: $*p < 0.05$, $**p < 0.01$, $***p < 0.001$, and $***p < 0.001$. Coloured stars denote differences between the corresponding mutant and WT values, whereas black stars between mutants.

Taken together, the data showed that the intergenic and *vfmE* mutations have antagonistic consequences for antibiotic production. A substantial increase in prodigiosin levels was found in the IGR strain, whilst *vfmE* provoked a significant reduction. The same trend was followed for carbapenem synthesis, but on a lower scale. However, only prodigiosin biosynthesis is modulated at the transcriptional level, as no expression changes were found after early exponential growth in the carbapenem cluster expression upon the addition of both the intergenic and *vfmE* mutations.

5.3. Intergenic and vfmE mutations are pleiotropic

As the IGR and *vfmE* strains were shown to elicit opposite effects on antibiotic synthesis, it was investigated whether this tendency could be extended to other phenotypic features of S39006. Thus, both strains were characterised by analysing their gas vesicle production, swimming ability, cellwall degrading enzymes, plant virulence, and quorum sensing signalling.

5.3.1. Intergenic and vfmE mutations reduce transcription of gas vesicle operons

For analysing the influence of the intergenic and *vfmE* mutations on gas vesicle production, flotation and transcriptional assays were conducted. For the latter, both mutations were transduced into the *gvpA1*::*lacZ* and *gvrA*::*lacZ* fusion strains, the genes leading the two operons of the gas vesicle biosynthesis cluster (Ramsay *et al*, 2011; Tashiro *et al*, 2016).

No discernible differences between the IGR and WT cells were noticed in the flotation assay (Fig. 5.6 A), as both stayed afloat at a comparable level. However, *vfmE* cells possessed an enhanced ability to float relative to those of WT. In terms of transcriptional activity, both mutations impacted in the same manner on *gvpA1* and *gvrA* expression. Both intergenic and *vfmE* mutations significantly (p <0.0043 and p <0.021, respectively) reduced the expression of *gvpA1* compared to the parental reporter strain, from mid exponential to stationary phase (Fig. 5.6 B). The *gvrA* transcriptional fall for each mutation relative to the isogenic strain was less pronounced than in *gvpA1*, and it took place from mid exponential growth for the intergenic mutation (p <0.033) and later for *vfmE* (p <0.037), which on average was slightly higher than that of the IGR strain (Fig. 5.6

C). Thus, the two mutations caused a drop in transcription of both operons of the gas vesicle cluster, *gvpA1-gvpY* and *gvrA-gvrC*, but this was not obviously reflected in the flotation capacity of the mutants, which exhibited an unchanged (IGR) and enhanced capacity (*vfmE*).

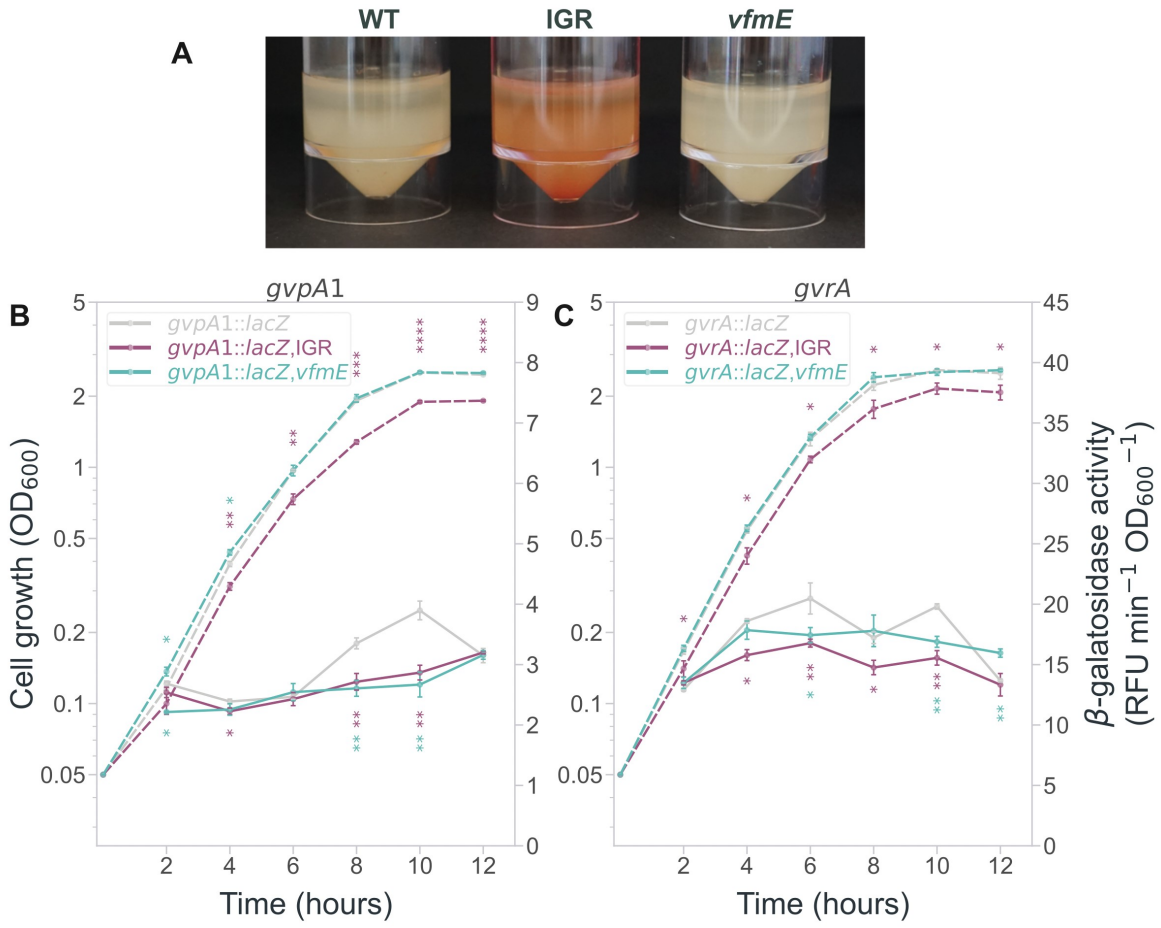


Fig. 5.6. Intergenic and *vfmE* mutations diminish expression of the gas vesicle gene clusters. A: Cultures of WT, IGR, and *vfmE* strains used for the flotation assay were left static for 48 h. For transcription assays (B,C), growth is shown as dashed lines (OD_{600} ;left Y axes) whereas solid lines indicate normalised βgalatosidase activity expressed as relative fluorescence units (RFU; right Y axes). Data from three biological replicates are displayed as means ± standard deviation. Statistical analysis was conducted at each time point by multiple unpaired Student's t-test: *$p < 0.05$, **$p < 0.01$, ***$p < 0.001$, ****$p < 0.0001$. Coloured stars denote differences between the corresponding mutant and WT values.

5.3.2. Intergenic mutation antagonises the VfmE effect on swimming but not on cellulase production

To continue with the characterisation, potential effects of the intergenic and *vfmE* mutations on the capacity of S39006 to produce its cell wall-degrading enzymes (pectate lyase and cellulase) plus its swimming ability, were examined via plate assays. As observed in antibiotic production, both mutations had contrary effects on swimming capacity of cells (Fig. 5.7, left). This capacity was diminished by approximately 35% (p =0.003) in the intergenic mutant strain, while it rose by the same magnitude (p =0.018) in a *vfmE* background. In the case of degrading enzymes, this contrasting effect of the two mutations was not observed. Pectate lyase activity was unaffected by the mutations, and cellulase activity was only impacted by the *vfmE* loss (p =0.021), presenting a nearly 20% decline relative to WT levels (Fig. 5.7, middle and right, respectively). These findings showed that although the intergenic and *vfmE* mutations played an antagonistic role in swimming

motility, this was not replicated in cellulase synthesis, where the disruption by insertion caused no changes.

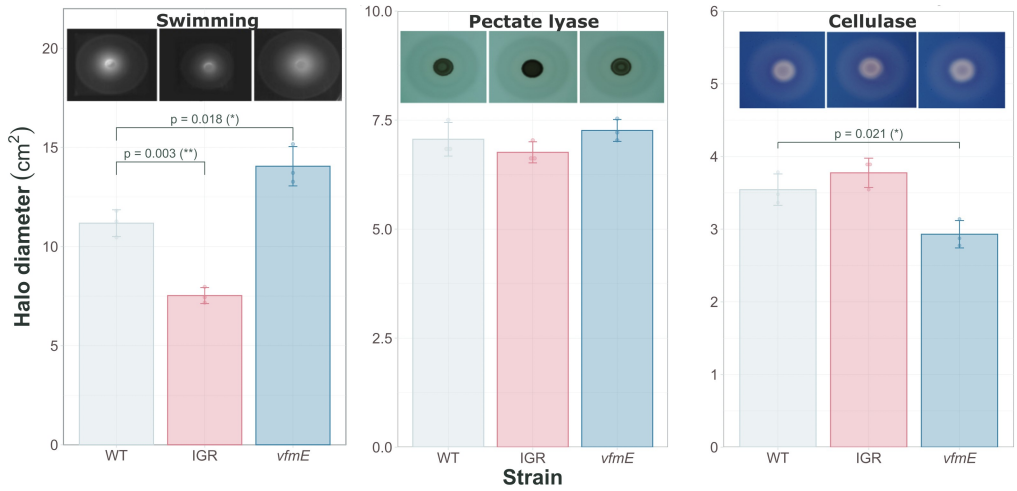


Fig. 5.7. The *vfmE* mutation reduced swimming and cellulase secretion, and intergenic mutation boosted motility. Swimming ability, pectate lyase, and cellulase production were measured as halo diameters formed by bacteria from normalised cultures (OD_{600}=1) spots. Data from three biological replicates are shown as means ± standard deviation. Statistical analysis was conducted by Student's t-test (p <0.05). Insets show a representative plate assayed for each attribute.

5.3.3. Intergenic and vfmE mutations weaken virulence in plants

It was hypothesised that since only the *vfmE* inactivation led to a reduced production of cellulase, one of the two degrading exoenzymes used for plant invasion, this may have an effect on virulence compared with the IGR strain. To test this, both strains were subjected to the potato tuber rotting assay. In this assay, the weight of the necrotic tissue generated by the bacterial infection is indicative of virulence capacity. The virulence in both strains was debilitated in comparison to the WT's ability. A reduction of approximately 75% of rotten tissue was obtained for the cells harbouring the intergenic mutation (p =5.39e^{-5}), which barely generated a cavity around the stabbed-inoculated area (Fig. 5.8, left). Likewise, a more modest but significant drop, equivalent to a quarter less rotting tissue weight, was detected for *vfmE* cells relative to those of WT (p =0.0279; Fig. 5.8, right).

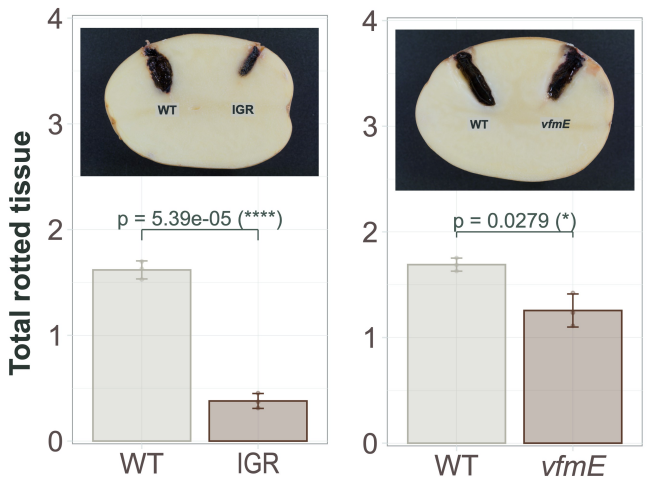


Fig. 5.8. The intergenic and *vfmE* mutations diminish virulence in plants to different extents. Tubers were infected with a normalised cell number (10^7 CFU) and scraped-off rotted tissue was weighted after four days. The average weights of three biological replicates (± standard deviation) and significance (Student's t-test, p <0.05) are displayed. Insets: cross section of a representative infected potato (iodine-stained rotten cavities for enhanced visualisation).

Thus, the intergenic mutation unexpectedly showed a more profound detrimental effect on infection capacity than *vfmE*, which possesses a diminished cellulase synthesis. This fact might be explained by impaired cell growth *in planta*; hence, cells extracted from the rotting extract were plated on minimal medium plates in serial dilutions. For the intergenic strain, the normalised cell count (normalised per gram of tissue) was a log-fold lower (10^5 CFU) than for WT cells. This agrees with the previously observed negative effect from the intergenic insertion on normal growth. On the other hand, the CFU count found for cells deprived of *vfmE* was the same as that of WT, as seen before. Thus, both mutants have an attenuated virulence capacity, with the intergenic mutation displaying a more severe effect, even though cells preserve intact both pectate lyase and cellulase synthesis.

5.3.4. Intergenic and vfmE mutations do not affect acyl-homoserine lactone synthesis

To assess whether the intergenic or *vfmE* mutations can modify the synthesis of acyl-homoserine lactones, and thus the quorum sensing (QS) communication system in S39006, both mutations were transduced into the synthase reporter strain (*smaI*::*lacZ*) background. Although both the intergenic and *vfmE* mutations lowered on average the *smaI* expression levels in relation to the parental strain (Fig. 5.9), this reduction was not significantly different. Notably, contrary to previously determined, the double mutant *smaI*::*lacZ*, IGR grew as well as the *vfmE* double and the isogenic reporter, for which no statistical differences were found. This was the only genetic background where no defective growth is observed when the intergenic mutation is present.

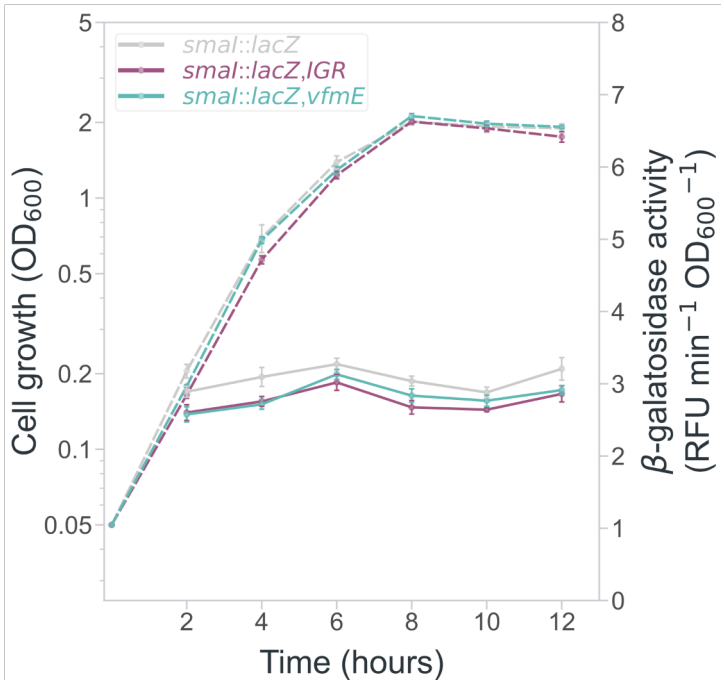


Fig. 5.9. Neither of the intergenic nor *vfmE* mutations alter synthesis of acyl-homoserine lactones. Cell growth is depicted as dashed lines (OD_{600}; left Y axis) whereas normalised β-galatosidase activity is indicated as solid lines (right Y axis). Transcription activity is expressed as relative fluorescence units (RFU). Data from three biological replicates are shown as means ± standard deviation. Statistical analysis was conducted at each time point by multiple unpaired Student's t-test (p <0.05).

Taken together, both intergenic and *vfmE* mutations only displayed contrasting effects as observed for antibiotic production for swimming capacity. The two mutants had the same effect but to different extents on transcription of gas vesicles and virulence in plants, which were reduced compared to WT strain, and only the *vfmE* strain showed a lower cellulase synthesis.

5.4. VfmE phenotype is epistatic to the intergenic

As the intergenic and *vfmE* mutations exhibit antagonistic effects in some phenotypic features but not all, the double mutant IGR, *vfmE* was generated via phage transduction. A previously generated intergenic strain (Wilf, 2011) harbouring the closest insertion to the current was used, since the *vfmE* strain carries a *cat* insertion as well as the transposon present in the intergenic mutant. This new double strain displayed a "light pink" colour phenotype, apparently identical to that of *vfmE* (Fig. 5.10). To corroborate this observation and to determine if this also applies to the carbapenem, quantitation of antibiotic production over time was performed for the intergenic (IGR), *vfmE*, and the double (IGR,*vfmE*) mutants.

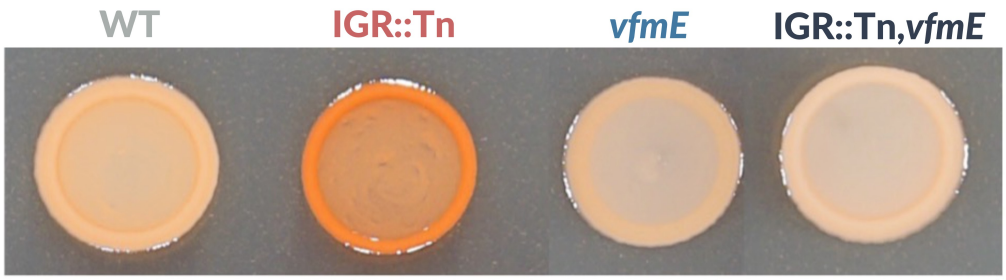


Fig. 5.10. The IGR, *vfmE* double mutant has same level of pigmentation as the *vfmE* isogenic strain. Patches were grown from normalised cells (OD_{600}=1) and spotted onto LBA plates for 18 h. The colour intensity indicates prodigiosin production.

The prodigiosin production of both *vfmE* and IGR,*vfmE* was significantly lower than WT strain (p <0.033 and p <0.012, respectively), but there was no difference between them (Fig. 5.11, left). The same pattern was repeated for carbapenem synthesis, with a reduced synthesis for single and double mutants in relation to the WT strain (p < 0.0008 and p <0.021, respectively) but not to each other, from late exponential phase onwards (Fig. 5.11, right). Data thus showed that the *vfmE* phenotype prevails over the intergenic, in terms of synthesis of antibiotics.

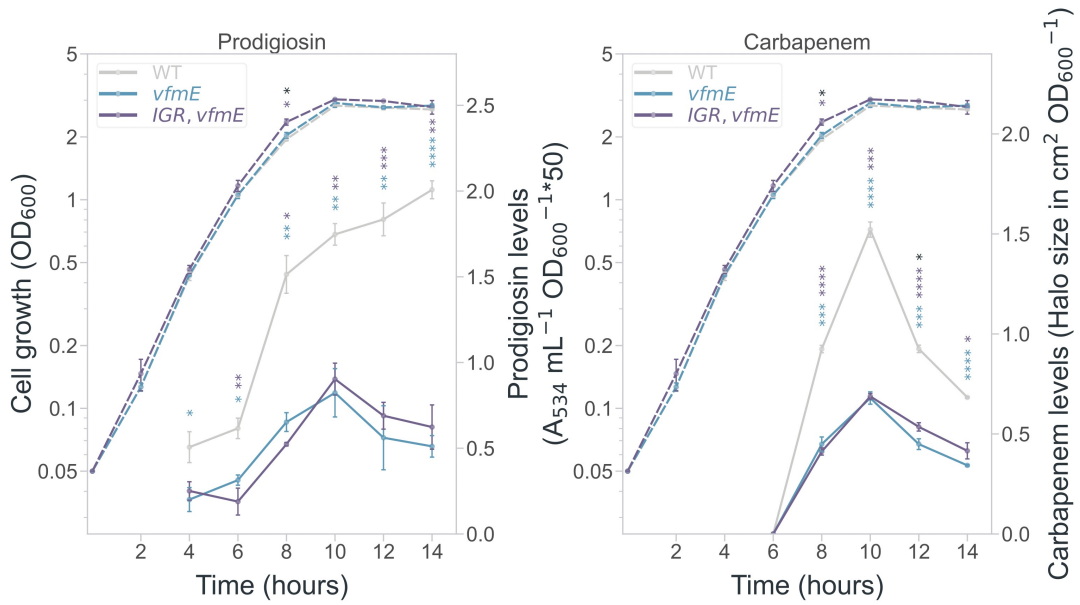


Fig. 5.11. The IGR, *vfmE* double mutant displays the same reduced antibiotic production as the *vfmE* strain. Cell growth is depicted as dashed lines (OD_{600}; left Y axes) whereas normalised antibiotic synthesis is indicated as solid lines (right Y axes). Prodigiosin was quantified by spectrophotometry (A_{534}) and the carbapenem by halo formation on an indicator strain. Data from three biological replicates are shown as means ± standard deviation. The synthesis of the intergenic mutant is not shown for ease of antibiotic production analysis of mutants. Statistical analysis was conducted at each time point by multiple unpaired Student's t-test: *p <0.05, **p <0.01, ***p <0.001. Coloured stars denote differences between the correspondent mutant and WT values, whereas black stars between mutants.

To investigate whether this result is also replicated in motility capacity, the same set of strains was used for swimming and swarming assays. The three mutants exhibited a differentiated swimming capacity compared to the WT cells. As found previously, the intergenic mutation decreased this ability (p =0.007), in contrast to *vfmE*-lacking cells, which showed a boosted motility (p =0.001), like the double mutant (p =0.002; Figure 5.12, top). In swarming, the intergenic strain displayed a highly enhanced spreading capacity compared to all the other strains, whilst *vfmE* and the double mutant showed the same tendency but to a much lesser extent relative to WT (Figure 5.12, bottom).

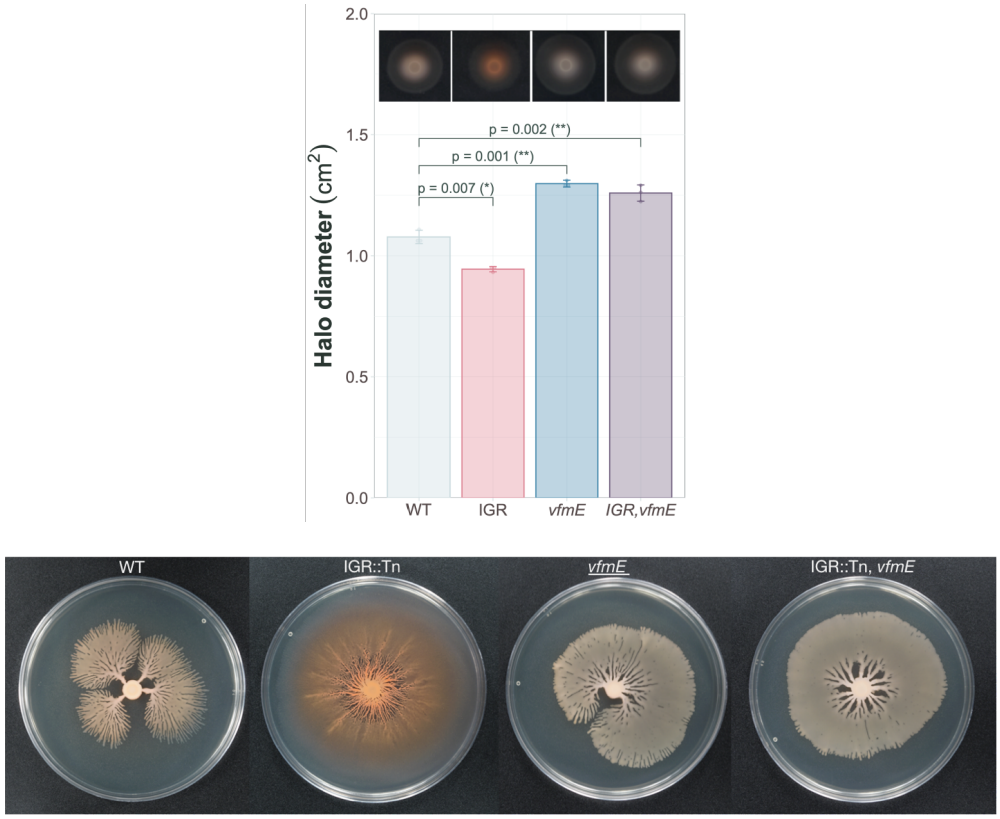


Figure 5.12. The *vfmE* mutant and the double IGR, *vfmE* mutant show the same motility phenotype. Top: Swimming ability was measured as the halo diameter formed by bacteria from normalised culture (OD_{600}=1) spots. Data from three biological replicates are shown as means ± standard deviation. Statistical analysis was conducted by Student's t-test: *p < 0.05, **p < 0.01. Insets show a representative plate assayed for each strain. Bottom: Swarming motility was assessed from normalised culture spotted onto Eiken agar plates and grown for 2 days. Representative images from three biological replicates are displayed.

To further test phenotypic differences between the single and double *vfmE* strains, an additional plant virulence assay was performed. Again, the double mutant showed a reduced infection ability in comparison to WT strain (p =0.0102; Fig. 5.13), and this drop was of the same magnitude as that of the isogenic *vfmE* previously attained (Fig. 5.8).

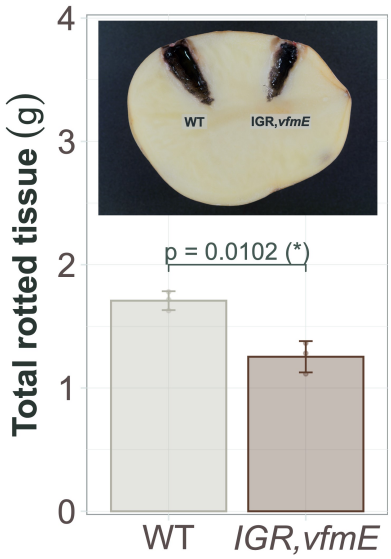


Fig. 5.13. The IGR, *vfmE* double mutant showed a decreased virulence in plants. Tubers were infected with a normalised cell number (10^7 CFU) and scraped-off rotted tissue was weighted after 4 days. The average weights of three biological replicates (± standard deviation) and significance (Student's t-test, p <0.05) is displayed. Inset: cross section of a representative infected potato (iodine-stained rotten cavities for enhanced visualisation).

Thus, the analyses showed that the IGR, *vfmE* double mutant exhibits the same phenotype as the *vfmE* strain, at least for antibiotic production, motility, and virulence. This may suggest that the intergenic mutant overproduction of antibiotics might be generated by a higher activity of *vfmE*; when absent, its phenotype is dominant.

5.5. VfmE promotes expression of a putative gene in the intergenic region

The previous work on this intergenic region found six independent transposon insertions, spanning 127 bp, that triggered the hyperpigmented phenotype (Wilf, 2011). As the precise location of such insertions was not known, the random-primed PCR technique was used to determine the two farthest insertion sites (NMW4 and NMW5 strains), finding the transposon location from this study in between. Moreover, as the transposon used carries a promoterless *lacZ* gene, it was shown that four insertions generated a Lac^+ phenotype, whereas others in the opposite orientation were Lac^- (Fig. 5.14). This demonstrated unidirectional promoter activity for mutants when driving transcription in the orientation convergent with *vfmE*.

Given that *vfmE* expression is increased in the intergenic genetic background (Fig. 5.4), it was investigated whether the regulatory protein modulates the expression of a hypothetical gene disrupted by the transposon, which could negatively regulate *vfmE*. For this, the LacZ activity from the reporter gene present in the intergenic strain used to generate the double mutant, was monitored over time. The β-galactosidase assay showed that the IGR mutant transcription is relatively stable over time, which suggests that any potential gene encoded in this region would be constitutively expressed (Fig. 5.15). When the VfmE regulator, encoded immediately

downstream of the insertion in opposite direction, is missing, the transcription of the putative intergenic gene is almost completely lost. This outcome implies a relationship between VfmE and an unknown gene, whose expression strongly relies on regulator activation.

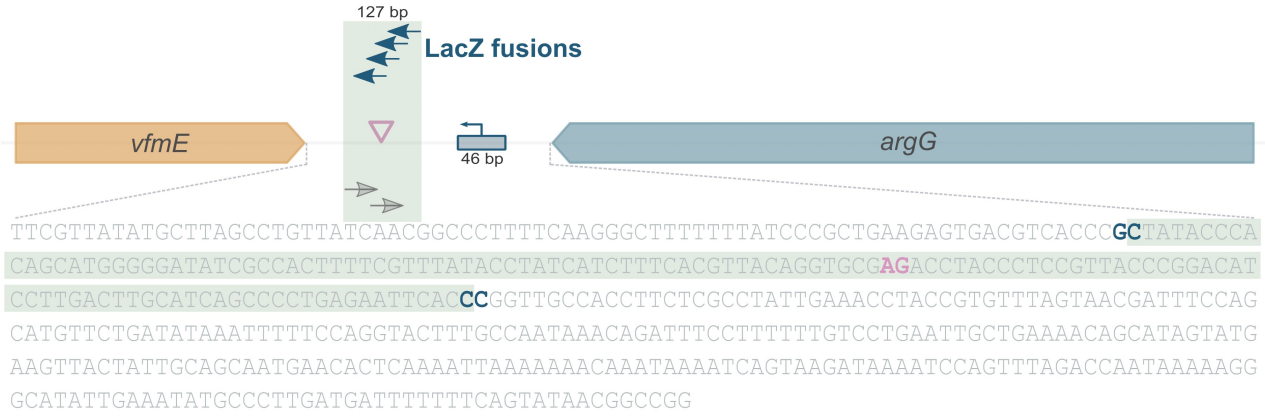


Fig. 5.14. Transcription direction in the transposon disrupted region is opposite to *vfmE*. The highlighted DNA region (127 bp) between *vfmE* and *argG* coding regions (coloured arrows) depicts the zone that, when interrupted, generated hyperpigmented strains. Four filled arrows indicate transcription direction (LacZ fusions), and the insertion from this study is shown as a pink triangle. The upstream blue box (46 bp) depicts the region with maximal promoter activity (adapted from Wilf, 2011).

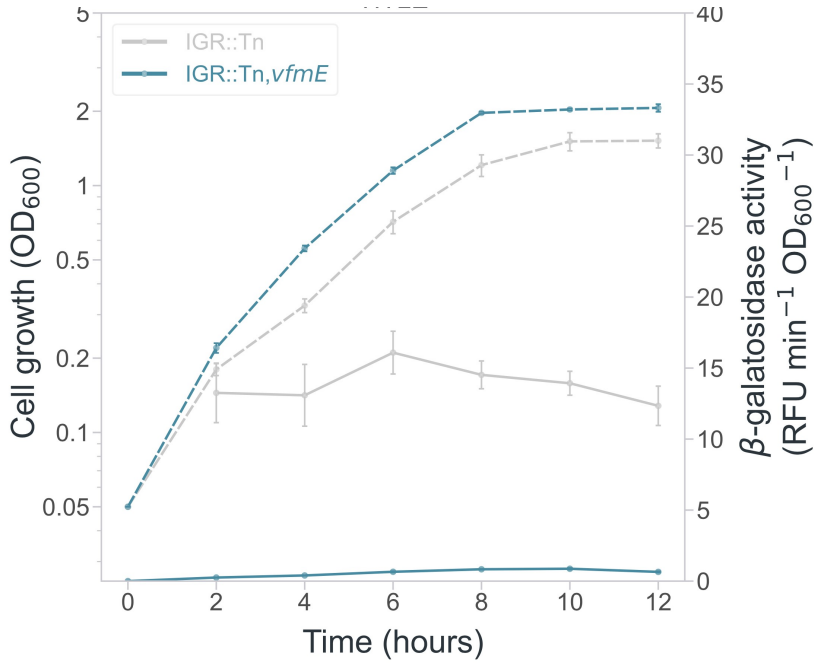


Fig. 5.15. VfmE activates expression of a putative gene interrupted by the transposon insertion. Cell growth is depicted as dashed lines (OD_{600}; left Y axis) whereas normalised β-galactosidase activity is indicated as solid lines (right Y axis). Transcription activity is expressed as relative fluorescence units (RFU). Data from three biological replicates are shown as means ± standard deviation.

Furthermore, by progressive deletion analysis, a 146 bp region (pNB9) upstream of the transposon insertions was found to contain the maximal promoter activity (Fig. 5.16). The 100 bp last fragment tested (pNB10) showed no activity. Thus, the 46 bp long region located before the start codon of the previously predicted gene *prf* was used for promoter prediction.

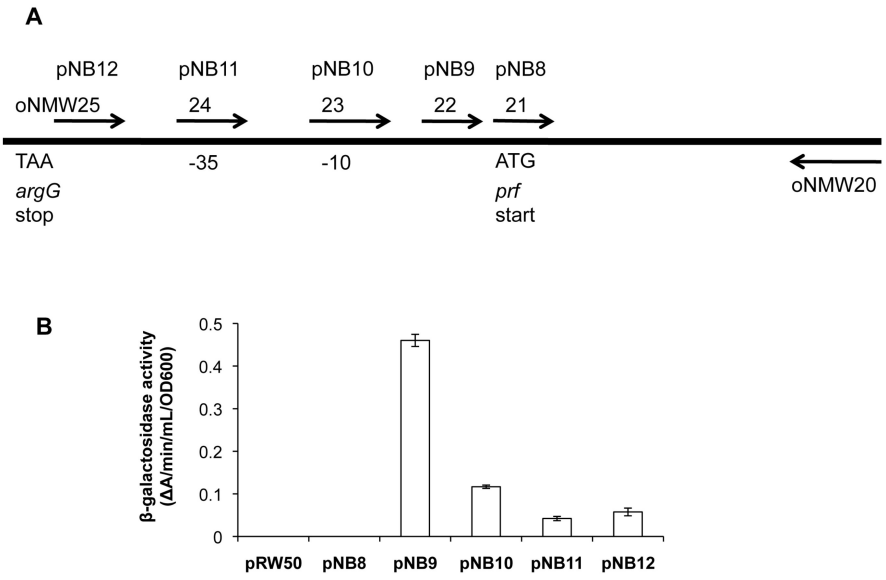


Fig. 5.16. pNB9 region has maximal promoter activity. **A**. Progressive 5' deletions of the *prf* promoter were cloned into the promoterless lacZ vector pRW50. Arrows indicate the primers used to amplify the regions (constructs pNB8-12) and -35 and -10 are predicted promoter boxes. **B**. Promoter activity expressed as β-galactosidase activity in *E. coli* DH5α after 10 h growth (Wilf, 2011).

Elements resembling an alternative Sigma 54 (σ54; RpoN) binding site were predicted for this region. Additionally, as the 146 bp zone with maximal promoter activity was detected by progressive deletions, and its 100 bp 3' portion (Fig. 5.17 A, dotted line) exhibited undetectable activity, there is also a possibility for the promoter being in the junction between the 46-100 bp. Thus, another prediction analysis was performed, incorporating the first 50 bp downstream of the 46 bp region. This analysis yielded another putative sigma region downstream of σ54, this time displaying features of a Sigma 38 (σ38; RpoS) binding site. The two predicted binding sites had a motif in common, which is the -12 and -35 box for σ54 and σ38, respectively (Fig. 5.17 B).

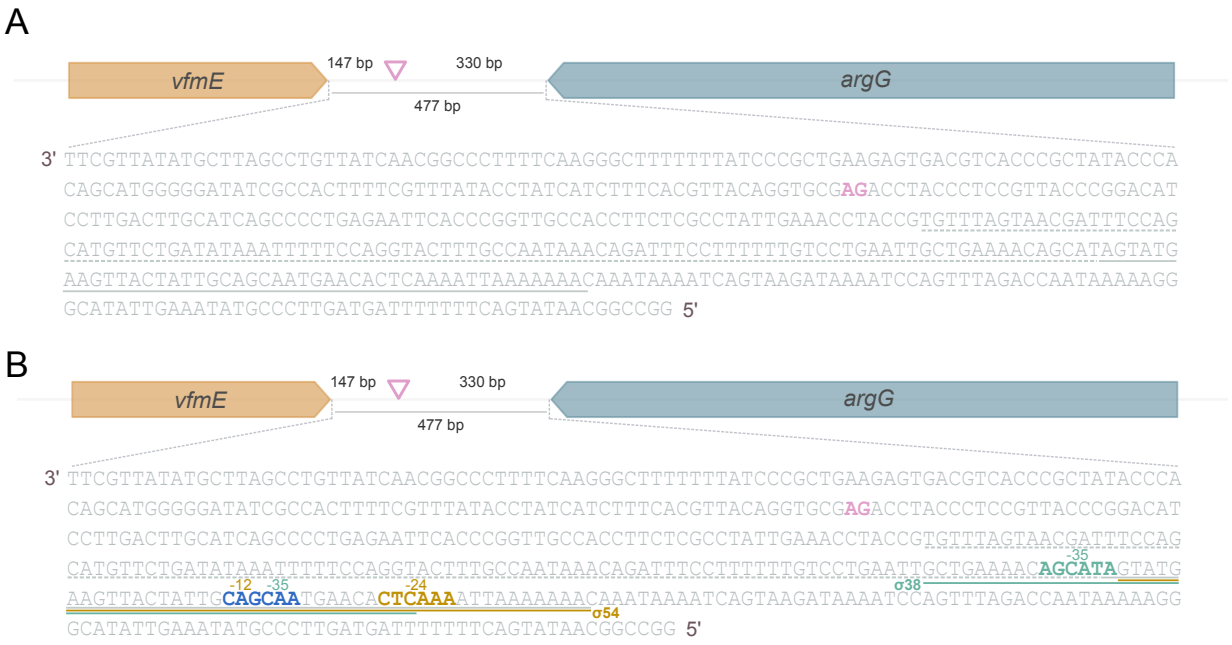


Fig. 5.17. Predicted promoters for the region displaying maximal activity upstream of the insertion sites. 5' to 3' view of the transposon-altered intergenic region. A: the 146 bp zone containing promoter activity is underlined in grey, and the dotted-lined portion has no activity. B: σ54 (-24 and -12 motifs) and σ38 (-35 and -10 motifs) are the predicted promoters. The blue-emboldened sequence is the overlapped motif between the predictions.

Therefore, to determine which prediction is the likely promoter site for a putative gene activated by VfmE, the -10 box and the half of the -24 box (Fig. 5.18 A) were excluded in the inserts used to test the σ54 and σ38 binding regions, respectively. These two fragments, as well as the portion containing both promoters (σ54-38) were cloned into the promoterless *lacZ* plasmid pRW50, to give the plasmid constructs pσ54, pσ38, and pσ54-38. These plasmids were used to transform *E. coli* DH5α, along with the empty vector control. Thus, the promoter activity of each construct, including the cells harbouring pNB9 (maximal promoter activity) as positive control, was assayed.

Both pNB9 and pσ54-38 constructs had the highest levels of β-galactosidase activity detected, with no statistical difference between them (Fig. 5.18 B). The pσ38 construct had circa 55% less activity than the longest fragments (p =0.00086), but it was higher than the pσ54 construct (p =0.00015), which had only residual LacZ activity comparable to the empty pRW50 vector. Therefore, from the two predicted promoter regions, it is likely that the putative σ38 binding site is the promoter of an unknown gene interrupted by the transposon and not the σ54. Moreover, the promoter activity difference found between the long fragments and pσ38, suggested that the bases upstream the active σ38 promoter are a binding site for a transcription activator.

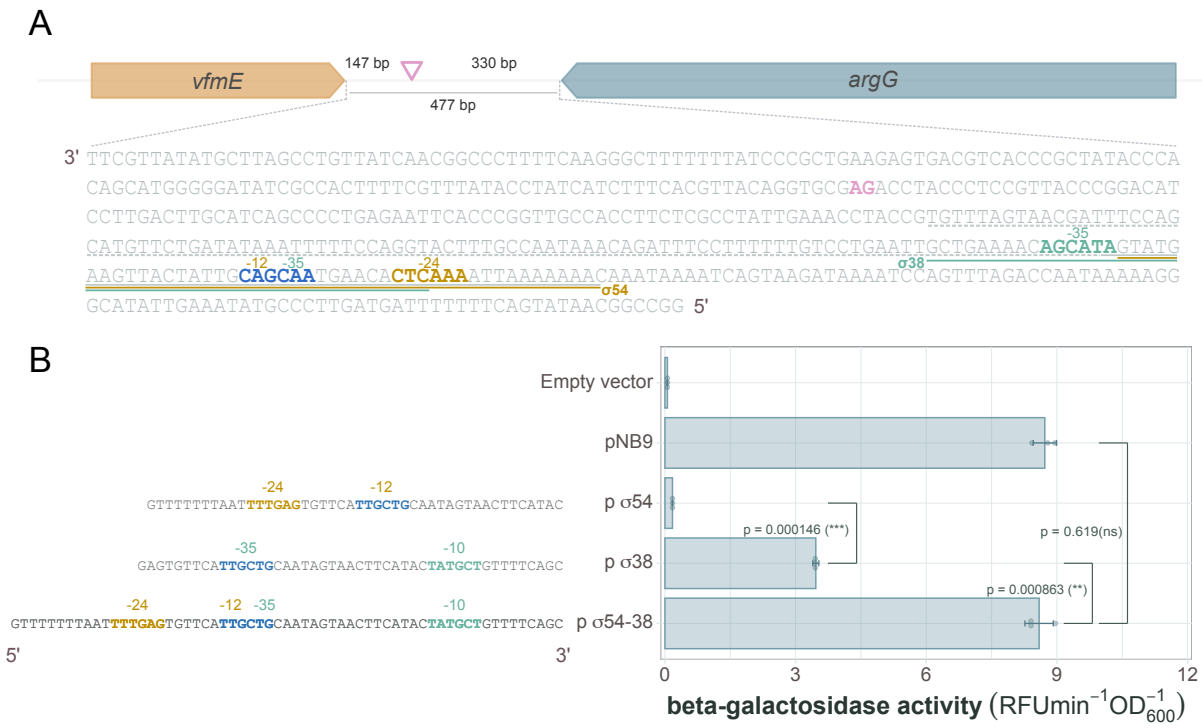


Fig. 5.18. A putative sigma 38 factor binding site drives transcription of the putative intergenic gene. A: 5' to 3' zoomed view of the intergenic region depicting the promoters predicted. The underlined zones in yellow and green, corresponding to σ54 and σ38, plus the zone that contains both (σ54-38), were experimentally tested for activity. B: *In vivo* β-galactosidase assay for the putative promoters and the combined region. Promoter activity of the empty vector, p (pRW50), and its derivative constructs in *E. coli* DH5α was measured at 10 h growth. Average data from three biological replicates ± standard deviation is shown. Statistical significance was tested by an unpaired Student's t-test: **p* < 0.05, ***p* < 0.01, ****p* < 0.001.

This 14-nt-long binding site (Fig. 5.19, left) was queried in the CollecTF database, which contains experimentally validated regulatory sites, to seek similar sequences. This search produced a single hit from *Vibrio cholerae* O395, a binding site for ToxT (Fig. 5.19, right), also known as toxin coregulated pilus (TCP) virulence regulatory protein, TcpN. This regulator is a member of the AraC family as well as VfmE, and its amino acidic sequence was Blasted against the S39006 genome to look for similar proteins. The search generated only one hit, XylR (31.3% identity), whose gene is located upstream of *argG*, which surrounds the intergenic insertion opposite to *vfmE* (Fig. 5.1).

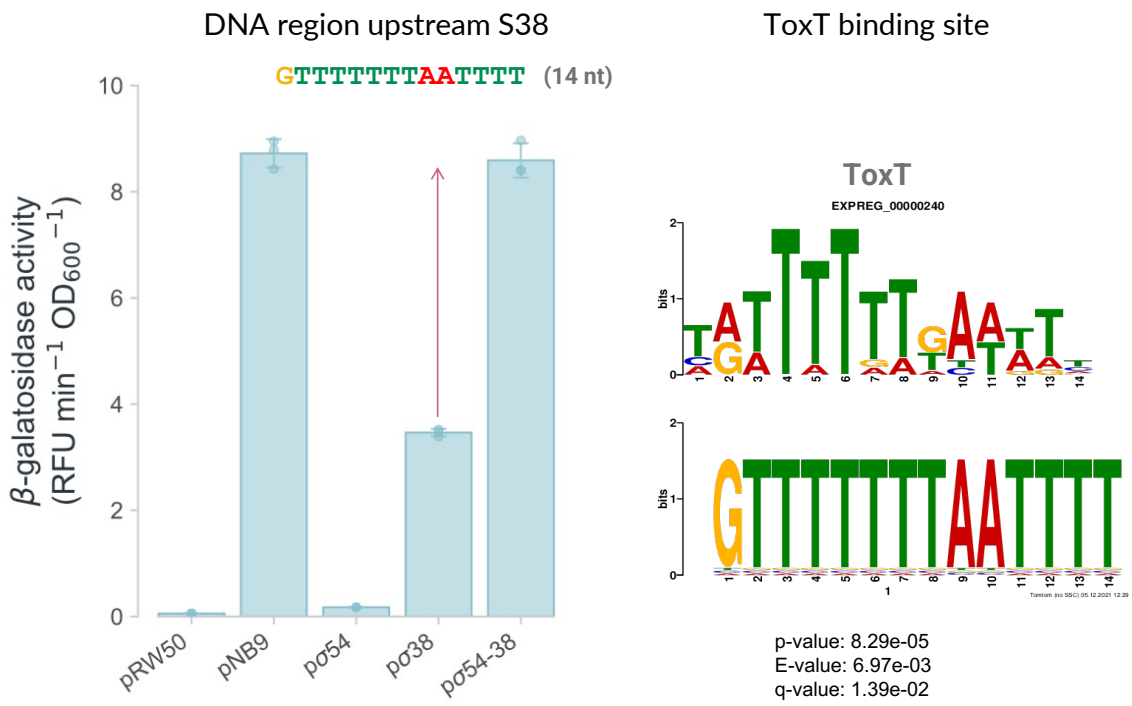


Fig. 5.19. The region upstream S38 might be a binding site for a ToxT homologue. Left: the 14 nt region presence in the pσ54-38 construct augments the promoter activity in *E. coli* DH5a. Right: CollecTF database predicted the 14 nt region (bottom) to be a ToxT homologue transcription factor binding site (top). Significance of the motif search is indicated underneath sequences.

Thereafter, in addition to VfmE, XylR was also incorporated into the analysis given the significant similarity of the testing site with that of the ToxT found in the CollecTF database. Thus, to test whether VfmE or XylR regulators can increase the promoter activity by acting on the presumptive 14-nt binding site, the correspondent genes were cloned into the pQE-80-oriT system. Each plasmid or the empty vector were then used to transform *E. coli* DH5α harbouring pσ38, lacking the testing site, or pσ54-38, to inspect promoter activity as described previously (Fineran *et al*, 2005). No significant changes were found in the LacZ activity from cells containing pσ38 (S38), but in those containing the insert pσ54-38 (S54-38) a significant increase was shown when VfmE (p =0.024) and XylR (p =0.003) were overproduced from the multicopy plasmid (Fig. 5.20). This result suggests that VfmE activates a putative gene encoded in the intergenic region, as well as XylR, which is encoded upstream of *argG*.

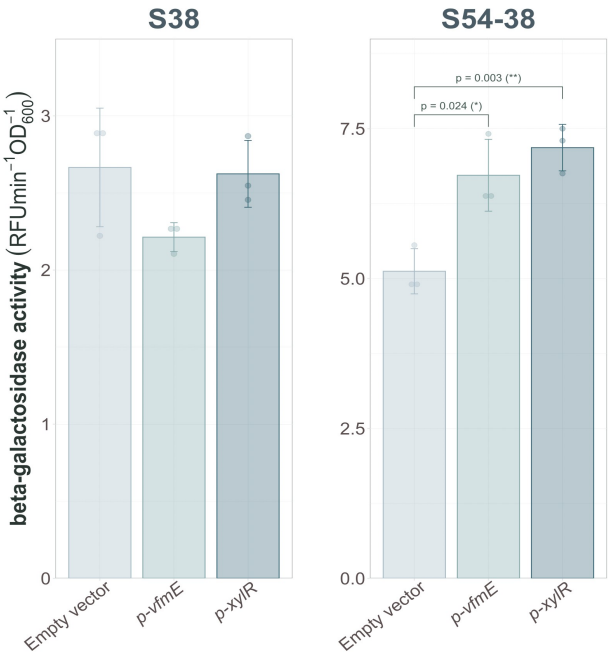


Fig. 5.20. VfmE and XylR regulators increase promoter activity of a putative intergenic gene. βgalactosidase activity was employed to assess promoter activity *in vivo*. *E. coli* DH5α cells harbouring the pσ38 (S38) or pσ54-38 (S54-38) constructs, were transformed using the high-copy-number vector pQE80oriT alone (empty vector) or incorporating *vfmE* (p-*vfmE*) or *xylR* (p-*xylR*) reading frames. Leaky expression effect of pQE80-oriT and its derivatives on cells containing pσ38 and pσ54-38 was measured at 10 h growth. Average data from three biological replicates ± standard deviation is shown. Statistical significance was tested by an unpaired Student's t-test: **p* < 0.05, ***p* < 0.01.

Collectively, the findings show that an alternative promoter σ38 binding site is located upstream of the region where transposon insertions provoked the intergenic phenotype. Furthermore, this promoter activity largely depends on VfmE activation in S39006, whose binding site contains at least the 14 nt region upstream of the σ38 promoter tested. However, XylR, another AraC-type regulator, also activated the promoter.

5.6. Gene prediction and complementation attempts for the intergenic mutation

Given that no genes are annotated within the intergenic region in the S39006 genome, BLASTnbased searches were performed to find similar DNA sequences. When using the entire intergenic region that contains the transposon insertion, only small regions from completely unrelated genera, such as *Prunus persica* (peach), were shown. New searches with smaller portions (e.g. half thereof) of this region were next performed, which resulted in two matches that were investigated to glean insights into a possible function altered by the transposon. A 52 nt hit matched to a *Dickeya paradisiaca* Ech703 region, while downstream of it, another segment matched to two genomes: *Dickeya chrysanthemi* Ech1591 and *Phytobacter ursingii* strain CAV1151. The latter result (111 nt long) contained the transposon insertion site of the intergenic mutant (Fig. 5.21, bottom).

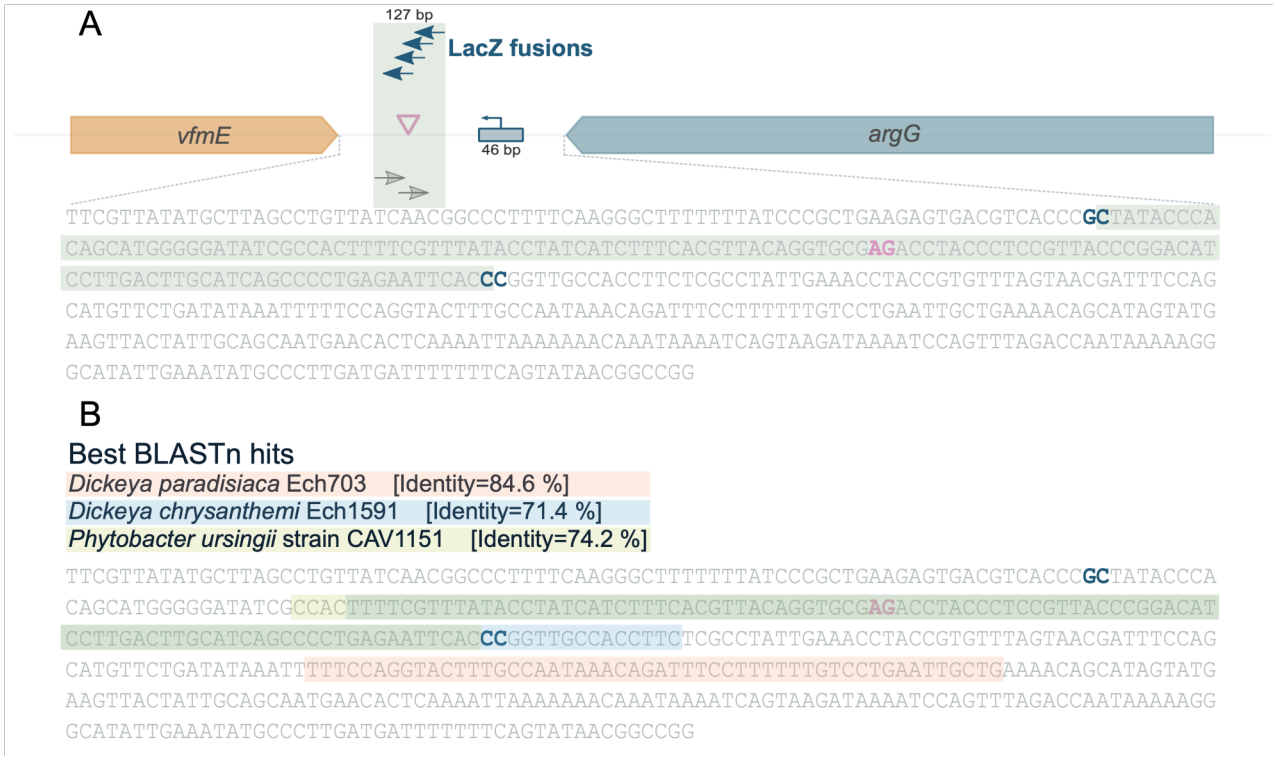


Fig. 5.21. Schematic of the intergenic transposon insertions and similar regions in other bacteria. A: The highlighted 127 bp zone indicates the region hit by transposons, and the filled arrows indicate that transcription occurs opposite to *vfmE*. Pink triangle and letters illustrate the insertion found in this study. B: The best BLASTn hits that have been mapped into the intergenic region. Hit1 (light red box) locates upstream the region of insertions (blue letters) and Hit2, within the region of insertions (blue/green boxes).

To examine the two sequences matching the S39006 disrupted region, arbitrarily named Hit1 and Hit2 (which includes the transposon insertion site), the genomes of both *D. paradisiaca* Ech703 and *D. chrysanthemi* Ech1591 strains were downloaded from NCBI and explored using Artemis software. In short, in the case of the Hit1 sequence (*D. paradisiaca* Ech703), it was located just upstream of the *vfmA* (*0089*) ORF, another homologue belonging to the *vfm* cluster, followed by *pecM* (*0088*). Further upstream of these genes, *argG* (*0086*) and the MarR regulator family member *pecS* (*0087*) were also seen. The Hit2 fragment was found in an intergenic region between an esterase/lipase gene (*3247*) and a nitrite reductase, *nrfC* (*3248*) gene. Nonetheless, these matches did not reveal any putative similar genes or conserved regulatory regions.

A *de novo* gene prediction approach was followed to find a putative coding sequence encompassing the 127 nt region of insertions, transcribed opposite to *vfmE*, and downstream of the region of maximal promoter activity. Thus, the tool ORFfinfer (NCBI) predicted a putative gene (261 nt) fulfilling these features (Fig. 5.22 A). Nevertheless, this gene was discarded as it was the same predicted in the past work (named *prf*), which was used for failed attempts at genetic complementation of the insertion mutant (Wilf, 2011). Therefore, it was hypothesised that a longer gene might complement the intergenic mutation. Thus, as no other start codon was

predicted, the start of the insert was set upstream of the -10-promoter box (Fig. 5.22 B). Inspection of the sequence downstream of the previous predicted reading frame revealed the presence of three stop codons, the two closest to the insertion area were UGA. Moreover, it was searched for the presence of *rho*-independent transcription terminators. To accomplish this, ARNold and FindTerm tools were employed, and a stem-loop (possible terminator sequence) was predicted. One of the stop codons was in the middle of this loop, while the other was 3 nt downstream of it. Hence, the end of the insert was chosen to cover both stop codons (Fig. 5.21 B, purple sequence).



Fig. 5.22. Location of the predicted genes in the intergenic region. The region between the blue letters corresponds to the region of insertions that generate the hyper-red phenotype. A: The pink-highlighted region indicates the predicted open reading frame (261 nt) and the green zone is the previous region found to contain the maximal promoter activity. The start codon is in bold. B: The possible small RNA (330 nt) is highlighted in light green, and the predicted *rho*-independent transcription terminator is in bold in purple letters. -10 and -35 boxes are also shown.

Thus, the 330 nt candidate transcript, that might correspond to a small RNA (sRNA) given the type of terminator, was tested in genetic complementation assays. Furthermore, the whole intergenic region (477 bp), was also tested. Both fragments were cloned into the pQE80-oriT system and used to transform *E. coli* β2163, which was then used to transfer the empty vector and each construct into WT, IGR, *vfmE* and IGR,*vfmE* strains via conjugation. Results showed that neither the predicted sRNA nor the entire intergenic region added *in trans* generated changes in prodigiosin production in any of the recipient strains assayed (Fig. 5.23).

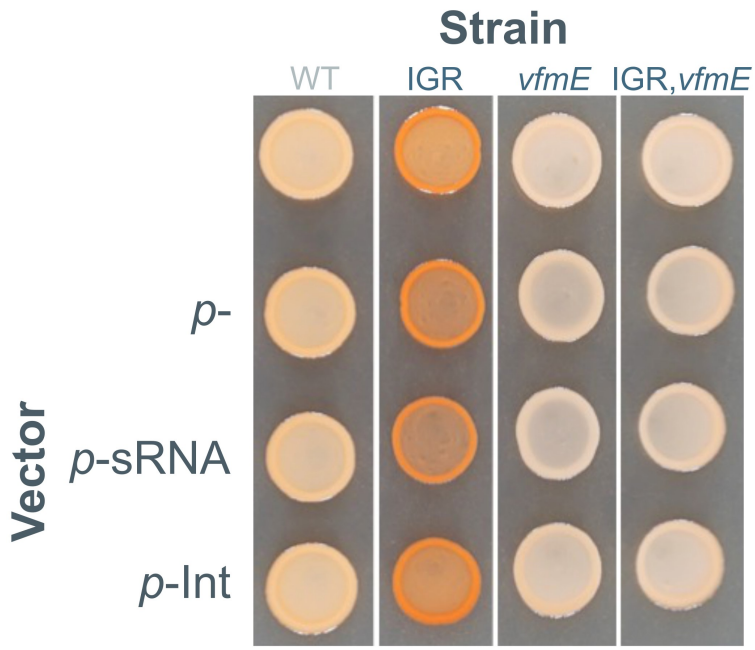


Figure 5.23. Putative small RNA and the intergenic region *in trans* do not restore prodigiosin production. The two constructs incorporating the small RNA (*p*-sRNA) or the intergenic region (*p*-Int) were expressed from the high-copy-number vector pQE-80-oriT (*p*-) with no induction. Bacterial patches of WT, IGR, *vfmE* and IGR,*vfmE* strains with or without plasmids were obtained from normalised cells (OD_{600}=1) spotted onto LBA plates for 18 h. The colour intensity indicates prodigiosin production level.

As it has been previously determined that IGR and *vfmE* mutations have contrary effects on swimming motility, it was tested whether the inserts in multicopy affected this feature. No perceptible differences in swimming haloes were observed for WT, IGR, or IGR,*vfmE* strains harbouring either the sRNA or the intergenic region. However, both inserts led to enhanced swimming ability in *vfmE* mutant cells (Fig. 5.24). The halo size from VfmE mutant cells increased upon *trans* addition of the candidate sRNA - which expanded even more when the full region that covers the candidate sRNA was overexpressed. Hence, only the swimming capacity of *vfmE* strain is affected by *in trans* addition of the tested fragments.

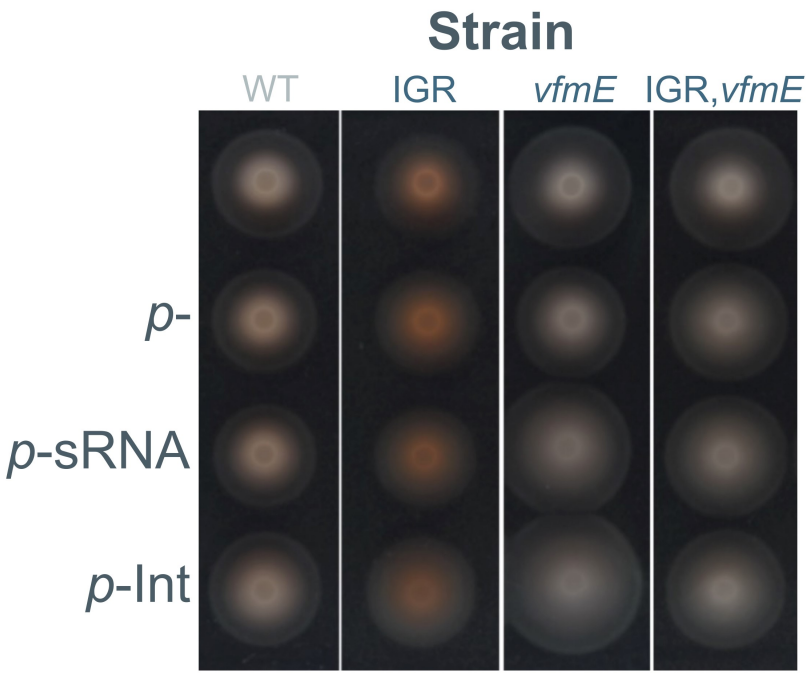


Figure 5.24. Putative small RNA and the intergenic region in trans boost swimming capacity of *vfmE* cells. The two constructs incorporating the small RNA (*p*-sRNA) or the intergenic region (*p*-Int) were expressed from the high-copy-number vector pQE-80-oriT (*p*-) with no induction. Bacterial patches of WT, IGR, *vfmE* and IGR,*vfmE* strains with or without plasmids were obtained from normalised cells (OD_{600}=0.2) spotted onto swimming plates for 14 h. The halo size is indicative of higher swimming capacity of cells.

As none of the tested fragments restored prodigiosin production levels, it was speculated that a larger fragment, probably acting as an antisense RNA (asRNA), might complement the intergenic (IGR) phenotype. Therefore, a new fragment starting from the same predicted place, spanning this time all the *vfmE* reading frame, plus a 300 bp region upstream from the start codon, was tested. This new 1,231 bp fragment, was cloned into the vector and then conjugated into the four strains tested earlier, WT, IGR, *vfmE*, and the double mutant IGR,*vfmE*. Again, the overexpression of this insert did not cause any change on any of the strains carrying the plasmids. Since this new attempt was unsuccessful, two final strategies were conceived: (i) two new forward primers with one and two extra single nucleotides added to test possible frames, and (ii), to discard that a putative long gene might start its transcription upstream of the intergenic promoter found previously, an insert spanning the entire IGR plus the antisense *vfmE* coding sequence and the 300 bp upstream of it, was also used for complementation. A summary of the fragments tested in complementation assays is shown in Fig. 5.25.

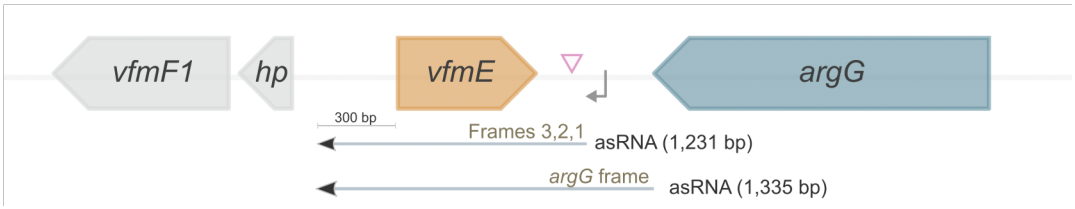


Figure 5.25. Summary of inserts tested in genetic complementation of the intergenic mutant: The three reading frames of a fragment starting downstream of the intergenic promoter until 300 bp upstream of the start codon of *vfmE* (putative asRNA), and a fragment starting immediately downstream of *argG* that covers up to the same end (a longer asRNA), are displayed.

All the last fragments followed the above-mentioned complementation procedure, as well as the strains, and once more, none could restore prodigiosin to WT levels upon their overexpression from plasmids.

5.7. Several transcripts convergent to vfmE start in the intergenic region

Since none of the different inserts used, with diverse lengths and reading frames opposite of *vfmE*, reverted the overproduction of prodigiosin, the next question was to what extent the antisense transcription relative to *vfmE*, evidenced by the IGR fusion strains, is found in the WT. Transcriptomic profiles should provide evidence about genes being actively transcribed and their direction. Hence, to find out the DNA extension covered by the antisense transcripts and whether there is transcriptional activity downstream of *vfmE*, the available transcriptomic data of S39006 was sought at Sequence Read Archive (SRA; NCBI) database. Paired-End RNA-seq raw files (control set) from the accession PRJNA635824 (Chilczuk *et al*, 2020) were chosen and dissected. Reads were mapped and sorted by position to the reference genome, generating files (BAM) separated by direction (sense and antisense). Directional reads in the intergenic area disclosed extensive transcriptional activity in the antisense strand, the opposite direction of *vfmE* reads (Fig. 5.26).

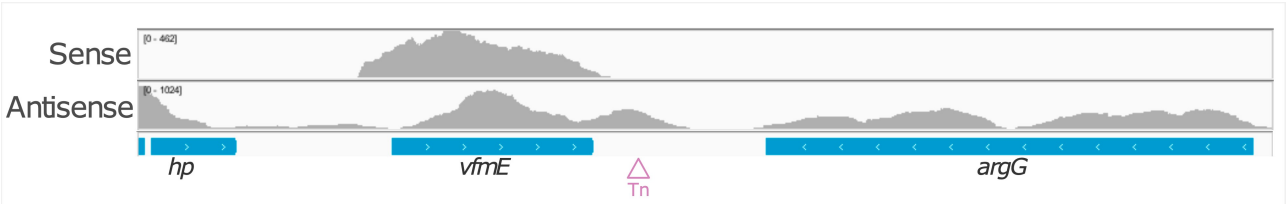


Figure 5.26. Extensive transcriptional activity in the opposite direction of *vfmE*. RNA-seq reads were mapped and aligned to the intergenic insertion (pink triangle) neighbourhood. A 3-kbp zoomed view of the zone shows the direction of reads as sense (top) and antisense (bottom) and the number of reads mapping to each position (read coverage) is displayed above genes (blue boxes). BAM files for each strand were indexed and inspected by using the Integrative Genome Viewer (IGV) software.

These reads apparently extend from half of the intergenic region between *vfmE* and *argG*, and overlap the *vfmE* reading frame (558 bp), with a possible stop at the start of this coding. Thus, the

reads mapped in the antisense strand of *vfmE* hint that the transposon interrupted a potential asRNA, which might have initiated its transcription upstream of the insertion site.

It is still unclear why, despite trying to complement the IGR mutant by trans-adding the three reading frames in this direction –encompassing the total length of *vfmE* coding region plus around 300 bp–, the phenotype restoration was not possible. One possible scenario would be that an even longer antisense RNA is operating, or perhaps there is more than one RNA being transcribed in the antisense direction, and somehow, they interact with each other. Another option is the transcription of a regulatory RNA encoded in the 3' UTR of *vfmE*. However, the transcriptomic data showed that this UTR appears to be rather short, and no reads are observed in the sense strand for the intergenic region. To gain more information about the length and localisation of a putative asRNA, the transcriptomic data was utilised for a genome-wide regulatory RNA prediction. Thus, by using the Rockhopper tool, a total of 1,258 predicted asRNAs were found in S39006's genome, including the RNA spanning the *vfmE* coding sequence, which was predicted to be 1,461 bp long. Bearing this information, the next stage of the analysis was the determination of the transcription start and end of this putative asRNA. For this, the Rapid amplification of cDNA ends (RACE) method was employed to identify the 5′ and 3′ ends of the antisense regulatory gene. Briefly, to begin with, the two furthest ends were sought, and surprisingly, from the determined start, a short transcript was uncovered. Next, as this revealed the presence of more than one transcript encoded in this region, a series of different primer sets were designed to determine all the potential transcripts encoded along the initially suspected asRNA. Thus, a total of three transcription start sites (TSS) were determined, all of them within the intergenic region. Likewise, only two transcription termination sites (TTS) could be found (Fig. 5.27 A). Downstream of the promoter region previously resolved, the first and shortest transcript (T1) was 182 bp long, which overlaps the second transcript (T2), starting 15 bp upstream of where T1 transcription halts. T2 was longer than T1 (546 bp) but shorter than the last transcript (T3), which transcribes from 109 bp downstream of T2 start. Unfortunately, the last 3' end, the TTS of T3, was not determined, but it is longer than 999 nt since no other TTS was found preceding this region.

Thus, it was found that up to three antisense transcripts, are transcribed in opposite direction to *vfmE*. Moreover, the T1 coincided with the predicted TSS from the promoter that was experimentally determined. Both T1 and T2 are the transcripts that, when affected by the insertions, would trigger the hyperpigmented phenotype.

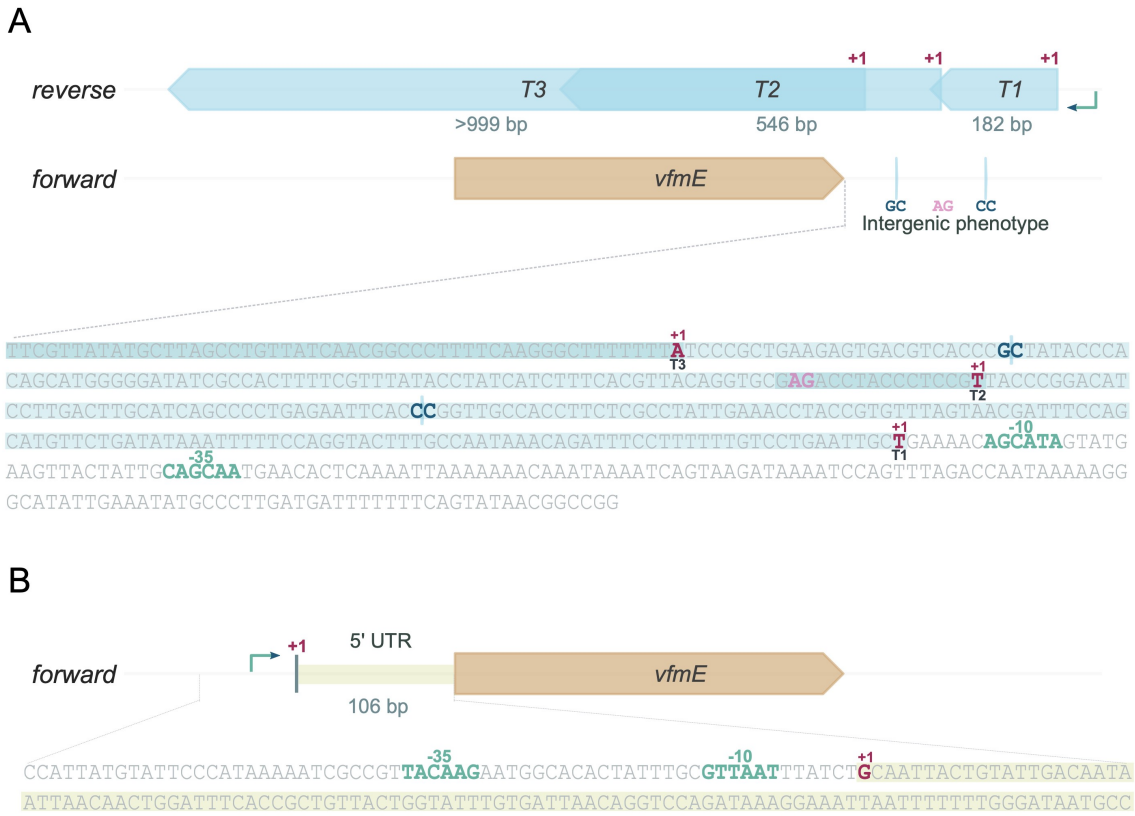


Figure 5.27. Up to three transcripts are transcribed opposite to *vfmE*. A: The reverse and forward strands containing the three possible antisense transcripts (light blue boxes) and the *vfmE* coding sequence (dark yellow box), respectively, are depicted. Names assigned to transcripts (T1-T3) are based on their position relative to the intergenic promoter (bended arrow). The length of each transcript in base pairs (bp) is shown underneath them. Downstream of the *vfmE* coding sequence (forward strand), the zone between the brackets GC-CC is the intergenic region previously found to increase the synthesis of prodigiosin when mutated, and AG (pink letters) indicates the approximate localisation of the transposon insertion found in this work. B: Map of *vfmE* upstream genetic elements. Only the forward strand containing the *vfmE* coding sequence and its elements is illustrated. Upstream of the coding sequence (dark yellow box), the 5' untranslated region (UTR) is highlighted in light green, and its length (bp) is shown below. Further upstream, the promoter is indicated by a bended arrow. The putative promoter boxes of *vfmE* (-35 and -10) are indicated in green letters in a zoom of the forward strand. Transcription start sites (+1 and purple letters) are indicated both in schematics and sequences.

In addition to the antisense transcripts, to incorporate the genetic elements present in the sense strand into the analysis, RACE attempts were also carried out for *vfmE*. Only the TSS of this gene was determined, unveiling a 106 bp long 5'UTR (Fig. 5.27 B). Furthermore, a putative promoter region (–10 and –35 boxes) was also inferred based on the TSS localisation. Unfortunately, due to time constraints, these transcripts in the intergenic region were not tested in complementation assays to investigate their effect on the strains.

5.8. VfmE in trans augments prodigiosin synthesis and perturbs cell growth

To check whether a plasmid-encoded VfmE can complement its corresponding mutant, and to test its effects on the other strains, the coding sequence was cloned into the pQE80-oriT system, and

the construct was used to transform *E. coli* β2163, and conjugated into WT, IGR, *vfmE* and IGR,*vfmE* strains. All the strains harbouring the overexpressed regulatory gene in the absence of induction displayed a hyperpigmented phenotype, except the double mutant IGR,*vfmE* (Fig. 5.28). Next, to test whether higher expression of the regulator was required for augmenting the prodigiosin synthesis in this strain, bacteria were grown in the presence of 0.1 mM IPTG. In this medium, all the strains produced higher levels of the pigment including, this time, the double mutant. Thus, this shows the hyperpigmentation is caused by the elevated activity of the VfmE regulator.

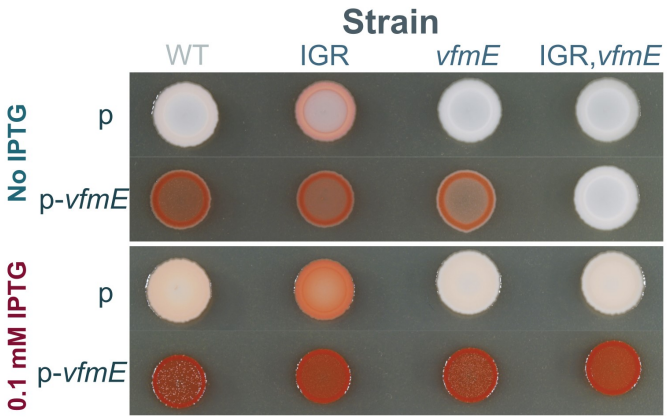


Fig. 5.28. Overexpression of *vfmE* leads to increased production of prodigiosin. WT, the intergenic (IGR), *vfmE*, and the double (IGR,*vfmE*) mutants, incorporating either the empty vector pQE80-oriT (*p*) or its *vfmE* derivative construct (*p-vfmE*) were grown in the absence or presence of the inducer IPTG. When present, the inducer was added to 0.1 mM. Bacterial patches were obtained from normalised cells (OD_{600}=1) spotted onto LBA plates for 18 h. The colour intensity indicates prodigiosin production level.

Furthermore, as it was previously shown that the intergenic mutation caused a detrimental effect on cell growth (e.g. Fig. 5.5), it was speculated that this might be due to increased VfmE activity. To test this, WT cells carrying either the empty vector or the *vfmE* construct were serially diluted and grown in LB medium, in the absence or presence of the expression inducer (IPTG). Comparable number of colonies from cells transformed with both plasmids, were obtained in plates lacking IPTG (Fig. 5.29). However, the addition of IPTG in two increasing concentrations (0.1 and
0.5 mM) provoked a dramatic reduction in the number of colonies and their sizes, compared to those incorporating the empty vector. No extra effect was observed from the five-fold increase in the inducer relative to 0.1 mM in the number of colonies. Therefore, the data suggests that the intergenic phenotype may be related to an enhanced production of VfmE.

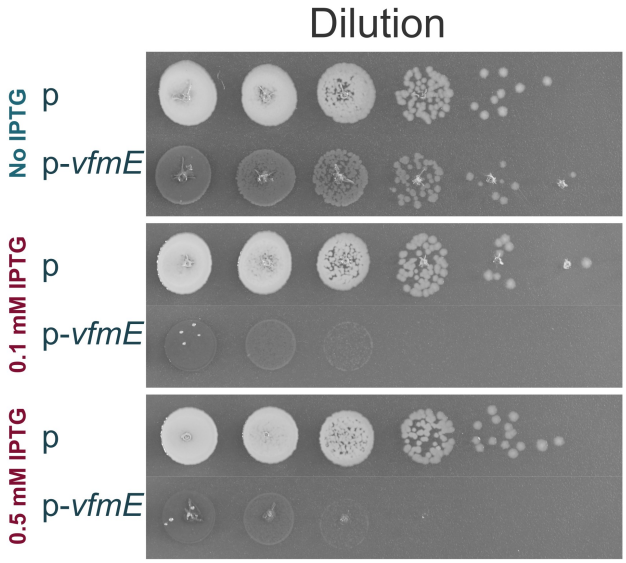


Fig. 5.29. Overexpression of *vfmE* negatively affects cell growth. the WT strain incorporating either the empty vector pQE80-oriT (*p*) or its *vfmE* derivative construct (*p-vfmE*) were serially diluted and grown in the absence or presence of the inducer IPTG. When present, the inducer was added to 0.1 and 0.5 mM. 5 µL of normalised cell density (OD_{600}=1) were spotted onto LBA plates containing inducer, when indicated, for 18 h.

5.9. Intergenic and vfmE mutations are epistatic to several known regulators

The intergenic phenotype seemed to be related to hyperactivity of the transcriptional regulator VfmE. To investigate potential mechanisms that drive overproduction of the antibiotics upon the intergenic insertion, and their decrease in the VfmE minus strain, double mutants with 14 previously investigated antibiotic regulators were created by phage transduction. Thus, by contrasting the antibiotic levels of double and isogenic strains, potential connections with known mechanisms might be elucidated. Moreover, expression changes of the fusion strains induced by the intergenic and the *vfmE* mutations were assessed.

As initially determined for prodigiosin production, transposon interruption of the intergenic region also increased the production in most of the regulatory genetic backgrounds tested (Fig. 5.30, top). This increase occurred for ten of the regulators, above their altered pigment synthesis, except for the *pigT* and *rsmA* mutations. The overproduction of prodigiosin in regulatory mutant backgrounds was approximately 1.3 to over 14 times higher than in their isogenic strains. In increasing magnitude, significant changes were found for *pigR* (p =0.0011), *pigX* (p =6.58e^{-5}), *phoB* (p =7.43e^{5}), *carR* (p =0.0024), *pigZ* (p =2.46e^{-5}), *pigS* (p =0.002), *rsmB* (p =0.0032), *pigW* (p =0.005), *pigU* (p =0.0015), and *pigP* (p =0.00063). The transposon insertion did not reinstate the prodigiosin synthesis in cells lacking *hfq* or *rap*.

On the contrary, a mutation of *vfmE* in these regulatory mutants reduced pigment production in eight strains, except *pigR* and *pigT* mutants, whose levels did not experience modifications (Fig. 5.30, bottom). A significant drop starting from 24% to up to 66 % in pigment production was observed, in increasing impact order, for *pigW* (p =0.043), *rsmA* (p =0.00012), *phoB* (p =0.0095), *pigS* (p =0.016), *pigZ* (p =0.0048), *pigP* (p =0.0002), *pigX* (p =1.63e-5), and *rsmB* (p =0.0097). Curiously, this extra *vfmE* mutation in the *carR* mutant generated the opposite effect, elevating prodigiosin synthesis to WT average (p =0.021). No pigment changes were detected in the strains *hfq*, *pigU*, and *rap* nor their double mutants.

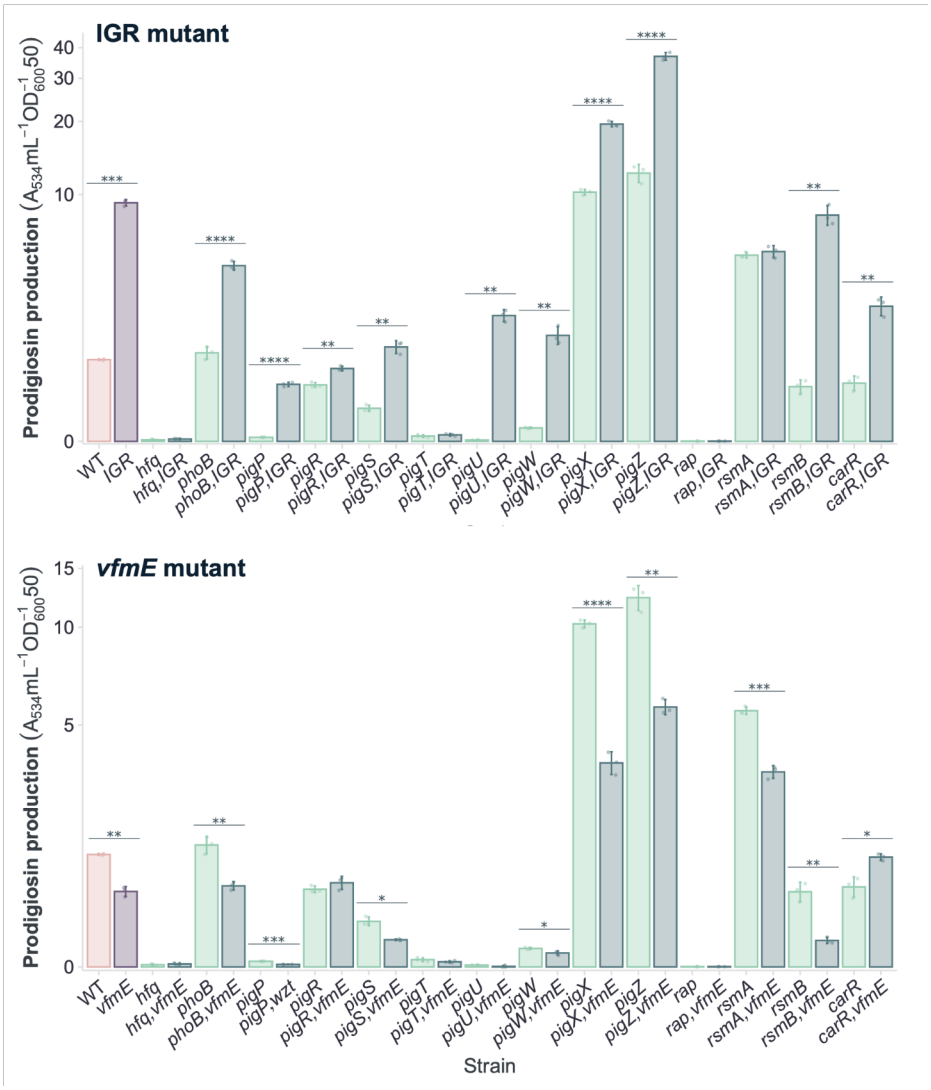


Fig. 5.30. The intergenic and *vfmE* mutations bypassed prodigiosin production in several known regulatory mutants. Prodigiosin synthesis was quantified by spectrophotometry (A_{534}) and normalised by cell growth (OD_{600}). Darker-coloured bars indicate the presence of either the intergenic (IGR; top) or *vfmE* (bottom) mutation. The means of data ± standard deviation from three biological replicates taken at an early stationary phase are shown. Statistical analysis was conducted by Student's t-test: *$p < 0.05$, ** $p < 0.01$, *** $p < 0.001$, **** $p < 0.0001$.

For carbapenem production, the opposite effects of the two mutations investigated were once more observed. Higher levels of this antibiotic were found for strains containing the intergenic insertion, but only in four mutant strains: *phoB* (p =0.0077), *pigW* (p =0.0142), *pigZ* (p =0.0045), presenting a 1.4–1.8-fold increase, and *pigU*, in which the abolished synthesis was restored upon the extra mutation (p =0.002; Fig. 5.31, top). On the contrary, the intergenic mutation caused a drop in *rsmB* strain's production (p =0.00019). No changes in carbapenem production between the double and isogenic strains *pigR*, *pigS*, and *pigX* were encountered. Also, in agreement with the pigment synthesis, the restoration of carbapenem production was not observed in *hfq* and *rap* mutants, in addition to *pigP*, *rsmA*, and *carR*. Strikingly, the intergenic mutation completely suppressed carbapenem production in the *pigT* background.

The *vfmE* mutation in regulatory mutant strains had the same effect as on prodigiosin synthesis, diminishing carbapenem biosynthesis, but only in six mutants (Fig. 5.31, bottom). In them, a 44% to 66 % decay in production compared to their isogenic levels occurred in the following order: *pigZ* (p =0.0027), *phoB* (p =0.015), *pigS* (p =0.0024), *pigT* (p =0.0046), *pigW* (p =2.12e^{-5}), and *pigX* (p =7.48e^{-5}). In *pigR* and *rsmB* backgrounds, no differences in production by the double mutants relative to the parental strain were found. For the rest of the regulators, *hfq*, *pigP*, *pigU*, *rap*, *rsmA*, and *carR*, no carbapenem halo formation was detected for either double or isogenic strains.

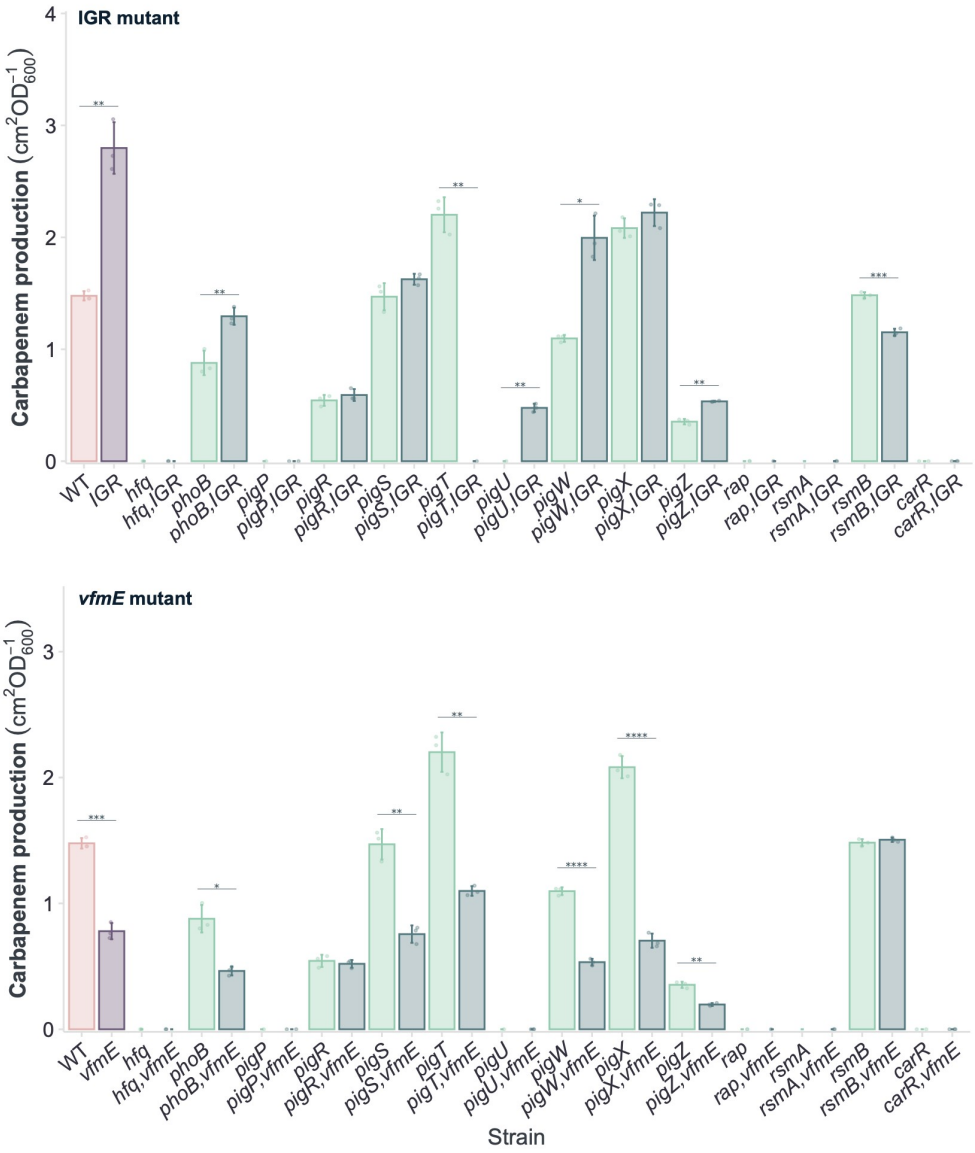


Fig. 5.31. The intergenic and *vfmE* mutations bypassed carbapenem production of several known regulators. Carbapenem synthesis was quantified by halo formation using an indicator strain and normalised by cell growth (OD_{600}). Darker-coloured bars indicate the presence of either the intergenic (IGR; top) or *vfmE* (bottom) mutation. The means of data ± standard deviation from three biological replicates taken at an early stationary phase are shown. Statistical analysis was conducted by Student's t-test: *$p < 0.05$, ** $p < 0.01$, *** $p < 0.001$, **** $p < 0.0001$.

From the set of known regulatory mutants, ten strains are LacZ fusions, and the impact of both the intergenic and *vfmE* mutations on their expression was investigated. The insertions were shown to influence the transcription of five known regulators. The intergenic mutation significantly reduced the expression of *pigP* (p =0.0157) and *carR* (p =0.0251) and augmented that of *pigT* (p =0.0022; Fig. 5.31). The expression of *pigP* and *carR* was decreased by 35% and 20% on average, whilst that of *pigT* was notably 2.4 times higher than its isogenic strain. The *vfmE* mutation, on the other hand, reduced *pigR* (p =0.0099) by approximately 10% of the transcriptional levels, and increased *pigW* (p =0.0094), nearly doubling its isogenic values (Fig. 5.32).

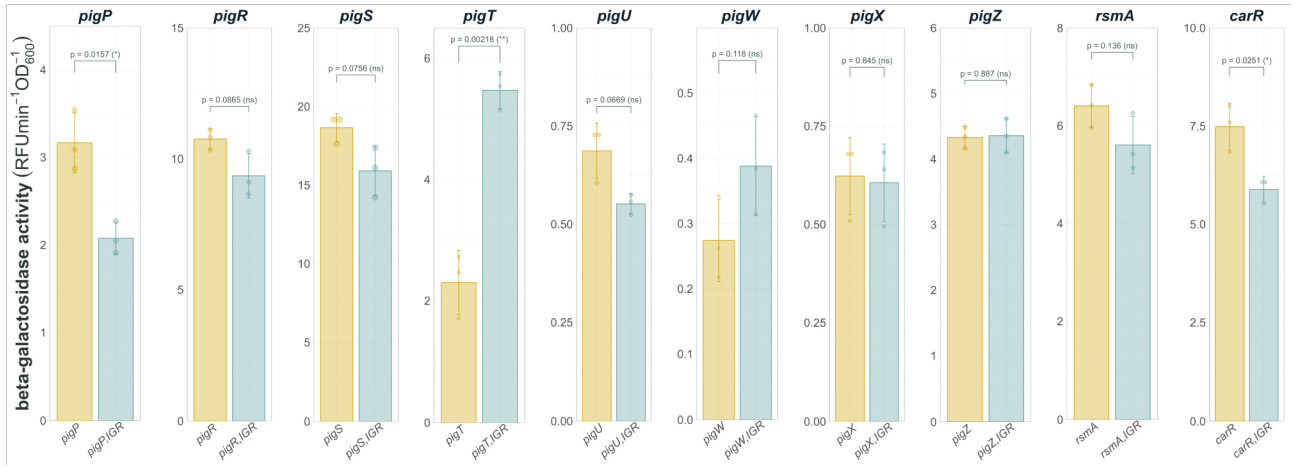


Fig. 5.32. Mutation in the intergenic region augments transcription of *pigT* and decreases that of *pigP* and *caR*. Normalised β-galatosidase (LacZ) activity was measured at early stationary phase and expressed as relative fluorescence units (RFU). The average of three biological replicates (± standard deviation) and significance (Student's *t*-test, p <0.05) are shown.

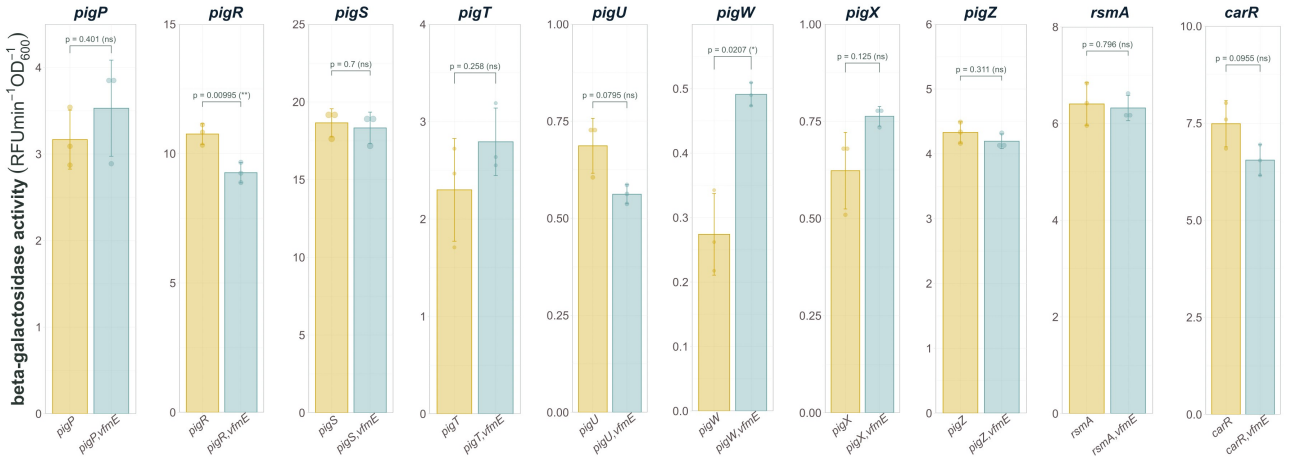


Fig. 5.33. Mutation of *vfmE* diminishes transcription of *pigR* and augments that of *pigW*. Normalised β-galatosidase (LacZ) activity was measured at early stationary phase and expressed as relative fluorescence units (RFU). The average of three biological replicates (± standard deviation) and significance (Student's *t*test, p <0.05) are shown.

Altogether, these findings showed that both the intergenic and *vfmE* mutations are epistatic over several of the known regulatory mutants tested, but displaying contrary effects. Neither of the mutations under study were able to bypass the effect of *hfq* or *rap* mutations in antibiotic production. In prodigiosin production, the regulators *pigT*, *pigR*, and *rsmA* might form part of the same regulating pathway as the intergenic and *vfmE* mutants. The *pigP*, *rsmA* and *carR* mutants were not bypassed by the tested mutations in carbapenem synthesis, and *pigR*, *pigS*, *pigX*, and *rsmB* showed no additive effects compared to that of the intergenic or *vfmE* double mutants.

5.10. Discussion

In the present chapter, an intergenic mutation that prompted overproduction of antibiotics led to the discovery of VfmE, a novel transcriptional regulator in S39006. The *vfmE* and intergenic mutations showed opposite effects on some phenotypic features, but not all. The dominance of the *vfmE* phenotype over the intergenic one showed its regulatory role, which was physiologically pleiotropic.

The intergenic insertion was between two convergently transcribed genes and displayed an increased pigmentation compared to the WT strain, and it was therefore further studied. The transposon was localised downstream relative to a sole reading frame, *argG*, which encodes the argininosuccinate synthetase. This enzyme participates in the synthesis pathway that converts citrulline to arginine, along with ArgH, the argininosuccinate lyase (Charlier and Bervoets, 2019). Both are generally found forming an operon, however, *argH* was not located nearby in the S39006 genome. Instead, upstream of *argG* two apparently unrelated genes were located. The first one encodes a ThiJ/PfpI domain-containing protein, and the second the transcription factor, XylR. In the opposite position to *argG*, surrounding the inserted transposon, an AraC-family regulator gene was situated. Homology search revealed its similarity to *vfmE*, which encodes a protein previously shown to direct virulence in *Dickeya* strains, through modulating a secondary quorum sensing (QS) system (Nasser *et al*, 2013). In this system, an unknown signalling molecule termed *vfm* (**v**irulence **f**actor **m**odulating) operates. A gene coding for a hypothetical protein was discovered immediately upstream of *vfmE*, followed by two more *vfm*-related genes, homologues of *vfmF* and *vfmJ* (see chapter 6 for details), and finally, the gas vesicle biosynthesis cluster.

Both the ArgG and VfmE phylogenetic trees revealed that ArgG was highly similar to that of other bacterial species and genera, whilst VfmE-similar proteins were only found in a reduced group of genera. Regardless of their conservation, in both cases, the S39006 proteins clustered with homologues from *Dickeya* strains, but no *Serratia* genus homologues were obtained for VfmE. This relatedness of S39006 to *Dickeya* agreed with previous work on the taxonomic relationship (Duprey *et al*, 2019; discussed in section 4.6).

The intergenic region that was the site of the transposon insertion was also previously found to stimulate pigment production in S39006. This study reported six independent transposon insertions, spanning a 127 bp zone, that provoked the hyper-red phenotype (Wilf, 2011). It was also shown that *vfmE* expression was higher when the intergenic region was interrupted, while the transcription of *argG* was unaltered. Due to these facts, both the intergenic and the *vfmE* mutants were examined for other effects on S39906 phenotypes. These mutations had contrary effects on antibiotic production and swimming capacity, in which the intergenic insertion enhanced the

synthesis of both compounds and diminished the flagellum-based cell motility, just the opposite to the *vfmE* deficient. Moreover, it was shown that impact on prodigiosin synthesis is controlled at the transcriptional level whereas, expression of the carbapenem operon, *carA-H*, did not change in the presence of either the intergenic or *vfmE* mutations, from early log phase onwards. A previous study of transposon mutants derived from *D. dadantii* 3937 reported that the *vfmE* mutant produced decreased levels of indigoidine –a blue pigment– compared with theWT strain, in the presence of polygalacturonic acid. The biosynthetic genes of this pigment are located upstream of the *vfm* operons in this strain, and the authors suggested a link between indigoidine and the *vfm* region. Moreover, this mutation decreased the swimming capacity of cells compared to WT strain (Monson *et al*, 2015). This capacity in *D. solani* was later shown to be strain-dependent. It was also reported that *D. dadantii* 3937 lacking this regulatory gene showed no differences in swimming motility in comparison to WT (Potrykus *et al*, 2018). Therefore, unlike *Dickeya* species, VfmE exerts a negative control on this type of cellular locomotion in S39006. For gas vesicle production, it was observed in the flotation assay that the *vfmE* cultures displayed an enhanced buoyancy compared to that of WT. Nonetheless, the transcription of the two biosynthesis operons (*gvpA1* and *gvrA)* was reduced compared to the correspondent isogenic fusion strains with the additional intergenic and *vfmE* mutations. In terms of virulence, both mutations led to an attenuated pathogenicity in the potato tuber assay, but the intergenic mutation had a more detrimental impact than *vfmE*. This is contradicted by the intact ability of the intergenic strain to produce both pectate lyase and cellulase, the degradative enzymes that enable cells to infect plants. Furthermore, even though the *vfmE* mutant had a reduced cellulase activity, it was more virulent than the intergenic mutant strain. This might be caused by a combination of the impaired growth and poor swimming motility displayed by the intergenic mutant strain. Similarly to S39006, decreased cellulase synthesis was observed in *D. dandantii* 3937 *vfmE*, but no variation in pectate lyase production was observed (Monson *et al*, 2015). A deletion of this gene ultimately leads to attenuated virulence in potato tubers (Banerjee *et al*, 2022). As shown for swimming capacity, *D. solani* strains production of both degrading enzymes varies from strain to strain, as well as the degree of potato tissue maceration (Potrykus *et al*, 2018).

Since VfmE activates a secondary QS in *D. dadantii* 3937 (Nasser *et al*, 2013), it was relevant to investigate whether this regulator impacts the synthesis of the QS primary signalling molecules in S39006, as well as the intergenic mutation. The production of these molecules, acyl-homoserine lactones, is carried out by the SmaI synthase, a LuxI homologue (Thomson *et al*, 2000; Slater *et al*, 2003), which was used to monitor transcriptional changes over time. Thus, the *smaI*::*lacZ* strain, to which either the intergenic or the *vfmE* mutations were added, showed no expression changes compared to the parental fusion. Hence, both the intergenic and *vfmE* modulate antibiotic

production in a QS-independent fashion. The corresponding LuxIR homologues in *Dickeya* strains are ExpIR, which are also based on synthesis and reception of acyl-homoserine lactones (Reverchon *et al*, 1998; Crépin *et al*, 2012; Feng *et al*, 2019). Mutants of these two genes in *D. solani* have been shown to possess reduced virulence (Potrykus *et al*, 2014) and double mutants with *vfmE* showed no additive effect, as pathogenicity was not further reduced compared to the single mutant (Potrykus *et al*, 2018). ExpI-lacking strains in *D. zeae* show enhanced motility and reduced virulence in potato tubers (Hussain *et al*, 2007), whereas in *D. dadantii* this mutation caused no effect on virulence in witloof chicory leaves (Ham *et al*, 2004). The double mutant between the intergenic and *vfmE* mutations, IGR,*vfmE*, exhibited the same phenotype as *vfmE* in antibiotic synthesis, motility, and virulence, which shows its dominance over the intergenic mutation, suggesting that at least some phenotypic characteristics are due to VfmE action. This regulator positively controls the expression of a putative gene encoded in the intergenic region, in opposite direction to *vfmE*. Also, it was experimentally shown to increase the activity of the putative Sigma 38 (RpoS) promoter found in the intergenic region. RpoS belongs to the Sigma 70 family, and it is a pivotal stress-responsive gene regulator in the stationary growth phase (Schellhorn, 2020). Its absence in S39006, leads to overproduction of antibiotics (Wilf and Salmond, 2012). From the results, VfmE might regulate its own expression by activating a repressor that transcribes in opposite direction. Increased antisense transcription may thus reduce *vfmE* expression. Intriguingly, the 14 nt region upstream of the intergenic promoter not only allows VfmE to increase this activity but also XylR, another AraC family regulator. This binding site is comparable to that of ToxT (TcpN) from *Vibrio cholerae*, as a virulence-expression activator (Higgins *et al*, 1992; Champion *et al*, 1997). Another similar motif for the S39006 query was CovR (data not shown), a response regulator of the two-component system CovSR in *Streptococcus agalactiae* (Lamy *et al*, 2004), which is also associated with virulence (Mazzuoli *et al*, 2004).

Bioinformatic predictions to find a gene within the intergenic region affected by the transposons identified a putative reading frame of 261 nt. This sequence had been previously shown not to restore the effects of the intergenic mutant phenotype (Wilf, 2011). Next, a longer sequence (330 nt) was tested along the entire intergenic region, and again, neither was able to recover the WT prodigiosin production in the hyperpigmented strains. However, testing of swimming ability of cells carrying these two inserts in multicopy revealed they may improve this capacity. Nonetheless, it remains to be determined whether the differences observed are significant. The speculation that an even longer transcript should be transcribed in the opposite direction to *vfmE* was then assayed. The antisense transcripts enable specific fine-tuning of their cognate gene activity, by either forming double-strand RNA that is later degraded, or by collision of RNA

polymerases (ToledoArana and Lasa, 2019; Lejan and Hajnsdorf, 2020; Chia *et al*, 2021; Millar and Raghavan, 2021). The recent transcriptome of *D. dadantii* revealed that 83 transcripts had their respective antisense transcripts, one of them being *vfmE*. In that strain, this gene is transcribed opposite to the transcription unit *vfmAZBCDFG*, which generates overlapping mRNAs and might mutually regulate their expression (Forquet *et al*, 2022). However, upon testing of a fragment spanning the *vfmE* reading frame plus 300 bp upstream in opposite direction to *vfmE*, the intergenic mutation pigmentation remained unchanged. Additionally, the other two frames of this putative asRNA were also tested, but did not turn down the prodigiosin levels. As the fragments employed in genetic complementation were not capable of reverting the hyperpigmented phenotype, it was suspected that other type of regulator might be involved. Thus, it was sought to find riboswitches by scanning the intergenic region. These alternative cis-acting controllers of gene expression are proteinindependent and usually rely on small molecules (Bastet *et al*, 2018; Pavlova *et al*, 2019). However, none was predicted. By analysing the directional reads from the WT transcriptome, it was found that there was profuse activity convergent to *vfmE*. This fact would support the hypothesis of a large asRNA negatively controlling *vfmE*, but it was not the case with the inserts assayed, as the intergenic mutation could not be complemented. The dissection of the transcript ends that are oppositely transcribed in relation to *vfmE* showed an unexpected result. Three transcripts were determined, all of them commencing within the intergenic region. Unfortunately, they could not be experimentally tested in complementation assays due to time limitations. Testing of each individually could clarify their roles.

The *vfmE* phenotype was complemented by *in trans* addition of its coding sequence, which agreed with the previous work, but that data was not provided (Wilf, 2011). Multicopy, but leaky expression of VfmE increased production of prodigiosin in three out of four strains tested. These were WT, IGR, and *vfmE* strains, whilst the double IGR,*vfmE* mutant displayed no colour change upon addition of the regulator. IPTG-induced strains exhibited even more pigmentation, including this time the double mutant strain, confirming that the higher production of prodigiosin is provoked by higher VfmE levels. Furthermore, the intergenic mutant strain showed a slight growth defect in addition to elevated antibiotic synthesis. Thus, the intergenic phenotype is caused by an increased VfmE action.

Through comparisons of antibiotic production by single and double mutants with fourteen known regulatory mutations, potential connections affecting antibiotic production were investigated. The intergenic mutation increased prodigiosin production in ten regulatory mutants while it did in four strains for the carbapenem antibiotic. In regulatory mutants made defective for VfmE, prodigiosin synthesis declined in eight strains and in six strains for carbapenem. Neither the

intergenic nor *vfmE* mutation could supress the *hfq* and *rap* phenotypes, whose absence completely abolishes the synthesis of antibiotics in S39006, supporting their place at the top of the regulatory hierarchy. In prodigiosin synthesis, the *pigT* mutant did not experience any significant change in pigment levels with either of the two additional mutations. Furthermore, in cells carrying the intergenic insertion, *pigT* expression increased significantly, whereas in cells lacking *vfmE*, there was no change in its expression. This PigT regulator is a homologue of GntR *E. coli* that was predicted to directly activate the prodigiosin operon at low levels of gluconate (Fineran *et al*, 2005). Moreover, it is noteworthy that in the region upstream (201 bp) of the *pigT* start codon, two motifs similar to the one shown to increase the intergenic promoter activity by VfmE and XylR are present (data not shown). This hints that VfmE may activate *pigT* expression. These results support the idea that the intergenic mutation alleviates a negative control on *vfmE*, which in turn might increase the production of prodigiosin via PigT activity. In addition to *pigT*, *rsmA* also showed no pigment modification in the presence of the intergenic mutation, but its synthesis was reduced by the *vfmE* mutation. RsmA, a CsrA homologue, is an RNA-binding protein that controls many processes in prokaryotes and it represses antibiotic synthesis in S39006 (Williamson *et al*, 2008; Wilf *et al*, 2013). The expression of this global regulator was not altered by the intergenic mutation or *vfmE*. Earlier transcriptomic data from S39006 revealed that *rsmA* inactivation diminishes the expression of *vfmE* and *rap* (Wilf *et al*, 2013), and therefore, a reduced VfmE activity in this background might explain the unchanged prodigiosin synthesis when the intergenic insertion was present. It is not known whether *pigT* modulates *rsmA* expression or vice-versa; although there could be a connection through the use of carbon sources such as glucose and gluconate. Finally, synthesis of prodigiosin in the *pigR* mutant did not decrease in the absence of *vfmE*, and, in this background, the expression of this regulator decreased. PigR has been predicted to encode a class IV adenylate cyclase that presumably modulates the synthesis of both antibiotics by the intracellular messenger 3',5'-cyclic adenosine monophosphate (cAMP; Fineran *et al*, 2005). However, its regulatory mechanisms remain elusive. This signalling molecule is found across all life kingdoms and its producing enzymes are grouped in six classes (I-VI; Khannpnavar *et al*, 2020). The membranebound class IV, encoded by *cyaB*, is associated with virulence (Ante *et al*, 2021) and synthesis of capsule polysaccharide and biofilm formation (Regmi *et al*, 2022). The transcription factor CRP (cAMP receptor protein, also termed Catabolite Activator Protein, CAP) forms a complex with cAMP, enabling it to regulate gene expression (Harman, 2001). In another prodigiosin-producer *Serratia* strain, *S. marcescens*, it was demonstrated that CRP negatively regulates the synthesis of prodigiosin at the transcriptional level (Kalivoda *et al*, 2010; Shanks *et al*, 2013). A *crp* mutation in *E. coli* was shown to boost expression of the S39006 pigment synthesis operon, and a potential

CRP binding site was found on its promoter, which overlaps half of the PigT binding motif (Fineran *et al*, 2005). The authors also pointed out that, in *E. coli*, the *gntR* promoter is controlled by GntR and CRP (Peekhaus and Conway, 1998). Therefore, there may be a rational linkage linkage between PigT and PigR regulation.

In the case of carbapenem, more actors might be involved in the regulation of its production. In addition to *hfq* and *rap*, neither the intergenic nor *vfmE* mutations reinstated carbapenem synthesis in the absence of *pigP*, *rsmA*, and *carR*. This implies they are in higher positions in the regulating hierarchy. PigP is a major transcriptional regulator that modulates antibiotic production through expression activation of *pigQ*, *pigS*, *rap* and *carR* and repression of *pigR*, *pigV*, and *pigX* (Fineran *et al*, 2005). CarR is a LuxR-type activator of the carbapenem biosynthesis operon (McGowan *et al*, 1995). The intergenic mutation decreased the transcription of both *pigP* and *carR*. No changes in double mutant synthesis relative to their parental strain were detected for the *pigR* strain carrying either the intergenic or *vfmE* mutations. Moreover, *pigS* and *pigX* synthesis were unaffected by the intergenic mutation, as well as *rsmB* when devoid of *vfmE*. PigS is an ArsR/SmtB family transcription factor that activates prodigiosin synthesis at the transcriptional level and it is under regulation by PigP (Fineran *et al*, 2005; Gristwood *et al*, 2011) and it has no known participation in carbapenem synthesis. PigX is a phosphodiesterase (PDE) that degrades the intracellular messenger cyclic dimeric guanosine monophosphate (c-di-GMP) (Fineran *et al*, 2005; Fineran *et al*, 2007). Finally, the non-coding RNA RsmB, a homologue of CsrB, decreases RsmA activity by binding to it (Williamson *et al*, 2008). The *vfmE* mutation reduced expression of *pigW*, which codes for the response regulator partner of PigQ in a two-component system, but it was bypassed by both mutations when tested.

Thus, the *pigR* phenotype is dominant for carbapenem production over both mutations, suggesting they may be in the same regulatory pathway. Interestingly, *pigX* has been correlated with the Rsm regulating route through swarming motility, and it was demonstrated that this PDE repressed expression of *rsmB*, probably by adjusting the c-di-GMP cellular levels (Williamson *et al*, 2008). This messenger exerts its control on cellular machinery through the use of signal-responsive effectors (Valentini and Filloux, 2019) and it was recently demonstrated that VfmE from *D. dadantii* is one of them (Banerjee *et al*, 2022). This regulator, moreover, positively regulates *gcpA* and *egcpB*, a diguanylate cyclase (DGC) and a PDE, respectively. However, inactivation of *vfmE* had no effects on intracellular c-di-GMP levels, and high levels of this signal repress the regulator transcription. It has been also reported that cAMP can directly interact with a c-di-GMP-responsive effector (Liu *et al*, 2022), thus VfmE could be a messenger-based effector that might respond to more than one intracellular signal. Further investigation is needed to resolve how these regulators interact to ultimately control antibiotic production.

This chapter showed that the intergenic mutation impacted an unknown mechanism that negatively controls the expression of the transcription factor VfmE, which may correspond to a self-regulatory system. This regulator activates antibiotic biosynthesis and modulates other phenotypic features. Moreover, by assessing a large library of known regulators, some functional interactions of both the intergenic and the *vfmE* mutations and members of the extremely complex antibiotic production network were exposed. Thus, regulators linked to carbon source utilisation and intracellular signal sensing are likely features involved in the physiological complexity of antibiotic production in S39006.

Chapter 6. VfmE is essential in *vfm* secondary quorum sensing system

Through investigating the intergenic insertion mutant and its impact on cell physiology, the driver of antibiotic synthesis was shown to be the transcriptional regulator VfmE. This AraC-type protein in *Dickeya* strains fulfils a central role in coordinating a secondary quorum sensing (QS) system, which relies on an unidentified extracellular messenger. This chapter describes a linkage between VfmE and this unknown signalling system in S39006.

6.1. S39006 has the vfm quorum sensing system components

The transcription regulator VfmE is a pivotal player in a secondary QS system linked to virulence. The *vfm* (**v**irulence **f**actor **m**odulating) gene cluster was discovered in *D. dadantii* 3937 and it directs the synthesis, export, and sensing of an extracellular signal termed Vfm, which triggers expression of virulence genes (Nasser *et al*, 2013). This signalling molecule levels rise from the middle to the end of the logarithmic growth phase and then fall in this strain. The Vfm molecule has not been isolated, and its structure remains unknown. Based on individual protein functions, it was inferred that this signal contains amino acid and fatty acid moieties (Nasser *et al*, 2013). This cluster was also reported to be present in the genomes of *D. paradisiaca* Ech703 (recently renamed as *Musicola paradisiaca*), *D. chrysanthemi* Ech1591, *D. zeae* Ech586, *D. zeae* EC1 (Zhou *et al*, 2015) and in *D. solani* (Potrykus *et al*, 2018). The *vfm* cluster in *D. dadantii* 3937 is comprised of 25 genes, which are grouped into five transcriptional units: *vfmAZBCD*, *vfmE*, *vfmFGHIJ*, *vfmKLMNOPQRSTUVW* and *ID16066* (Fig. 6.1, top). Given that VfmE was shown to control antibiotic biosynthesis in S39006, and that two *vfm* system homologues (*vfmF* and *vfmJ*) were discovered upstream of *vmfE*, it was hypothesised that other proteins from this QS system would be found elsewhere in the genome. Hence, a Blastp-based search was performed using the amino acidic sequences of the remaining 22 *vfm* proteins from *D. dadantii* 3937, and genes encoding similar proteins were mapped in the *Serratia* genome (Fig. 6.1, bottom).



Fig. 6.1. Comparison of *vfm* clusters of *Dickeya dadantii* 3739 and *Serratia* sp. ATCC 39006. Gene colours denote genes belonging to experimentally determined transcriptional units (boxes on the right) in *D. dadantii* 3937 (Nasser *et al*, 2013). The *vfm* cluster in *D. dadantii* occupies a single genomic position,

whilst that of *Serratia* is split into two locations (indicated by '//'). Genes in red were only found in the *Serratia* genome, albeit the *hp* (encoding a hypothetical protein) between *vfmR* and *vfmT1* might encode a VfmStype protein. Genes were drawn to scale using their nucleotide length.

Protein	Length	Gene	Uniprot ID	Identity (%)	Function (GO)	Predicted activity
VfmA	286	Ser39006_016235	A0A2I5T9K6	37.6	Acyltransferase (Thiolase-like)	3-oxoacyl-ACP synthase
VfmZ	84	Ser39006_016240	A0A2I5T9H4	58.1	Phosphopantetheine binding ACP domain	Acyl carrier protein
VfmB	222	Ser39006_016245	A0A2I5TQQ5	56.2	Oxidoreductase	Acyl-CoA dehydrogenase
VfmC	452	Ser39006_016250	A0A2I5T9H7	45.9	Transmembrane MatE	Na^+-driven multidrug efflux pump
VfmD	329	Ser39006_016255	A0A2I5T9J0	45.6	Serine aminopeptidase, S33	Alpha/beta hydrolase
VfmE	185	Ser39006_001310	A0A2I5TEA0	82.4	DNA-binding transcription factor	AraC family regulator
VfmF1	235	Ser39006_001300	A0A2I5TEA1	83	ATP-binding protein (untA)	ABC transporter (MacB)
VfmF2	235	Ser39006_016275	A0A2I5T9I9	63.1	ATP-binding protein (untA)	ABC transporter (MacB)
VfmG	847	Ser39006_016270	A0A2I5TLV9	41.2	FtsX-like permease	Peptide ABC transporter permease
VfmH	483	Ser39006_016265	A0A2I5T9I4	50.9	ATP-binding (Response regulator)	Sigma-54-dependent Fis family
VfmI	438	Ser39006_016260	A0A2I5T9H2	40	Histidine kinase	FixL homologue
VfmJ	254	Ser39006_001295	A0A2I5TEB0	53.2	Holo-[acyl-carrier-protein] synthase	4'-phosphopantetheinyl transferase
VfmK	476	Ser39006_016230	A0A2I5TLX0	53.6	Pyridoxal-dependent decarboxylase	Diaminopimelate decarboxylase
VfmL	291	Ser39006_016225	A0A2I5TLW3	33.8	Acyltransferase (Thiolase-like)	3-oxoacyl-ACP synthase
VfmM	526	Ser39006_016215	A0A2I5TDC5	51.6	AMP-dependent synthetase/ligase	Long-chain fatty acid-CoA ligase
VfmN	86	Ser39006_016210	A0A2I5T9M3	44.2	Phosphopantetheine binding ACP domain	Acyl carrier protein
VfmO	505	Ser39006_016205	A0A2I5T9H3	43.9	AMP-dependent synthetase/ligase	Alanine-phosphoribitol ligase
VfmP	513	Ser39006_016200	A0A2I5T9G0	44.3	AMP-dependent synthetase/ligase	Alanine-phosphoribitol ligase
VfmR	388	Ser39006_016195	A0A2I5T9I0	48.5	Oxidoreductase	Acyl-CoA dehydrogenase
VfmT1	316	Ser39006_016185	A0A2I5TLV2	45.5	Acyltransferase (Thiolase-like)	3-oxoacyl-ACP synthase
VfmT2	328	Ser39006_016220	A0A2I5T9H9	22.2	Acyltransferase (Thiolase-like)	3-oxoacyl-ACP synthase
VfmU	362	Ser39006_016180	A0A2I5TDG0	47.3	Butyryl-CoA Dehydrogenase	Acyl-CoA dehydrogenase
VfmV	286	Ser39006_016175	A0A2I5TLU8	42.9		Uncharacterized protein
VfmW	325	Ser39006_016170	A0A2I5TLW0	42.2	Acyltransferase (Thiolase-like)	3-oxoacyl-ACP synthase
ID16066	224	Ser39006_016160	A0A2I5TLU7	36.2		DUF2807 domain
HlyD	418	Ser39006_016280	A0A2I5TLX4	-	Secretion protein HlyD	HlyD_D23 domain
Hp	229	Ser39006_016190	A0A2I5TLU9	30.5		Uncharacterized protein
P450	462	Ser39006_016165	A0A2I5T9J1	-	Cytochrome P450 (heme/iron binding)	Cytochrome P450

Table 6.1. Proteins of the *vfm* cluster present in *Serratia* sp. ATCC 39006. Lengths are expressed as amino acid residues, and their identity percentages are relative to the correspondent homologue in *Dickeya dadantii* 3937. GO (Gene Ontology) terms were extracted from Interpro. ACP= acyl carrier protein and Hp is a putative VfmS.

To examine if any of the *vfm* proteins in S39006 share similar functions, their predicted domains were extracted and mapped into each protein. For 22 proteins, putative domains were found, and some of them have similar architecture (Fig. 6.2).

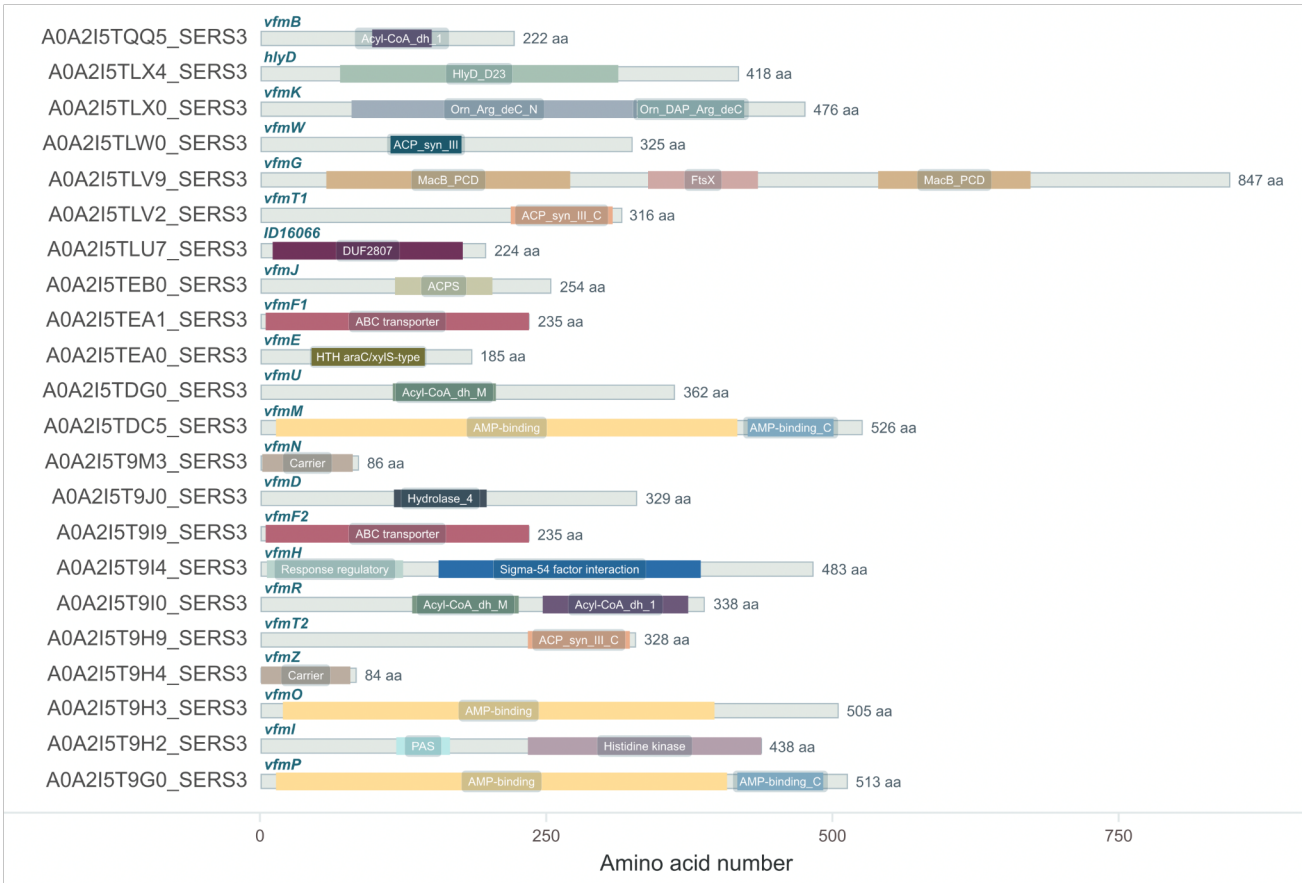


Fig. 6.2. Domain architecture of *vfm* proteins in *Serratia* sp. ATCC 39006. Domains were extracted from the Uniprot platform based on Pfam predictions. Corresponding Uniprot IDs precede each protein, and their lengths are indicated at their ends. Proteins and domains were drawn to scale using their residue lengths and locations, respectively.

No predictions were obtained for VfmA, VfmC, VfmL, VfmV, P450, and the putative VfmS (Hp). Proteins VfmB, VfmU, and VfmR share an Acyl-CoA dehydrogenase domain (Acyl-CoA_dh_1), and the latter carries an extra domain of a different class (Acyl-CoA_dh_M). Acyl carrier domains were found for VfmW, VfmT1, and VfmT2, and although VfmA's domain did not appear in the search, it may serve a similar function. VfmF is an ABC transporter and along with VfmG, presenting two MacB and a FtsX domains, were previously thought to export the undefined Vfm molecule (Nasser *et al*, 2013). Notably, three proteins encoded in the Locus2 (*vfmK-16066*) locus, VfmM, VfmO, and VfmP, have AMP-binding domains, implying that this intracellular messenger may play a role. From the same locus, both VfmN and VfmZ are carrier proteins and might be involved in the transport of the Vfm signal. Finally, VfmI and VfmH potentially comprise a twocomponent system, with the former acting as the histidine kinase and the latter as a Sigma-54 transcription factor dependent response regulator.

This QS system was shown to modulate the cell wall-degrading enzymes (CWDE) and the *vfm* genes at transcriptional level in a dose-dependent fashion in *D. dandantii* (Nasser *et al*, 2013). The *ID16066* gene deactivation in that strain did not affect the system function, and hence, it was not investigated further. Activation of *vfm* genes proceeds through a hierarchical control system. The external Vfm signal is likely exported by using the VfmFG system and sensed by the putative twocomponent system, VfmH-VfmI, which then triggers the *vfmE* expression (Fig. 6.3). Next, this regulator directly activates the transcription of CWDE genes (*pelE* and *celZ*) as well as the expression of *vfmA*, *vfmF*, *vfmK*, and itself (autoinducible), i.e., all the *vfm* transcriptional units. In *D. zeae* EC1, Fis protein also regulates transcription of *vfmE* by binding to its promoter (Lv *et al*, 2018).

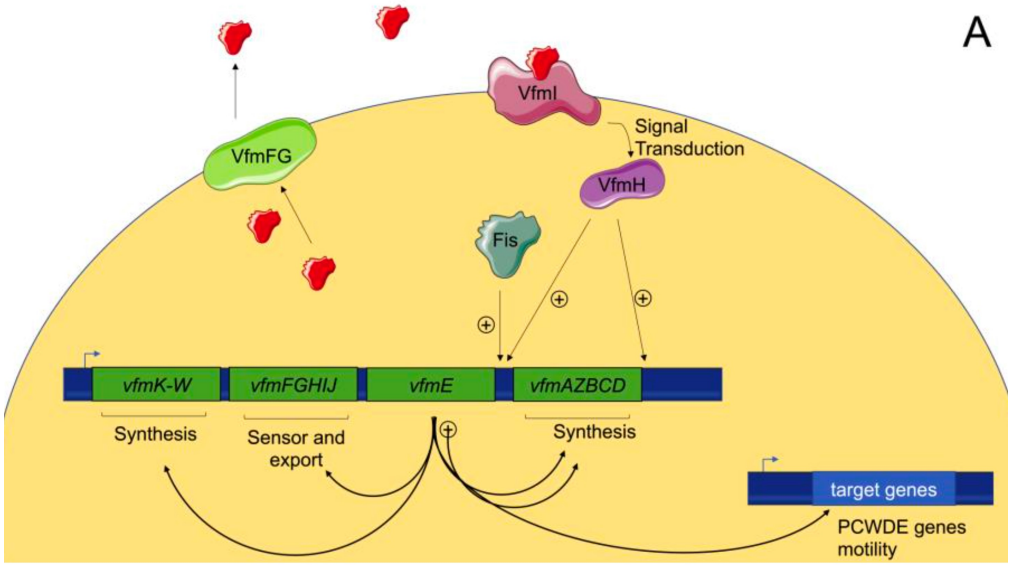


Fig. 6.3. Schematic of *vfm* quorum sensing system regulation in *Dickeya dadantii* 3937. The green boxes denote the transcriptional units and their putative role in the system. The Vfm signal (in red) is exported via VfmFG and sensed by VfmI, which transduces the signal to *vfmH*, which in turn induces the expression of *vfmE*. This regulator then activates all the *vfm* transcriptional units and cell wall-degrading enzymes (*celZ* and *pelE*). In addition to VfmH, Fis also controls *vfmE* expression in *D. zeae* EC1. Image taken from Baltenneck *et al* (2021).

6.2. VfmE is predicted to interact with Vfm proteins

As this is the first study demonstrating that VfmE modulates antibiotic synthesis, it was of interest to predict other proteins that may form part of its regulatory network, in particular, to infer whether the secondary QS system based on the Vfm messenger controls the production of antimicrobials through VfmE. To achieve this goal, the VfmE sequence was utilised as a query in the STRING (Search Tool for the Retrieval of Interacting Genes/Proteins) database. This tool predicts proteinprotein interactions based on either direct (physical) or indirect (functional)

associations from known and predicted partners by experimental or computational methods (Szklarczyk *et al*, 2019). The VfmE network of the ten closest putative interactors comprises seven *vfm* product proteins (Fig.6.4). These proteins are VfmA, VfmD, VfmG, VfmI, VfmJ, VfmT1, and VfmT2. From this set, only VfmJ is encoded near *vfmE* (Locus1). The others were 13465, 14990, and 22715. The 13465 product is a ferritin-like domain protein, 14990 is a putative diguanylate cyclase, and 22715 is a major facilitator superfamily (MFS) transporter. The interaction network presented a high enrichment *p*-value (1.63e-11) that indicates this set is likely to be collectively connected, and therefore, the *vfm* QS system might regulate antibiotic production in S39006.

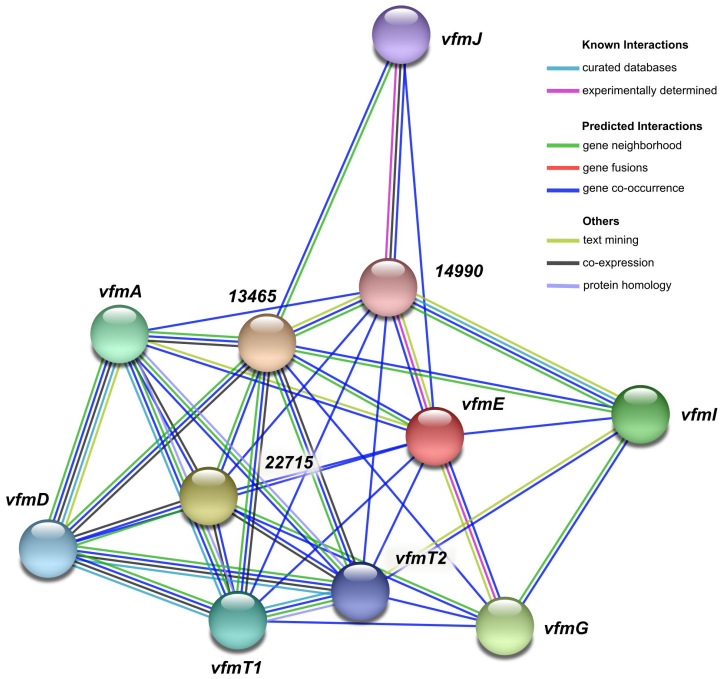


Fig. 6.4. Protein-protein interaction network predicted for S39006 VfmE. The network predicts functional protein association with the query sequence (VfmE; red balloon). The first shell of 10 proteins that may interact with VfmE are shown. Coloured lines connecting proteins indicate the type of evidence for each interaction (legend). PPI enrichment *p*-value= 1.63e-11. Uniprot IDs of non-*vfm* proteins: 13465 (A0A2I5TD76), 14990 (A0A2I5TL86), and 22715 (A0A2I5TCP5).

6.3. A *vfm* gene *in trans* modulates transcription of the intergenic gene and contributes to producing the Vfm signal

Since VfmE was shown to activate the intergenic gene affected by transposon insertions, other mutations that activate this transcription, probably linked to the *vfm* system, were sought. A random transposon mutagenesis approach based on LacZ activity as a readout was designed for this. Given that VfmE might repress its own activity by activating a gene or a set of genes convergently transcribed from the intergenic region, a *vfmE* strain resulting from the mutagenesis should display a less “blue” colouration in X-Gal-containing plates, compared to the intergenic

mutation carrying the *lacZ*. Hence, this fusion mutation located within the transposon (NMW2 strain, Wilf, 2011) was transferred into a *pigC* genetic background via phage transduction. The aim was to generate a strain unable to synthesise prodigiosin to avoid a misleading selection based on blue colour intensity. Thus, the double mutant IGR, *pigC* was generated and used as the parental strain for mutagenesis.

From independent conjugation events, 6,265 transconjugant colonies were screened from X-Gal LBA plates, which enabled identification of 136 colonies displaying phenotypes ranging from "white" to "light blue" (lower "blueness" compared to that of the parental strain). For visual colour comparisons, all these colonies were re-streaked on X-Gal selection plates, along with the parental strain (Fig. 6.5).

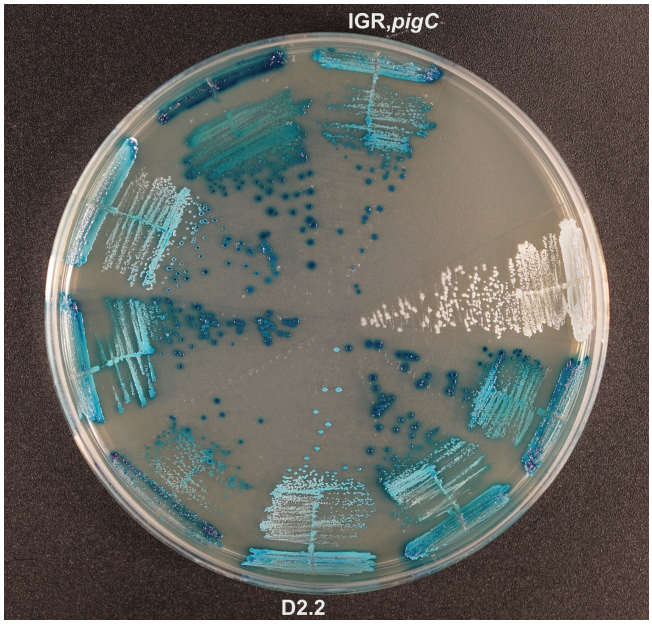


Figure 6.5. An example of transconjugants displaying different blue intensities that translate into diverse alteration levels of the intergenic transcription. Strains were streaked on X-Gal LBA plates and grown for two days. The colour intensity indirectly indicates transcriptional activity of the intergenic gene. The parental (IGR, *pigC*) and a confirmed "light blue" phenotype mutant (D2.2, *cyaA*) are indicated.

Because it was difficult to determine how different they were from the parental strain in some cases, aliquots from overnight cultures grown for 16 hours were used to quantify β-galactosidase activity in microplate assays, allowing any mutation that did not truly affect transcription to be discarded (data not shown). Thus, insertion strains that did not modify the transcription of the intergenic fusion were not considered further. A RP-PCR strategy was followed to find the transposon insertion sites for the remaining strains. From a first set of confirmed strains, four genes affected by transposon insertions were found (Table 6.2).

Code	Target	Predicted function	Fusion	Match (bp)	Phenotype
D2.2	*cyaA*	Adenylate cyclase	Yes	78	Light blue
D11	*hlyD*	Type I secretion system	No	76	Light blue
D12	*fliD*	Flagellum structure	Yes	74	Light blue
D29	*20775*	AMP-dependent synthetase	Yes	49	Light blue

Table 6.2. Transposon-disrupted genes displaying reduced expression of the intergenic gene.
Fusion: indicates if the transposon-incorporated *uidA* forms a transcriptional fusion strain; Match: genome overlap length that was used to confirm the transposon location in base pairs (bp).
Uniprot ID: CyaA (A0A2I5TFP0), HlyD (A0A2I5TLX4), FliD (A0A2I5TJG3), 20775 (A0A2I5TBQ8).

The first gene identified was *cyaA*, a single transcriptional unit that encodes an adenylate cyclase (851 amino acids) involved in synthesising cAMP, as well as the known regulator PigR (a CyaB homologue; Fineran *et al*, 2006). A cAMP-related protein (20775; 851 amino acids) was also identified from a possible operonic arrangement. It is the second of a four-gene arrangement. Next, a flagellum-related gene, *fliD*, was discovered as the first gene of a potential tripartite operon. Its product (490 amino acids) is important for morphogenesis and elongation of the filament. Finally, a *hlyD* homologue was also found. The protein encoded by this gene is a key member of a Type I secretion system in bacteria. This gene was mapped to Locus2 (the large portion) of the *vfm* cluster as previously predicted, which is not present in the corresponding cluster in *D. dandantii*. This mutation was transduced out into a WT and the intergenic background to examine their resulting phenotype. The isogenic *hlyD* presents the same phenotype displayed by the *vfmE* strain (light pink) as well as the double mutant, akin to what was observed for the IGR, *vfmE* double mutant (Fig.
6.6).

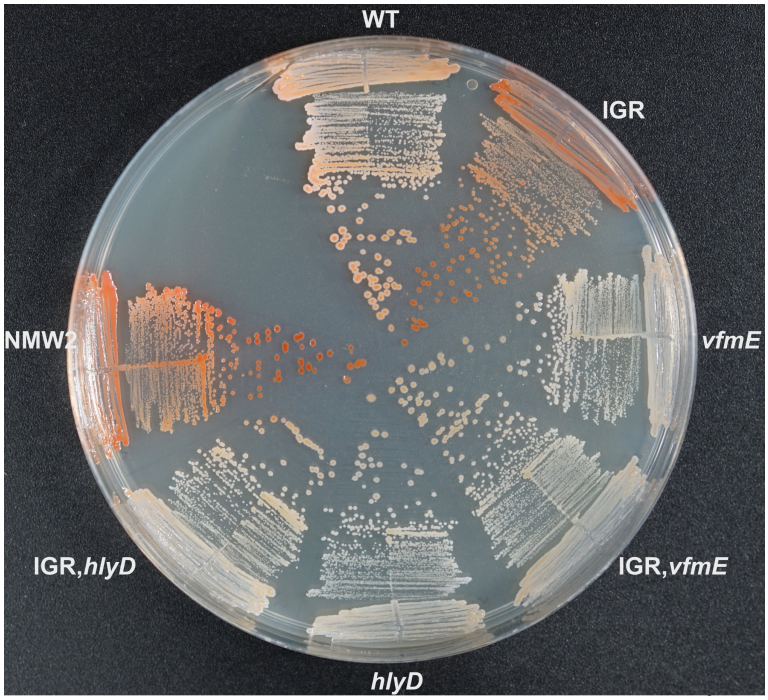


Figure 6.6. The *hlyD* and IGR, *hlyD* transductants have the *vfmE* phenotype. Both transductants and previous strains used in complementation assays were streaked in LBA plates and grown for two days. Colour intensity indicates prodigiosin synthesis.

Therefore, it was experimentally confirmed that *hlyD*, forming a putative *vfm* operon made up of 5 genes, modulates expression of the intergenic gene and alters prodigiosin synthesis. Furthermore, its phenotype is dominant over that of the intergenic mutation, like *vfmE*. Interestingly, although the *vfm* cluster in S39006 is not confined to a single locus as in *Dickeya* strains, these results hint that both *vfm* loci act together to control, at least, prodigiosin production. This also suggests that VfmE might modulate the distant *vfm* second cluster to produce, export, and sense the Vfm molecule, which would orchestrate collective action in a new quorum sensing system in S39006.

Since two different genes, *vfmE* and *hlyD*, both belonging to the *vfm* QS system, provoked the same effect on prodigiosin production, it was hypothesised that the Vfm QS signal is produced, and it is involved in this production. To test its presence and potential effects on antibiotic production, crossfeeding assays were carried out. In these experiments, two bacterial patches are grown together close enough to assess whether the nearest area to the next patch exhibits higher pigmentation upon receiving an extracellular signal. The same principle was employed for carbapenem production, which was assessed by halo formation in the presence of an *E. coli* beta-lactam supersensitive strain. The assessment focused on the effect of several "sender" strains on cells lacking *vfmE* and *hlyD*, representing the two *vfm* loci in S39006. The "senders" were WT, *vfmE*, *hlyD*, IGR, the double IGR,*vfmE*, and the double IGR, *hlyD*. Furthermore, to investigate

any effect of the primary QS system signal, AHL, *vfmE*, *hlyD*, and the intergenic mutations were transduced out into the *smaI* genetic background (encoding the AHLs synthase) by phage transduction. Cells were grown in (i) peptone medium as it improves prodigiosin synthesis and (ii) LBA plus a lawn of the carbapenemsensitive indicator strain. The effects were visible after 14 hours, and no further variation was observed at a later time. No discernible pigmentation or carbapenem production changes were observed in the cells devoid of *vfmE* when placed alongside all the "sender" strains (Fig. 6.7, right side patches). On the other hand, *hlyD* cells only displayed increased lateral pigmentation when grown along with WT, IGR, *smaI*, and *smaI*,IGR. This indicates enhanced synthesis of prodigiosin via cross-feeding. Nonetheless, no perceptible halo size increase was observed. These findings suggest that the (i) Vfm extracellular signal promotes prodigiosin synthesis in an AHL-independent manner, (ii) both VfmE and HlyD are indispensable for the signal to be made and/or exported, (iii) VfmE and not HlyD is required to augment pigment production upon reception of the signal, and (iv) the intergenic mutation may boost VfmE activity. Additionally, when AHLs are absent, an enhanced swarming motility was observed when the intergenic region is interrupted in the carbapenem production assay.

Hence, it was shown via a transposon mutagenesis approach that HlyD, encoded in the large section of the *vfm* QS system, regulates the intergenic gene. Furthermore, the Vfm signalling molecule is likely to be produced, and it increases the pigment levels, only in the presence of VfmE. These results show that the *vfm* system operates in S39006, and it modulates antibiotic biosynthesis.

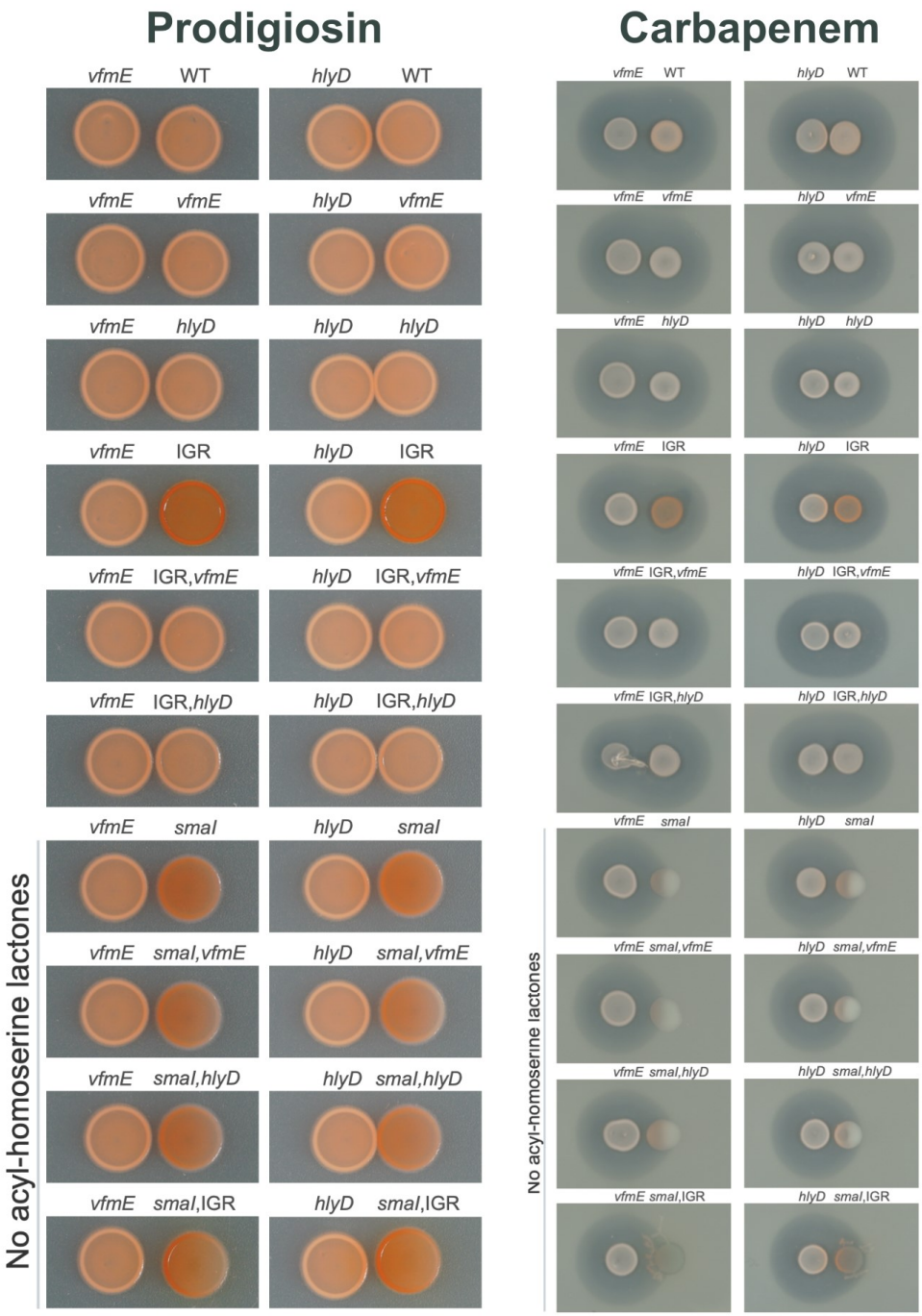


Figure 6.7. Cross-feeding assay for antibiotic production. Cell cultures grown overnight were normalised to OD_{600}=1, spotted onto plates, and incubated for up to 36 h. Images were taken at 14, 16, 18, 30, and 36 hours and were similar to 14 h growth (this figure). For prodigiosin synthesis, peptone medium was employed, while for carbapenem, LBA plates and top lawn containing the *E. coli* (super sensitive) indicator strain were employed. Double mutants with *smaI* are unable to synthesise acyl-homoserine lactones, the primary quorum-sensing signalling molecule.

6.4. Inactivation of all *vfm* transcription units reduces prodigiosin production

As deactivation of either *vfmE* or *hlyD* diminishes transcription of the intergenic gene disrupted by the transposons, leading to prodigiosin-overproducing cells, it was reasoned that mutations able to bypass the intergenic hyperpigmented phenotype should be in *vfm* genes. Therefore, to

study the *vfm* system, a new random transposon mutagenesis was carried out, this time aiming to find "lightpink" transconjugant colonies by using the intergenic mutant as parental strain. From independent conjugation events, a total of 12,703 colonies derived from the intergenic (IGR) strain were screened on LBA selection plates. From all mutagenesis experiments, 155 transconjugant colonies displaying altered phenotypes –compared to the parental strain– were isolated and streaked twice in selection plates. From this set, based on visual inspection, 112 colonies correspond to pink/lightpink (Fig. 6.8), 26 to hyperpigmented (redder than the IGR parental strain), and 17 displaying very little or no pigmentation (either whitish or translucent colonies). Next, sets of light-pink mutants were subjected to RP-PCR, to find the transposon locations.

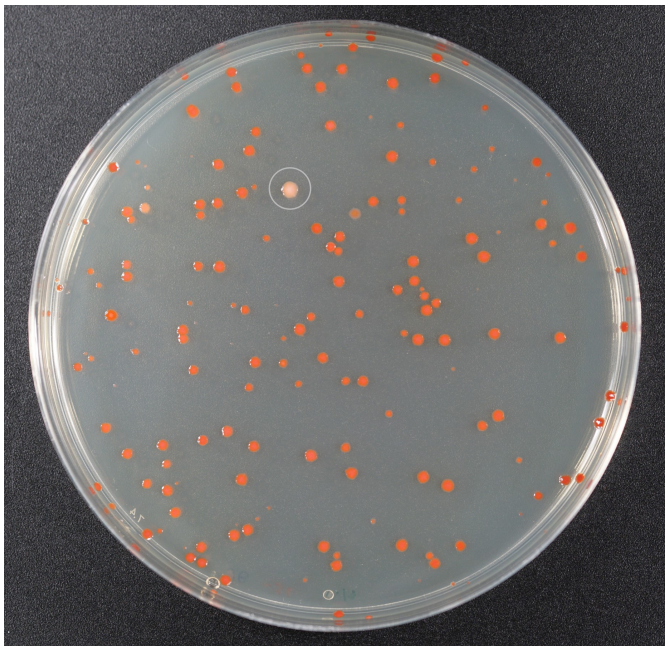


Figure 6.8. An example of a transconjugant colony displaying a light-pink (*vfm*) phenotype. Transconjugant cells were grown for two days on LBA plates. The colour intensity reflects prodigiosin production. The circled colony mutation reverted the parental (IGR) hyper-red phenotype.

As a proof of concept, mutants displaying white phenotypes were also subjected to RP-PCR. From this, genes from the prodigiosin biosynthesis operon (*pigA*, *pigF*, *pigH*, *pigJ*, and *pigK*) were also found to be hit by transposons. Furthermore, known regulators such as *rap* and *rbsR* were also disrupted by transposon insertions. From the light-pink phenotype set, a third of the total, i.e., 38 transposon insertion sites, were determined. As expected, all the transposons were found within a *vfm* coding region or in possible promoters (Fig. 6.9). Transposons were mostly inserted into the *vfmE* reading frame (13 insertions), then *vfmA* and *vfmK* after, with 6 and 4 insertions each (Fig. 6.9). These counts also includes putative promoters. For *vfmA* and *vfmK*, 3 insertions in each case were located in putative promoters. All the genes of the *vfmA-vfmD*

transcriptional unit were hit by transposons, except *vfmZ*. Other insertions were localised within the *vfmK-ID16066* unit, in genes *vfmM*, *vfmN*, *vfmO*, and *vfmV*. No insertions in genes upstream of *vfmE* (Locus1) nor *hlyD-vfmI* units were detected.

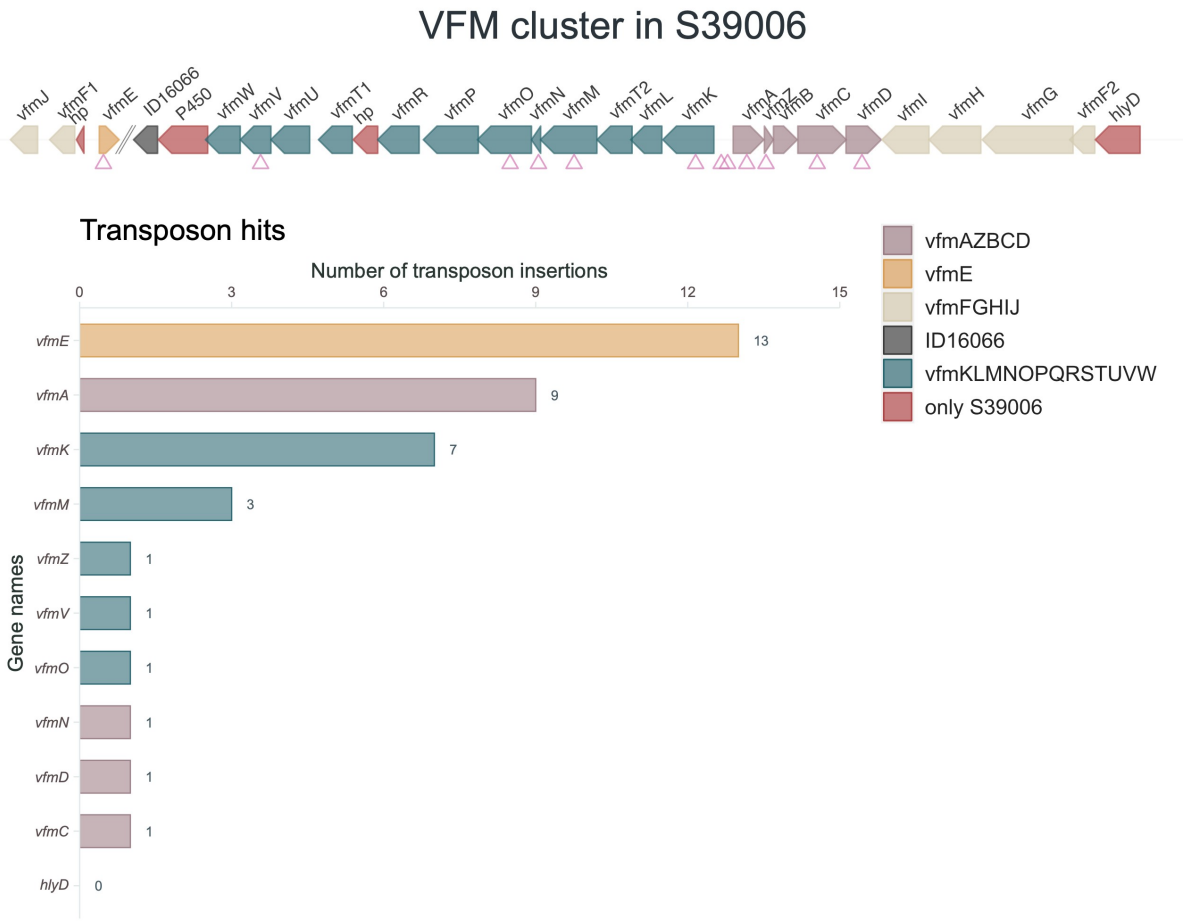


Fig. 6.9. Map and number of *vfm* genes hit by the transposons. Transposon-inserted genes from the *vfm* cluster are indicated by pink triangles. Triangles indicate genes affected regardless of the number of times that transposons were inserted. Transposon insertions in *vfmA* and *vfmK* include possible promoters affected. The rank chart of transposon-interrupted genes is coloured based on the transcriptional unit they belong to (legend on the right side).

In *D. dadantii*, *vfmE* activates transcription of all *vfm* units, *vfmA*, *vfmF*, *vfmK*, and itself (Nasser *et al*, 2013), all of which are the first genes of their corresponding transcriptional units. In S39006, the equivalent key genes representing the putative *vfm* operons are *vfmA*, *vfmK*, *hlyD*, and *vfmE*, which are reduced for prodigiosin production in an intergenic background. To examine their isogenic phenotype, all these mutations were transduced into the WT strain via phage transduction. All the resulting transductants exhibited the same light-pink phenotype (Fig. 6.10). Nonetheless, in the case of *vfmE*, the single insertion mutant was not obtained because to the intergenic mutation was too close to the *vfmE* coding sequence. Efforts to obtain the *vfmE* strain

from the double strain were made via streaking 140 transductant colonies on plates containing one of the two selection markers (single strain should be sensitive to one).

Altogether, the random transposon mutagenesis, plus transduction, approach enabled the construction of all the first genes of the potential *vfm* transcription units. The strains *vfmA*, *vfmE*, *vfmK*, and *hlyD*, present a reduction in prodigiosin synthesis and are epistatic to the intergenic phenotype.

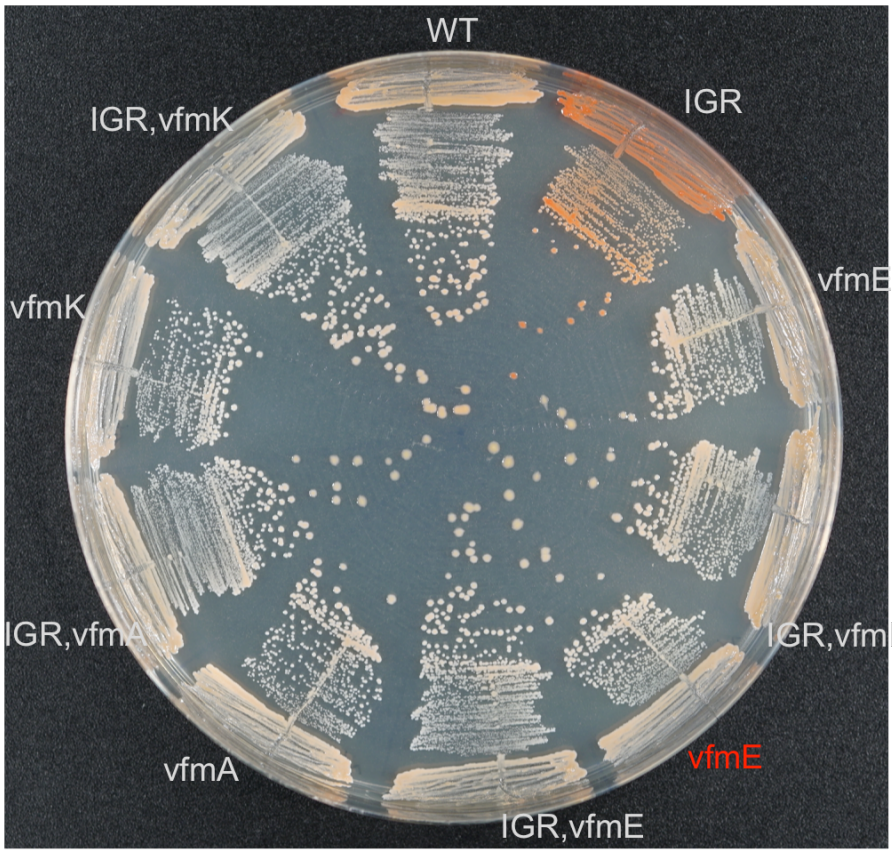


Figure 6.10. Single and double *vfmA*, *vfmE*, and *vfmK* strains with the intergenic mutation display reduced prodigiosin synthesis. Strains were streaked in LBA plates and grown for two days. Strain *vfmE* in red is the transductant found resistant to both selection markers (it includes the intergenic mutation).

6.5. *vfmA* and *vfmE* inactivation attenuates virulence and overexpression of *vfmE* increases the Vfm signal

The Vfm-based QS system was discovered as a virulence modulator in *D. dadantii* (Nasser *et al*, 2013). Hence, since all the first genes of the putative *vfm* transcriptional units were obtained, it was sought to determine whether they control plant virulence. Thus, the mutant strains *vfmA*, *vfmE*, *vfmK*, and *hlyD* were tested along with WT in the potato rotting assay. The infection assay showed that only *vfmA* and *vfmE* are relevant for tuber rotting. On average, both *vfmA* and *vfmE* mutants showed virulence capacity reductions by approximately 30% (p =0.0267 and p =0.0279, respectively), whereas no significant differences were determined for *vfmK* or *hlyD* necrotic

tissue compared to that of WT (Fig. 6.11). Further, the WT cell count from serially diluted cultures was 10^6 colony forming units (CFU) per gram of tissue, the same as that obtained for all the *vfm* strains.

Hence, the effects of both *vfmA* and *vfmE* are not due to cell growth impairment *in planta*.

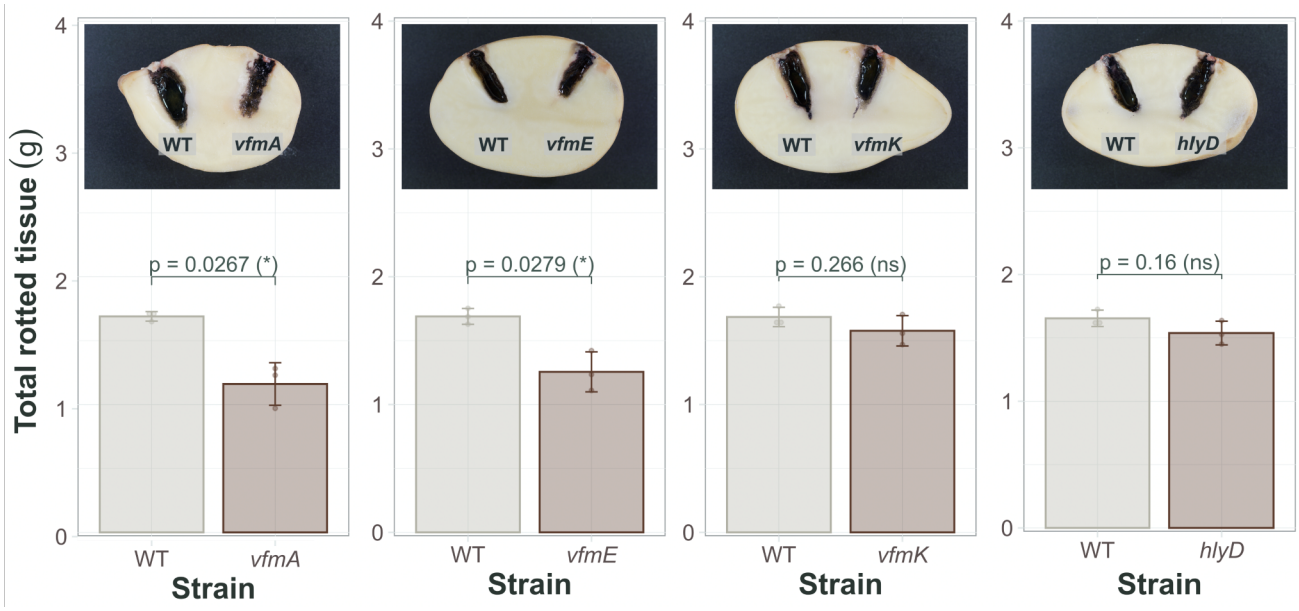


Fig. 6.11. The *vfmA* and *vfmE* mutation decreases virulence in plants. Tubers were infected with a normalised cell number (10^7 CFU) and scraped-off rotted tissue was weighted after 4 days. The average weights of three biological replicates (± standard deviation) and significance (Student's t-test, p <0.05) are displayed. Inset: cross section of a representative infected potato (iodine-stained rotten cavities for enhanced visualisation).

VfmE in S39006 is important in Vfm messenger signaling, which modulates prodigiosin synthesis. To assess the role of this regulator on carbapenem production via the extracellular signal, a new cross-feeding assay was designed. This time, the WT strain harbouring either the empty pQE80-oriT plasmid or the plasmid encoding *vfmE* was used as the Vfm "sender" strain. On its side, the WT and mutants *vfmA*, *vfmE*, *vfmK*, *hlyD*, and the intergenic (IGR) served as the Vfm "recipient" strains. Additionally, as all the bacterial patches were spotted manually on plates and the distance between the pairs is relevant, the shortest distance between "sender" and "recipient" strains was measured. This distance was next multiplied by the halo generated, since the closer the cells are, the larger the effect of the putative signal, due to diffusion. The normalised carbapenem production of all the "recipient" strains was higher upon reception of the extracellular signal coming from the "sender" overexpressing *vfmE* than from the control (Fig. 6.12). Likewise, the "recipients" also appeared to be more pigmented. Notably, in the WT receiver cells, the upturn in carbapenem synthesis was more than double that of the control. Among the "recipient" strains belonging to *vfm*, *vfmE* and *vfmA* mutants exhibited the lowest carbapenem levels when the signal came from cells incorporating the empty vector (native VfmE

levels). From these basal carbapenem levels, strains *vfmK* and *hlyD* showed a stepping rise in production, with the latter being even higher than the WT cells. On the other hand, the *vfm* recipient mutants displayed a relatively steady carbapenem synthesis when sensing the signal coming from the WT overexpressing the regulator. In the case of the intergenic recipient, upon reception of signal from both "senders", the levels of carbapenem remained below WT synthesis, albeit the cells receiving the signal from *vfmE* overexpressing cells were higher than control.

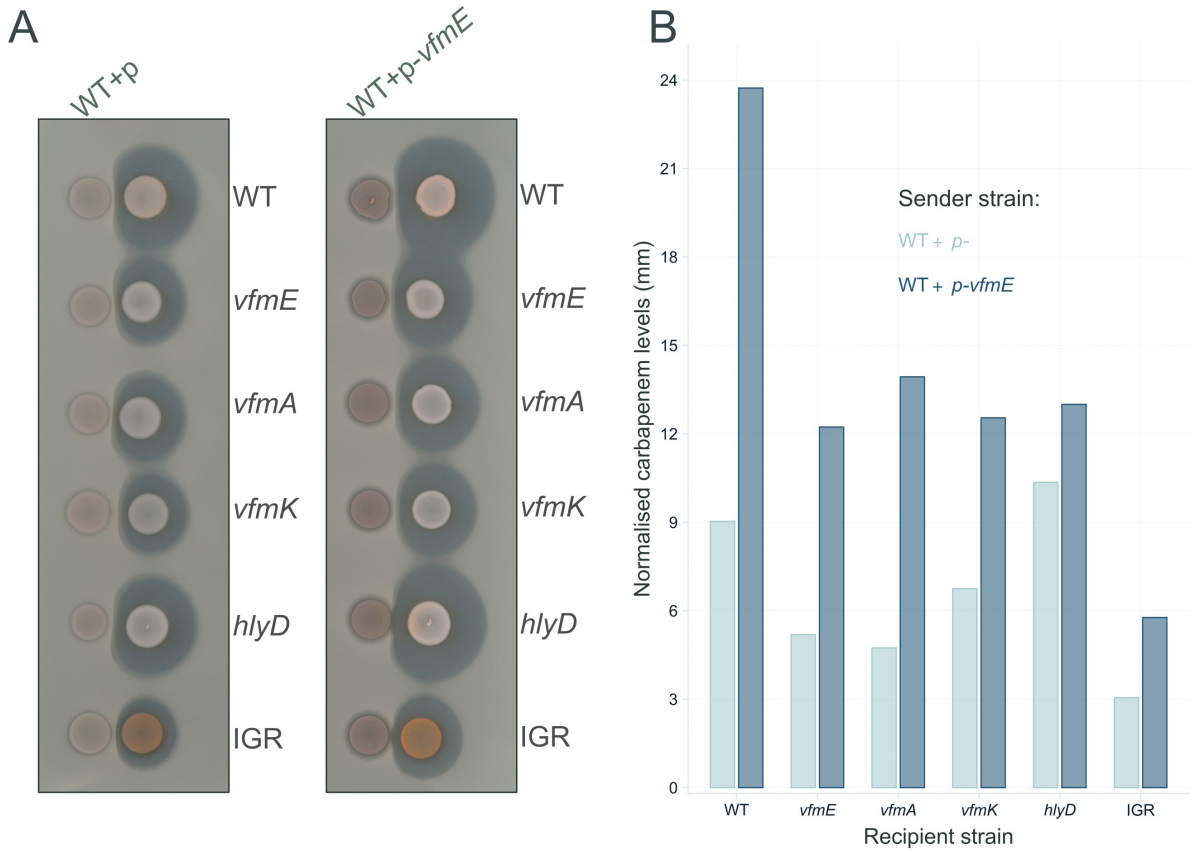


Fig. 6.12. Overexpression of *vfmE* increases production of an extracellular signal that augments carbapenem synthesis. A: Cross-feeding assays. Two "sender" strains (left columns), WT harbouring either the empty pQE80-oriT vector (WT+p) or the one carrying the *vfmE* (WT+p-*vfmE*), were employed to test the signal delivery. The "recipient" strains, named on the right columns, were used to test the potential Vfm signal response. Cell cultures grown overnight were normalised to OD_{600}=1, spotted onto LBA plates, and incubated for 14 h. A top lawn containing the *E. coli* (super sensitive) indicator strain was utilised to detect carbapenem synthesis. B: Normalised carbapenem production by the "recipient" strains upon detection of the extracellular signal produced by the two "sender" strains. Normalised levels refer to halo formation measured from bacterial patch edges to halo borders, multiplied by the distance between the cell patches.

Overall, these findings indicate that *vfmA* and *vfmE* have a greater impact on the *vfm* system than *vfmK* and *hlyD*, as their absence reduced virulence. Also, these mutants exhibited a lower capacity to produce carbapenem when sensing low levels of the putative Vfm signal. Finally, *in trans* addition of VfmE leads to higher levels of the signal, which in turn increases antibiotic production.

6.6. VfmE increases *vfmA* promoter activity and decreases that of *hlyD;* VfmH does not act on any *vfm* promoter

In *D. dadantii*, the AraC-family regulator VfmE was shown to activate the four transcriptional units of the *vfm* system, *vfmA*, *vfmE*, *vfmK*, *vfmF*, by direct binding to their promoter regions, in addition to those of *pelE* and *celZ*, from the exoenzymes pectate lyase and cellulase (Nasser *et al*, 2013). Therefore, it was hypothesised that there might be a common motif among the promoters of the known VfmE regulon in this strain. Thus, based on the ChIP-seq analysis used in that study, the six promoter regions were used to find a shared motif, to infer the VfmE binding site in *D. dandantii*, which may be similar to that of S39006, given the highly similar VfmE sequences (Fig.
6.13).

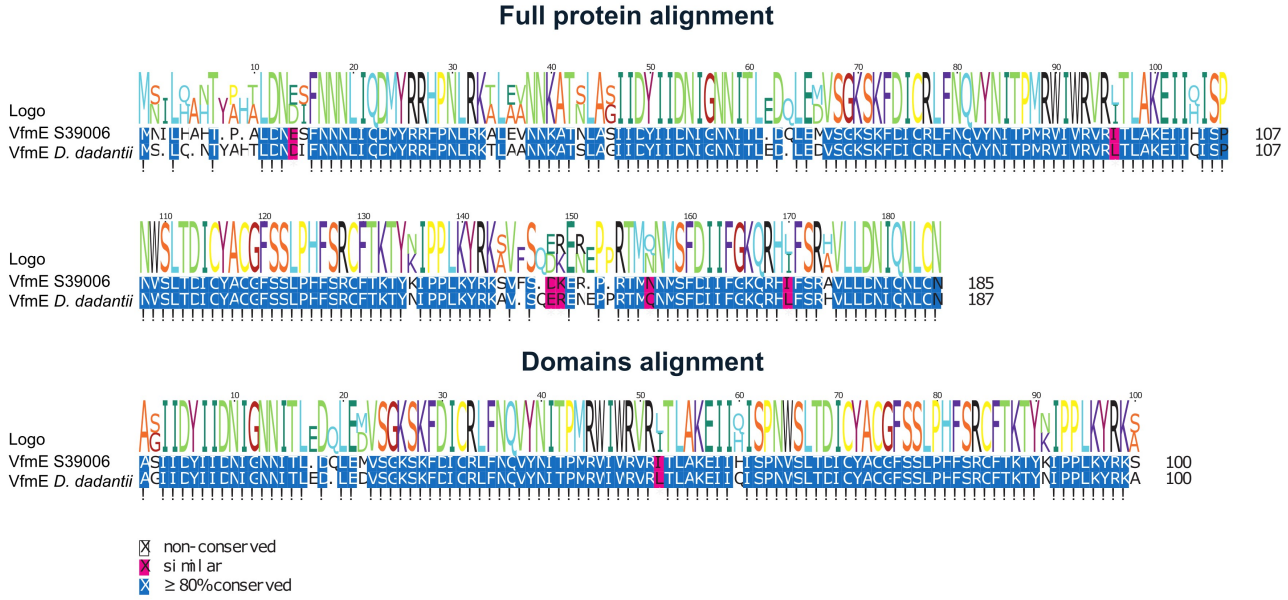


Fig. 6.13. **VfmE from S39006 and *Dickeya dadantii* are highly similar at the sequence level**. The VfmE amino acid sequence from S39006 (185 residues) and *D. dadantii* 3937 (187 residues) were aligned by Muscle (Top). Where found, consensus is denoted by "!" under the alignment. The AraC (HTH_18, Pfam) domain from the strains (both located at 45-155 position) was also compared separately (bottom).

Thus, two strategies were followed: the six promoter regions were (i) scanned using PePPER (de Jong *et al*, 2012) to search for known motifs, and (ii) subjected to a *de novo* discovery of overrepresented motif(s) via MEME suite (MEME and GLAM2 tools) and the Regulatory Sequence Analysis Tools (RSAT) suite. The motif scanning analysis, intended to find known transcription factor (TF) binding sites (TFBSs) in the six promoters bound by VfmE in *D. dadantii*, found several candidates, but none related to AraC regulators (data not shown). MEME did not find a motif shared by the six promoters, but GLAM2 did. Five putative binding sites were provided by this tool, whereas RSAT predicted a single shared motif (Fig. 6.14).

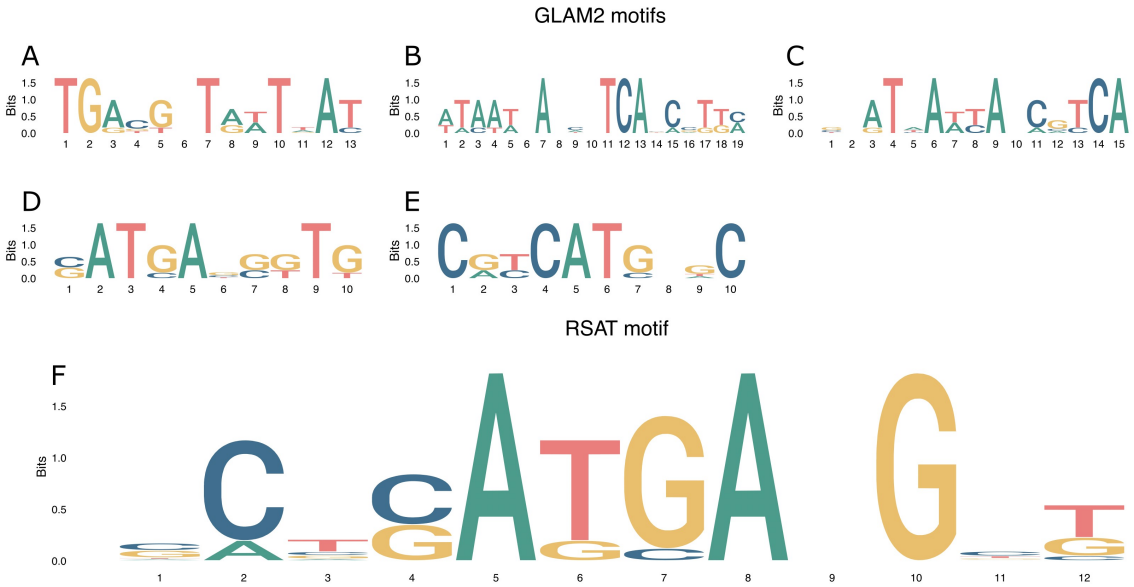


Fig. 6.14. Motif prediction for the six regions bound by VfmE in *Dickeya dadantii*. GLAM2 (A-E) and RSAT (F) motifs were predicted by using the 6 promoter sequences experimentally validated (Nasser *et al*, 2013). GLAM2 motif score rank: A= 43.67, B= 42.34, C= 39.18, D= 38.86, and E= 38.72.

The prediction made by RSAT showed similarities to one of the motifs provided by GLAM2 (Fig. 6.14, see motif D and F). Nevertheless, this motif differs from the one found in S39006 that increases the intergenic promoter activity (Fig. 5.18).

Given that VfmE possibly controls the *vfm* transcriptional units to produce the Vfm QS signal in a similar fashion as in *D. dadantii*, *in vivo* assays were carried out to test this presumption. This consisted of cloning approximately 300 bp of the upstream region of the initiation codon, plus around 20 bp of coding sequence of *vfmA*, *vfmE*, *vfmF1*, *vfmK*, and *hlyD*, into the pRW50 promoterless LacZ system. Next, the five constructs were used to transform *E. coli* DH5a. Finally, these strains were additionally transformed with either the empty vector pQE80-oriT or the vector containing the *vfmE*. Furthermore, since VfmH, a response regulator, was pointed out as the activator of *vfmE* expression in *D. dadantii* (Nasser *et al*, 2013), it was also incorporated into the analysis. VfmE was found to only increase the promoter activity of *vfmA* (p =5.03e^{-5}), and surprisingly, it reduced that of *hlyD* (p =0.015; Fig. 6.15). No other significant changes were detected for the rest of the promoters tested. The same was observed for cells overexpressing VfmH, which was found to play no role in modulating the DNA regions examined.

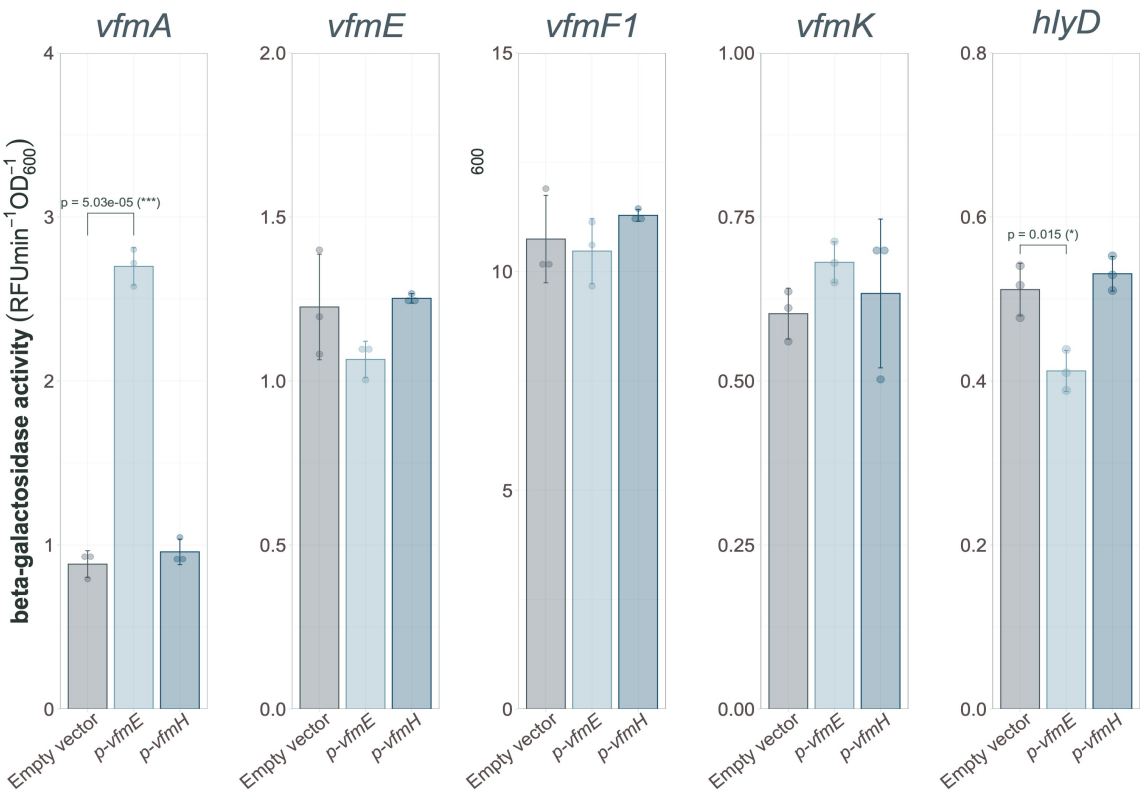


Fig. 6.15. VfmE activates *vfmA* and represses *hlyD* promoter activity in S39006. β-galactosidase activity was employed to assess promoter activity *in vivo*. *E. coli* DH5α cells harbouring the pRW50 derivative constructs containing promoter regions of *vfmA*, *vfmE*, *vfmF1*, *vfmK*, and *hlyD*, were transformed with the high-copy-number vector pQE80-oriT alone (empty vector) or incorporating *vfmE* (p-*vfmE*) or *vfmH* (p- *vfmH*) coding sequences. A leaky expression effect of pQE80-oriT and its derivatives on cells containing the pRW50 constructs was measured at 10 h growth. Average data from three biological replicates ± standard deviation is shown. Statistical significance was tested by an unpaired Student's t-test: *$p < 0.05$, **$p < 0.01$, ***$p < 0.001$.

Thus, the predicted binding motifs for the VfmE in *D. dadantii* were different from the one uncovered in this study. In S39006, VfmE positively regulates *vfmA* transcription while negatively regulating *hlyD* transcription *in vivo*. Moreover, VfmH, thought to be at the top of the regulating hierarchy, did not control any of the promoters tested.

6.7. VfmE and VfmH do not influence expression of antibiotic operons, *carR*, or *rap* regulators

Production of prodigiosin and the carbapenem in S39006 is driven by proteins encoded in two operons, *pigA-O* and *carA-H*, and the latter is positively regulated by a LuxR-type protein termed CarR. Moreover, Rap is a key transcriptional regulator that activates both antibiotics. In *D. zeae* EC1, VfmE regulates *slyA*, the *rap* homologue (Lv *et al*, 2019). Previously, it was shown that the *vfmE* mutant presents a reduced synthesis of both compounds (Fig. 5.5). To investigate if VfmE directly regulates the expression of biosynthesis clusters and two crucial regulators, an *in vivo* assay was performed. For this, *E. coli* DH5a cells harbouring promoter regions of *pigA* (Fineran *et al*, 2005), *carA*, *carR*, and *rap* (Gristwood *et al*, 2009) were transformed with either the vector

pQE80-oriT with no insert or its derivative incorporating *vfmE*. Moreover, the same procedure was conducted with the *vfmH* coding sequence.

The β-galactosidase activity of all four LacZ constructs carrying either a *vfmE* or *vfmH* overexpressing plasmid did not differ significantly from that of the corresponding empty vector (Fig. 6.16). These results show that none of the putative major regulators of the *vfm* QS system controls the expression of antibiotics or two of their main transcriptional activators.

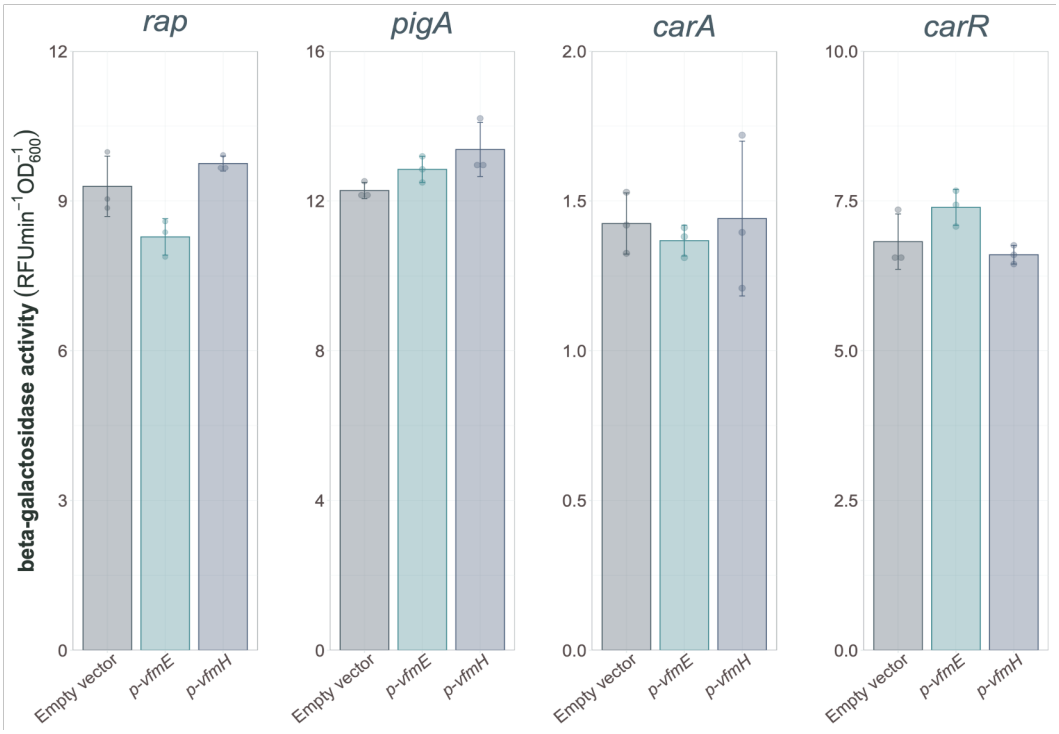


Fig. 6.16. Overexpression of *vfmE* or *vfmH* has no effect on expression of biosynthesis clusters or *carR* or *rap* regulators. β-galactosidase activity was used to monitor promoter activity *in vivo*. *E. coli* DH5α cells containing the pRW50 including the regions pTA14 (*rap*), pTA15 (*pigA*), pTA16 (*carA*), and pTA23 (*carR*), were transformed with the high-copy-number vector pQE80-oriT alone (empty vector) or incorporating *vfmE* (p-*vfmE*) or *vfmH* (p-*vfmH*) coding sequences. Leaky expression from pQE80-oriT and its derivatives on cells containing the pRW50 contructs was measured at 10 h growth. Average data from three biological replicates ± standard deviation is shown. Statistical significance was tested by an unpaired Student's t-test: $p < 0.05$.

6.8. Discussion

This chapter explored the presence and role of the secondary QS system *vfm* in regulating antibiotic synthesis in S39006. A genomic search unveiled the presence of *vfm* members, and a mutagenesis approach demonstrated that potential operons are connected to antibiotic production. The regulatory role of VfmE in this novel signalling phenomenon was hence investigated. *Dickeya* spp. have been recognised as important phytopathogens owing to their virulence against a wide range of plant hosts, causing relevant economic impact (Charkowski, 2018). This virulence had been previously linked to ExpIR, the acyl-homoserine lactone-based QS system (Nasser *et al*, 1998), but latterly, a new QS system, was discovered to play a more significant

role. In the strain *D. dadantii* 3937, the study model, this secondary system was indeed found to direct virulence through activating cell wall-degrading enzymes. This system, as explained before, relies on the release and sensing of the extracellular signal termed Vfm (Nasser *et al*, 2013). In parallel with the present work, the presence of proteins belonging to this system was also found in the S39006 genome (Duprey *et al*, 2019). Here, the search and dissection of these proteins showed that only one *vfm* homologue protein from the *Dickeya* model is missing (VfmQ). Moreover, two proteins that compose the *vfm* system in S39006, HlyD and P450, are not encoded in *Dickeya*. HlyD is the membrane-bound part of the Type I secretion system in bacteria, which is usually encoded along with the rest of the members, HlyB and TolC (Alav *et al*, 2021). These proteins were found elsewhere in the S39006 genome, forming an operon (data not shown), and therefore the *vfm* HlyD is a duplicate. The other unique *vfm* protein in the *Serratia* strain was the Cytochrome P450, which is a mono-oxidase that contains heme groups (Khmelevtsova *et al*, 2017). Some *vfm* proteins were detected to share some domains among them. Interestingly, in three members, VfmM, VfmO, and VfmP, AMP-binding domains were identified. This insight may be a link between this secondary extracellular signalling system and the intracellular messenger cAMP, since a putative adenylate cyclase named PigR, a CyaB homologue, is involved in antibiotic production regulation (see section 5.8). Furthermore, another adenylate cyclase, CyaA, was found to modulate the intergenic gene transcription via transposon mutagenesis, as well as an unknown AMP-dependent synthase. Thus, the *vfm* QS system and cAMP signalling might be integrated in S39006 and act together to modulate antibiotic production. The mutagenesis approach also uncovered that the *hlyD* (*vfm* system) inactivation diminishes the transcription of the intergenic gene, akin to the lack of *vfmE*. Also, the *hlyD* cells exhibited the same light-pink phenotype as those of *vfmE*. This finding then led to the observation in cross-feeding experiments that there is an extracellular signal, possibly the Vfm, that seems to enhance antibiotic synthesis, upon cell reception. This occurs independently of the AHLs from the primary QS system, at least in a *hlyD* genetic background. In VfmE-lacking cells, the extracellular signal does not provoke visible changes, pointing to this regulator as crucial in this regulating QS system. It has been previously stated that this regulator activates all the *vfm* operons and the signalling molecule, Vfm, induces its expression (Nasser *et al*, 2013).

The bypass mutants of the hyperpigmented intergenic phenotype, displaying the light-pink phenotype, were all mapped to the *vfm* system. Thus, the first genes of all the potential transcriptional units, *vfmA*, *vfmK*, and *hlyD*, were obtained via mutagenesis. However, only *vfmA* and *vfmE* affected the pathogenicity in the plant virulence assays. These four genes that represent the putative *vfm* operons were used to test the sensing of the potential Vfm molecule, using a *vfmE*overexpressing plasmid as a sender of the signal. The cross-feeding assays showed that

when VfmE was in multicopy, the production of carbapenem was higher compared to the WT levels, although this effect was more dramatic in WT as a receptor, which suggests that every transcriptional unit is needed to produce more of the putative signal to maintain the high synthesis of this compound. In the case of prodigiosin, the effect might be similar, but further investigation is needed to corroborate this observation.

Given the VfmE sequence similarity between *D. dadantii* 3937 and S39006, it was reasoned that a motif prediction should find a binding site similar to what was found upstream of the intergenic promoter (chapter 5). However, none of the motifs predicted using the binding sites from *D. dadantii* were similar to the likely VfmE binding motif in S39006. Unfortunately, due to time constraints, *in vitro* binding assays to ensure that the motif is bound by the regulator could not be performed. Surprisingly, overproduction of VfmE *in trans* only affected two out of five promoter regions tested. This regulatory protein increased the promoter activity of *vfmA* and decreased that of *hlyD*, whereas the other *vfm* regulator investigated, VfmH, had no effects on any assayed promoter. However, these regulators might interact with more distant regions than the ones tested to control transcription. Curiously, following these findings, VfmE reduces the expression of *vfmI* and *vfmH*, as they would belong to the *hlyD* operon, and the latter is supposedly its activator. Regarding the Locus1, the smaller region containing *vfmE*, *vfmF1* expression was not affected by either of the two regulators, and its participation, or not, in the *vfm* system is unknown. In the *Dickeya* model, VfmE activates all the operons through direct promoter binding, including its own. Further, VfmH was defined as the mediator of Vfm signalling in *D. dadantii* by activating *vfmE* expression, and it also activates that of *vfmA* (Nasser *et al*, 2013). This regulator, in addition to modulating these two genes, also controls *vfmF* expression in *D. zeae* EC1 (Lv *et al*, 2019). Hence, the hierarchical regulatory *vfm* network in S39006 differs from that of *Dickeya* strains and awaits to be experimentally determined.

The potential action of VfmE and VfmH on promoter activity of the two biosynthesis operons and two key regulators was also tested via *in vivo* assays. Strains incorporating each promoter construct were transformed with plasmids overproducing VfmE or VfmH, or with the empty vector. It was found that none of the two regulators affected expression of the promoters tested. This shows that they exert action on antibiotic production through other mechanisms.

The present work discovered that a secondary QS system, believed to be only in *Dickeya* strains, is active in S39006. Furthermore, it is not only involved in antibiotic synthesis regulation but also in virulence. Notably, VfmE is capable of trans-controlling at least two *vfm* genes that are in a distant locus, to possibly act coordinately and both produce and sense the extracellular signalling molecule. This study thus exposes a new QS system as a novel player in the field of antibiotic production.

Chapter 7. Proteomes of the intergenic mutant and its *vfmE* double mutant exhibit opposite changes in antibiotic and *vfm* synthesis proteins

The VfmE regulator was shown to fulfill an essential role in regulating antibiotic production. This role was uncovered by the intergenic disruption, and the *vfmE* phenotype is the epistatic one. Here, the consequences of these two related mutations on antibiotics and the new signalling system are explored at a global scale.

7.1. The intergenic mutation induces more protein changes than the double mutant with *vfmE*

The VfmE regulator modulates the synthesis of both antibiotics in S39006. The intergenic mutation, on the other hand, generates a similar hyper-red phenotype in prodigiosin production in cells overexpressing *vfmE*. Moreover, the antibiotic synthesis of the double mutant carrying both the intergenic and *vfmE* mutations was the same as of the isogenic *vfmE*. Hence, it was speculated that the intergenic insertion disrupted an unknown mechanism that negatively controls VfmE activity. Thus, to investigate the global impact of the mutations in the intergenic (IGR) and the double (IGR,*vfmE*) strain, a proteomic analysis was carried out. For this approach, the experimental work was conducted in collaboration with Dr. Katherine Hucks and Dr. Carlo Sandoval. Four culture samples of each mutant and the WT strain were taken at stationary growth phase for antibiotic production quantitation and protein quality controls, to finally select three representative samples for proteomics (see Materials and Methods section 2.15). The purified intracellular protein samples in triplicates were subjected to a tandem mass tagging (TMT)-based proteomic analysis at the Cambridge Centre for Proteomics.

The labelling efficiency obtained for all samples was 95.6% and the final filtered dataset contained 2,851 values for unique proteins, equivalent to 64.6% of the predicted proteome (4,413) for S39006 (Fineran *et al*, 2013). The data correlation among all the samples submitted for this analysis were evaluated via principal component analysis (PCA). This analysis allowed separation and estimation of the overall closeness among the biological replicates and the strains they involve, based on their differential expression of proteins. The overview of proteome variability showed that the replicates cluster together according to their respective strain (Fig. 7.1). Moreover, the comparison reveals that the double mutant (orange circles) has a more similar profile to the WT strain (black circles) than the intergenic strain (green circles), which is by far the strain exhibiting the most different proteomic outcome. Thus, the protein expression profiles demonstrate that the two mutants display substantial differences relative to that of the WT strain.

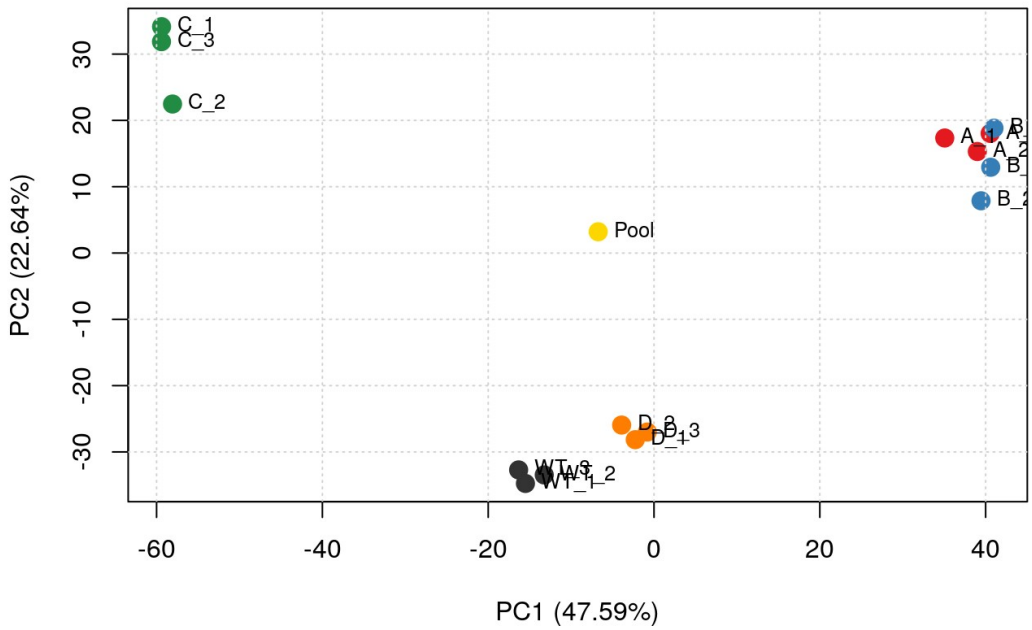


Fig. 7.1. Principal component analysis of the proteomes profiles. The circles represent individual samples and the colours indicate whether they belong to the pool sample (yellow), the WT strain (black), the intergenic mutant (Green), or the double mutant (orange). The other two strains (A and B) correspond to other investigations. The distance between circles denotes their degree of similarity.

The quantitative proteomic data enabled to identify a total of 2,851 unique proteins belonging to S39006. The proteins that were up- or down-regulated compared to the WT strain were visualised using a Volcano plot. In this graphic, the Log_2 fold-change of the protein datasets versus their statistical significance are plotted. Differentially expressed proteins were those with adjusted *p*values <0.05 and displaying a threshold of a 1-fold change in abundance relative to the WT values. It was observed that in the two mutants, changes in protein concentration relative to the WT strain occurred to a different extent. The highest number of proteins up-regulated was found in the intergenic's proteome, which has fold change values oscillating between 1.023 to 5.53, whereas the proteome of the double strain presents mostly down-regulated proteins, with changes ranging from -1.23 to -2.65. The total number of proteins that were significantly up-regulated in the intergenic strain was 62, whereas the down-regulated number was 4. In stark contrast, only 2 proteins were found to be up- and 16 down-regulated in the double mutant (Fig. 7.2).

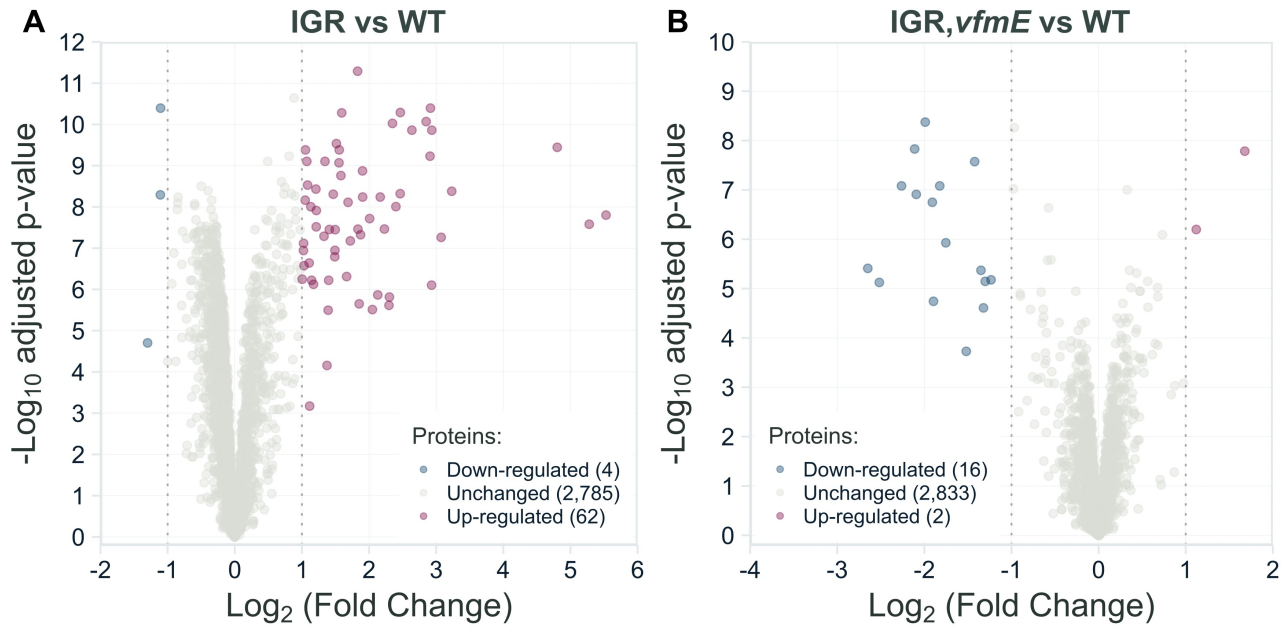


Fig. 7.2. Volcano plots of the intergenic and double mutant's proteomes. The blue and red scattered circles represent proteins with low and high expression levels, respectively. The adjusted *p*-values were transformed by -Log_{10} (Y axis) versus the Log_2 protein fold change (FC; X axis) for the (A) intergenic (IGR) and (B) double mutant (IGR,*vfmE*) relative to the WT values. Vertical dotted lines indicate the limit of the values considered as differentially expressed (-1 and 1 FC). The adjusted $p < 0.05$ was used to determine significant differences. The total number of proteins that have been up- and down-regulated is shown in the correspondent inset.

To dissect the composition of these protein groups differentially expressed, their assigned identities were checked by Blastp searches and then manually classified. Thus, all of these proteins were grouped into 5 major classes, according to their predicted functions. Interestingly, from the 62 up regulated proteins in the intergenic mutant, 21 correspond to members of the *vfm* cluster, the largest group with known function (Fig. 7.3 A). Opposed to this, all the down-expressed proteins (16) in the double mutant coincide with *vfm* members (Fig. 7.3 B). The following group from the intergenic dataset was constituted by 7 proteins of the prodigiosin biosynthesis operon. No members of this group were observed in the double mutant data with the fold change threshold used. The next group in the intergenic strain contains 5 members, which are involved in flagellar synthesis and assembly. The last one is comprised of four transcriptional regulators, three of them up-regulated and only one is down. The remaining proteins, 26 up and 3 down-regulated in the intergenic data and 2 upregulated proteins in the double mutant, were not classified.

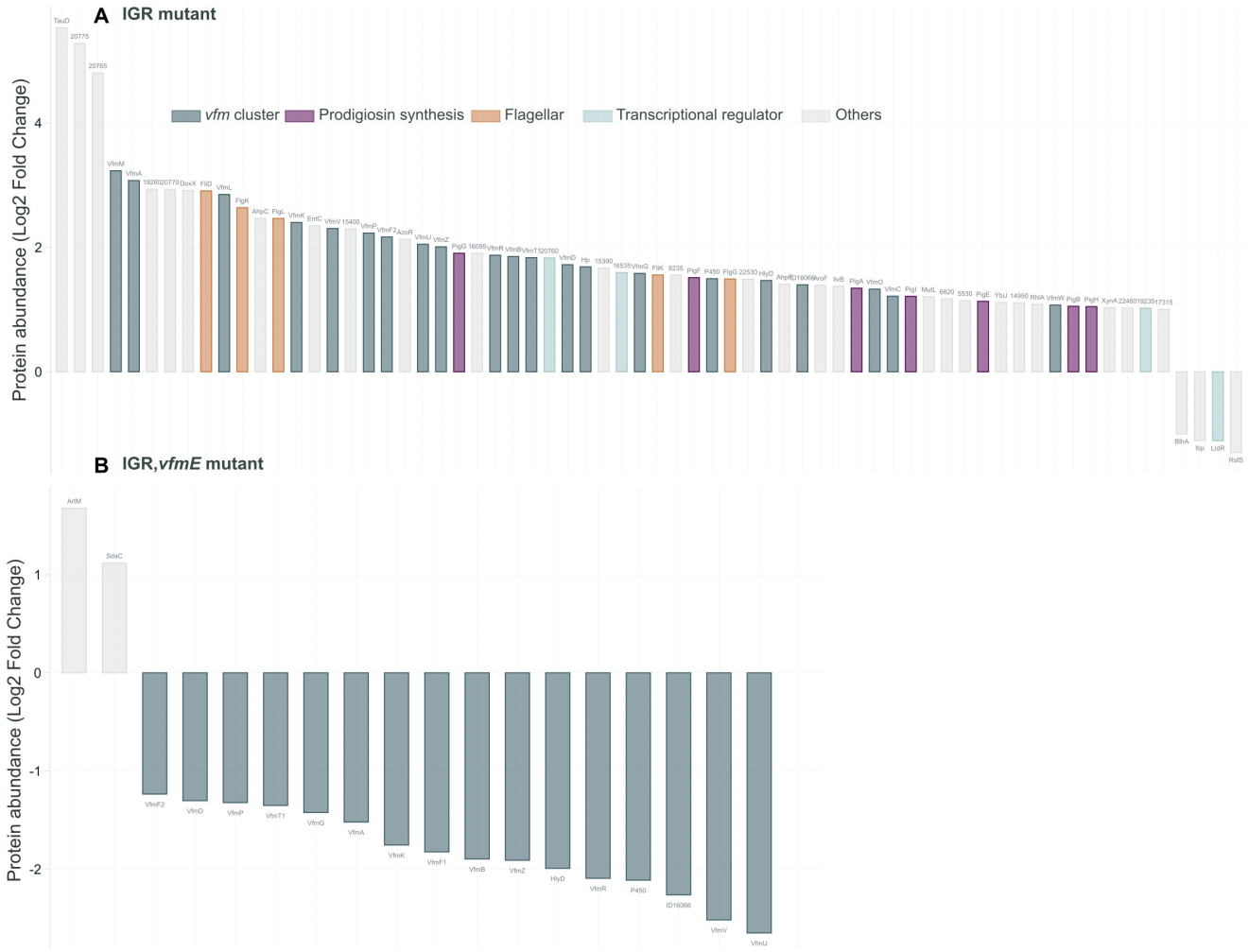


Fig. 7.3. Relative abundance of differentially expressed proteins in the intergenic and double mutants' proteomes. The protein abundance, expressed as Log2 fold change relative to the WT values, is shown for the (A) intergenic (IGR) and (B) double mutant (IGR,*vfmE*). The FC threshold of 1 was employed. The classification was performed based on known or predicted functional activities (colour codes in A legend).

The differentially expressed proteins, except for members of *vfm* and prodigiosin operons, are listed in Table 7.1. Among the top up-regulated proteins in the intergenic proteome, a putative operon comprised of four members was found. Its components are TauD (20780), 20775, 20770, and 20765, whose fold-change ratio varies from 2.93 (20770) to 5.53 (TauD), the latter being the most upregulated protein. This is a taurine dioxygenase, preceded in the operon by 20770, a putative hemolysin, 20765, a drug resistance efflux transporter, and 20770, an AMP-dependent synthase. Intriguingly, this protein was previously found in the mutagenesis screening and shown to augment transcription of the intergenic gene, as well as HlyD from the *vfm* cluster (Table 6.2). Flagellarelated proteins were also highly up-regulated in this proteome, with fold-change values ranging from 1.49 for FlgG up to 2.9 for FliD, which was also uncovered in the same mutagenesis screening as the two above-mentioned proteins. Four transcriptional regulators also

suffered modifications in their cellular concentration. In the up-regulated group, two LysR-family members and one from the MarR family were up-regulated, whilst LldR, a GntR-type regulator, was down-regulated. Other down-regulated proteins in this list are a heat-shock protein and RsfS (also known as YbeB), a ribosome hibernation factor. In the case of the double mutant proteome, the two up-regulated proteins are part of uptake systems of arginine (ArtM) and serine (SdaC).

Protein	Uniprot ID	Fold change	Predicted function
Intergenic mutant			
TauD	A0A2I5TP40	5.53	Taurine catabolism dioxygenase
20775	A0A2I5TBQ8	5.279	AMP-dependent synthetase
20765	A0A2I5TBQ2	4.803	Bcr/CflA family efflux transporter
19260	A0A2I5TB24	2.935	Uncharacterized protein
20770	A0A2I5TBS2	2.932	Thermostable hemolysin
DoxX	A0A2I5TIH1	2.915	DoxX family protein
FliD	A0A2I5TJG3	2.908	Flagellar hook-associated protein 2 (Flagellar cap protein)
FlgK	A0A2I5T713	2.638	Flagellar hook-associated protein 1
AhpC	A0A2I5T4S7	2.466	Alkyl hydroperoxide reductase C
FlgL	A0A2I5T773	2.464	Flagellar hook-filament junction protein
EntC	A0A2I5TQG4	2.349	Isochorismate synthase
15400	A0A2I5TLF4	2.297	ATP-grasp domain-containing protein
AzoR	A0A2I5T7L6	2.13	FMN dependent NADH:quinone oxidoreductase
16095	A0A2I5T9F6	1.903	3-oxoacyl-ACP synthase
20760	A0A2I5TBQ0	1.829	LysR family transcriptional regulator
15390	A0A2I5T923	1.666	Uncharacterized protein
16535	A0A2I5T9Q7	1.593	MarR family transcriptional regulator
FliK	A0A2I5T725	1.556	Flagellar hook-length control protein
8235	A0A2I5T5G1	1.553	B3_4 domain-containing protein
FlgG	A0A2I5T723	1.492	Flagellar basal-body rod protein (Distal rod protein)
22530	A0A2I5TPZ1	1.489	Aminotransferase
AhpF	A0A2I5TH12	1.408	Alkyl hydroperoxide reductase subunit F
AroF	A0A2I5THV9	1.391	Phospho-2-dehydro-3-deoxyheptonate aldolase
IlvB	A0A2I5TGR4	1.374	Acetolactate synthase
MutL	A0A2I5T434	1.208	DNA mismatch repair protein
6820	A0A2I5T4R1	1.172	ATP-grasp domain-containing protein
5530	A0A2I5TGF3	1.144	Uncharacterized protein
YbiJ	A0A2I5TF45	1.115	DUF1471 domain-containing protein
14950	A0A2I5T8U3	1.108	Phage major tail tube protein
RhlA	A0A2I5T9G2	1.084	Alpha/beta hydrolase
XynA	A0A2I5T195	1.031	Xylanase

22480	A0A2I5TQZ0	1.025	Amidohydrolase
19235	A0A2I5TAY6	1.022	LysR family transcriptional regulator
17315	A0A2I5TA11	1.004	Cysteine synthase family protein
BlhA	E7BBI9	-1	MBL fold metallo-hydrolase (Metallo-beta-lactamase fa
Ibp	A0A2I5T9L7	-1.105	Heat-shock protein
LldR	A0A2I5TN43	-1.109	Transcriptional regulator
RsfS	A0A2I5TMY3	-1.299	Ribosomal silencing factor
Double mutant			
ArtM	A0A2I5TLQ5	1.678	Arginine transporter permease subunit ArtM
SdaC	A0A2I5TIG5	1.12	HAAAP family serine/threonine permease

Table 7.1. Differentially expressed proteins in the intergenic and double mutants' proteomes. List of proteins with significant differences relative to the WT values. The *vfm* and prodigiosin synthesis proteins are not included. The numbers in the Protein column represent the name assigned by the corresponding coding gene. Predicted functions were taken from the Uniprot database.

7.2. The intergenic and the *vfmE* double mutant display opposite changes in antibiotic-synthesis protein levels

As some of the prodigiosin biosynthesis proteins were up-regulated in the intergenic mutant, but none was found using the fold change threshold chosen in the double mutant, it was reasoned that the rest of the members should exhibit lower values given their contrasting phenotypes in antibiotic production. Hence, to test this, all the proteins belonging to this operon (Fig. 7.4 A) were sought in the corresponding dataset. For the intergenic mutant strain, most of these proteins were found to be up-regulated, except for PigK, PigL, and PigM, which were not detected (Fig. 7.4 B). Values starting from 0.747 for PigC up to PigG with 1.9 were observed. The opposite case was observed for the double mutant, in which the same proteins were down-regulated, mirroring in most cases the increment observed in the intergenic, but at lower scale. Abundance ratios in this proteome ranged between -0.166 and -0.575 for PigB and PigG, respectively. Likewise, the same procedure was followed to find proteins of the carbapenem synthesis operon (Fig. 7.5 A). The same pattern was observed for the proteins detected, showing them up-regulated in the intergenic proteome, except for CarF (-0.006 variation; Fig. 7.4 B), and down-regulated in the double mutant dataset (Fig. 7.4 C). The proteins CarR, CarD, and CarE were not detected. Altogether, these results confirm the previous findings showing that antibiotic levels are higher in the intergenic cells and lower in the double mutant with *vfmE*.

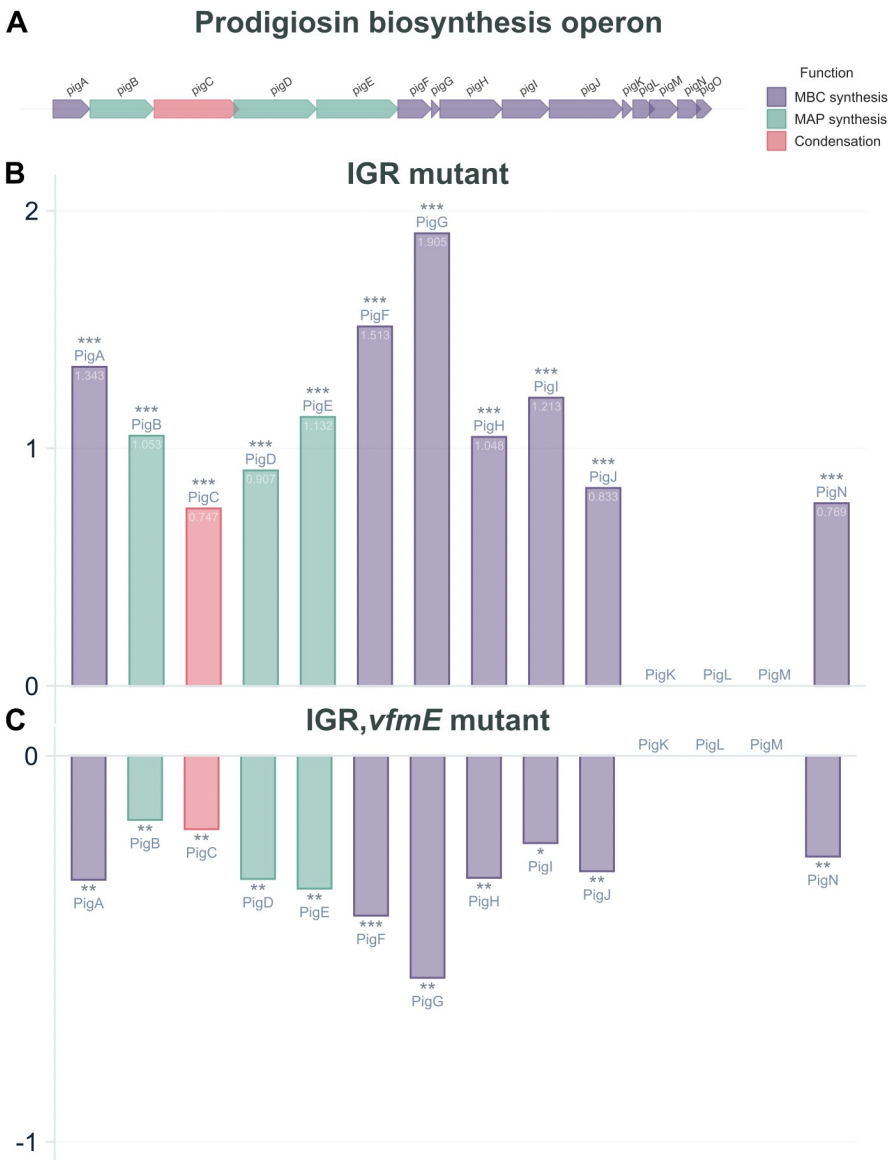


Fig. 7.4. Relative abundance of differentially expressed prodigiosin synthesis proteins in the intergenic and double mutants' proteomes. Bar colours correspond to the protein function in the biosynthetic operon (A). The protein abundance, expressed as Log2 fold change relative to the WT values, is shown for the (B) intergenic (IGR) and (C) double mutant (IGR,*vfmE*). The FC threshold of 1 was employed. The significance of protein changes is indicated by adjusted *p*-values: *$p < 0.05$, **$p < 0.01$, ***$p < 0.001$.

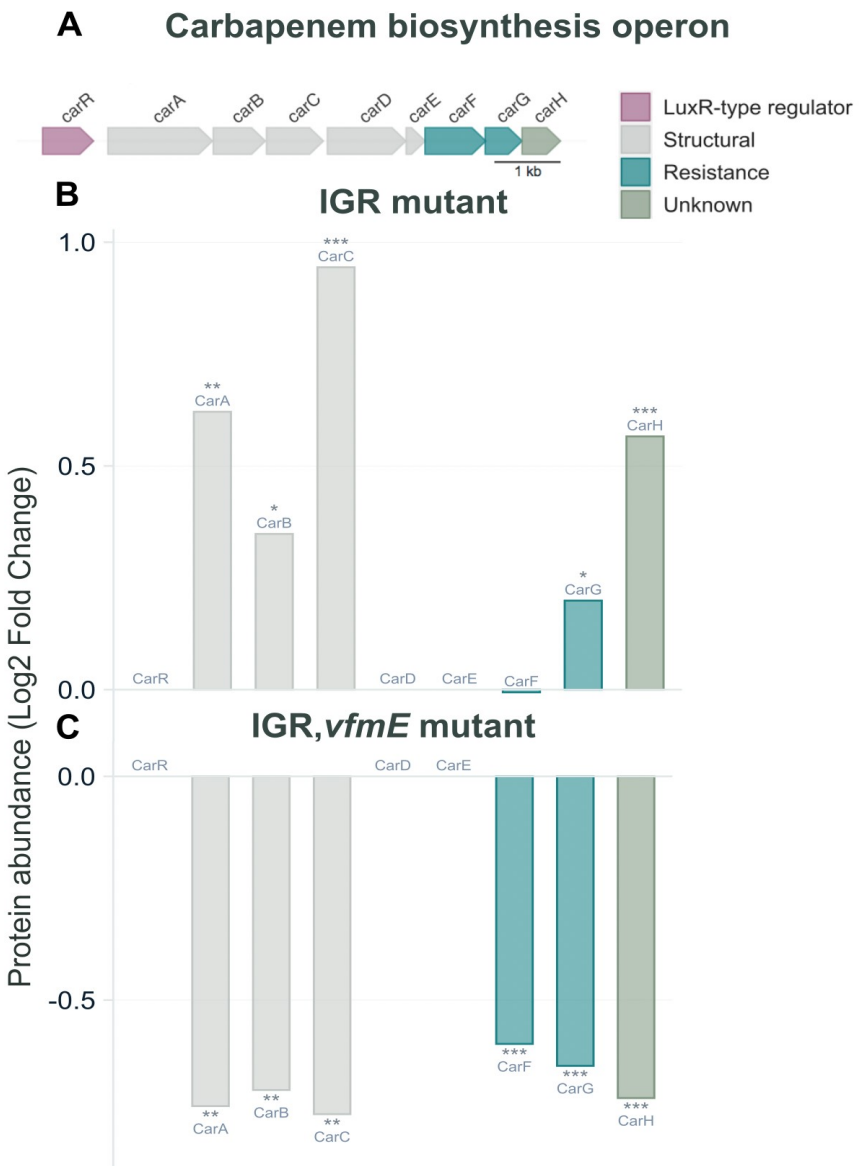


Fig. 7.5. Relative abundance of differentially expressed carbapenem synthesis proteins in the intergenic and double mutants' proteomes. Bar colours correspond to the protein function in the biosynthetic operon (A). The protein abundance, expressed as Log2 fold change relative to the WT values, is shown for the (B) intergenic (IGR) and (C) double mutant (IGR,*vfmE*). The FC threshold of 1 was employed. The significance of protein changes is indicated by adjusted *p*-values: *$p < 0.05$, **$p < 0.01$, ***$p < 0.001$.

7.3. The intergenic and the vfmE double mutant display opposite changes in *vfm* protein levels

In addition to antibiotic production regulation, the transcriptional regulator VfmE is also essential in the novel QS system based on the extracellular signal called Vfm. To investigate whether the intergenic mutation causes higher protein expression of only some *vfm* cluster members (seen in 7.3 A) or all of them, the remaining proteins from each *vfm* operon (Fig. 7.6 A) were sought in the proteomes. As expected, most of the detected *vfm* proteins were overproduced in the intergenic background (Fig. 7.6 B), conversely to the effect of the additional mutation of *vfmE* (Fig. 7.6 C). Only 4 proteins were not detected in the analysis: VfmJ, VfmE (expected solely in

the intergenic strain), VfmN, and VfmT2. For the intergenic strain, protein change values were from 0.435 up to 3,23-fold for VfmF1 and VfmM, respectively. The negative values in the double strain were observed in the range of -0.108 and -2.517 for the hypothetical protein (potentially a VfmS-like protein) and VfmV, respectively.

Therefore, these findings point that VfmE somehow activates all the operons of the *vfm* QS system. Unfortunately, owing to the time limitation, a deeper analysis of the proteomic data could not be performed. Moreover, the mutants *vfmA*, *vfmE*, *vfmK*, and *hlyD*, the first genes of each potential *vfm* operon, were also submitted to the proteomics facility for processing, but the time frame made it impossible to analyse this data and include it in this work.

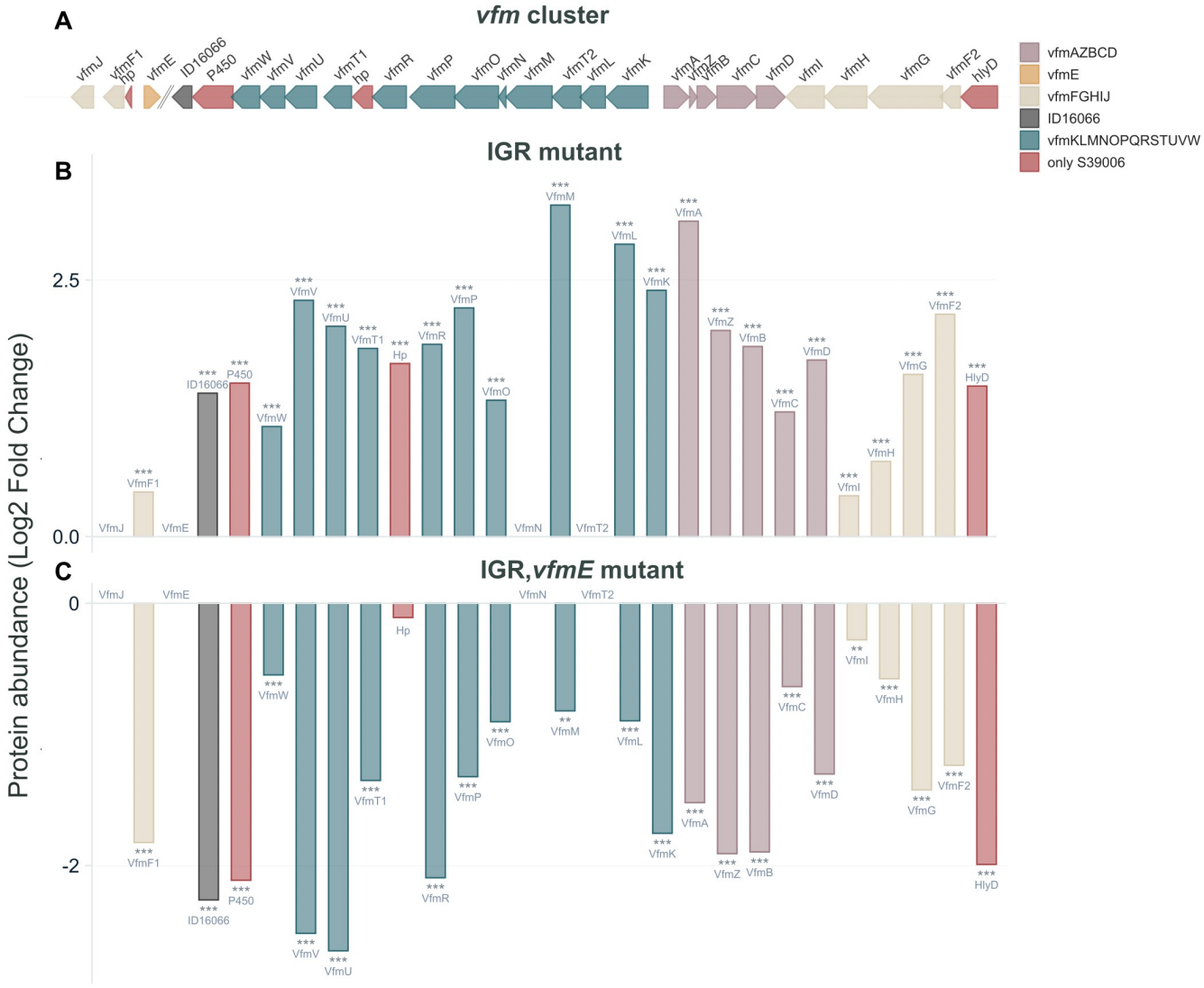


Fig. 7.6. Relative abundance of differentially expressed *vfm* proteins in the intergenic and double mutants' proteomes. Bar colours correspond to the putative operon the proteins belong to (A). The protein abundance, expressed as Log2 fold change relative to the WT values, is shown for the (B) intergenic (IGR) and (C) double mutant (IGR,*vfmE*). The FC threshold of 1 was employed. The significance of protein changes is indicated by adjusted *p*-values: *$p < 0.05$, **$p < 0.01$, ***$p < 0.001$.

7.4. Discussion

This chapter revealed the contrasting effects of the intergenic insertion and the additional mutation of *vfmE* on key features of S39006. Both the proteins involved in antibiotic production and in the Vfm-based QS system exhibited the opposite changes in their concentration. This supports the experimental results provided in previous chapters about the interplay between the two mutations investigated.

Regarding the overall similarity between the two mutant proteomes analysed, the intergenic insertion triggered far more changes than the double mutant. By setting the FC ratio to 1, the number of differentially overexpressed proteins in the intergenic proteome was 60-fold higher than in the double, whilst the downregulated in the latter were only four-times higher than the isogenic mutant. Notably, a third of all the up-regulated proteins in the intergenic strain were members of the *vfm* QS system, some of which were turned down upon the additional mutation of *vfmE*. The search of all the *vfm* constituent proteins showed that all the detected were either up or downregulated in the single or double mutant proteomes, respectively. This proves that this new extracellular signalling system is operative in S39006, as previously deduced by the cross-feeding assays, and it relies on VfmE action. On the other hand, the high expression of these proteins in the intergenic proteome underpins the hypothesis that the effects are provoked by a higher activity of VfmE. The four undetected *vfm* proteins were VfmJ, VfmE, VfmN, and VfmT2. Since *vfmE* was mutated in the double mutant strain, it should not appear in the analysis, however, it was not found either in the intergenic proteome, presumably due to low abundance. The predicted functions for the other three are a phosphopantetheinyl transferase (PPTase), Acyl carrier protein (ACP), and a 3-oxoacyl-ACP synthase, respectively. Another gap filled by the proteomic analysis was the activity of the proteins belonging to the termed “Locus1”, located upstream of the *vfmE* (the small group). Although VfmJ was not detected, the other member, VfmF1, experienced the same changes as the rest of the member from the large cluster (“Locus2”), indicating that it is also in the VfmE regulon.

with regard to the antibiotic biosynthesis proteins, they changed accordingly with the previous results: both operons were up-regulated in the intergenic proteome and down-regulated in that of the double. Moreover, the expression increase was also higher in the prodigiosin cluster than in the carbapenem cluster compared to the double mutant, again, in agreement with their production. The prodigiosin proteins PigK, PigL, and PigM were not detected. The function of PigK is unknown, PigL is a PPTase like VfmJ, and PigM is a dehydrogenase. The protein changes were more dissimilar in the carbapenem operon compared to that of prodigiosin. CarA, CarB, CarC, and CarH have more or less similar changes depending on the mutations. Nonetheless, the two

proteins providing the intrinsic resistance to the strain, CarF and CarG, they behaved differently. CarF concentration showed no significant changes in the intergenic proteome, while CarG was significantly increased. In the double mutant, both were downregulated to a comparable extent. The remaining components of this operon, CarD, and CarE were not found, nor the operon activator CarR either.

Another group of proteins found up-regulated in the intergenic proteome were linked to flagella. This finding was surprising as this mutant was shown to have a diminished swimming capacity, unlike the enhanced double mutant's ability. More of these proteins displaying lower expression levels could have helped to explain this mutant's behaviour. Another motility-related protein that was high in the intergenic mapping, the hydrolase RhlA, which is responsible for the production of surfactant that is used by the cells for swarming. The high *rhlA* expression in this background was previously confirmed by qPCR (Wilf, 2011), and it might explain the increased capacity observed in the intergenic strain. Unfortunately, due to time constraints, a more detailed analysis of the proteomic alterations caused by the mutations could not be conducted. Nevertheless, this chapter sheds light on protein changes induced by the new regulator VfmE, which modulates both the antibiotic production and a novel extracellular signalling system.

Chapter 8. Final discussion

The search for novel regulators of antibiotic production in S39006 by following a random transposon mutagenesis approach proved to be effective. The pigmentation differences in colonies after conjugation successfully enabled to identify directly from plates the strains of interest. The phenotypes observed varied from non-pigmented to hyper-producing pigment strains. The presence of known regulatory genes harbouring transposon insertions validated this approach. Mutants carrying insertions on genes of interest were verified via phage transduction to assure that those mutations actually triggered the phenotypic effects observed. The present chapter summarises the most relevant findings regarding the selected regulatory mutants derived from the mutagenesis.

An overview of the transposon mutagenesis process and the selection of mutants exhibiting altered pigmentation was presented in Chapter 3. From the set of selected strains from the screening, three insertion mutants were introduced. Two of them displayed an enhanced colouration relative to the WT parental strain, and one had a more "whitish" pigmentation. The first hyperpigmented strain had the insertion on a phosphopantetheinyl transferase (PPTase) gene, a *yieE* homologue. The next strain had the *cysW* (a sulfate transporter) altered, which reduced the production of both antibiotics. Since the protein is involved in cysteine/sulfate transport (via the CysAWPT complex), this strain was grown in a minimal medium and it was found to be auxotrophic. Finally, the last insertion strain, with the *5465* interrupted by the transposon, showed a redder phenotype in plates. However, its antibiotic synthesis did not significantly differ from the parental strain. Hence, from this point, the main focus of this work moved onto two other mutations: *wzt* and an intergenic region.

In Chapter 4, in addition to the *wzt* strain, its downstream gene *1186* also had inserted a transposon, and hence both were considered. These insertions into the two sequential genes were mapped and predicted to be part of a putative operon comprised of six genes (*1182-1187*). Both insertions increased the synthesis of antibiotics and led to a rough colony morphology. However, the *wzt* disruption had a more profound effect on prodigiosin, and it was therefore selected for analysis. This gene encodes the predicted partner of Wzm to form the ABC transport system of the Oantigen. Cells devoid of this gene showed an enhanced production of both antibiotics, and this upturn is regulated at the transcriptional level. Moreover, the mutation of this gene caused a reduced motility and attenuated virulence, which confirms pleiotropy. Assessing the production of antibiotics by double mutants of *wzt* with a large set of known regulators, led to uncover that the transcription regulator Rap was needed to produce the two antibacterial compounds.

Moreover, in the case of prodigiosin, PigX, a cyclic dimeric phosphodiesterase (PDE), was also involved. Thus, Rap and c-di-GMP concentration are likely related to, at least, Wzt, and possibly its operon, due to the similar effects observed on its downstream gene *1186*, suggesting polarity. For the carbapenem production, clear regulatory candidates controlling this molecule's levels were not ascertained. In this case, in addition to *rap*, mutations in *pigP*, *pigU*, and *carR*, made not possible the synthesis of this molecule in the *wzt* genetic background, which hints that they might participate in regulating the carbapenem production. Hence, possible regulatory routes for the Wzt operon are suggested (Fig. 8.1).

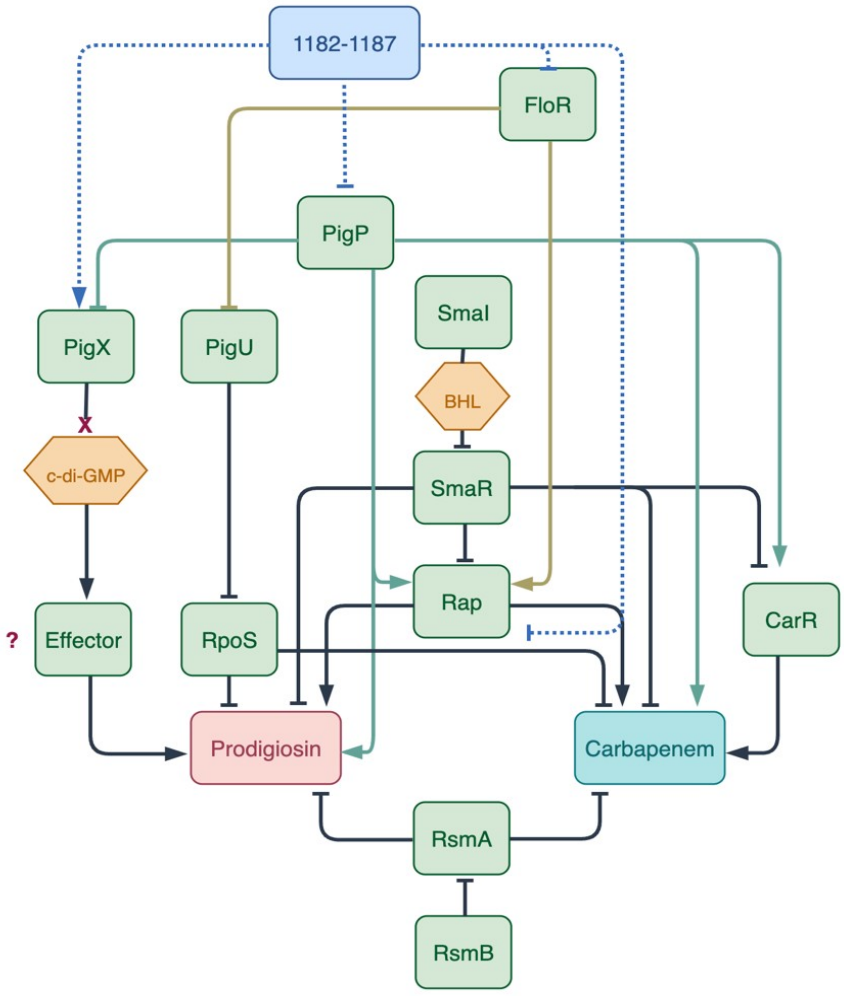


Fig. 8.1. Proposed model of antibiotic production regulation by the Wzt operon. The operon is proposed to act as a whole given that disruption of gene 1186, downstream of *wzt*, led to a similar phenotype (polar effects). It is displayed as a blue box (*1182-1187*) at the top. Transcriptional activation is illustrated by arrow heads and repression by flat arrow heads. Blue dotted lines indicate the possible regulatory by which the Wzt operon represses the biosynthesis operon of prodigiosin (red box) and the carbapenem (light blue box). These suggested pathways should be driven by a yet unknown transcriptional regulator as none is present in the Wzt operon. The green and dark yellow connecting lines correspond to the PigP and FloR regulon that might be involved in the antibiotic regulating process. PigX degrades ("x" sign) c-di-GMP molecules which might decrease activity of an unknown regulator that depends on this signal's presence.

Given that the active operon ultimately represses the production of both compounds at the transcriptional level, Rap activity might be the driver. This regulator directly activates both antibiotic biosynthesis operons and it is positively controlled by PigP (Fineran *et al*, 2005) and FloR (Quintero-Yanes *et al*, 2020). Thus, the Wzt operon could repress Rap activity through one of these proteins or via an unknown regulator. However, FloR also represses PigU, an HexA homologue, which in turn negatively modulates RpoS activity. The latter is a specialised sigma factor that represses the production of both antibiotics. Additionally, in the case of prodigiosin, PigX represses transcription of prodigiosin operon, presumably via indirect action. Its activity is negatively controlled by PigP, whose reduction leads to an increase of intracellular pool of c-diGMP via PigX (a PDE) degradation. Therefore, in the absence of PigX, the higher levels of c-diGMP may direct the rise of the operon transcription through an unknown effector. Finally, it cannot be ruled out that the Wzt operon may increase PigX activity in another way. Further research is hence needed to clarify how the Wzt operon modulates the synthesis of antibiotics in S39006.

The last mutant derived from the mutagenesis screening was examined in more detail in the chapter 5. Akin the *wzt* strain, this mutant exhibited hyperpigmentation. It carries a transposon insertion in the intergenic region between *argG* and *vfmE*, both transcribing convergently. Solely the *vfmE* and not the *argG* expression was previously shown to be increased in the intergenic background, and this mutant was therefore examined alongside the intergenic strain (named IGR). The regulatory gene encodes an AraC-type regulator that is associated with virulence modulation in *Dickeya* strains.

Antibiotic quantitation showed that the intergenic and the *vfmE* mutations have antagonistic effects. The former increases the synthesis of both compounds, particularly prodigiosin, whereas the lack of *vfmE* reduces their production. This phenomenon was also observed in flagella-based motility. Nevertheless, the plant's virulence was not affected in this way.

When investigating the double strain IGR,*vfmE*, it was noticed that the *vfmE* isogenic phenotype prevailed at least in antibiotic synthesis, motility, and virulence. The VfmE was then found to activate a potential intergenic gene using an intergenic LacZ fusion mutant. After, a predicted promoter showed activity *in vivo*. Multicopies of VfmE in cells harbouring this promoter were demonstrated to augment its activity.

Genetic complementation of the intergenic mutant was sought by employing fragments of varied length in the opposite transcription direction of *vfmE*. However, the reversion of the elevated pigmentation was not possible. Following RNA-seq data analysis of this region and transcription end determination, the presence of up to three transcripts convergently transcribed to *vfmE* was revealed.

To investigate related regulating pathways, the set of known regulators was used to generate double mutants with both the intergenic and the *vfmE* mutations. In general, the trend previously found in antibiotic synthesis, with the intergenic insertion increasing and the *vfmE* decreasing the production, was maintained. Given that the antibiotic regulation is directed by VfmE, the analysis revealed that the regulators PigT and PigR might drive the prodigiosin upturn. Further, in the intergenic background, the expression of *pigT* was increased, whilst that of *pigR* had no change. Thus, VfmE would activate the GntR regulator PigT, which in turn, directly activates the expression of prodigiosin biosynthesis cluster (Fig. 8.2). Also, VfmE activity might depend on PigR, which synthesises cAMP.

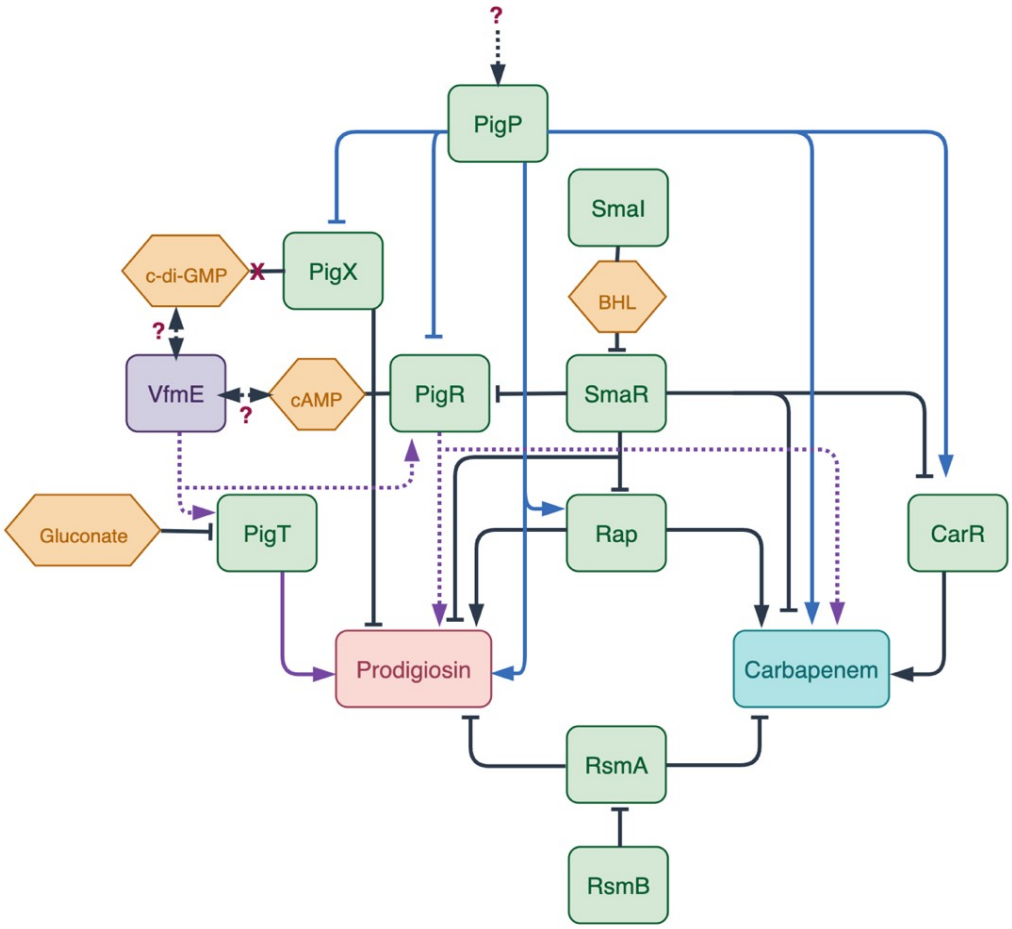


Fig. 8.2. Proposed model of antibiotic production regulation by VfmE. The VfmE transcriptional regulator (purple box) is proposed to activate the production of prodigiosin (red box) and the carbapenem (light blue box) mainly via two regulators, PigR (both compounds) and PigT (only prodigiosin). The former synthesises cAMP and it is unknown whether it acts or not at transcriptional level through an effector protein. PigT, a transcription regulator repressed by gluconate, activates expression of the pigment synthesis cluster. Moreover, VfmE activity may be influenced by either cAMP or c-di-GMP, or both. PigX degrades ("x" sign) c-di-GMP molecules. Transcriptional activation is illustrated by arrow heads and repression by flat arrow heads. Purple dotted lines indicate the possible regulatory routes in which VfmE operates. The blue connecting lines correspond to the PigP regulon.

For the carbapenem case, the scenario is more complex. In addition to PigR, a mutation on *pigX* also impeded the rise of this compound in the intergenic background. This regulator decreases the expression of both prodigiosin and the carbapenem operons by diminishing the intracellular levels of c-di-GMP. Notably, VfmE has been recently shown to be a c-di-GMP-based effector in *D*. *dadantii* (Banerjee *et al*, 2022). Thus, the activity of VfmE may also be dependent of these two intracellular signals. Nonetheless, to ascertain the exact mechanisms underpinning its regulon, more research is necessary.

Given that VfmE has been reported to control a secondary quorum sensing (QS) system in *Dickeya* strains, homologues of this system and the role of VfmE beyond antibiotic synthesis in S39006 were explored in Chapter 6. By homology search, the *vfm* cluster was confirmed to be present in S39006. Its main difference to that of *Dickeya* spp. is that it occupies two loci instead of one. Most of the components are localised in the cluster opposite to where *vfmE* is placed. Nonetheless, some of the *vfm* members were predicted to interact with VfmE. To look into this prediction, it was used a new transposon mutagenesis approach, using the LacZ activity from an intergenic fusion strain. This approach disclosed that another *vfm* member, encoding a HlyD homologue, also modulates the intergenic gene alike VfmE, which demonstrated a linkage between the two distant *vfm* clusters. Additionally, this mutant had the same *vfmE* colony phenotype. This fact raised the question whether the unknown molecule, termed Vfm, may tune the antibiotic synthesis. Cross-feeding assays suggest that this extracellular signal is formed, and it enhances pigmentation. Altogether, these findings led to the hypothesis that mutants able to bypass the hyperpigmented phenotype of IGR should belong to the *vfm* cluster, which was later corroborated by another mutagenesis. All of the new *vfm* members exhibited the ligh-pink phenotype of *vfmE* strain, which was also found several times in the screening. Next, as the genes leading all the putative operons that comprise the *vfm* system were obtained, their contribution to virulence and Vfm signalling was assessed. Afterwards, to examine if the VfmE can control the promoter activity of the potential *vfm* operons, *in vivo* assays were carried out. Additionally, the VfmH effect was also tested since it has been pointed out as the major controller of the *vfm* system (Nasser *et al*, 2013). Data showed that VfmE activates and reduces slightly the expression of *vfmA* and *hlyD*, respectively. VfmH, however, played no role. Cells overexpressing these two regulators had no effect on the expression of antibiotic synthesis operons (*pigA-O* and *carA-H*), *rap*, and *carR*. This supports a model in which VfmE regulation of antibiotic production is exerted via other regulators. Therefore, this chapter evidenced that VfmE not only activates antibiotic synthesis, but it also modulates a new QS system that is based on a mysterious molecule.

Since previous findings hint that the intergenic mutation alleviates an unknown mechanism that negatively controls the VfmE activity, a proteomics analysis was conducted to examine the insertion effects on a global scale. Additionally, to contrast the protein changes, the double mutant containing both the intergenic and *vfmE* mutations was also analysed. Thus, Chapter 7 delved into the protein changes of antibiotic synthesis and *vfm* clusters induced by the mutations under study. Overall, the intergenic strain prompted changes in a higher number of proteins compared to the double mutant's proteome. The former proteome had nearly four-fold more proteins differentially expressed than its double strain counterpart. Moreover, these proteins possess an ample diversity of functions, unlike the proteins differentially regulated in the other proteome. It was corroborated that changes in all the biosynthetic proteins detected from the two antibiotic operons correlate with the corresponding synthesis levels previously quantitated for the two strains. Likewise, this omics approach also allowed to confirm that all the *vfm* members detected suffered contrasting concentration changes in the mutants assayed. As observed in the antibiotic production, the intergenic insertion elicited the up-regulation of all the found *vfm* members, whilst the opposite effect was observed for its double mutant. Overall, this technique, in addition to confirming the interplay between the intergenic region and VfmE, it strongly supports that the effects observed in the intergenic strain are owing to higher levels of the transcription regulator.

In summary, this study identified and characterised novel regulators of antibiotic synthesis using random transposon mutagenesis and a straightforward visual screening method. The work was centred on two mutations, *wzt*, from an operon related to O-antigen transport, and the other to an intergenic region. The former was shown to repress the biosynthesis of antibiotics, and the intergenic disruption led the attention to the AraC regulator VfmE as the regulatory driver. Thus, this regulator, previously only associated with virulence modulation, was here demonstrated to also activate the production of antibiotics. Furthermore, a new cell-to-cell communication system in S39006 was unearthed when studying VfmE, which was speculated to be solely operative in *Dickeya* species. The evidence shown also suggests that higher levels of the Vfm extracellular signal, stimulate antibiotic synthesis. Thus, the findings provided in this work not only expands the arsenal of regulators used by S39006 to fine-tune its production of antibacterials but also discloses a novel communication system, which warrants further research. The importance lies in the new players added to the known regulatory network of antibiotic biosynthesis in a non-canonical model. This advances our understanding of the mechanisms underpinning natural antibiotic production, which may impact future developments in their controlled manufacturing.

9. References

Abràmoff, M. D., Magalhães, P. J., & Ram, S. J. (2004). Image processing with ImageJ. *Biophotonics International*, *11*(7), 36–42.

Aminov, R. (2017). History of antimicrobial drug discovery: Major classes and health impact. *Biochemical Pharmacology*, *133*, 4–19.

Andro, T., Chambost, J.-P., Kotoujansky, A., Cattaneo, J., Bertheau, Y., Barras, F., Van Gijsegem, F., & Coleno, A. (1984). Mutants of Erwinia chrysanthemi defective in secretion of pectinase and cellulase. *Journal of Bacteriology*, *160*(3), 1199–1203.

Ante, V. M., Farris, L. C., Saputra, E. P., Hall, A. J., O'Bier, N. S., Oliva Chávez, A. S., Marconi, R. T., Lybecker, M. C., & Hyde, J. A. (2021). The *Borrelia burgdorferi* adenylate cyclase, CyaB, is important for virulence factor production and mammalian infection. *Frontiers in Microbiology*, *12*, 676192.

Aravind, L., Anantharaman, V., Balaji, S., Babu, M. M., & Iyer, L. M. (2005). The many faces of the helix-turn-helix domain: Transcription regulation and beyond. *FEMS Microbiology Reviews*, *29*(2), 231–262.

Arivizhivendhan, K., Mahesh, M., Murali, R., Mary, R. R., Thanikaivelan, P., & Sekaran, G. (2019). Prodigiosin–iron-oxide–carbon matrix for efficient antibiotic-resistant bacterial disinfection of contaminated water. *ACS Sustainable Chemistry & Engineering*, *7*(3), 3164–3175.

Bainton, N. J., Stead, P., Chhabra, S. R., Bycroft, B. W., Salmond, G., Stewart, G. S., & Williams, P. (1992). N-(3-oxohexanoyl)-L-homoserine lactone regulates carbapenem antibiotic production in *Erwinia carotovora*. *Biochemical Journal*, *288*(3), 997–1004.

Banerjee, B., Zeng, Q., Yu, M., Hsueh, B. Y., Waters, C. M., & Yang, C.-H. (2022). Quorum-Sensing Master Regulator VfmE Is a c-di-GMP Effector That Controls Pectate Lyase Production in the Phytopathogen *Dickeya dadantii*. *Microbiology Spectrum*, *10*(2), e01805-21.

Barquist, L., Boinett, C. J., & Cain, A. K. (2013). Approaches to querying bacterial genomes with transposon-insertion sequencing. *RNA Biology*, *10*(7), 1161–1169.

Barton, L. L. (2005). Biometals. *Structural and Functional Relationships in Prokaryotes*, 721–774.

Bastet, L., Turcotte, P., Wade, J. T., & Lafontaine, D. A. (2018). Maestro of regulation: Riboswitches orchestrate gene expression at the levels of translation, transcription and mRNA decay. *RNA Biology*, *15*(6), 679–682.

Beld, J., Sonnenschein, E. C., Vickery, C. R., Noel, J. P., & Burkart, M. D. (2014). The phosphopantetheinyl transferases: Catalysis of a post-translational modification crucial for life. *Natural Product Reports*, *31*(1), 61–108.

Berry, M. C., McGhee, G. C., Zhao, Y., & Sundin, G. W. (2009). Effect of a waaL mutation on lipopolysaccharide composition, oxidative stress survival, and virulence in *Erwinia amylovora*. *FEMS Microbiology Letters*, *291*(1), 80–87.

Bertani, B., & Ruiz, N. (2018). Function and biogenesis of lipopolysaccharides. *EcoSal Plus*, *8*(1).

Blum, M., Chang, H.-Y., Chuguransky, S., Grego, T., Kandasaamy, S., Mitchell, A., Nuka, G., PaysanLafosse, T., Qureshi, M., & Raj, S. (2021). The InterPro protein families and domains database: 20 years on. *Nucleic Acids Research*, *49*(D1), D344–D354.

Boratyn, G. M., Schäffer, A. A., Agarwala, R., Altschul, S. F., Lipman, D. J., & Madden, T. L. (2012). Domain enhanced lookup time accelerated BLAST. *Biology Direct*, *7*(1), 1–14.

Borić, M., Danevčič, T., & Stopar, D. (2011). Prodigiosin from *Vibrio* sp. DSM 14379; a new UVprotective pigment. *Microbial Ecology*, *62*(3), 528–536.

Brown, E. D., & Wright, G. D. (2016). Antibacterial drug discovery in the resistance era. *Nature*, *529*(7586), 336–343.

Buchan, D. W., & Jones, D. T. (2019). The PSIPRED protein analysis workbench: 20 years on. *Nucleic Acids Research*, *47*(W1), W402–W407.

Bush, K., & Bradford, P. A. (2016). β-Lactams and β-lactamase inhibitors: An overview. *Cold Spring Harbor Perspectives in Medicine*, *6*(8), a025247.

Cain, A. K., Barquist, L., Goodman, A. L., Paulsen, I. T., Parkhill, J., & van Opijnen, T. (2020). A decade of advances in transposon-insertion sequencing. *Nature Reviews Genetics*, *21*(9), 526–540.

Cao, Y., Jin, X., Huang, H., Derebe, M. G., Levin, E. J., Kabaleeswaran, V., Pan, Y., Punta, M., Love, J., & Weng, J. (2011). Crystal structure of a potassium ion transporter, TrkH. *Nature*, *471*(7338), 336–340.

Carver, T., Harris, S. R., Berriman, M., Parkhill, J., & McQuillan, J. A. (2012). Artemis: An integrated platform for visualization and analysis of high-throughput sequence-based experimental data. *Bioinformatics*, *28*(4), 464–469.

Champion, G. A., Neely, M. N., Brennan, M. A., & DiRita, V. J. (1997). A branch in the ToxR regulatory cascade of *Vibrio cholerae* revealed by characterization of toxT mutant strains. *Molecular Microbiology*, *23*(2), 323–331.

Charkowski, A. O. (2018). The changing face of bacterial soft-rot diseases. *Annual Review of Phytopathology*, *56*, 269–288.

Charlier, D., & Bervoets, I. (2019). Regulation of arginine biosynthesis, catabolism and transport in *Escherichia coli*. *Amino Acids*, *51*(8), 1103–1127.

Chen, N., Liu, Y., Li, Y., & Wang, C. (2020). Chemical Proteomic Profiling of Protein 4′Phosphopantetheinylation in Mammalian Cells. *Angewandte Chemie*, *132*(37), 16203–16209.

Chen, Y., Luo, G., Chen, S., Zhang, D., Xie, W., Wang, Z., Zheng, W., & Xu, H. (2021). The potential of prodigiosin for control of Prorocentrum donghaiense blooms: Algicidal properties and acute toxicity to other marine organisms at various trophic levels. *Ecotoxicology and Environmental Safety*, *228*, 112913.

Chen, Y., Xia, J., Su, Z., Xu, G., Gomelsky, M., Qian, G., & Liu, F. (2017). *Lysobacter* PilR, the regulator of type IV pilus synthesis, controls antifungal antibiotic production via a cyclic di-GMP pathway. *Applied and Environmental Microbiology*, *83*(7), e03397-16.

Chen, Y., Zhou, J., Lv, M., Liang, Z., Parsek, M. R., & Zhang, L. (2020). Systematic analysis of c-diGMP signaling mechanisms and biological functions in *Dickeya zeae* EC1. *MBio*, *11*(6), e0299320.

Chia, J. Y., Khoo, K. S., Ling, T. C., Croft, L., Manickam, S., Yap, Y. J., & Show, P. L. (2021). Description and detection of excludons as transcriptional regulators in gram-positive, gramnegative and archaeal strains of prokaryotes. *Biocatalysis and Agricultural Biotechnology*, *32*, 101933.

Chilczuk, T., Monson, R., Schmieder, P., Christov, V., Enke, H., Salmond, G., & Niedermeyer, T. H. J. (2020). Ambigols from the Cyanobacterium Fischerella ambigua increase Prodigiosin Production in *Serratia* spp. *ACS Chemical Biology*, *15*(11), 2929–2936.

Choi, S. Y., Lim, S., Yoon, K., Lee, J. I., & Mitchell, R. J. (2021). Biotechnological activities and applications of bacterial pigments violacein and prodigiosin. *Journal of Biological Engineering*, *15*(1), 1–16.

Church, N. A., & McKillip, J. L. (2021). Antibiotic resistance crisis: Challenges and imperatives. *Biologia*, *76*(5), 1535–1550.

Clarke, B. R., Cuthbertson, L., & Whitfield, C. (2004). Nonreducing terminal modifications determine the chain length of polymannose O antigens of *Escherichia coli* and couple chain termination to polymer export via an ATP-binding cassette transporter. *Journal of Biological Chemistry*, *279*(34), 35709–35718.

Coulthurst, S. J., Barnard, A. M., & Salmond, G. P. (2005). Regulation and biosynthesis of carbapenem antibiotics in bacteria. *Nature Reviews Microbiology*, *3*(4), 295–306.

Coulthurst, S. J., Kurz, C. L., & Salmond, G. P. (2004). LuxS mutants of *Serratia* defective in autoinducer-2-dependent 'quorum sensing'show strain-dependent impacts on virulence and production of carbapenem and prodigiosin. *Microbiology*, *150*(6), 1901–1910.

Couturier, M., Bhalara, H. D., Chawrai, S. R., Monson, R., Williamson, N. R., Salmond, G. P., & Leeper, F. J. (2020). Substrate flexibility of the flavin-dependent dihydropyrrole oxidases PigB and HapB involved in antibiotic prodigiosin biosynthesis. *ChemBioChem*, *21*(4), 523–530.

Crépin, A., Barbey, C., Beury-Cirou, A., Hélias, V., Taupin, L., Reverchon, S., Nasser, W., Faure, D., Dufour, A., & Orange, N. (2012). Quorum sensing signaling molecules produced by reference and emerging soft-rot bacteria (*Dickeya* and *Pectobacterium* spp.). *PLoS One*, *7*(4), e35176.

Crépin, A., Beury-Cirou, A., Barbey, C., Farmer, C., Hélias, V., Burini, J.-F., Faure, D., & Latour, X. (2012). N-acyl homoserine lactones in diverse *Pectobacterium* and *Dickeya* plant pathogens: Diversity, abundance, and involvement in virulence. *Sensors*, *12*(3), 3484–3497.

Crofts, T. S., Gasparrini, A. J., & Dantas, G. (2017). Next-generation approaches to understand and combat the antibiotic resistome. *Nature Reviews Microbiology*, *15*(7), 422–434.

Crooks, G. E., Hon, G., Chandonia, J.-M., & Brenner, S. E. (2004). WebLogo: A sequence logo generator. *Genome Research*, *14*(6), 1188–1190.

Cuthbertson, L., Kos, V., & Whitfield, C. (2010). ABC transporters involved in export of cell surface glycoconjugates. *Microbiology and Molecular Biology Reviews*, *74*(3), 341–362.

Darshan, N., & Manonmani, H. (2015). Prodigiosin and its potential applications. *Journal of Food Science and Technology*, *52*(9), 5393–5407.

Darshan, N., & Manonmani, H. (2016). Prodigiosin inhibits motility and activates bacterial cell death revealing molecular biomarkers of programmed cell death. *Amb Express*, *6*(1), 1–12.

de Jong, A., Pietersma, H., Cordes, M., Kuipers, O. P., & Kok, J. (2012). PePPER: a webserver for prediction of prokaryote promoter elements and regulons. *BMC Genomics*, *13*(1), 1–10.

Den Hengst, C. D., Tran, N. T., Bibb, M. J., Chandra, G., Leskiw, B. K., & Buttner, M. J. (2010). Genes essential for morphological development and antibiotic production in Streptomyces coelicolor are targets of BldD during vegetative growth. *Molecular microbiology*, *78*(2), 361-379.

Di Lorenzo, F., Duda, K. A., Lanzetta, R., Silipo, A., De Castro, C., & Molinaro, A. (2021). A journey from structure to function of bacterial lipopolysaccharides. *Chemical Reviews*.

Dolan, S. K., Kohlstedt, M., Trigg, S., Vallejo Ramirez, P., Kaminski, C. F., Wittmann, C., & Welch, M. (2020). Contextual flexibility in *Pseudomonas aeruginosa* central carbon metabolism during growth in single carbon sources. *MBio*, *11*(2), e02684-19.

Dudek, C.-A., & Jahn, D. (2022). PRODORIC: state-of-the-art database of prokaryotic gene regulation. *Nucleic Acids Research*, *50*(D1), D295–D302.

Duprey, A., Taib, N., Leonard, S., Garin, T., Flandrois, J., Nasser, W., Brochier-Armanet, C., & Reverchon, S. (2019). The phytopathogenic nature of *Dickeya aquatica* 174/2 and the dynamic early evolution of *Dickeya* pathogenicity. *Environmental Microbiology*, *21*(8), 2809–2835.

El-Gamal, M. I., Brahim, I., Hisham, N., Aladdin, R., Mohammed, H., & Bahaaeldin, A. (2017). Recent updates of carbapenem antibiotics. *European Journal of Medicinal Chemistry*, *131*, 185–195.

Esquerré, T., Bouvier, M., Turlan, C., Carpousis, A. J., Girbal, L., & Cocaign-Bousquet, M. (2016). The Csr system regulates genome-wide mRNA stability and transcription and thus gene expression in *Escherichia coli*. *Scientific Reports*, *6*(1), 1–13.

Evans, T., Crow, M., Williamson, N., Orme, W., Thomson, N., Komitopoulou, E., & Salmond, G. (2010). Characterization of a broad-host-range flagellum-dependent phage that mediates highefficiency generalized transduction in, and between, *Serratia* and *Pantoea*. *Microbiology*, *156*(1), 240–247.

Felden, B., & Augagneur, Y. (2021). Diversity and Versatility in Small RNA-Mediated Regulation in Bacterial Pathogens. *Frontiers in Microbiology*, *12*, 719977. https://doi.org/10.3389/fmicb.2021.719977

Feng, L., Schaefer, A. L., Hu, M., Chen, R., Greenberg, E. P., & Zhou, J. (2019). Virulence factor identification in the banana pathogen *Dickeya zeae* MS2. *Applied and Environmental Microbiology*, *85*(23), e01611-19.

Fineran, P. C., Everson, L., Slater, H., & Salmond, G. P. (2005). A GntR family transcriptional regulator (PigT) controls gluconate-mediated repression and defines a new, independent pathway for regulation of the tripyrrole antibiotic, prodigiosin, in *Serratia*. *Microbiology*, *151*(12), 3833–3845.

Fineran, P. C., Iglesias Cans, M. C., Ramsay, J. P., Wilf, N. M., Cossyleon, D., McNeil, M. B., Williamson, N. R., Monson, R. E., Becher, S. A., & Stanton, J.-A. L. (2013). Draft genome sequence of *Serratia* sp. Strain ATCC 39006, a model bacterium for analysis of the biosynthesis and regulation of prodigiosin, a carbapenem, and gas vesicles. *Genome Announcements*, *1*(6), e01039-13.

Fineran, P. C., Slater, H., Everson, L., Hughes, K., & Salmond, G. P. (2005). Biosynthesis of tripyrrole and β-lactam secondary metabolites in *Serratia*: Integration of quorum sensing with multiple new regulatory components in the control of prodigiosin and carbapenem antibiotic production. *Molecular Microbiology*, *56*(6), 1495–1517.

Fineran, P. C., Williamson, N. R., Lilley, K. S., & Salmond, G. P. (2007). Virulence and prodigiosin antibiotic biosynthesis in *Serratia* are regulated pleiotropically by the GGDEF/EAL domain protein, PigX. *Journal of Bacteriology*, *189*(21), 7653–7662.

Fischbach, M. A., & Walsh, C. T. (2009). Antibiotics for emerging pathogens. *Science*, *325*(5944), 1089–1093.

Forquet, R., Jiang, X., Nasser, W., Hommais, F., Reverchon, S., & Meyer, S. (2022). Mapping the complex transcriptional landscape of the phytopathogenic bacterium *Dickeya dadantii*. *Mbio*, *13*(3), e00524-22.

Gatto, L., & Lilley, K. S. (2012). MSnbase-an R/Bioconductor package for isobaric tagged mass spectrometry data visualization, processing and quantitation. *Bioinformatics*, *28*(2), 288–289.

Gligorijević, V., Renfrew, P. D., Kosciolek, T., Leman, J. K., Berenberg, D., Vatanen, T., Chandler, C., Taylor, B. C., Fisk, I. M., & Vlamakis, H. (2021). Structure-based protein function prediction using graph convolutional networks. *Nature Communications*, *12*(1), 1–14.

Goff, J., & Yee, N. (2017). Tellurate enters *Escherichia coli* K-12 cells via the SulT-type sulfate transporter CysPUWA. *FEMS Microbiology Letters*, *364*(24), fnx241.

Gomez Valdez, L., Rondan Dueñas, J. C., Andrade, A. J., Del Valle, E. E., Doucet, M. E., & Lax, P. (2022). In *vitro* and in *vivo* nematicidal activity of prodigiosin against the plant-parasitic nematode *Nacobbus celatus*. *Biocontrol Science and Technology*, *32*(6), 741–751.

Grazziotin, A. L., Vidal, N. M., & Venancio, T. M. (2015). Uncovering major genomic features of essential genes in Bacteria and a methanogenic Archaea. *The FEBS Journal*, *282*(17), 3395–3411.

Green, B., Bouchier, C., Fairhead, C., Craig, N. L., & Cormack, B. P. (2012). Insertion site preference of Mu, Tn5, and Tn7 transposons. *Mobile DNA*, *3*(1), 1–6.

Green, M. R., & Sambrook, J. (2012). Molecular cloning. *A Laboratory Manual 4th*.

Greenfield, L. K., & Whitfield, C. (2012). Synthesis of lipopolysaccharide O-antigens by ABC transporter-dependent pathways. *Carbohydrate Research*, *356*, 12–24.

Grimont, F., & Grimont, P. A. (2006). The genus *Serratia*. *Prokaryotes*, *6*(219), 44.

Gristwood, T., Fineran, P. C., Everson, L., & Salmond, G. P. (2008). PigZ, a TetR/AcrR family repressor, modulates secondary metabolism via the expression of a putative four-component resistance-nodulation-cell-division efflux pump, ZrpADBC, in *Serratia* sp. ATCC 39006. *Molecular Microbiology*, *69*(2), 418–435.

Gristwood, T., McNeil, M. B., Clulow, J. S., Salmond, G. P., & Fineran, P. C. (2011). PigS and PigP regulate prodigiosin biosynthesis in *Serratia* via differential control of divergent operons, which include predicted transporters of sulfur-containing molecules. *Journal of Bacteriology*, *193*(5), 1076–1085.

Grognot, M., & Taute, K. M. (2021). More than propellers: How flagella shape bacterial motility behaviors. *Current Opinion in Microbiology*, *61*, 73–81.

Gupta, K., Gupta, A., & Shrivastava, D. (2017). The last resort antibiotics: Carbapenems. *Int. J. Adv. Res*, *5*(4), 1410–1413.

Gupta, S., Stamatoyannopoulos, J. A., Bailey, T. L., & Noble, W. S. (2007). Quantifying similarity between motifs. *Genome Biology*, *8*(2), 1–9.

Hagelueken, G., Huang, H., Clarke, B. R., Lebl, T., Whitfield, C., & Naismith, J. H. (2012). Structure of WbdD: a bifunctional kinase and methyltransferase that regulates the chain length of the O antigen in *Escherichia coli* O9a. *Molecular Microbiology*, *86*(3), 730–742.

Ham, J. H., Cui, Y., Alfano, J. R., Rodríguez-Palenzuela, P., Rojas, C. M., Chatterjee, A. K., & Collmer, A. (2004). Analysis of *Erwinia chrysanthemi* EC16 pelE:: uidA, pelL:: uidA, and hrpN:: uidA mutants reveals strain-specific atypical regulation of the Hrp type III secretion system. *Molecular Plant-Microbe Interactions*, *17*(2), 184–194.

Hamed, R. B., Gomez-Castellanos, J. R., Henry, L., Ducho, C., McDonough, M. A., & Schofield, C. J. (2013). The enzymes of β-lactam biosynthesis. *Natural Product Reports*, *30*(1), 21–107.

Hampton, H. G., McNeil, M. B., Paterson, T. J., Ney, B., Williamson, N. R., Easingwood, R. A., Bostina, M., Salmond, G. P., & Fineran, P. C. (2016). CRISPR-Cas gene-editing reveals RsmA and RsmC act through FlhDC to repress the SdhE flavinylation factor and control motility and prodigiosin production in *Serratia*. *Microbiology*, *162*(6), 1047.

Han, M.-J., & Lee, S. Y. (2006). The *Escherichia coli* proteome: Past, present, and future prospects. *Microbiology and Molecular Biology Reviews*, *70*(2), 362–439.

Harman, J. G. (2001). Allosteric regulation of the cAMP receptor protein. *Biochimica et Biophysica Acta (BBA)-Protein Structure and Molecular Enzymology*, *1547*(1), 1–17.

Harris, A. K., Williamson, N. R., Slater, H., Cox, A., Abbasi, S., Foulds, I., Simonsen, H. T., Leeper, F. J., & Salmond, G. P. (2004). The *Serratia* gene cluster encoding biosynthesis of the red

antibiotic, prodigiosin, shows species-and strain-dependent genome context variation. *Microbiology*, *150*(11), 3547–3560.

Hatzios, S. K., & Bertozzi, C. R. (2011). The regulation of sulfur metabolism in *Mycobacterium tuberculosis*. *PLoS Pathogens*, *7*(7), e1002036.

Hejazi, A., & Falkiner, F. (1997). *Serratia marcescens*. *Journal of Medical Microbiology*, *46*(11), 903– 912.

Herron, P. R., Hughes, G., Chandra, G., Fielding, S., & Dyson, P. J. (2004). Transposon Express, a software application to report the identity of insertions obtained by comprehensive transposon mutagenesis of sequenced genomes: analysis of the preference for in vitro Tn 5 transposition into GC-rich DNA. Nucleic acids research, 32(14), e113-e113.

Henderson, J. C., Zimmerman, S. M., Crofts, A. A., Boll, J. M., Kuhns, L. G., Herrera, C. M., & Trent, M. S. (2016). The power of asymmetry: Architecture and assembly of the Gram-negative outer membrane lipid bilayer. *Annu Rev Microbiol*, *70*(6), 255–278.

Hengge, R. (2009). Proteolysis of σS (RpoS) and the general stress response in *Escherichia coli*. *Research in Microbiology*, *160*(9), 667–676.

Hentchel, K. L., & Escalante-Semerena, J. C. (2015). Acylation of biomolecules in prokaryotes: A widespread strategy for the control of biological function and metabolic stress. *Microbiology and Molecular Biology Reviews*, *79*(3), 321–346.

Higgins, C. F. (1992). ABC transporters: From microorganisms to man. *Annual Review of Cell Biology*, *8*(1), 67–113.

Hill, A. M., & Salmond, G. P. (2020). Microbial gas vesicles as nanotechnology tools: Exploiting intracellular organelles for translational utility in biotechnology, medicine and the environment. *Microbiology*, *166*(6), 501.

Holmqvist, E., & Vogel, J. (2018). RNA-binding proteins in bacteria. *Nature Reviews Microbiology*, *16*(10), 601–615.

Hong, X., Wang, X., & Wang, Z. (2017). A rare case report of acyclovir-induced immune thrombocytopenia with tongue hematomas as the first sign, and a literature review. *BMC Pharmacology and Toxicology*, *18*(1), 1–5.

Hu, D. X., Withall, D. M., Challis, G. L., & Thomson, R. J. (2016). Structure, chemical synthesis, and biosynthesis of prodiginine natural products. *Chemical Reviews*, *116*(14), 7818–7853.

Huang, G., Zhang, L., & Birch, R. G. (2000). Albicidin antibiotic and phytotoxin biosynthesis in *Xanthomonas albilineans* requires a phosphopantetheinyl transferase gene. *Gene*, *258*(1–2), 193–199.

Huang, Y., He, L., Li, G., Zhai, N., Jiang, H., & Chen, Y. (2014). Role of helicity of α-helical antimicrobial peptides to improve specificity. *Protein & Cell*, *5*(8), 631–642.

Hussain, M. B., Zhang, H.-B., Xu, J.-L., Liu, Q., Jiang, Z., & Zhang, L.-H. (2008). The acyl-homoserine lactone-type quorum-sensing system modulates cell motility and virulence of *Erwinia chrysanthemi* pv. Zeae. *Journal of Bacteriology*, *190*(3), 1045–1053.

Hwang, K.-S., Kim, H. U., Charusanti, P., Palsson, B. Ø., & Lee, S. Y. (2014). Systems biology and biotechnology of Streptomyces species for the production of secondary metabolites. *Biotechnology Advances*, *32*(2), 255–268.

Iguchi, A., Iyoda, S., Kikuchi, T., Ogura, Y., Katsura, K., Ohnishi, M., Hayashi, T., & Thomson, N. R. (2015). A complete view of the genetic diversity of the *Escherichia coli* O-antigen biosynthesis gene cluster. *DNA Research*, *22*(1), 101–107.

Ji, K., & Kim, Y. T. (2019). Antimicrobial activity of prodigiosin from Serratia sp. PDGS 120915 against intestinal pathogenic bacteria. *Microbiology and Biotechnology Letters*, *47*(3), 459–464.

Kalivoda, E. J., Stella, N. A., Aston, M. A., Fender, J. E., Thompson, P. P., Kowalski, R. P., & Shanks, R. M. (2010). Cyclic AMP negatively regulates prodigiosin production by *Serratia marcescens*. *Research in Microbiology*, *161*(2), 158–167.

Kalvari, I., Nawrocki, E. P., Argasinska, J., Quinones-Olvera, N., Finn, R. D., Bateman, A., & Petrov, A. I. (2018). Non-coding RNA analysis using the Rfam database. *Current Protocols in Bioinformatics*, *62*(1), e51.

Kalynych, S., Morona, R., & Cygler, M. (2014). Progress in understanding the assembly process of bacterial O-antigen. *FEMS Microbiology Reviews*, *38*(5), 1048–1065.

Kanehisa, M., Araki, M., Goto, S., Hattori, M., Hirakawa, M., Itoh, M., Katayama, T., Kawashima, S., Okuda, S., & Tokimatsu, T. (2007). KEGG for linking genomes to life and the environment. *Nucleic Acids Research*, *36*(suppl_1), D480–D484.

Kavita, K., de Mets, F., & Gottesman, S. (2018). New aspects of RNA-based regulation by Hfq and its partner sRNAs. *Current Opinion in Microbiology*, *42*, 53–61.

Kearns, D. B. (2010). A field guide to bacterial swarming motility. *Nature Reviews Microbiology*, *8*(9), 634–644.

Kelley, L. A., Mezulis, S., Yates, C. M., Wass, M. N., & Sternberg, M. J. (2015). The Phyre2 web portal for protein modeling, prediction and analysis. *Nature Protocols*, *10*(6), 845–858.

Kertesz, M. A. (2001). Bacterial transporters for sulfate and organosulfur compounds. *Research in Microbiology*, *152*(3–4), 279–290.

Khannpnavar, B., Mehta, V., Qi, C., & Korkhov, V. (2020). Structure and function of adenylyl cyclases, key enzymes in cellular signaling. *Current Opinion in Structural Biology*, *63*, 34–41.

Khmelevtsova, L., Sazykin, I., Sazykina, M., & Seliverstova, E. Y. (2017). Prokaryotic cytochromes P450. *Applied Biochemistry and Microbiology*, *53*(4), 401–409.

Kim, J. H., Komatsu, M., Shin-Ya, K., Omura, S., & Ikeda, H. (2018). Distribution and functional analysis of the phosphopantetheinyl transferase superfamily in Actinomycetales microorganisms. *Proceedings of the National Academy of Sciences*, *115*(26), 6828–6833.

Kulmanov, M., Khan, M. A., & Hoehndorf, R. (2018). DeepGO: predicting protein functions from sequence and interactions using a deep ontology-aware classifier. *Bioinformatics*, *34*(4), 660–668.

Kumar, K., & Kumar, V. (2015). Prodigiosin alkaloids: Recent advancements in total synthesis and their biological potential. *RSC Advances*, *5*(15), 10899–10920.

Kumar, S., Stecher, G., Li, M., Knyaz, C., & Tamura, K. (2018). MEGA X: molecular evolutionary genetics analysis across computing platforms. *Molecular Biology and Evolution*, *35*(6), 1547.

Kutschera, A., Schombel, U., Wröbel, M., Gisch, N., & Ranf, S. (2019). Loss of wbpL disrupts Opolysaccharide synthesis and impairs virulence of plant-associated *Pseudomonas* strains. *Molecular Plant Pathology*, *20*(11), 1535–1549.

Kwon, Y. M., Ricke, S. C., & Mandal, R. K. (2016). Transposon sequencing: Methods and expanding applications. *Applied Microbiology and Biotechnology*, *100*(1), 31–43.

Labrie, S. J., Mosterd, C., Loignon, S., Dupuis, M.-È., Desjardins, P., Rousseau, G. M., Tremblay, D. M., Romero, D. A., Horvath, P., & Fremaux, C. (2019). A mutation in the methionine aminopeptidase gene provides phage resistance in *Streptococcus thermophilus*. *Scientific Reports*, *9*(1), 1–11.

Lamy, M., Zouine, M., Fert, J., Vergassola, M., Couve, E., Pellegrini, E., Glaser, P., Kunst, F., Msadek, T., & Trieu-Cuot, P. (2004). CovS/CovR of group B streptococcus: A two-component global regulatory system involved in virulence. *Molecular Microbiology*, *54*(5), 1250–1268.

Lapenda, J., Silva, P., Vicalvi, M., Sena, K., & Nascimento, S. (2015). Antimicrobial activity of prodigiosin isolated from *Serratia marcescens* UFPEDA 398. *World Journal of Microbiology and Biotechnology*, *31*(2), 399–406.

Larsson, D., & Flach, C.-F. (2022). Antibiotic resistance in the environment. *Nature Reviews Microbiology*, *20*(5), 257–269.

Lee, C. M., Monson, R. E., Adams, R. M., & Salmond, G. P. (2017). The LacI–family transcription factor, RbsR, is a pleiotropic regulator of motility, virulence, siderophore and antibiotic production, gas vesicle morphogenesis and flotation in *Serratia*. *Frontiers in Microbiology*, *8*, 1678.

Leisico, F., Godinho, L. M., Gonçalves, I. C., Silva, S. P., Carneiro, B., Romão, M. J., Santos-Silva, T., & de Sá-Nogueira, I. (2020). Multitask ATPases (NBDs) of bacterial ABC importers type I and their interspecies exchangeability. *Scientific Reports*, *10*(1), 1–17.

Lejars, M., Kobayashi, A., & Hajnsdorf, E. (2019). Physiological roles of antisense RNAs in prokaryotes. *Biochimie*, *164*, 3–16.

Leonard, S., Hommais, F., Nasser, W., & Reverchon, S. (2017). Plant–phytopathogen interactions: Bacterial responses to environmental and plant stimuli. *Environmental Microbiology*, *19*(5), 1689– 1716.

Letunic, I., & Bork, P. (2019). Interactive Tree Of Life (iTOL) v4: Recent updates and new developments. *Nucleic Acids Research*, *47*(W1), W256–W259.

Lewinson, O., & Livnat-Levanon, N. (2017). Mechanism of action of ABC importers: Conservation, divergence, and physiological adaptations. *Journal of Molecular Biology*, *429*(5), 606–619.

Lewis, K. (2020). The science of antibiotic discovery. *Cell*, *181*(1), 29–45.

Li, H., Handsaker, B., Wysoker, A., Fennell, T., Ruan, J., Homer, N., Marth, G., Abecasis, G., & Durbin, R. (2009). The sequence alignment/map format and SAMtools. *Bioinformatics*, *25*(16), 2078– 2079.

Li, Y., Feng, T., & Wang, Y. (2022). The role of bacterial signaling networks in antibiotics response and resistance regulation. *Marine Life Science & Technology*, 1–16.

Lim, S., Bhak, J., Jeon, S., Mun, W., Bhak, J., Choi, S. Y., & Mitchell, R. J. (2022). The Kiss of Death: *Serratia marcescens* Antibacterial Activities against *Staphylococcus aureus* Requires Both de novo Prodigiosin Synthesis and Direct Contact. *Microbiology Spectrum*, e00607-22.

Lin, L., Xu, K., Shen, D., Chou, S., Gomelsky, M., & Qian, G. (2021). Antifungal weapons of *Lysobacter*, a mighty biocontrol agent. *Environmental Microbiology*, *23*(10), 5704–5715.

Lin, S.-R., Chen, Y.-H., Tseng, F.-J., & Weng, C.-F. (2020). The production and bioactivity of prodigiosin: Quo vadis? *Drug Discovery Today*, *25*(5), 828–836.

Liu, X., Wang, Y., Sun, S., Zhu, C., Xu, W., Park, Y., & Zhou, H. (2013). Mutant breeding of *Serratia marcescens* strain for enhancing prodigiosin production and application to textiles. *Preparative Biochemistry and Biotechnology*, *43*(3), 271–284.

Liu, Z., Hossain, S. S., Morales Moreira, Z., & Haney, C. H. (2022). Putrescine and its metabolic precursor arginine promote biofilm and c-di-GMP synthesis in *Pseudomonas aeruginosa*. *Journal of Bacteriology*, *204*(1), e00297-21.

Llarrull, L. I., Testero, S. A., Fisher, J. F., & Mobashery, S. (2010). The future of the β-lactams. *Current Opinion in Microbiology*, *13*(5), 551–557.

Lodge, J., Fear, J., Busby, S., Gunasekaran, P., & Kamini, N. R. (1992). Broad host range plasmids carrying the *Escherichia coli* lactose and galactose operons. *FEMS Microbiology Letters*, *95*(2–3), 271–276.

Low, K. E., & Howell, P. L. (2018). Gram-negative synthase-dependent exopolysaccharide biosynthetic machines. *Current Opinion in Structural Biology*, *53*, 32–44.

Lowe, T. M., & Chan, P. P. (2016). tRNAscan-SE On-line: Integrating search and context for analysis of transfer RNA genes. *Nucleic Acids Research*, *44*(W1), W54–W57.

Lu, Y.-W., San Roman, A. K., & Gehring, A. M. (2008). Role of phosphopantetheinyl transferase genes in antibiotic production by *Streptomyces coelicolor*. *Journal of Bacteriology*, *190*(20), 6903–6908.

Lv, M., Chen, Y., Hu, M., Yu, Q., Duan, C., Ye, S., Ling, J., Zhou, J., Zhou, X., & Zhang, L. (2022a). OhrR is a central transcriptional regulator of virulence in *Dickeya zeae*. *Molecular Plant Pathology*, *23*(1), 45–59.

Lv, M., Chen, Y., Hu, M., Yu, Q., Duan, C., Ye, S., Ling, J., Zhou, J., Zhou, X., & Zhang, L. (2022b). OhrR is a central transcriptional regulator of virulence in *Dickeya zeae*. *Molecular Plant Pathology*, *23*(1), 45–59.

Lv, M., Hu, M., Li, P., Jiang, Z., Zhang, L., & Zhou, J. (2019). A two-component regulatory system VfmIH modulates multiple virulence traits in *Dickeya zeae*. *Molecular Microbiology*, *111*(6), 1493–1509.

Mahlen, S. D. (2011). Serratia infections: From military experiments to current practice. *Clinical Microbiology Reviews*, *24*(4), 755–791.

Makitrynskyy, R., Tsypik, O., Nuzzo, D., Paululat, T., Zechel, D. L., & Bechthold, A. (2020). Secondary nucleotide messenger c-di-GMP exerts a global control on natural product biosynthesis in streptomycetes. *Nucleic Acids Research*, *48*(3), 1583–1598.

Mann, E., Kimber, M. S., & Whitfield, C. (2019). Bioinformatics analysis of diversity in bacterial glycan chain-termination chemistry and organization of carbohydrate-binding modules linked to ABC transporters. *Glycobiology*, *29*(12), 822–838.

Marchler-Bauer, A., Derbyshire, M. K., Gonzales, N. R., Lu, S., Chitsaz, F., Geer, L. Y., Geer, R. C., He, J., Gwadz, M., & Hurwitz, D. I. (2015). CDD: NCBI's conserved domain database. *Nucleic Acids Research*, *43*(D1), D222–D226.

Marchler-Bauer, A., Lu, S., Anderson, J. B., Chitsaz, F., Derbyshire, M. K., DeWeese-Scott, C., Fong, J. H., Geer, L. Y., Geer, R. C., & Gonzales, N. R. (2010). CDD: a Conserved Domain Database for the functional annotation of proteins. *Nucleic Acids Research*, *39*(suppl_1), D225–D229.

Masschelein, J., Jenner, M., & Challis, G. L. (2017). Antibiotics from Gram-negative bacteria: A comprehensive overview and selected biosynthetic highlights. *Natural Product Reports*, *34*(7), 712–783.

Mattatall, N. R., & Sanderson, K. E. (1996). *Salmonella typhimurium* LT2 possesses three distinct 23S rRNA intervening sequences. *Journal of Bacteriology*, *178*(8), 2272–2278.

Mauzy, C., & Hermodson, M. (1992). Structural and functional analyses of the repressor, RbsR, of the ribose operon of *Escherichia coli*. *Protein Science*, *1*(7), 831–842.

Mazzuoli, M.-V., Daunesse, M., Varet, H., Rosinski-Chupin, I., Legendre, R., Sismeiro, O., Gominet, M., Kaminski, P. A., Glaser, P., & Chica, C. (2021). The CovR regulatory network drives the evolution of Group B *Streptococcus virulence*. *PLoS Genetics*, *17*(9), e1009761.

McGowan, S. J., Barnard, A. M., Bosgelmez, G., Sebaihia, M., Simpson, N. J., Thomson, N. R., Todd, D. E., Welch, M., Whitehead, N. A., & Salmond, G. P. (2005). Carbapenem antibiotic biosynthesis in *Erwinia carotovora* is regulated by physiological and genetic factors modulating the quorum sensing-dependent control pathway. *Molecular Microbiology*, *55*(2), 526–545.

McKay, M. J., Martfeld, A. N., De Angelis, A. A., Opella, S. J., Greathouse, D. V., & Koeppe II, R. E. (2018). Control of transmembrane helix dynamics by interfacial tryptophan residues. *Biophysical Journal*, *114*(11), 2617–2629.

McNeil, M. B., Clulow, J. S., Wilf, N. M., Salmond, G. P., & Fineran, P. C. (2012). SdhE is a conserved protein required for flavinylation of succinate dehydrogenase in bacteria. *Journal of Biological Chemistry*, *287*(22), 18418–18428.

McNeil, M. B., & Fineran, P. C. (2013). The conserved RGxxE motif of the bacterial FAD assembly factor SdhE is required for succinate dehydrogenase flavinylation and activity. *Biochemistry*, *52*(43), 7628–7640.

McNeil, M. B., Hampton, H. G., Hards, K. J., Watson, B. N., Cook, G. M., & Fineran, P. C. (2014). The succinate dehydrogenase assembly factor, SdhE, is required for the flavinylation and activation of fumarate reductase in bacteria. *FEBS Letters*, *588*(3), 414–421.

McNeil, M. B., Iglesias-Cans, M. C., Clulow, J. S., & Fineran, P. C. (2013). YgfX (CptA) is a multimeric membrane protein that interacts with the succinate dehydrogenase assembly factor SdhE (YgfY). *Microbiology*, *159*(7), 1352–1365.

Mesarich, C. H., Rees-George, J., Gardner, P. P., Ghomi, F. A., Gerth, M. L., Andersen, M. T., Rikkerink, E. H., Fineran, P. C., & Templeton, M. D. (2017). Transposon insertion libraries for the characterization of mutants from the kiwifruit pathogen *Pseudomonas syringae* pv. Actinidiae. *PloS One*, *12*(3), e0172790.

Millar, J. A., & Raghavan, R. (2021). Modulation of bacterial fitness and virulence through antisense RNAs. *Frontiers in Cellular and Infection Microbiology*, *10*, 596277.

Mistry, J., Chuguransky, S., Williams, L., Qureshi, M., Salazar, G. A., Sonnhammer, E. L., Tosatto, S. C., Paladin, L., Raj, S., & Richardson, L. J. (2021). Pfam: The protein families database in 2021. *Nucleic Acids Research*, *49*(D1), D412–D419.

Monson, R., Smith, D. S., Matilla, M. A., Roberts, K., Richardson, E., Drew, A., Williamson, N., Ramsay, J., Welch, M., & Salmond, G. P. (2015). A plasmid-transposon hybrid mutagenesis system effective in a broad range of Enterobacteria. *Frontiers in Microbiology*, *6*, 1442.

Nakamura, T., Yamada, K. D., Tomii, K., & Katoh, K. (2018). Parallelization of MAFFT for large-scale multiple sequence alignments. *Bioinformatics*, *34*(14), 2490–2492.

Nasser, W., Dorel, C., Wawrzyniak, J., Van Gijsegem, F., Groleau, M., Déziel, E., & Reverchon, S. (2013). Vfm a new quorum sensing system controls the virulence of *Dickeya dadantii*. *Environmental Microbiology*, *15*(3), 865–880.

Naville, M., Ghuillot-Gaudeffroy, A., Marchais, A., & Gautheret, D. (2011). ARNold: A web tool for the prediction of Rho-independent transcription terminators. *RNA Biology*, *8*(1), 11–13.

Nguyen, V. B., Nguyen, D. N., Nguyen, A. D., Ngo, V. A., Ton, T. Q., Doan, C. T., Pham, T. P., Tran, T. P. H., & Wang, S.-L. (2020). Utilization of crab waste for cost-effective bioproduction of prodigiosin. *Marine Drugs*, *18*(11), 523.

Nuzzo, D., Makitrynskyy, R., Tsypik, O., & Bechthold, A. (2020). Cyclic di-GMP cyclase SSFG_02181 from *Streptomyces ghanaensis* ATCC14672 regulates antibiotic biosynthesis and morphological differentiation in streptomycetes. *Scientific Reports*, *10*(1), 1–15.

Olsthoorn, M. M., Petersen, B. O., Duus, J., Haverkamp, J., Thomas-Oates, J. E., Bock, K., & Holst, O. (2000). The structure of the linkage between the O-specific polysaccharide and the core region of the lipopolysaccharide from *Salmonella enterica* serovar Typhimurium revisited. *European Journal of Biochemistry*, *267*(7), 2014–2027.

Pan, M.-Y., Shen, Y.-C., Lu, C.-H., Yang, S.-Y., Ho, T.-F., Peng, Y.-T., & Chang, C.-C. (2012). Prodigiosin activates endoplasmic reticulum stress cell death pathway in human breast carcinoma cell lines. *Toxicology and Applied Pharmacology*, *265*(3), 325–334.

Pandey, R., Chander, R., & Sainis, K. B. (2007). Role of interleukin-2 regulated proteins in immunosuppression by the N-alkylated prodigiosin analogue. *International Immunopharmacology*, *7*(13), 1695–1703.

Papireddy, K., Smilkstein, M., Kelly, J. X., Salem, S. M., Alhamadsheh, M., Haynes, S. W., Challis, G. L., & Reynolds, K. A. (2011). Antimalarial activity of natural and synthetic prodiginines. *Journal of Medicinal Chemistry*, *54*(15), 5296–5306.

Papp-Wallace, K. M., Endimiani, A., Taracila, M. A., & Bonomo, R. A. (2011). Carbapenems: Past, present, and future. *Antimicrobial Agents and Chemotherapy*, *55*(11), 4943–4960.

Paritala, H., & S Carroll, K. (2013). New targets and inhibitors of mycobacterial sulfur metabolism. *Infectious Disorders-Drug Targets (Formerly Current Drug Targets-Infectious Disorders)*, *13*(2), 85–115.

Parker, W. L., RATHNUM, M. L., JERRY, J., TREJO, W. H., PRINCIPE, P. A., & SYKES, R. B. (1982). SQ 27, 860, a simple carbapenem produced by species of *Serratia* and *Erwinia*. *The Journal of Antibiotics*, *35*(6), 653–660.

Paterson, D. L., & Bonomo, R. A. (2005). Extended-spectrum β-lactamases: A clinical update. *Clinical Microbiology Reviews*, *18*(4), 657–686.

Paul, T., Bandyopadhyay, T. K., Mondal, A., Tiwari, O. N., Muthuraj, M., & Bhunia, B. (2020). A comprehensive review on recent trends in production, purification, and applications of prodigiosin. *Biomass Conversion and Biorefinery*, 1–23.

Pavlova, N., Kaloudas, D., & Penchovsky, R. (2019). Riboswitch distribution, structure, and function in bacteria. *Gene*, *708*, 38–48.

Peekhaus, N., & Conway, T. (1998). Positive and negative transcriptional regulation of the *Escherichia coli* gluconate regulon gene *gntT* by GntR and the cyclic AMP (cAMP)-cAMP receptor protein complex. *Journal of Bacteriology*, *180*(7), 1777–1785.

Pérez Tomás, R. E., & Montaner Ramoneda, B. (2003). Effects of the proapoptotic drug prodigiosin on cell cycle-related proteins in Jurkat T cells. *Histology and Histopathology, 2003, Vol. 18, Num. 2, p. 379-385*.

Perez-Tomas, R., & Vinas, M. (2010). New insights on the antitumoral properties of prodiginines. *Current Medicinal Chemistry*, *17*(21), 2222–2231.

Pfeifer, F. (2012). Distribution, formation and regulation of gas vesicles. *Nature Reviews Microbiology*, *10*(10), 705–715.

Pfeifer, F. (2015). Haloarchaea and the formation of gas vesicles. *Life*, *5*(1), 385–402.

Piłsyk, S., & Paszewski, A. (2009a). Sulfate permeasesphylogenetic diversity of sulfate transport. *Acta Biochimica Polonica*, *56*(3).

Piłsyk, S., & Paszewski, A. (2009b). Sulfate permeasesphylogenetic diversity of sulfate transport. *Acta Biochimica Polonica*, *56*(3).

Potrykus, M., Golanowska, M., Hugouvieux-Cotte-Pattat, N., & Lojkowska, E. (2014). Regulators involved in *Dickeya solani* virulence, genetic conservation, and functional variability. *Molecular Plant-Microbe Interactions*, *27*(7), 700–711.

Potrykus, M., Hugouvieux-Cotte-Pattat, N., & Lojkowska, E. (2018). Interplay of classic Exp and specific Vfm quorum sensing systems on the phenotypic features of *Dickeya solani* strains exhibiting different virulence levels. *Molecular Plant Pathology*, *19*(5), 1238–1251.

Potrykus, M., Sledz, W., Golanowska, M., Slawiak, M., Binek, A., Motyka, A., Zoledowska, S., Czajkowski, R., & Lojkowska, E. (2014). Simultaneous detection of major blackleg and soft rot bacterial pathogens in potato by multiplex polymerase chain reaction. *Annals of Applied Biology*, *165*(3), 474–487.

Potter, R. F., D'Souza, A. W., & Dantas, G. (2016). The rapid spread of carbapenem-resistant Enterobacteriaceae. *Drug Resistance Updates*, *29*, 30–46.

Poulter, S., Carlton, T. M., Su, X., Spring, D. R., & Salmond, G. P. (2010). Engineering of new prodigiosin-based biosensors of *Serratia* for facile detection of short-chain N-acyl homoserine lactone quorum-sensing molecules. *Environ Microbiol Rep 2:322–328*.

Pourciau, C., Lai, Y.-J., Gorelik, M., Babitzke, P., & Romeo, T. (2020). Diverse mechanisms and circuitry for global regulation by the RNA-binding protein CsrA. *Frontiers in Microbiology*, *11*, 601352.

Quintero-Yanes, A., Lee, C. M., Monson, R., & Salmond, G. (2020). The FloR master regulator controls flotation, virulence, and antibiotic production in *Serratia* sp. ATCC 39006. *Environmental Microbiology*, *22*(7), 2921–2938.

Quintero-Yanes, A., Monson, R. E., & Salmond, G. P. (2019). Environmental potassium regulates bacterial flotation, antibiotic production and turgor pressure in *Serratia* through the TrkH transporter. *Environmental Microbiology*, *21*(7), 2499–2510.

Raetz, C. R., & Whitfield, C. (2002). Lipopolysaccharide endotoxins. *Annual Review of Biochemistry*, *71*, 635.

Ramsay, J. P., & Salmond, G. P. (2012). Quorum sensing-controlled buoyancy through gas vesicles: Intracellular bacterial microcompartments for environmental adaptation. *Communicative & Integrative Biology*, *5*(1), 96–98.

Ramsay, J. P., Williamson, N. R., Spring, D. R., & Salmond, G. P. (2011). A quorum-sensing molecule acts as a morphogen controlling gas vesicle organelle biogenesis and adaptive flotation in an enterobacterium. *Proceedings of the National Academy of Sciences*, *108*(36), 14932–14937.

Rancati, G., Moffat, J., Typas, A., & Pavelka, N. (2018). Emerging and evolving concepts in gene essentiality. *Nature Reviews Genetics*, *19*(1), 34–49.

Ranjan, M., Khokhani, D., Nayaka, S., Srivastava, S., Keyser, Z. P., & Ranjan, A. (2021). Genomic diversity and organization of complex polysaccharide biosynthesis clusters in the genus *Dickeya*. *PloS One*, *16*(2), e0245727.

Rashidi, M., & Jebali, A. (2019). Liposomal prodigiosin and plasmid encoding serial GCA nucleotides reduce inflammation in microglial and astrocyte cells by ATM/ATR signaling. *Journal of Neuroimmunology*, *326*, 75–78.

Regmi, A., Tague, J., & Boyd, E. F. (2022). A class IV adenylate cyclase CyaB is required for capsule polysaccharide production and biofilm formation in *Vibrio parahaemolyticus*. *BioRxiv*.

Retchless, A. C., & Lawrence, J. G. (2010). Phylogenetic incongruence arising from fragmented speciation in enteric bacteria. *Proceedings of the National Academy of Sciences*, *107*(25), 11453–11458.

Romeo, T., & Babitzke, P. (2018). Global regulation by CsrA and its RNA antagonists. *Microbiology Spectrum*, *6*(2), 6–2.

Ryazantseva, I., Andreyeva, I., Klementyeva, G., Ogorodnikova, T., & Petrov, V. Y. (1995). Pigmentdependent light influence on the energetics of Serratia marcescens. *Thermochimica Acta*, *251*, 63– 67.

Saha, R. P., Samanta, S., Patra, S., Sarkar, D., Saha, A., & Singh, M. K. (2017). Metal homeostasis in bacteria: The role of ArsR–SmtB family of transcriptional repressors in combating varying metal concentrations in the environment. *Biometals*, *30*(4), 459–503.

Saigí, F., Climent, N., Piqué, N., Sanchez, C., Merino, S., Rubirés, X., Aguilar, A., Tomás, J. M., & Regué, M. (1999). Genetic analysis of the *Serratia marcescens* N28b O4 antigen gene cluster. *Journal of Bacteriology*, *181*(6), 1883–1891.

Samrot, A. V. (2011). IJMBR International Journal of Medicobiological Research. *Int J Med Res*, *1*(3), 145–150.

Scheepers, G. H., Lycklama a Nijeholt, J. A., & Poolman, B. (2016). An updated structural classification of substrate-binding proteins. *FEBS Letters*, *590*(23), 4393–4401.

Schellhorn, H. E. (2020). Function, evolution, and composition of the RpoS regulon in *Escherichia coli*. *Frontiers in Microbiology*, *11*, 560099.

Shanks, R. M., Lahr, R. M., Stella, N. A., Arena, K. E., Brothers, K. M., Kwak, D. H., Liu, X., & Kalivoda, E. J. (2013). A *Serratia marcescens* PigP homolog controls prodigiosin biosynthesis, swarming motility and hemolysis and is regulated by cAMP-CRP and HexS. *PloS One*, *8*(3), e57634.

Shimada, T., Fujita, N., Yamamoto, K., & Ishihama, A. (2011). Novel roles of cAMP receptor protein (CRP) in regulation of transport and metabolism of carbon sources. *PloS One*, *6*(6), e20081.

Shomar, H., Gontier, S., van Den Broek, N. J., Tejeda Mora, H., Noga, M. J., Hagedoorn, P.-L., & Bokinsky, G. (2018). Metabolic engineering of a carbapenem antibiotic synthesis pathway in Escherichia coli. *Nature Chemical Biology*, *14*(8), 794–800.

Sillitoe, I., Bordin, N., Dawson, N., Waman, V. P., Ashford, P., Scholes, H. M., Pang, C. S., Woodridge, L., Rauer, C., & Sen, N. (2021). CATH: increased structural coverage of functional space. *Nucleic Acids Research*, *49*(D1), D266–D273.

Simpson, B. W., & Trent, M. S. (2019). Pushing the envelope: LPS modifications and their consequences. *Nature Reviews Microbiology*, *17*(7), 403–416.

Slater, H., Crow, M., Everson, L., & Salmond, G. P. (2003). Phosphate availability regulates biosynthesis of two antibiotics, prodigiosin and carbapenem, in *Serratia* via both quorum-sensingdependent and-independent pathways. *Molecular Microbiology*, *47*(2), 303–320.

Smyth, G. K. (2005). Limma: Linear models for microarray data. In *Bioinformatics and computational biology solutions using R and Bioconductor* (pp. 397–420). Springer.

Solovyev, V. V., Salamov, A. A., Seledtsov, I. A., Vorobyev, D., & Bachinsky, A. G. (2011). *Automatic Annotation of Bacterial Community Sequences and Application to Infections Diagnostic.* 346–353.

Sperandeo, P., Martorana, A. M., & Polissi, A. (2017). Lipopolysaccharide biogenesis and transport at the outer membrane of Gram-negative bacteria. *Biochimica et Biophysica Acta (BBA)-Molecular and Cell Biology of Lipids*, *1862*(11), 1451–1460.

Spížek, J., Sigler, K., Řezanka, T., & Demain, A. (2016). Biogenesis of antibiotics—Viewing its history and glimpses of the future. *Folia Microbiologica*, *61*(4), 347–358.

Sprouffske, K., & Wagner, A. (2016). Growthcurver: an R package for obtaining interpretable metrics from microbial growth curves. *BMC bioinformatics*, *17*(1), 1-4.

Stanton, T. B. (2013). A call for antibiotic alternatives research. *Trends in Microbiology*, *21*(3), 111–113.

Stapon, A., Li, R., & Townsend, C. A. (2003). Carbapenem biosynthesis: Confirmation of stereochemical assignments and the role of CarC in the ring stereoinversion process from L-proline. *Journal of the American Chemical Society*, *125*(28), 8486–8493.

Sun, D., Liu, W., Zhou, X., Ru, Y., Liu, J., Zhu, J., & Liu, C. (2022). Organic Hydroperoxide Induces Prodigiosin Biosynthesis in *Serratia* sp. ATCC 39006 in an OhrR-Dependent Manner. *Applied and Environmental Microbiology*, *88*(5), e02041-21.

Sun, D., Zhou, X., Liu, C., Zhu, J., Ru, Y., Liu, W., & Liu, J. (2021). Fnr negatively regulates prodigiosin synthesis in *Serratia* sp. ATCC 39006 during aerobic fermentation. *Frontiers in Microbiology*, 2642.

Surette, M. D., & Wright, G. D. (2017). Lessons from the environmental antibiotic resistome. *Annual Review of Microbiology*, *71*, 309–329.

Suryawanshi, R. K., Patil, C. D., Koli, S. H., Hallsworth, J. E., & Patil, S. V. (2017). Antimicrobial activity of prodigiosin is attributable to plasma-membrane damage. *Natural Product Research*, *31*(5), 572–577.

Suvorova, I. A., Korostelev, Y. D., & Gelfand, M. S. (2015). GntR family of bacterial transcription factors and their DNA binding motifs: Structure, positioning and co-evolution. *PloS One*, *10*(7), e0132618.

Szabo, M., Bronner, D., & Whitfield, C. (1995). Relationships between rfb gene clusters required for biosynthesis of identical D-galactose-containing O antigens in *Klebsiella pneumoniae* serotype O1 and *Serratia marcescens* serotype O16. *Journal of Bacteriology*, *177*(6), 1544–1553.

Szklarczyk, D., Gable, A. L., Nastou, K. C., Lyon, D., Kirsch, R., Pyysalo, S., Doncheva, N. T., Legeay, M., Fang, T., & Bork, P. (2021). The STRING database in 2021: Customizable protein–protein networks, and functional characterization of user-uploaded gene/measurement sets. *Nucleic Acids Research*, *49*(D1), D605–D612.

Tambong, J. T. (2013). Phylogeny of bacteria isolated from *Rhabditis* sp.(Nematoda) and identification of novel entomopathogenic *Serratia marcescens* strains. *Current Microbiology*, *66*(2), 138–144.

Tashiro, Y., Monson, R. E., Ramsay, J. P., & Salmond, G. P. (2016). Molecular genetic and physical analysis of gas vesicles in buoyant enterobacteria. *Environmental Microbiology*, *18*(4), 1264–1276.

Thomson, N., Crow, M., McGowan, S., Cox, A., & Salmond, G. (2000). Biosynthesis of carbapenem antibiotic and prodigiosin pigment in *Serratia* is under quorum sensing control. *Molecular Microbiology*, *36*(3), 539–556.

Thorvaldsdóttir, H., Robinson, J. T., & Mesirov, J. P. (2013). Integrative Genomics Viewer (IGV): High-performance genomics data visualization and exploration. *Briefings in Bioinformatics*, *14*(2), 178–192.

Tichy, E., Luisi, B., & Salmond, G. (2014). Crystal structure of the carbapenem intrinsic resistance protein CarG. *Journal of Molecular Biology*, *426*(9), 1958–1970.

Tichy, E. M., Hardwick, S. W., Luisi, B. F., & Salmond, G. P. (2017). 1.8 Å resolution crystal structure of the carbapenem intrinsic resistance protein CarF. *Acta Crystallographica Section D: Structural Biology*, *73*(7), 549–556.

Toledo-Arana, A., & Lasa, I. (2020). Advances in bacterial transcriptome understanding: From overlapping transcription to the excludon concept. *Molecular Microbiology*, *113*(3), 593–602.

Townsend, C. A. (2016). Convergent biosynthetic pathways to β-lactam antibiotics. *Current Opinion in Chemical Biology*, *35*, 97–108.

Umarov, R. K., & Solovyev, V. V. (2017). Recognition of prokaryotic and eukaryotic promoters using convolutional deep learning neural networks. *PloS One*, *12*(2), e0171410.

Updegrove, T. B., Zhang, A., & Storz, G. (2016). Hfq: The flexible RNA matchmaker. *Current Opinion in Microbiology*, *30*, 133–138.

Vakulskas, C. A., Leng, Y., Abe, H., Amaki, T., Okayama, A., Babitzke, P., Suzuki, K., & Romeo, T. (2016). Antagonistic control of the turnover pathway for the global regulatory sRNA CsrB by the CsrA and CsrD proteins. *Nucleic Acids Research*, *44*(16), 7896–7910.

Van Der Meer, J. R., & Belkin, S. (2010). Where microbiology meets microengineering: Design and applications of reporter bacteria. *Nature Reviews Microbiology*, *8*(7), 511–522.

Van der Meij, A., Worsley, S. F., Hutchings, M. I., & van Wezel, G. P. (2017). Chemical ecology of antibiotic production by actinomycetes. *FEMS Microbiology Reviews*, *41*(3), 392–416.

Van Dyk, T. K., Wei, Y., Hanafey, M. K., Dolan, M., Reeve, M. J. G., Rafalski, J. A., Rothman-Denes, L. B., & LaRossa, R. A. (2001). A genomic approach to gene fusion technology. *Proceedings of the National Academy of Sciences*, *98*(5), 2555–2560.

Walters, R. F., & Degrado, W. F. (2006). Helix-packing motifs in membrane proteins. *Proceedings of the National Academy of Sciences*, *103*(37), 13658–13663.

Wang, Z., Li, B., Zhou, L., Yu, S., Su, Z., Song, J., Sun, Q., Sha, O., Wang, X., & Jiang, W. (2016). Prodigiosin inhibits Wnt/β-catenin signaling and exerts anticancer activity in breast cancer cells. *Proceedings of the National Academy of Sciences*, *113*(46), 13150–13155.

Wass, M. N., Kelley, L. A., & Sternberg, M. J. (2010). 3DLigandSite: Predicting ligand-binding sites using similar structures. *Nucleic Acids Research*, *38*(2), 469–473.

Whitfield, C., & Trent, M. S. (2014). Biosynthesis and export of bacterial lipopolysaccharides. *Annual Review of Biochemistry*, *83*, 99–128.

Whitfield, C., Williams, D. M., & Kelly, S. D. (2020). Lipopolysaccharide O-antigens—Bacterial glycans made to measure. *Journal of Biological Chemistry*, *295*(31), 10593–10609.

Whitney, J., & Howell, P. (2013). Synthase-dependent exopolysaccharide secretion in Gram-negative bacteria. *Trends in Microbiology*, *21*(2), 63–72.

Wilf, N. (2011). *The role of post-transcriptional regulators in pathogenesis and secondary metabolite production in Serratia sp. ATCC 39006.*

Wilf, N. M., Reid, A. J., Ramsay, J. P., Williamson, N. R., Croucher, N. J., Gatto, L., Hester, S. S., Goulding, D., Barquist, L., & Lilley, K. S. (2013). RNA-seq reveals the RNA binding proteins, Hfq and RsmA, play various roles in virulence, antibiotic production and genomic flux in *Serratia* sp. ATCC 39006. *BMC Genomics*, *14*(1), 1–17.

Wilf, N. M., & Salmond, G. P. (2012). The stationary phase sigma factor, RpoS, regulates the production of a carbapenem antibiotic, a bioactive prodigiosin and virulence in the enterobacterial pathogen *Serratia* sp. ATCC 39006. *Microbiology*, *158*(3), 648–658.

Wilf, N. (2011). The role of post-transcriptional regulators in pathogenesis and secondary metabolite production in *Serratia* sp. ATCC 39006. (Doctoral thesis).

Wilf, N. M., Williamson, N. R., Ramsay, J. P., Poulter, S., Bandyra, K. J., & Salmond, G. P. (2011a). The RNA chaperone, Hfq, controls two luxR-type regulators and plays a key role in pathogenesis

and production of antibiotics in *Serratia* sp. ATCC 39006. *Environmental Microbiology*, *13*(10), 2649–2666.

Wilf, N. M., Williamson, N. R., Ramsay, J. P., Poulter, S., Bandyra, K. J., & Salmond, G. P. (2011b). The RNA chaperone, Hfq, controls two luxR-type regulators and plays a key role in pathogenesis and production of antibiotics in *Serratia* sp. ATCC 39006. *Environmental Microbiology*, *13*(10), 2649–2666.

Wilkens, S. (2015). Structure and mechanism of ABC transporters. *F1000prime Reports*, *7*.

Williamson, N. R., Fineran, P. C., Gristwood, T., Chawrai, S. R., Leeper, F. J., & Salmond, G. P. (2007). *Anticancer and immunosuppressive properties of bacterial prodiginines*.

Williamson, N. R., Fineran, P. C., Leeper, F. J., & Salmond, G. P. (2006). The biosynthesis and regulation of bacterial prodiginines. *Nature Reviews Microbiology*, *4*(12), 887–899.

Williamson, N. R., Fineran, P. C., Ogawa, W., Woodley, L. R., & Salmond, G. P. (2008). Integrated regulation involving quorum sensing, a two-component system, a GGDEF/EAL domain protein and a post-transcriptional regulator controls swarming and RhlA-dependent surfactant biosynthesis in *Serratia*. *Environmental Microbiology*, *10*(5), 1202–1217.

Wingett, S. W., & Andrews, S. (2018). FastQ Screen: A tool for multi-genome mapping and quality control. *F1000Research*, *7*.

Wohlleben, W., Mast, Y., Stegmann, E., & Ziemert, N. (2016). Antibiotic drug discovery. *Microbial Biotechnology*, *9*(5), 541–548.

Wright, E. S. (2022). FindNonCoding: Rapid and simple detection of non-coding RNAs in genomes. *Bioinformatics*, *38*(3), 841–843. https://doi.org/10.1093/bioinformatics/btab708

Xu, F., Nazari, B., Moon, K., Bushin, L. B., & Seyedsayamdost, M. R. (2017). Discovery of a cryptic antifungal compound from *Streptomyces albus* J1074 using high-throughput elicitor screens. *Journal of the American Chemical Society*, *139*(27), 9203–9212.

Xu, J., Platt, T. G., & Fuqua, C. (2012). Regulatory linkages between flagella and surfactant during swarming behavior: Lubricating the flagellar propeller? *Journal of Bacteriology*, *194*(6), 1283–1286.

Xu, K., Shen, D., Han, S., Chou, S., & Qian, G. (2021). A non-flagellated, predatory soil bacterium reprograms a chemosensory system to control antifungal antibiotic production via cyclic di-GMP signalling. *Environmental Microbiology*, *23*(2), 878–892.

Xu, Z., Li, Y., Wang, Y., Deng, Z., & Tao, M. (2019). Genome-wide mutagenesis links multiple metabolic pathways with actinorhodin production in *Streptomyces coelicolor*. *Applied and Environmental Microbiology*, *85*(7), e03005-18.

Yang, J., & Zhang, Y. (2015). Protein structure and function prediction using I-TASSER. *Current Protocols in Bioinformatics*, *52*(1), 5–8.

Yip, C.-H., Mahalingam, S., Wan, K.-L., & Nathan, S. (2021). Prodigiosin inhibits bacterial growth and virulence factors as a potential physiological response to interspecies competition. *Plos One*, *16*(6), e0253445.

Zallot, R., Oberg, N., & Gerlt, J. A. (2019). The EFI web resource for genomic enzymology tools: Leveraging protein, genome, and metagenome databases to discover novel enzymes and metabolic pathways. *Biochemistry*, *58*(41), 4169–4182.

Zhou, J., Cheng, Y., Lv, M., Liao, L., Chen, Y., Gu, Y., Liu, S., Jiang, Z., Xiong, Y., & Zhang, L. (2015). The complete genome sequence of *Dickeya zeae* EC1 reveals substantial divergence from other Dickeya strains and species. *BMC Genomics*, *16*(1), 1–15.